Turbulent combustion in opposed jet flows

by

Epaminondas Mastorakos

Thesis submitted for the degree of
Doctor of Philosophy
in the University of London
and for the
Diploma of Membership of the Imperial College

Imperial College of Science, Technology and Medicine
(Mechanical Engineering Department)

July 1993

Abstract

The extinction of turbulent flames is technologically and scientifically interesting and stretched counterflow flames are used in the investigations of this thesis to study the phenomenon. Non–premixed, partially–premixed diffusion, and fully premixed flames have been established in turbulent opposed jet flows and the velocity, temperature, and mixing characteristics of inert and reactive flows have been measured with laser–doppler velocimetry, numerically–compensated fine–wire thermocouples, and aspiration–probe respectively and an eddy–viscosity model has been formulated to predict the width of the mixing layer and the level of the mixture fraction fluctuations.

The results showed that the appoach to extinction, caused by increased bulk and/or turbulent stretch rates, led to smaller product concentrations, and that the influence of the heat release associated with the reaction zone had an effect on the mean and fluctuating velocity field that depends on whether the flame is diffusion or premixed. Measurements of the mixture fraction fluctuations in inert flows exhibited the unexpected feature of small probability of well–mixed fluid, and this is explained by the fact that in the counterflow geometry there is little time available for turbulent mixing because the fluid is rapidly convected outside the stagnation region by the action of the relatively high bulk strain rate. This observation is used to interpret the reactive flow data, motivates suggestions for the appropriateness of standard turbulence models for this flow, and suggests a physical description for mixing based on the Flapping Model of scalar turbulence.

The extinction limits of non–premixed and partially–premixed diffusion flames have been measured and analysis showed that the mean dissipation rate of the mixture fraction had a critical value at extinction, a result that highlights the prominent position of this quantity in the description of turbulent diffusion flame stability. The extinction limits of turbulent counterflow diffusion flames in natural gas jets opposed by preheated air and by air vitiated by combustion products, and of lean premixed flames opposed by hot reaction products, have also been measured to relate the extinction of flames in the opposed–jet flow to the more practically–interesting configuration of flames stabilised by recirculation zones and, in conjunction with estimates of the scalar dissipation rate, resulted in new predictions of recirculating flame stability.

Acknowledgements

The research described in this thesis was performed from September 1989 to July 1993 and has been supervised by Prof. J. H. Whitelaw and Dr. A. Taylor. They both deserve my sincerest thanks for their warm interest, useful suggestions, and constructive criticisms on the work and on this thesis, and for their efforts to obtain the financial support that made my stay at Imperial College possible. My gratitude is deeper than I express for Prof. Whitelaw's long effort to teach me how scientific research should be done and for Dr. Taylor's insistence that real understanding of physical phenomena comes only with the capability to explain these, as well as for his teaching me fluid mechanics over many a beer. It needs a lot of work from my part, but I must try to ensure that their efforts were not wasted.

Many colleagues at Imperial College have helped me in various ways during these years and I acknowledge their assistance. Dr. C. Vafidis found laser-doppler signals when I was ready to give up; Dr. Enotiadis always solved my serious computer problems; I have benefitted from discussions and the co–operation with Dr. Y. Hardalupas; Dr. P. Lindstedt provided constructive advice and useful data; Drs. P. Costen and S. Godoy and Mr. J. R. Laker advised me on experimental methods; and the technical staff of the Thermofluids Section have done everything they could to help, and in an expert way.

Outside Imperial College, I wish to acknowledge suggestions from Prof. P. A. Libby, whose interest in this work was always a strong motivation to do more, and help from Dr. L. W. Kostiuk for sharing his experiences on counterflow flames during the early stages of this work.

Friends in the lab, including Rebeca Perez–Ortiz and David Symon, have helped enormously with technical suggestions and answers to philosophical questions, while late–evening support came invariably from my friend Nikos Orfanoudakis. Special thanks go to the unknown white–haired man that made sure the coffee machine outside the Combustion Lab was up–and–running; without it, life would be different and much more boring.

On a personal level, I must thank my family for their support and the others who were close to me. Although I let them down often by excusing myself as too busy, I wouldn't have made it without them.

Table of Contents

Abstract 2

Acknowledgments 3

List of Tables 9

List of Figures 10

List of commonly used symbols 18

Chapter 1. Introduction 21

1.1 BACKGROUND 21
1.1.1 The topic of this thesis 21
1.1.2 Structure of this Chapter 22

1.2 LAMINAR COUNTERFLOW FLAMES 23
1.2.1 Historical overview and motivation 23
1.2.2 Stagnation point flows 24
1.2.3 Extinction limits 25
Diffusion flames 25
Premixed flames 26

1.3 TURBULENT COUNTERFLOW FLAMES 28
1.3.1 Premixed flames on solid plates 28
1.3.2 Premixed flames in opposed jets 29
1.3.3 Non–premixed opposed jet flames 30

1.4 THE PRESENT CONTRIBUTION 34
1.4.1 Structure of turbulent counterflow flames (Chapter 3) 34
1.4.2 Extinction of turbulent counterflow flames (Chapter 4) 34
1.4.3 Extinction of flames in recirculation zones (Chapter 5) 34
1.4.4 The structure of this thesis 35

Chapter 2. Experimental methods 36

2.1 FLOW CONFIGURATION 36
2.1.1 Straight–tube burner 36
2.1.2 Contoured–nozzle burner 37
2.1.3 Burners for flames with hot product dilution 38

2.2 NOMENCLATURE, FLUID PROPERTIES, AND FLOW CONDITIONS 39

2.3 PHOTOGRAPHIC METHODS 41

2.4 SPECIES CONCENTRATIONS MEASUREMENTS 42
2.4.1 Sampling circuit 42
2.4.2 Operation, calibration, and analytical uncertainties 43
CO, CO2, and O2 analysers 43
H2 analyser 43
Unburnt hydrocarbons analyser 43
2.4.3 Calculation of the mean mixture fraction 45
2.4.4 Probes used 47

2.4.5 Spatial averaging effects 48
2.4.6 Comparison of the two probes and sample results 50
2.4.7 Uncertainties 51

2.5 TEMPERATURE MEASUREMENTS 51
2.5.1 Thermocouples 52
2.5.2 Data acquisition 52
2.5.3 Compensation 52
2.5.4 Numerical methods 54
2.5.5 Sample results 55
Surface catalysis 56
Time constant 56
Instantaneous temperature 57
2.5.6 Two–point measurements 58
2.5.7 Uncertainties 59
Radiation loss 59
Statistical and positional 60
Uncertainties due to the time constant 61

2.6 VELOCITY MEASUREMENTS 61
2.6.1 LDV systems 61
2.6.2 Uncertainties 62

2.7 SUMMARY OF CHAPTER 2 64

Figures for Chapter 2 65

Chapter 3. The structure of opposed jet turbulent flames 78

3.1 INTRODUCTION 78
3.1.1 The structure of this Chapter 78
3.1.2 Flow conditions and nomenclature 78
Varying and constant parameters 78
Nomenclature and normalisations 79
3.1.3 Correspondence between measurements 79

3.2 INERT OPPOSED JET FLOWS 81
3.2.1 Background and structure of this Section 81
3.2.2 Visualisation 81
3.2.3 Initial conditions 82
Single jet 82
Opposed jets 83
3.2.4 Velocity traverses 83
3.2.5 Mixing – Theoretical results 85
Formulation 86
Numerical results 90
3.2.6 Mixing – Experimental results 91
3.2.7 Mixing – Comparison of experiment with theory 93

3.3 REACTING OPPOSED JET FLOWS 95
3.3.1 Background and structure of this Section 95
3.3.2 Visualisation 95
Pure diffusion flames 95
Partially premixed diffusion flames 96
Premixed flames 96
3.3.3 Scalar fields – diffusion flames 97

Temperature measurements 97
Species concentrations measurements 99
3.3.4 Velocity fields – diffusion flames 99
Initial conditions 99
Centreline variations 100
Off–axis variations 102
3.3.5 Scalar fields – premixed flames 102
Temperature measurements 103
Species concentrations measurements 103
3.3.6 Velocity fields – premixed flames 104
Initial conditions 104
Centreline variations 104
Off–axis variations 106

3.4 DISCUSSION 107
3.4.1 Scale estimates and combustion regimes 107
Turbulent combustion regimes 107
Scale estimates 108
3.4.2 Comparison of reacting with inert flow 109
Velocities 109
Mixing 110
3.4.3 Transition from diffusion to premixed flames 111
3.4.4 Flame motion 113
Frequency content 113
Two–point measurements 114
3.4.5 The approach to extinction and the strain rate on the flame 115
Species concentrations 116
Temperatures 118
Bulk stretch rate 118
Turbulent stretch rate 120
3.4.6 Mixing in opposed jet flows 120
Short residence times 121
Instantaneous scalar structure 121
Flapping Model for inert mixing 122
Flapping Model for flames 123
Discussion on the Flapping Model 124
The scalar dissipation rate 125

3.4 SUMMARY OF CHAPTER 3 126

Figures for Chapter 3, Section 3.2 129

Figures for Chapter 3, Section 3.3 151

Figures for Chapter 3, Section 3.4 194

Chapter 4. Extinction of turbulent counterflow flames 210

4.1 INTRODUCTION 210
4.1.1 Structure of this Chapter 210
4.1.2 Background on extinction of laminar flames 210
4.1.3 Extinction of turbulent premixed flames 211
Flamelet combustion 211
Combustion in Kolmogorov–scale vortices 211
4.1.4 Extinction of turbulent diffusion flames 212

Flamelet flames 212
Non–flamelet flames 214
4.1.5 Application of extinction theories: the lifted jet flame 214
4.1.6 Localised extinction: the piloted jet diffusion flame of Masri *et al.* (1990) 215
4.1.7 The turbulent counterflow premixed flames of Kostiuk *et al.* (1989) 216
4.1.8 Present contribution 216

4.2 EXPERIMENTAL METHODS 218
4.2.1 Flow configuration 218
4.2.2 Determination of extinction points 218
Cold reactants, diffusion flames 218
Cold reactants, premixed flames 219
Electrically heated reactants 219
Reactants diluted by hot products 219
Flames with fuels other than natural gas 220

4.3 RESULTS 221

4.3.1 General observations 221
4.3.2 Premixed flames 222
Single and twin flames 222
Heated opposed stream 223
Structure of ultra–lean counterflow premixed flames 224
Discussion and comparison with laminar flames 226
4.3.3 Diffusion flames 229
4.3.4 Discussion and correlations of the extinction of diffusion flames 230
Correlation in terms of total strain rate 230
Correlation in terms of the scalar dissipation rate 232
Comparison with laminar flames – strain rate 233
Comparison with laminar flames – dissipation rate 234
Comparison with laminar flames – partial premixing 234
Discussion on the proposed correlations 235
4.3.5 Diffusion flames with vitiated air 238
Background and structure of this Section 238
Air stream preheat without dilution 239
Fuel stream preheat without dilution 239
Air dilution with and without preheat 240
Flames with hot combustion products as oxidiser 240
Comparison with laminar flames – analysis 241
Comparison with laminar flames – results 244
Application to recirculating flames 246
4.3.6 Extensions to other fuels 247
H_2/CH_4 flames 247
$CO/H_2/N_2$ flames 247

4.4 SUMMARY OF CHAPTER 4 249

Figures for Chapter 4 252

Chapter 5. Conjectures on the extinction of non–premixed flames stabilised by recirculation zones 272

5.1 INTRODUCTION 272
5.1.1 Purpose of this Chapter 272

5.1.2 Stability of recirculating premixed flames 272
5.1.3 Stability of recirculating non–premixed flames 274
5.1.4 Structure of this Chapter 276

5.2 STABILISATION OF NON–PREMIXED RECIRCULATING FLAMES 277

5.3 EXTINCTION OF NON–PREMIXED RECIRCULATING FLAMES 279
5.3.1 Operational parameters of a recirculation–stabilised diffusion flame 279
5.3.2 Mixing of the fuel jet 279
5.3.3 Scalar dissipation rate in the mixing layer 280
5.3.4 The temperature of the recirculation zone 281
5.3.5 Final expressions 282
5.3.6 Qualitative prediction of extinction 283
5.3.6 Discussion 284
Comparison with experiment 284
Scaling laws 285
Extinction correlations 286
Justification of assumptions 286
Quantitative predictions 287

5.4 SUMMARY OF CHAPTER 5 288

Chapter 6. Closure 291

6.1 CONCLUSIONS FROM THIS WORK 291

6.2 SUGGESTIONS FOR FURTHER RESEARCH 293

Appendix 2.1. Calculation of oxygen mole fraction in the vitiated air burner 295

Appendix 6.1. Published work 296

References 297

List of Tables

		page
Table 1.1	Flow arrangements for turbulent counterflow premixed flame experiments.	31
Table 1.2	Flow arrangements for turbulent counterflow diffusion flame experiments.	33
Table 2.1	Reactants compositions and counterflow flame definitions.	41
Table 2.2	Time constant measurements in isothermal turbulent air flow and Monte–Carlo calculations based on the expression of Collis and Williams (1959).	57
Table 2.3	Uncompensated and compensated mean and r.m.s. temperature measurements.	58
Table 2.4	Principal characteristics of the laser–doppler velocimeter.	63
Table 3.1	Estimates of relevant scales for diffusion flames.	108
Table 3.2	Estimates of relevant scales for premixed flames.	109

List of Figures

		page
Figure 2.1	The burner arrangements used for most measurements.	65
Figure 2.2	The contractions used for stabilising laminar counterflow flames.	66
Figure 2.3	The burner used for the experiments with air diluted by hot products ("vitiated air") in some extinction experiments in Chapter 4.	67
Figure 2.4	Outline of the sampling circuit showing the various drying and filtering stages, valves, and analysers.	69
Figure 2.5	The mole fraction of methane in methane–air mixtures measured by the FID with and without subsequent correction using Eq. (2.4.1).	70
Figure 2.6	Sketches of the probes used for extracting samples from the flames.	71
Figure 2.7	Sketch of the way spatial averaging effects arise and the way in which these are calculated.	72
Figure 2.8	Broadening of profiles due to spatial averaging.	73
Figure 2.9	Comparison of measurements with the small and large probes of Fig. 2.6 in partially–premixed diffusion and fully premixed turbulent counterflow flames.	74
Figure 2.10	The ratio of the time constant of a 40μm wire at 1m/s based on air properties (Eq. 2.5.2 with Eq. (2.5.3) to that based on the local properties across a laminar counterflow diffusion flame calculated by Jones and Lindstedt (1988).	75
Figure 2.11	Typical probability density function of compensated temperature at conditions of high partial premixing of the fuel stream with air (X=0.8) that shows signal contamination by catalytic effects on the wire surface.	75
Figure 2.12	Typical temperature traces, pdfs, and frequency spectra in turbulent counterflow diffusion flames.	76

Figure 3.2.1	Photograph of the light scattered from alumina particles seeded in the upper jet of an inert opposed jet flow with H=25mm, H_p=55mm, and U_1=U_2=3.0m/s.	129
Figure 3.2.2	Mean and r.m.s. axial velocity radial variation across the exit plane of a single jet (z/D=0.08) for two locations of the perforated plate, H_p.	130
Figure 3.2.3	Variation of the turbulence intensity q' (Eq. 3.2.1) at r=0 at the exit of a single jet with bulk velocity for different locations of the perforated plate.	130
Figure 3.2.4	Variation of the anisotropy and the turbulence intensity (Eq. 3.2.1) at r=0 at the exit of a single jet with H_p for different bulk velocities.	131
Figure 3.2.5	Comparison of the axial velocity radial variation at z=2mm in the jet exit of the single and the opposed jets with H=20mm.	132
Figure 3.2.6	Radial variation of the mean and r.m.s. axial velocity at different axial locations for the inert opposed jet flow with H=25mm.	133
Figure 3.2.7	Axial traverses along the centreline of the inert opposed jet flow with H=20mm and U_o=1.64m/s for different H_p.	134
Figure 3.2.8	Radial variation close to the stagnation plane (z=10mm) of the axial and radial mean and r.m.s. velocity for an inert opposed jet flow.	135
Figure 3.2.9	Centreline variation of the mean axial and r.m.s. axial and radial velocities for inert flow for different jet separations.	136
Figure 3.2.10	Comparison of velocity measurements when both and when only one of the jets are seeded with LDV scattering particles.	137
Figure 3.2.11	Probability density functions of axial and radial velocities close to the stagnation point.	138
Figure 3.2.12	Theoretical predictions of the mean and r.m.s. fluctuations of the mixture fraction across the mixing layer.	139

Figure 3.2.13	Variation of the mixture fraction fluctuations and the normalised by the bulk strain rate ($\chi=2\alpha f'^2S$, Eq. 3.2.25) at $\eta=0$ as a function of α.	140
Figure 3.2.14	Axial variations of the production (1), convection (2), diffusion (3), and dissipation (4) terms in Eq. (3.2.24) for different values of α.	141
Figure 3.2.15	Contours of the mean temperature in the inert opposed jet flow with H=20mm, T_2=450K, U_1=1.88m/s and U_2=2.3m/s.	142
Figure 3.2.16	Mean centreline normalised temperature $(T-T_1)/(T_2-T_1)$, with T_2=450K, H=20mm, H_p=55mm, in the inert opposed jet flow.	143
Figure 3.2.17	Centreline variations of the mean and r.m.s. mixture fraction for different jet separations and perforated plate locations.	144
Figure 3.2.18	Probability density functions of the mixture fraction along the centreline of inert opposed jet flows. H_p=55mm.	145
Figure 3.2.19	Probability density functions of the mixture fraction along the centreline of inert opposed jet flows. H_p=120mm.	146
Figure 3.2.20	Time traces and frequency spectra of the mixture fraction.	147
Figure 3.2.21	Radial variation of the r.m.s. mixture fraction fluctuations and the crossing frequency.	148
Figure 3.2.22	Contours of r.m.s. temperature and crossing frequency.	149
Figure 3.2.23	Centreline variation of the measured mixture fraction compared with the predictions from Eq. (3.2.22).	150

Figure 3.3.1	Photograph of a pure diffusion turbulent counterflow flame.	151
Figure 3.3.2	Photographs of laminar counterflow partially premixed diffusion and rich premixed flames.	152
Figure 3.3.3	Photographs of a partially premixed diffusion flame and a single premixed flame.	153
Figure 3.3.4	Photographs of twin premixed flames.	154
Figure 3.3.5	Contours of mean and r.m.s. temperature in a diffusion flame.	155
Figure 3.3.6	Mean and r.m.s. temperature at r=10mm for diffusion flames.	156
Figure 3.3.7	Mean temperature profiles along the centreline of diffusion flames for different velocities and jet separations.	157
Figure 3.3.8	The maximum mean temperature at diffusion flames as a function of jet separation.	158
Figure 3.3.9	Probability density functions of the temperature of flames at H=10mm, H_p=55mm.	159
Figure 3.3.10	Probability density functions of the temperature of flames at H=20mm, H_p=55mm.	160
Figure 3.3.11	Probability density functions of the temperature of flames at H=20mm, H_p=120mm.	161
Figure 3.3.12	Probability density functions of the temperature of flames at H=30mm, H_p=55mm.	162
Figure 3.3.13	Probability density functions of the temperature of flames at H=20mm, H_p=55mm with air preheat.	163
Figure 3.3.14	Frequency spectra at the location of maximum mean temperature for the pure diffusion flames.	164
Figure 3.3.15	Mean species concentrations for diffusion flames with H=20mm, H_p=55mm, and X=0.0 at the indicated air bulk velocity.	165
Figure 3.3.16	Mean species concentrations for diffusion flames with H=20mm, H_p=55mm, and X=0.5 at the indicated air bulk velocity.	166

Figure 3.3.17	Mean species concentrations for diffusion flames with H=20mm, H_p=55mm, and X=0.8 at the indicated air bulk velocity.	167
Figure 3.3.18	Mean species concentrations for partially premixed diffusion flames.	169
Figure 3.3.19	Mean species concentrations for pure and partially premixed diffusion at low turbulence intensity.	170
Figure 3.3.20	Mean species concentrations for pure and partially premixed diffusion at H=25mm.	171
Figure 3.3.21	Mean and r.m.s. axial velocity radial variation at z=2mm for a diffusion flame.	172
Figure 3.3.22	Mean axial and r.m.s. axial and radial velocities along the centreline for pure and partially premixed diffusion flames for two jet separations.	173
Figure 3.3.23	Mean and r.m.s. velocities along the centreline for diffusion flames at different turbulence intensities.	176
Figure 3.3.24	Comparison of pure and partially premixed flames.	177
Figure 3.3.25	Comparison of partially premixed flames at two velocities.	178
Figure 3.3.26	Comparison of velocities along the centreline and at r=10mm.	179
Figure 3.3.27	Comparison of radial velocities at r=10mm for pure and partially premixed flames.	180
Figure 3.3.28	Comparison of radial velocities for inert and reacting flows.	181
Figure 3.3.29	The mean and r.m.s. temperature at r=10mm for a single premixed flame.	182
Figure 3.3.30	The probability density functions of the temperature measurements of Fig. 3.3.29.	183
Figure 3.3.31	Mean species concentrations of single lean premixed flames at two velocities.	184
Figure 3.3.32	Mean species concentrations of single rich premixed flames.	185
Figure 3.3.33	Mean species concentrations of twin lean premixed flames at two velocities.	186

Figure 3.3.34	Mean and r.m.s. velocity radial variation at z=2mm for a single premixed flame.	187
Figure 3.3.35	Centreline variation of the mean and r.m.s. velocities for a single premixed flame.	188
Figure 3.3.36	Centreline traverses of the mean and r.m.s. velocities in single premixed flames for different equivalence ratio.	189
Figure 3.3.37	Comparison of the velocities in inert flows and single and twin premixed flames.	190
Figure 3.3.38	Comparison of the velocities in twin premixed flames at two bulk velocities.	191
Figure 3.3.39	Axial variations of the axial and radial velocities at r=0 and r=10mm in single premixed flames.	192
Figure 3.3.40	Radial variations of the radial velocity at different axial positions in single premixed flames.	193
Figure 3.4.1	Comparison of the mean mixture fraction for reacting and inert flows.	194
Figure 3.4.2	Comparison of the mean mixture fraction for diffusion and premixed flames.	195
Figure 3.4.3	The pdf of temperature before and after high–pass filtering at 20Hz for diffusion flames.	196
Figure 3.4.4	The effect of high–pass filtering on the axial variation of the r.m.s. temperature and the skewness of the pdf of the temperatures of diffusion flames.	197
Figure 3.4.5	Correlation coefficient as a function of thermocouple separation.	198
Figure 3.4.6	Mean species measurements plotted against the mixture fraction.	199
Figure 3.4.7	The maximum mole fraction of reaction products plotted against $\chi / \chi_{ext.}$	201
Figure 3.4.8	The axial variation of $-\partial U/\partial z$ and $\partial V/\partial r$ along the centreline of diffusion flames with H=20mm.	202
Figure 3.4.9	The axial variation of $-\partial U/\partial z$ and $\partial V/\partial r$ along the centreline of diffusion flames with H=25mm.	203
Figure 3.4.10	The normalised strain rate $(\partial V/\partial r)/(U_o/H)$.	204
Figure 3.4.11	Schematic of the Flapping Model.	205

Figure 3.4.12	The mean and r.m.s. of a scalar predicted by the Flapping Model with an error–function profile.	206
Figure 3.4.13	The maximum scalar r.m.s. fluctuations at the location of $\langle F \rangle = 0.5$ and the associated probability density functions predicted by the Flapping Model.	207
Figure 3.4.14	The mean and r.m.s. of a scalar predicted by the Flapping Model with a gaussian profile.	208
Figure 3.4.15	The probability density functions and the correlation coefficient of scalar fluctuations predicted by the Flapping Model.	209
Figure 4.1	The extinction velocity of premixed flames as a function of equivalence ratio and turbulence intensity.	252
Figure 4.2	The leanest equivalence ratio for stable counterflow turbulent premixed flames as a function of the opposing stream temperature.	253
Figure 4.3	The mean and r.m.s. temperature in the mixing layer of a cold jet and a jet of hot combustion products.	254
Figure 4.4	The probability density functions of temperature for the conditions of Fig. 4.3.	255
Figure 4.5	The power spectral density of temperature for the conditions of Fig. 4.3.	256
Figure 4.6	Mean and r.m.s. velocities for the flow of Fig. 4.3.	256
Figure 4.7	Mean temperature across the mixing layer for different reactant jet compositions.	257
Figure 4.8	Mean concentrations of O_2 and CO_2 across the mixing layer for different reactant jet compositions.	257
Figure 4.9	Mean concentration of CO across the mixing layer for different reactant jet concentrations and hot–product stream temperatures.	258
Figure 4.10	The maximum CO concentration as a function of opposing stream temperature.	259

Figure 4.11	The CO mole fraction plotted against the local temperature.	259
Figure 4.12	Bulk velocity at extinction of diffusion flames as a function of tube separation H for different air volume fractions in the fuel stream.	260
Figure 4.13	Bulk velocity for extinction as a function of air volume fraction for two jet separations.	261
Figure 4.14	Bulk velocity for extinction as a function of air volume fraction for two turbulent intensities.	262
Figure 4.15	Total strain rate (Eq. 4.3.3) at extinction as a function of air volume fraction for different H and H_p.	262
Figure 4.16	Estimated scalar dissipation rate from Eq. (4.3.4) at extinction.	263
Figure 4.17	Bulk velocity at extinction from Fig. 4.15 plotted as a function of stoichiometric mixture fraction.	264
Figure 4.18	The turbulent mean scalar dissipation rate at extinction compared with the scalar dissipation rate at laminar flame extinction.	264
Figure 4.19	Bulk velocity at extinction of flames with preheated reactants.	265
Figure 4.20	The minimum oxygen mole fraction in the oxidiser stream for partially premixed flames.	266
Figure 4.21	The minimum oxygen mole fraction in the vitiated air as a function of the temperature for turbulent diffusion flames.	267
Figure 4.22	The predicted from Eq. (4.3.16) S_{vit}/S_{ref} for laminar counterflow diffusion flames.	268
Figure 4.23	Predictions of Eq. (4.3.16) for laminar counterflow pure diffusion flames for the special case of adiabatic hot product dilution.	269
Figure 4.24	Contours of S_{vit}/S_{ref} from Eq. (4.3.16) and data in the $X_{ox} - T_2$ plane.	270
Figurre 4.25	The extinction velocity and scalar dissipation rate of turbulent coutnerflow diffusion flames with H_2–CH_4 fuel.	271
Figure 5.1	A conceptual model for a diffusion flame stabilised by a recirculation zone.	290

List of commonly used symbols

C_q	normalised turbulence intensity, Eq. (3.2.2)
D	diameter of jet, Fig. 2.2. Also, throat diameter, Chapter 5
Da	Damköhler number
D_{inj}	diameter of fuel nozzle, Chapter 5
D_o	diameter of annular tube
d_w	diameter of thermocouple wire
d_p	diameter at aspiration probe tip
d_{str}	diameter of streamtube containing the extracted sample, Eq. (2.4.5)
F, $\langle F \rangle$	mean mixture fraction, Chapter 3.
f	mixture fraction
f_{st}	stoichiometric mixture fraction, Eq. (2.2.1)
f'	r.m.s. of mixture fraction fluctuations
H	jet separation, Fig. 2.2
H_{flame}	distance of laminar flame from upper tube exit, Fig. 2.3b
H_p	distance of perforated plate from tube exit, Fig. 2.2
k_g	thermal conductivity of fluid around the thermocouple
L_{flame}	estimated flame length in swirl burner, Chapter 5
L_{RZ}	estimated length of recirculation zone, Chapter 5
L_{turb}	estimated turbulence lengthscale, (4mm in the opposed jet flow)
q'	turbulence level, Eq. (3.2.1)
r	radial coordinate
R	inner tube radius
Re_w	Reynolds number of the flow around the thermocouple, Section 2.5.3
Re_t	turbulence Reynolds number, defined by $q'L_{turb}/\nu$
S_L	laminar flame speed
S	one half of strain rate, Eq. (3.2.11)
S_{bulk}	bulk flow strain rate, taken as $2U_o/H$
S_{turb}	small–scale turbulent strain rate, Eq. (4.3.2)
Sw	swirl number, Chapter 5
t	time
T	temperature
T'	r.m.s. temperature
T_2	centerline temperature of upper stream in the burners of Fig. 2.3
$U_{1,2}$	bulk axial velocity of subscripted stream
U_b	bulk air velocity, Chapter 5

U_f	bulk fuel velocity, Chapter 5
U_o	bulk velocity of air stream, equal to U_2 and used for normalisations
U	mean axial velocity in Chapter 3, and bulk velocity in Chapter 4.
u	instantaneous velocity
u'	axial r.m.s. velocity
V	radial velocity
v'	radial r.m.s. velocity
w	spatial averaging width, Section 2.4.5; also width of profile in Flapping Model, Section 3.4.6
X, X_{air}	air volume fraction in fuel stream
X_{ox}	oxygen mole fraction of upper stream in the burners of Fig. 2.3. Calculated in the manner shown in Appendix 2.1.
Y	mass fraction
z	axial coordinate, measured from the lower jet
Z_{st}	axial coordinate of stagnation plane
Z_{half}	axial coordinate where $\langle F \rangle = 0.5$
z*	reduced coordinate, $z-Z_{st}$ or $z-Z_{half}$
$\langle\ \rangle$	time–averaged quantity
[ ]	mole fraction

Greek

α	ratio of mean flow to turbulent timescales, Eq. (3.2.19)
β	parameter in Flapping Model, Section 3.4.6. Also, parameter in Section 4.3.5
η	non–dimensional axial coordinate, Eq. (3.2.15)
η_K	Kolmogorov lengthscale
μ	viscosity
ν	kinematic viscosity
ρ	density
τ_{wire}	thermocouple time constant, Eq. (2.5.2)
τ_{chem}	chemical timescale estimated by ν/S_L^2
ϕ	equivalence ratio
χ	mean turbulent scalar dissipation rate, Eq. (3.2.8)
χ_{ext}	estimated χ at extinction, Section 4.3.4
χ_{lam}	estimated scalar dissipation rate at extinction of laminar counterflow flames, Eq. (4.3.6)
χ_{flame}	estimated χ at recirculating flame, Chapter 5

Subscripts

1	lower stream
2	upper stream
b	bulk
g	gas
K	Kolmogorov–scale
st	stoichiometric

Chapter 1. Introduction

1.1 BACKGROUND

1.1.1 The topic of this thesis

Engineers dealing with the design of practical combustion devices require information that current theoretical descriptions of turbulent combustion cannot always provide. Existing models, in conjunction with numerical solutions of the modelled governing equations of the fluid flow, can give good results for mean flame lengths and fuel consumption rates for a range of flames of practical importance (Jones and Whitelaw, 1982). Difficulties arise, however, for the prediction of other aspects of turbulent flames: for example, the creation of combustion by–products, like NO_x and CO that are serious pollutants and whose emissions from industrial furnaces and aircraft engines come under stringent legislation, and flame stability, as when flames extinguish in gas–turbine combustors at high altitude and in internal combustion engines, are phenomena that combustion engineers have to consider but whose theoretical descriptions are not adequately developed.

Pollutant formation and flame stability involve finite–rate kinetic effects, where the times needed for the chemical reactions is on the same order as the turbulent mixing times, and this situation is more difficult to describe than the fast–chemistry limit because of the need to consider the mechanism in which the turbulence affects the chemical reactions through the fluctuations of velocity and species concentrations. Departures from the fast–chemistry limit in almost all flames of engineering interest are associated with *stretching*, which reduces the residence time through the reaction zone and leads to extinction if excessive. The flame stretch is defined as the fractional rate of increase of flame area, and can be found from the flow field velocity gradients for certain flows, for example, in straining flows where the stretch rate is equal to the *strain* rate. A straining flow is realised experimentally in opposed jet flows or flows stagnating on solid plates, and the simple velocity field in these configurations offers simplifications to theoretical treatments and allows the effects of stretching on the progress of the chemistry and on flame extinction to be quantified, as has been demonstrated over a number of years by research in laminar counterflow flames.

Counterflow diffusion flames are established in the mixing region of opposed jets of fuel and oxidant and counterflow premixed flames are stabilised when one (or both) of the jets carry a fuel/oxidant mixture, and the stretch rate is given roughly by the velocity of the jets divided by the jet separation. Recently, such flows have also been used for

turbulent premixed combustion experiments and particularly to examine separately the influence of the bulk stretching from those of the superimposed turbulent stretching.

In this thesis, counterflow turbulent premixed and diffusion flames are examined in terms of their aerodynamic and chemical structure and their extinction limits. The results highlight the changes in the reaction as extinction is approached with increases in stretch and suggest appropriate modelling approaches for the turbulent mixing in straining flows. The effects of partial premixing on diffusion flames, a factor often overlooked due to the prominence of theories that concentrate in the two idealisations of initially uniformly–mixed and initially fully–separate reactants, a prominence which is unjustifiable in view of the inevitable partial premixing in realistic flames with finite–kinetic effects and localised quenching, are also determined. The results are interpreted in the context of current theories of turbulent combustion and flame extinction and so are useful because the insight obtained applies to combustion in other geometries, for example, in the technologically–important flames stabilised by recirculation zones, as demonstrated in Chapter 5 of the thesis. Finally, in view of the current trend in combustion applications to employ exhaust gas recirculation, the extinction of flames with reactants diluted by hot combustion products is examined.

1.1.2 Structure of this Chapter

The next Section provides a review of the literature of combustion in the counterflow geometry and is divided in two parts, the first dealing with *laminar* counterflow flames and the second with corresponding works on *turbulent* counterflow flames. The purpose of the first part is to introduce certain basic aspects of the opposed jet flow and of flame extinction that will be used in later Chapters, and the second part aims to highlight omissions in previous works in turbulent counterflow flames, as well as demonstrate their relevence in the field of turbulent combustion reaserch. A detailed review of turbulent flame extinction is postponed to Chapters 4 and 5. Finally, the present contribution is summarised in Section 1.4 together with an outline of the thesis.

1.2 LAMINAR COUNTERFLOW FLAMES

In this Section, research on laminar counterflow flames is reviewed to introduce physical phenomena that will be discussed in the thesis. The review starts with a description of various counterflow flame arrangements, followed by a discussion of various aspects of stagnation point flows and flame extinction. The reader is referred to Tsuji (1982), Law (1988), and Dixon–Lewis (1990) for reviews emphasing diffusion flames, premixed flames, and their chemistry respectively.

1.2.1 Historical overview and motivation

Laminar counterflow flames have been used for a number of years to study the flame chemical structure and extinction, to validate detailed chemical kinetic mechanisms in conjunction with numerical solutions of the governing equations, and to provide information used in theoretical models of turbulent flames based on laminar flamelets.

Counterflow *diffusion* flames are established when a stream of fuel flows against a stream of oxidant and the flame is found in the neighbourhood of the stagnation surface, and many experimental configurations have been used by various authors to realise this concept. Wolfhard (1956) and Simmons and Wolfhard (1957) presented an arrangement with air flowing against a fuel stream injected through a porous metal sphere establishing thus an enveloping cylindrical flame with a hemispherical end and with the part at the forward stagnation point considered as a counterflow flame. Potter and Butler (1959) used two opposed straight pipes, while Pandya and Weinberg (1962) examined the opposed flows from nozzles fitted at their exits with porous plugs to provide uniform velocity profiles. Tsuji and Yamaoka (1966) established flames at the forward stagnation point of a porous cylinder immersed in an air stream, and recent practice is to establish flat axisymmetric flames in opposed flows issuing from contoured nozzles, as by Chelliah *et al.* (1990), to eliminate heat loss to solid surfaces. Theoretical results for mixing in laminar counterflows and flame extinction had already been obtained by Spalding (1961), Fendell (1965), and Liñan (1974) and will be discussed later.

Counterflow *premixed* flames, established when premixed fuel–air jets stagnate, were analysed theoretically by Libby and Williams (1981, 1983), Buckmaster and Mikolaitis (1982), Buckmaster and Ludford (1982), and Tien and Matalon (1991), and experimentally by Sato (1982), Ishizuka and Law (1982), and Law *et al.* (1986), among others, in similar arrangements as the diffusion flames. The effects of straining on reaction rates and extinction have been examined motivated to a great extent by the relevance of strained flames to laminar flamelet models of turbulent combustion (e.g. Peters, 1986), as discussed next.

In these models, the turbulent flame is treated as an ensemble of laminar flames or "flamelets" that are characterised by the local value of the strain rate in the turbulent flow. By making ensemble averages over the strain rate, the mean reaction rates can be calculated and, because laminar flames exhibit departures from infinitely–fast or equilibrium chemistry with increasing strain rates, the flamelet models provide a means of incorporating finite–chemistry effects in turbulent combustion descriptions. Finally, recent developments in chemical kinetic mechanisms for hydrocarbon combustion and their incorporation in numerical calculations of the flow and scalar fields in laminar flames have motivated experimental and numerical work in counterflow diffusion and premixed flames to validate the chemistry models, Dixon–Lewis (1990).

In the following Sections, certain aspects of the flow field in counterflows are introduced that will be referred to in later parts of the thesis and findings on flame extinction are reviewed.

1.2.2 Stagnation point flows

Consider an axisymmetric and irrotational flow of viscous fluid against a solid surface. The no–slip condition at the surface implies that there will be a region containing non–zero vorticity and a similarity analysis shows that this region (the boundary layer) remains of constant width if the external irrotational flow obeys

$$U = -2\,S\,z \qquad (1.2.1a)$$

and

$$V = S\,r \qquad (1.2.1b)$$

where U and V are the velocities normal and parallel to the plate, z and r the coordinates in the respective directions from the stagnation point, and S the strain rate (Schlichting, 1979, p. 95). Such a flow is called Hiemenz flow and has the property that the strain rate is uniform and that the boundary layer has width of the order of $\sqrt{\nu/S}$, with ν the kinematic viscosity, and these two properties also exist in the flow of two opposed fluids, if the external flow obeys Eqs. (1.2.1) (Dixon–Lewis, 1990). A similarity solution can be obtained in the case of variable density flows with appropriate definition of the spatial coordinates for both the velocity and transported scalars and shows that the scalars do not vary with radius (Spalding, 1961; Fendell, 1965). Therefore, flames in opposed jet flows that obey Eqs. (1.2.1) experience constant stretch rates equal to 2S but it is not always correct that Eqs. (1.2.1) adequately describe the flows realised experimentally, as discussed below and also in Chapter 3.

Jones and Lindstedt (1988), Kee *et al.* (1988), Dixon–Lewis (1990), and Chelliah *et al.* (1990), for example, have attributed differences between numerical predictions and

measurements to the fact that the flow issuing from opposed nozzles is not characterised by a constant strain rate because Eq. (1.2.1) implies a finite radial velocity everywhere, including the nozzle exit, which is physically unacceptable. A more realistic boundary condition at the nozzle exit that has been shown to give better results is that of plug flow, where the flow exiting the nozzles is uniform and with zero axial velocity gradient, so that the stretch rate is zero there and increases towards the stagnation point. This implies that care is needed in comparing results from different experimental arrangements and that the stretch rate is not uniform across the flame (but is uniform *along* the flame isotherms; Dixon–Lewis, 1990) and is different from the potential flow result. Since experimental conditions are usually reported in terms of global properties like bulk velocities and jet separations, there is an uncertainty in the actual value of the stretch rate acting on the flame and so comparisons between theoretical and experimental results are not straightforward. To overcome this problem partially, which is expected to be present in *turbulent* opposed jet flames as well, local measurements of the stretch rate are also given in this thesis (Section 3.4.5).

1.2.3 Extinction limits

The extinction of counterflow flames is discussed here separately for diffusion and premixed flames and it will be shown that extinction has been found to occur at critical values of the strain rate for both types of flame and physical explanations are given. These results will aid interpretation of the measurements of the stability limits of the *turbulent* counterflow flames examined in Chapter 4, where a detailed review of turbulent flame extinction is also presented. Descriptions of the stability of turbulent flames in realistic geometries, for example in recirculation zones, are also based on ideas presented here and are reviewed in Chapter 5.

Diffusion flames

Potter *et al.* (1960) used an opposed jet diffusion flame to measure the "flame strength", defined by these authors as the maximum bulk velocity of the flow which could sustain a stable flame, and found that the bulk velocity for extinction increased linearly with jet diameter and decreased with increasing dilution of the reactants by inerts. Spalding (1961) analysed theoretically the mixing field in opposed jet flows with velocities given by Eqs. (1.2.1), and using approximate expressions for the speed of chemical kinetics, found that combustion is not possible above a certain value of the bulk velocity. Although Spalding expressed his result in a slightly different algebraic form, his final expression for the flame extinction limit was equivalent to a comparison between the velocity gradient in the flow, taken as the jet velocity divided by the jet diameter, and the (inverse) kinetic timescale τ_{chem}, given by the molecular diffusion coefficient divided by the propagation speed of a laminar stoichiometric premixed flame (S_L) squared.

These predictions were confirmed by Anagnostou and Potter (1962) and suggest that, using more recent terminology, extinction of counterflow diffusion flames occurs at a critical value of the stretch rate that scales with the inverse of a kinetic timescale.

The ratio of a flow to a kinetic timescale is defined as a Damköhler number (Da) and Fendell (1965) analysed the stagnation point flow of oxidant against the vapour flow evaporated from the surface of a liquid fuel and showed by perturbation methods that for large Da, combustion occurs close to the Burke–Schumann limit of infinitely–fast chemistry, but that at smaller values the flame temperature decreases. A plot of flame temperature *vs.* Da revealed an S–shaped curve with the upper branch corresponding to stable combustion, the lower branch (at low T) corresponding to frozen flow, and the turning points joining these two branches through an unstable (physically unrealistic) regime, corresponding to ignition and extinction points. Liñan (1974) used activation energy asymptotics to describe the reaction zone in counterflow flames between gaseous oxidant and fuel jets and arrived at the same S–shaped curve of maximum temperature *vs.* Da and also concluded that, close to extinction, reactants penetrate the reaction zone unreacted, and Liñan's result motivates the following physical explanation for flame extinction.

As the strain rate increases, residence times decrease, reactants are supplied to the reaction zone faster than these can be consumed and hence the flame temperature decreases, the reaction becomes slower, and the flame eventually extinguishes. The *sudden* nature of the transition between stable burning and frozen flow has been revealed by Liñan (1974) to be due to the exponential dependence of the reaction rate on the temperature involved in the Arrhenius expressions, and this large sensitivity of the reaction rate on temperature has motivated efforts to correlate flame extinction limits with flame temperatures. In this context, Tsuji (1982) reviewed such works for counterflow diffusion flames with and without reactant dilution and showed that extinction occurs when the flame temperature falls below a certain value, a result that will be discussed in Chapter 4 together with results from experiments in this thesis and recent theoretical descriptions of the chemistry of hydrocarbon combustion.

Premixed flames

Twin premixed flames in the counterflow geometry extinguish when the strain rate increases above a critical value (Law *et al.*, 1986) and the physical mechanism depends, perhaps surprisingly, on the mixture Lewis number. If the Lewis number is smaller than unity (for example, as for lean propane–air mixtures), increasing the strain rate reduces the flame temperature and extinction can be explained by the same argument described previously for diffusion flames. For lean methane–air mixtures which have Le greater than unity, the presence of stretch, coupled with differential diffusion of heat and species, makes the mixture reaching the reaction zone closer to stoichiometric, the flame

temperature does not reduce with increasing strain rate, and the flame does *not* extinguish with stretch alone; additional mechanisms, such as loss of heat to a solid surface or incomplete combustion due to flame restraining with the two flames touching, are responsible for flame extinction (Law *et al.*, 1980; Sato, 1982; Law, 1988). The counterpart of this result for *turbulent* premixed flames approaching extinction is discussed in Chapter 3.

Premixed flames established in the stagnation flow of reactants against fully–burnt hot products, rather than against identical reactant jets, have been used as representative "elements" in laminar flamelet descriptions of turbulent flames (Libby and Williams, 1983), and have thus received attention. In this arrangement, the flame extinction points are found theoretically from the turning points of an S–shaped curve, but these exist *only* when the opposing flow of hot products have a sufficiently low temperature (Libby and Williams, 1983; Darabiha *et al.*, 1988). In contrast, when this is close to the adiabatic value, the flame might migrate inside the hot product stream and the flame does *not* extinguish with strain rate. These findings suggest that conditions may exist under which flames do not show abrupt extinction limits and will be compared with experimental results in turbulent premixed flames opposing hot products in Chapter 4.

1.3 TURBULENT COUNTERFLOW FLAMES

In this Section, a review of previous research on turbulent counterflow premixed and non–premixed flames is given that includes the situation of a premixed mixture stagnating on a solid surface because flames in this geometry show similar behaviour in certain aspects to flames established in counterflows. Research in turbulent flames in flows with stagnation point is recent, with theoretical descriptions still being developed (Bray, 1993), and with many aspects concerning their chemical structure and extinction unexplored. Tables 1.1 and 1.2 summarise the various configurations used in previous experiments together with those examined in the present work for ease of comparison.

1.3.1 Premixed flames on solid plates

Cho *et al.* (1986) examined a premixed flame formed in the stagnation region from a turbulent jet of reactants impinging on a solid plate. This flow, similarly to the laminar stagnation point flows discussed in Section 1.2.2, has the advantage of a uniform strain rate associated with the mean flow, and because the turbulence is created with a grid inside the reactant jet, offers the additional advantage over other turbulent flame configurations that turbulence is controlled independently of the mean flow. Therefore this arrangement offers easily controlled flow properties, has no complications involved with a flameholder (for example, due to vortex shedding) or a pilot flame, and provides an approximately one–dimensional flame, which is convenient to analyse theoretically.

Because of these advantages, many authors have since used this configuration to study a range of premixed flame phenomena. Turbulent flame speeds, defined as the flow speed upstream of the flame brush, have been correlated with the strength of the approach turbulence and resulted in new empirical expressions (Cho *et al.*, 1986; Liu and Lenze, 1988; Liu *et al.*, 1990, 1993). The turbulence before and after the flame has been examined by conditional measurements in the products and reactants which showed that the flame did not produce significant turbulent energy (Cho *et al.*, 1988), and the instantaneous flame motion has been analysed in the context of the Bray–Moss–Libby model of turbulent premixed combustion to give scalar integral lengthscales and flame area (Shepherd *et al.*, 1990), results of interest to premixed flame models (Bray and Libby, 1990).

The extinction of these flames has been predicted theoretically by Bray *et al.* (1992), as part of a series of papers dealing with the theory of premixed flames in stagnating flows, to occur at a critical value of a Damköhler number, and examined experimentally by Yahagi *et al.* (1992) who showed that the Lewis number of the mixture affects extinction in the same way as for laminar flames (Law *et al.*, 1980;

Section 1.2.3). This result suggests that theoretical approaches using equal molecular diffusivities for all species may be inadequate, and the same implication will be discussed in Chapters 3 from results in the present work.

Premixed flames in flows stagnating on a solid plate have the disadvantage that they are not adiabatic because heat is lost to the surface. To overcome this problem, while keeping the advantages of the stagnation–point flow, twin premixed flames in opposed turbulent jets have been examined and are reviewed in the next Section.

1.3.2 Premixed flames in opposed jets

The turbulent counterpart of the twin laminar premixed counterflow flames has been examined by Kostiuk *et al.* in a series of papers (Kostiuk *et al.*, 1989, 1993a, 1993b; Kostiuk, 1991). These flames were formed in the stagnation region of two identical turbulent opposed jets of premixed propane and air and measurements were made of velocities by laser–doppler velocimetry and reaction progress variable by planar Mie scattering. In addition, their extinction limits have been measured and correlated with the estimated total stretch rate acting on the flame, taken as the sum of the bulk flow strain rate and the small–scale turbulent strain rate (Kostiuk *et al.*, 1989). These papers complement the theoretical analysis of Bray *et al.* (1991) and will be referred to repeatedly in this thesis as comparisons will be made between these measurements and the present ones.

Mounaïm–Rousselle and Gökalp (1993) also used a twin–flame arrangement to study the velocity field in inert and reacting flows, but with the provision of a co–flow which offers two advantages. The first is that the phenomenon of "bouncing" is reduced, as found by the elimination of low–frequency peaks in velocity spectra; "bouncing" is a term used by Kostiuk (1991) to describe an unsteady axial motion of the flames that is not apparent at jet separations smaller than about two jet diameters. The second advantage of a co–flow is that, if the co–flow is of an inert gas, it eliminates the stabilisation of flames on the burner rim, which would occur for rich premixed flames, and so extends the use of the counterflow twin–flame geometry to a wide range of equivalence ratios.

Before closing this Section, mention is made to the opposed–jet flames of Abbas *et al.* (1991) who used jets of small diameters and hydrogen pilots to stabilise twin premixed flames on the jets' exits. These flames were not flat, and so are not convenient to analyse theoretically, and were located at the curved shear layers of the jets, rather than the stagnation point neighbourhood, and so, strictly speaking, do not have the advantages that stagnating flames offer. However, measurements of stable species concentrations showed that stretch decreases the formation of NO_x and of CO_2, so that these flames showed finite–rate kinetic effects induced by stretch.

1.3.3 Non–premixed opposed jet flames

A diffusion flame formed in the counterflow of a hydrogen jet against a wider and slower turbulent air stream was examined in terms of its instantaneous topology and strain rate by Goix and Talbot (1991). The flame was curved as it enveloped the fuel jet and the flow did not resemble the ideal stagnation point flow (Section 1.2.2), so that the stretch rate acting on the flame was not uniform and the flame's extinction was possibly affected by entrainment of reaction products at the shear layers between the reversed fuel jet and the air flow.

There are no measurements in *flat* turbulent counterflow diffusion flames, the turbulent counterpart of laminar counterflow diffusion flames, nor any theoretical results for such flames, although such theories are under development, for example by Libby (1993). The existence of such flames has been mentioned by Anagnostou and Potter (1962) in opposed jets issuing from straight pipes in which the flows approximated fully–developed turbulent pipe flow, but the absence of inert co–flow caused stabilisation of the flame on the fuel jet rim, and the effects of the turbulence on the flame were not examined.

Guidance for the design of the experiments in diffusion flames described in the following Chapters was provided by examining burners used to stabilise *laminar* counterflow diffusion flames (Section 1.2.1) and *turbulent* opposed jet *premixed* flames (1.3.2). The resulting burner, described in Chapter 2, incorporates perforated plates to create turbulence, co–flow of nitrogen to limit reaction in the stagnation region, and is usually operated at small jet separations (Chapters 3 and 4). These flames were flat and located around the stagnation point, and so the advantages of theoretical simplicity and radial uniformity are carried over from the corresponding laminar diffusion and turbulent premixed flames to the present ones.

Table 1.1

Flow arrangements for turbulent counterflow premixed flame experiments. Included are sketches of the flow configurations examined in the present work to facilitate comparison.

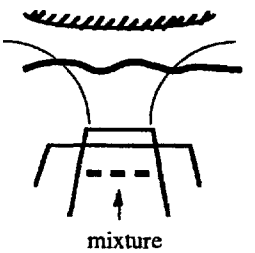
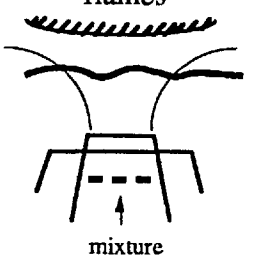
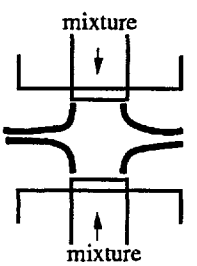
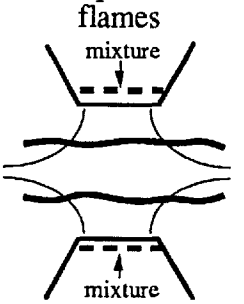
Authors	Flow arrangement	Measurements	Comments
Cho *et al.* (1986), Cho *et al.* (1988), Shepherd *et al.* (1990)	Single premixed flames 	Velocities, reaction progress variable, conditional measurements, turbulent flame speeds, topology of flame surface.	Methane–air and propane–air flames. Air co–flow.
Liu and Lenze (1988), Liu *et al.* (1990), Liu *et al.* (1993)	Single premixed flames 	Velocities, turbulent flame speeds.	Hydrogen–methane mixtures. Mention of flame extinction at high turbulence intensities. Air co–flow.
Abbas *et al.* (1991)	Twin piloted premixed flames 	Extinction limits, ionisation current, temperatures, stable species incl. NO_x.	No perforated plate, small tube diameter and large jet separation. Curved methane–air flame stabilised on jet rim by a hydrogen pilot. Air co–flow.
Kostiuk *et al.* (1989), Kostiuk (1991), Kostiuk *et al.* (1993a) and (1993b).	Twin premixed flames 	Extinction limits, velocities, reaction progress variable from tomographic images.	No co–flow, jet separations larger than one jet diameter. Inert flow has also been examined.

Table 1.1 Cont'd.

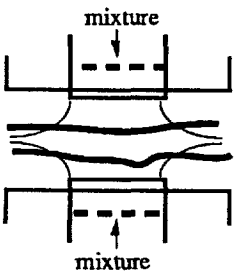
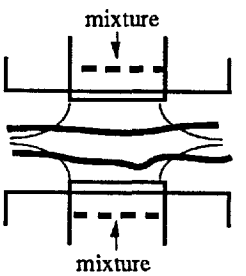
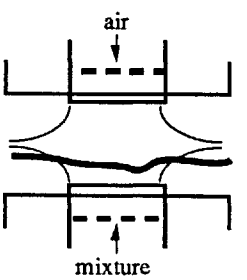
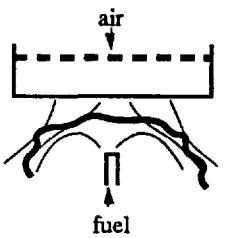
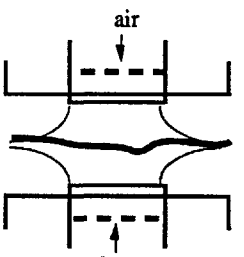
Authors	Flow arrangement	Measurements	Comments
Mounaïm–Rousselle and Gökalp (1993)	Twin premixed flames 	Velocities.	Influence of co–flow on combusting and inert flow.
Present work	Twin premixed flames 	Velocities, stable species concentrations, extinction limits.	Smaller separation than previous experiments, lower velocities.
Present work	Single premixed flames 	Velocities, temperatures, stable species concentrations, extinction limits.	New configuration, the single flame counterpart of twin flames. Extinction also examined with upper air stream replaced with hot reaction products (Chapter 4).

Table 1.2

Flow arrangements for turbulent counterflow diffusion flame experiments. Included are sketches of the present experiments.

Authors	Flow arrangement	Measurements	Comments
Goix and Talbot (1991)	Diffusion flames 	Velocities, tomographic images of flame surface.	Jet of hydrogen against wide and slow air flow. Curved flame.
Present work	Diffusion flames, pure and partially premixed 	Velocities, temperatures, stable species, extinction, mixing of the two jets in inert and reacting flow.	New configuration, the turbulent counterpart of laminar counterflow diffusion flames. Nitrogen co-flow. Partially premixed flames also examined. Extinction also measured with hot products as oxidant (Chapter 4).

1.4 THE PRESENT CONTRIBUTION

1.4.1 Structure of turbulent counterflow flames (Chapter 3)

The measurements of the velocity and scalar fields of inert and reacting flows provide information on the mixing between two turbulent opposed jets, quantify the turbulence and the stretch rate, and identify the separate effects of bulk and turbulent stretching on the stable species mole fractions in the flame. Results are presented for unpremixed and partially premixed diffusion, single premixed, and twin premixed flames, with more emphasis on the first two types because these flames have not been studied before, and for inert flows, for which a theoretical analysis of the mixing between the two jets is also given to assist interpretation of reacting flow results.

1.4.2 Extinction of turbulent counterflow flames (Chapter 4)

Extinction limits of diffusion flames have been measured as a function of turbulent and bulk stretching to find their relative importance and it is shown that the mean turbulent dissipation rate of the mixture fraction assumes a critical value at extinction conditions, showing hence that the appropriate Damköhler number describing the extinction of turbulent diffusion flames should be based on the scalar dissipation rate. The effect of partial premixing, reactant initial temperature, and reactant dilution are examined, and comparisons are made with corresponding results for laminar counterflow diffusion flames. Because flames in many practical configurations are stabilised by recirculation zones which mix hot reaction products with the incoming reactants, extinction limits of counterflow flames with the oxidant diluted by hot reaction products have also been measured and are discussed. Finally, the conditions under which turbulent diffusion and premixed flames do not show abrupt extinction have been determined.

1.4.3 Extinction of flames in recirculation zones (Chapter 5)

Estimates of the turbulent scalar dissipation rate and the chemical timescale in diffusion flames stabilised by recirculation zones have been made and are used to propose conjectures on the stability limits of such flames. These conjectures are physically correct because they represent turbulent flame extinction in a more fundamental way than others proposed previously which were mostly of empirical nature, and explain extinction trends that were not well–understood.

1.4.4 The structure of this thesis

The flow arrangements, measurement techniques and associated experimental uncertainties, definitions of terms, and details on the operation of the counterflow burner are presented in Chapter 2. Measurements of velocities and scalars in inert flows and diffusion and premixed flames are reported in Chapter 3 together with a theoretical analysis for mixing in the opposed jet flow and a discussion of these results. The extinction limits of various flame configurations and comparisons with laminar flame results and correlations for diffusion flame extinction are presented in Chapter 4 and conjectures on the stability of flames stabilised by recirculation zones, based on results from Chapter 4, in Chapter 5. Each Chapter ends with a summary of its conclusions and Chapter 6 closes the thesis with a presentation of the more important conclusions and with a discussion of possible directions for future research.

Chapter 2. Experimental methods

This Chapter presents the methods used to obtain the results shown in Chapters 3 and 4 of this thesis. The flow configuration is described first and details on the operational parameters of the different flames follow. The methods used to visualise the flames and for the measurement of species concentrations, temperature, and velocities are then presented and the Chapter closes with a summary.

2.1 FLOW CONFIGURATION

2.1.1 Straight–tube burner

Figure 2.1a shows the geometrical arrangement used in most of the experiments described in this thesis. It comprised two opposed straight brass tubes, each of inside diameter D=25.4mm and 40 diameters long, separated by a variable vertical distance H. To promote turbulence, perforated plates with holes of 4mm diameter giving 45% solidity were fixed within each of the tubes by the spring–action of four legs and this allowed variation of the distance, H_p, of the perforated plate from the tube lip. Outer straight tubes of D_o=51.8mm diameter and about 40cm long were also fitted to, and made concentric with, the inner tubes by adjusting three screws arranged as a "spider". Both assemblies were clamped to a frame and vertical alignment of the two assemblies was performed by adjusting the "spiders" until the two opposing inner tubes were facing each other to within 0.5mm as measured by a ruler. Further alignment was found to be redundant, because with this level of alignment, the flames were horizontal (i.e. normal to the burner axis, as judged visually) and preliminary measurements of temperature corroborated the visual finding to within ±0.5mm.

The reactants were fed to the inner tube about 35 D from the exit plane from two radially-symmetric inlets (Fig. 2.1b) and a third central inlet was also used in certain experiments, for example to introduce seeding particles for velocity measurements. The flanges closing the back end of the inner and the annular tubes were tight–fitted and sealed with vacuum grease at all contacts. Since the pressure of the flow in the pipes was only slightly above atmospheric, no leaks were expected and none were observed. The perforated plate was cut to size from a commercial–grade perforated sheet of mild steel and the legs were soldered on the plate close to its perimeter; velocity measurements, shown later in Chapter 3, quantify the uniformity of the mean and fluctuating velocities across the tube at the exit plane. Care was needed to keep the

perforated plate as normal as possible to the tube axis or asymmetric flow, easily diagnosed by a non–flat flame, would occur.

The flow in the annular space between the outer and the inner tubes was nitrogen and its purpose was to shield the inner reactant jets from entraining ambient air. It was found that for lean premixed flames (i.e. flames established between a fuel–air mixture and either a jet of air or an identical premixed jet), the presence of the nitrogen co–flow was redundant and the nitrogen could be replaced by air without changing the flame appearance or characteristics close to the centreline; for stoichiometric and rich premixed and for diffusion flames, however, the nitrogen was essential to limit reaction to the stagnation region between the two jets; failure to achieve this resulted in flames being attached on the fuel–nozzle rim.

The fuel in the present experiments was natural gas (with composition described later in Section 2.2) drawn from the mains network by a gas compressor in the laboratory and delivered at a pressure of 1 bar above atmospheric, the air was supplied by a shop compressor, and the nitrogen from cylinders. The air was at a pressure of about 6 bar, which was reduced by commercial pneumatic–air–quality pressure regulators and filtered for solid particles and oil droplets down to 2μm, before supplying a bank of rotameters. All flow rates were metered by rotameters calibrated by the manufacturers and were arranged such that each of the assemblies could be fed as follows: 0 – 100 l/min of air; 0 – 20 l/min of gas; 0 – 100 l/min of nitrogen. Extra rotameters for 0 – 100 l/min of gas and 0 – 500 l/min of air were also connected to provide sufficient measurement accuracy both for diffusion flames, which needed a large supply of gas, and for premixed flames, which needed a small flow rate of gas and a large flow rate of air. For certain extinction experiments described in Chapter 4, extra flow rates needed to be measured (e.g. oxygen and nitrogen separately; hydrogen added to gas etc.) and these were also metered by rotameters. The estimated uncertainties in the measured flow rates is expected to be ±5%, as suggested by the manufacturer and confirmed by a few area–integrations of velocity measurements.

The burner just described is different from the one used by Kostiuk *et al.* (1989) and Kostiuk (1991) in that straight pipes rather than contractions were used in each of the jets and in that annular co–flows were included. The former does not affect the flow, because it will be shown that the velocity profile across the tube exit plane is uniform, and the latter was found to be essential for obtaining flat diffusion flames, unlike the premixed flames of Kostiuk (1991).

2.1.2 Contoured–nozzle burner

Laminar counterflow diffusion flames were examined in a limited number of experiments in terms of their appearance and extinction limits. These flames were stabilised in a counterflow burner, Fig. 2.2, which comprised two vertically opposed

assemblies, each with a contraction of length L_{con} = 90mm and of area ratio 9 ending in a diameter of 30mm, a straight section after the contraction of length L_{noz} = 50mm, and an annular section of diameter 50mm. Irregularities in the flow were removed by multiple screens (rectangular meshes of wires 0.5mm thick and spaced 0.5mm apart) placed inside each of the burners along a length L_{str} = 30mm before the contraction and inside the co–flowing streams. The shape of the contraction was selected based on Morel's (1975) suggestions in order to ensure smooth flow inside the nozzle, and preliminary velocity measurements confirmed a uniform velocity profile with almost no fluctuations. Provision was made to fit perforated plates after the contraction and before the straight section so as to be able to use this burner for *turbulent* flames as well. With the exception of the perforated plates, this burner is very similar to that used by other researchers, for example Rolon *et al.* (1991) and Chelliah *et al.* (1990).

2.1.3 Burners for flames with hot product dilution

Some extinction experiments described in Chapter 4 were performed with air diluted by hot combustion products, usually termed vitiated air, and these flames were established in a slightly modified burner from the one shown in Fig. 2.1. To provide a flow of hot products, a second perforated plate, identical to the ones described in Section 2.1.1, was fitted inside the upper tube about 30 tube diameters upstream of the exit on which a lean, laminar premixed flame could be ignited through a plugged opening. As Fig. 2.3a shows, these products were further mixed with oxygen and nitrogen, metered separately, to form the final stream leaving the tube at temperatures, T_2, up to 1000K and oxygen mole fractions, X_{ox}, in the range $0.07<X_{ox}<0.20$. Higher temperatures, up to a maximum of 1750K and X_{ox} down to a minimum of 0.02, were achieved by stabilising the premixed laminar flame close to the tube exit on the perforated plate previously used to generate turbulence, Fig. 2.3b. In this configuration, T_2 was controlled by varying the distance, H_{flame}, of the laminar flame from the exit plane between 2 and 10 D and relying on the heat losses to decrease the temperature to the required value. The absence of a turbulence–promoting perforated plate in the top flow of oxidiser meant that the turbulence levels there were not as large as in the bottom stream, and the consequences of that are discussed in Chapter 4. Finally, a few experiments were performed with oxygen – nitrogen mixtures electrically heated by a heater with maximum capacity 4.8kW (Technical Heaters, Inc.) connected to the inlet of the upper tube of the burner in Fig. 2.3a.

2.2 NOMENCLATURE, FLUID PROPERTIES, AND FLOW CONDITIONS

In this thesis, flames established in the burner of Fig. 2.1 are mostly examined and below, details on how the flow conditions were calculated and how they are described are given. Symbols are defined as they are introduced and the most commonly–used ones have also been compiled in lists found in the beginning of the thesis.

"Stream 1" refers to the lower stream and "Stream 2" to the upper stream, and this convention is followed everywhere in this work. In most cases, the lower stream carried fuel, either pure or partially premixed with air, and the upper stream carried air, and Table 2.1 summarises the possibilities for most of the flames examined here. For each stream the bulk velocity, U, is calculated from the rotameter readings and the equivalence ratio ϕ of a mixture is calculated by

$$\phi = 9.524\ (\dot{Q}_{fuel} / \dot{Q}_{air})$$

where $\dot{Q}$ refers to the metered volume flow rate and the factor 9.524 is the stoichiometric air : methane molar ratio; the air volume fraction in the fuel stream, X, is calculated from

$$X = \dot{Q}_{air} / (\dot{Q}_{fuel} + \dot{Q}_{air})$$

and is used to describe the amount of partial premixing of the fuel when it corresponds to a mixture richer that the rich flammability limit for premixed flame propagation, which is taken as $\phi = 1.6$ (e.g., Kuo, 1986). The relationship between the equivalence ratio and the air volume fraction is

$$\phi = 9.524\ (1/X - 1)$$

and so the rich flammability limit corresponds to $X = 0.86$. Flames fired by fuel–air mixtures with $X < 0.86$ are deemed as "diffusion" and the partial premixing is described by X, while if $X > 0.86$, the flame is deemed as "premixed" and the mixture is described by the equivalence ratio ϕ. The term "pure diffusion" is reserved for a flame with no partial premixing, i.e. with $X=0$.

The composition of the natural gas used in the present experiments was approximately as follows: 95% CH_4, 1% C_3H_8, 2% N_2, 0.5% CO_2, and other inerts and traces of heavier hydrocarbons (Smith, 1992). This composition results in a fuel–air stoichiometric ratio of 1 : 9.286, i.e. 97% of the assumed value in the previous

paragraph. The mixture fraction of methane : air stoichiometric mixtures is $f_{st} = 0.055$, while for the natural gas of the above composition is $f_{st} = 0.059$. These numbers are considered to be close and therefore it will be assumed throughout this thesis that the fuel is 100% methane.

The stoichiometric mixture fraction for diffusion flames with partial premixing is found from

$$f_{st} = \frac{(1\text{-}X)R_{MW} + X}{(1\text{-}X)R_{MW} + (1\text{-}X)/R_{molar}} \quad , \qquad (2.2.1)$$

where $R_{MW} = MW_{fuel} / MW_{air}$, and R_{molar} is the fuel to air molar ratio at stoichiometry and equal to 0.105 for methane–air flames. This equation will be used in Chapters 3 and 4.

The density of natural gas is taken as 0.664 kg/m^3 (Kaye and Laby, 1986), of air 1.19 kg/m^3, and the kinematic viscosity of air is taken as equal to 1.52 x 10^{-5} m^2/s, all at 1 bar and 20 °C. Numerical values of transport properties are needed in Section 2.5 for the evaluation of the mixture conductivity in the calculation of the thermocouple time constant and are discussed further there. It was assumed that the air delivered by the shop compressor contained 21% oxygen and 79% nitrogen by volume and these values were used in the calibration of the oxygen analyser used for measuring the oxygen concentration of samples extracted from the flames with aspiration probes (Section 2.4).

Symmetry in the opposed jet flow dictated that the momentum flow rates of the two jets had to be equal, that is $\rho_1 U_1^2 = \rho_2 U_2^2$ where the subscripts 1 and 2 refer to the fuel and the air stream respectively, and this implied that most of the fuel was not consumed in the stagnation region since the stoichiometric fuel to air mass ratio, and hence mass flow rate ratio to complete combustion of the supplied fuel, is only 0.055. The annular nitrogen flow, discussed in Section 2.1, also served to quench the uninteresting buoyant flame which would otherwise form outside the burner, and it was found that nitrogen co–flows faster than 0.5 m/s were enough to achieve this, and such values were used for all experiments[1]. In most measurements presented in this thesis, the momentum flow rates between the two jets were equal, with the exception of a few extinction experiments in Chapter 4 which were performed with the fuel and air jet velocities, rather than their momenta, being equal and this resulted in a slightly asymmetric flow with the flame being located closer to the fuel nozzle, but this was inconsequential for the extinction limit (Chapter 4) and for the scalar measurements (Chapter 3).

[1] A flow rate of 0.5m/s corresponds to about 50l/min and so a standard nitrogen cylinder (containing 7000l at atmospheric conditions), that supplied both the upper and the lower co–flows, was exhausted in about 70min.

In the experiments with vitiated air as oxidant, the oxygen mole fraction was calculated from the metered flow rates, after assuming complete combustion of the laminar "supply" flame, according to the method outlined in Appendix 2.1.

Table 2.1
Reactants compositions and counterflow flame definitions. Diffusion flames are considered those which have $X < 0.86$, and premixed flames those with $X > 0.86$ (or $\phi < 1.6$); see Section 2.2.

Flame Type	Stream 1	Stream 2	Characterised by	Burner (Fig. No.)	Comments
laminar, diffusion	fuel or fuel–air	air	U, X, H	2.2	
laminar, premixed	fuel–air	air	U, ϕ_1, H	2.2	
turbulent, diffusion	fuel or fuel–air	air	U, X, H, H_p	2.1	The most common flame in this thesis
turbulent, single premixed	fuel–air	air	U, ϕ_1, H, H_p	2.1	$U_1=U_2$
turbulent, twin premixed	fuel–air	fuel–air	U, ϕ, H, H_p	2.1	$U_1=U_2$ and $\phi_1=\phi_2$ always

2.3 PHOTOGRAPHIC METHODS

Colour photographs of the flames were taken with a Nikon 35mm SLR camera on Scotch 1000 ASA slide film. Two–dimensional images at a plane containing the centerline of the turbulent opposed jet flow were made by seeding one of the streams with Al_2O_3 particles from a reverse–cyclone feeder and illuminating with a laser sheet formed by placing a cylindrical lens in front of an air–cooled Ar–Ion laser operated at its maximum power of 130mW and tuned at green light (wavelength: 514.5nm). High seeding rates were used in order to provide adequate illumination of the image in a direction normal to the light sheet.

2.4 SPECIES CONCENTRATIONS MEASUREMENTS

This Section presents the system used to measure the mean mole fractions of unburnt hydrocarbons, oxygen, carbon monoxide, carbon dioxide, and hydrogen in samples extracted from positions across the flow by aspiration probes. An overview of the sampling circuit is given first, followed by details on the analyser operation and the data processing used to convert the measured mole fractions in the dried specimens to values appropriate for the flame gases which contain water vapour. The sampling probes that were used are described in Section 2.4.4, which is followed by a discussion on spatial averaging effects. Some of the material in this Section is taken from an internal report that gives more details on the operation and the precautions needed for the accurate measurement of the sample concentrations (Mastorakos, 1992a). The system is based on that assembled by Godoy (1982), Heitor (1985), and Milosavljevic (1993), with specific improvements made on the sample filtering procedures and on the removal of the non–linearity involved in the FID measurements.

2.4.1 Sampling circuit

The flow of the sample from the sampling probe to the analysers is sketched in Fig. 2.4. A 10μm stainless steel filter was connected to the inlet of a heated sampling line, which terminated at a Tee–junction with one of the branches connected to the sample port of the Flame Ionisation Detector (FID) and the other feeding the other analysers. To avoid hydrocarbons dissolving in any condensate formed along the sampling line before the sample reached the FID, the heated line, powered by a custom–made feedback–controlled supply, was kept at a temperature of about 200 °C. The sample that did not enter the FID flowed to a cooling coil immersed in an ice bath and then to a drier. The drier consisted of a tube inside a bed of CaCl grains of 2 to 5 mm–diameter and an outlet at its top which directed the sample into a paper filter[2]. A diaphragm pump (fitted with PTFE coating) was connected after the filter and then the sample flowed through a second identical filter and a rotameter equipped with a needle valve to control the flow. Normally, this valve was fully open so as to employ the full capacity of the pump. Finally, the sample was divided into four branches, each feeding an analyser and fitted with a shut–off valve. All fittings were stainless steel Swagelok 1/4" OD type and all tubing was of stainless steel or flexible PTFE in order to facilitate connections without endangering leaks and to ensure chemical inactivity of the sample. The sample flow rate depended on the probe tip diameter (see also Section 2.4.5) and was in the range 1 – 2 l/min which resulted in a purge time of the circuit of about one

[2] A commonly–used drier is silica gel, but it is known that this material absorbs CO_2 and so should be avoided.

minute. The FID measured the concentration of unburnt hydrocarbons on a *wet* basis and the other analysers measured on a *dry* basis.

2.4.2 Operation, calibration, and analytical uncertainties

Emphasis is placed here on some results on the calibration and operation of the Flame Ionisation Detector used to measure the concentration of unburnt hydrocarbons because of the observed non–linear response of this instrument. For details on the operation of the other analysers, see Mastorakos (1992a) and Godoy (1982).

CO, CO_2, and O_2 analysers

The mole fraction of CO and CO_2 was measured by non–dispersive infra–red analysers manufactured by the Analytical Development Company and the mole fraction of O_2 was measured by a Servomex 540A paramagnetic analyser. For all three analysers, bottled nitrogen and bottled gases with known concentrations to within ±2% were used for setting the zero and the span respectively, apart from the oxygen analyser whose span was set by sampling ambient air. The uncertainties in the measured mole fractions were about ± 0.001.

H_2 analyser

The mole fraction of hydrogen was measured by a gas chromatograph (Pye Unicam, Series 146) fitted with a gas conductivity detector (katharometer), a molecular column to separate the hydrogen from the other components of the mixture, and a gas sampling valve, and nitrogen was used as the carrier gas. The measurement was made by comparing the height of the peak produced by the sample with that produced by a bottled mixture containing 5% H_2 in N_2 to within ±5%. The measurement uncertainty in the reported mole fraction is estimated to be about ±0.003 and is due to the uncertainty in the calibration gas, observed unsteadiness of the katharometer power supply, and error in determining the peak in the chromatogram on graph paper.

Unburnt hydrocarbons analyser

The mole fraction of unburnt hydrocarbons (UHC) was measured by a Flame Ionization Detector (FID) manufactured by Rotork Analysis Ltd. The principle of operation of this instrument is as follows: a small amount of the sample passes over a lean hydrogen–air flame where the hydrocarbon molecules react with the available oxygen at the high flame temperature and produce short–lived ions which form a current that is amplified and measured; the current is proportional to the mole fraction of unburnt hydrocarbons in the detector flame. The sample is drawn by a pump and most of the sample is by–passed to the exhaust, while a small amount enters the detector oven and the relative flow rates between the exhaust and the oven flows depend on the setting of a

pressure regulator. The pressure after the regulator, indicated by a dial gauge on the front panel of the instrument, has to be *identical* during calibration and measurement, so that the amount of sample, and therefore the partial pressure of the sample in the oven, is the same when calibrating and measuring. It is important to realise that it is the *volume flow rate* of the sample through the oven that is to be kept constant, with the *pressure* being the only available controlling parameter.

Two points are to be noted in connexion with the proper calibration of the FID. The first is that hydrocarbons of the molecular composition and in concentrations as close as possible to those expected in the flame, should be used as span gas. For example, for measurements in the exhaust gases of methane flames where ppm levels of UHC are expected, ppm levels of CH_4 in nitrogen should be used as calibration gas. If different hydrocarbons (e.g. propane) are used for calibration and measurement, errors may arise (Milosavljevic, 1993).

The second, and more important, point concerns the need to measure a *wide* range of UHC mole fractions, as in diffusion flames, and the practical requirement that this is done with a *single* calibration, and this would be possible if *both* the volume flow rate through the oven during calibration and measurement were identical *and* if the magnitude of the ion current formed during the combustion of the hydrocarbon were linear with UHC concentration. The manufacturer claims that the latter point is valid, and considerations of the magnitude of the ion current and the net amount of hydrocarbon in the detector flame suggest that ion current saturation, which would make the relationship between ion current and hydrocarbon concentration non–linear, probably does not occur (Lawton & Weinberg, 1969). Concerning the former point, however, it is argued below that the same volume flow rate of sample gas cannot always be achieved, even if the pressure indication is the same.

Examination of the flow diagram inside the instrument, provided in the manufacturer's Users' Manual, shows that the sample flows into the oven through a restriction and a capillary tube downstream of the pressure regulator; the volume flow rate of the sample will depend on the pressure, but also, in general, on the gas density and viscosity. For example, it is easy to show that if isentropic, adiabatic, and choked flow through the restriction is assumed (a situation unlikely to be realised in practice since the gauge pressure upstream of the restriction is only about 1psi), a given pressure will provide volume flow rates of two gases in the ratio equal to the inverse square root of their density ratio. If, as another example closer to reality, it is assumed that the pressure head is meant to overcome only the frictional resistance offered to the sample flow in the capillary tube, it can be shown that the volume flow rate ratio between two gases is equal to the inverse ratio of their viscosities. It is clear that differences in the amount of sample entering the detector will arise between calibration and measurement if the sample and the calibration gases have very different compositions.

The problem is intense in the measurements of UHC in diffusion flames, where the full spectrum of compositions from 100% fuel to pure air needs to be measured. Figure 2.5a shows that the FID, calibrated with 100% methane, underestimates the methane volume fraction in methane–air mixtures by a factor as large as 0.6 at low methane concentrations, as found by experiments with mixtures of known composition to within ±7.5% formed with the rotameters described in Section 2.1. Note that according to the manufacturer, the response of the instrument is *linear* for the full range of UHC compositions, but Fig. 2.5a shows that this is not the case. It has also been found that if the instrument is calibrated with a *low* concentration of methane in air, it *over–estimates* high UHC mole fractions (for example, an instrument calibrated with 0.2% CH_4 in nitrogen measures 100% CH_4 as 160%; Perez–Ortiz, 1992).

Figure 2.5a shows that it has proven possible to correct for the FID non–linearity by multiplying the indication by the ratio of the sample to the span gas viscosity, motivated by the expectation that the flow of the sample inside the FID is controlled by viscous forces along the capillary tubes. The proposed correction is then that

$$X_{UHC,true} = X_{UHC,indicated} * (\mu_{true} / \mu_{span}) \qquad (2.4.1)$$

where μ is the viscosity. Note that the viscosity of the sample mixture needs to be used, since it determines the flow through the capillary, and which is still unknown at this stage. An iteration procedure which has been found to converge satisfactorily consists of the calculation of the viscosity of the indicated mixture, estimating the true mixture composition based on Eq. (2.4.1), and then updating the viscosity estimate. The viscosity of the mixture has been calculated with Wilke's formula (Bird *et al.*, 1960). Note that, in contrast to the results shown in Fig. 2.5b for the viscosity of methane–air mixtures, gases in *flames* also include other species, but it is expected that the associated error is small.

The use of Eq. (2.4.1) allows the measurement of UHC over a large range of concentrations with a *single* span gas calibration to within ±7.5%. In the measurements presented here, the span was set by using 100% natural gas and the values indicated by the instrument were corrected according to Eq. (2.4.1)[3].

2.4.3 Calculation of the mean mixture fraction

The measured data were processed in the manner of Jones *et al.* (1992), also used by Milosavljevic (1993), to find the *wet* mole fractions from the *dry* mole fraction

[3] Further evidence that Eq. (2.4.1) accurately corrects measurements of concentrations of methane in air corresponding to lean flammable mixtures was provided by a few experiments performed with the help of Dr. Choku Nakamura of NKK, Japan, at one time visiting the Chemical Engineering Dept. of Imperial College, who provided samples of 5% CH_4 in air (by vol.) independently measured by rotameters to within 5%.

measurements of CO_2, CO, O_2, H_2, and the *wet* mole fraction of UHC. Expressions for the oxygen–to–nitrogen atom ratio being equal to that of the oxidiser and for the carbon–to–hydrogen atom ratio being equal to that of the parent fuel were used to assemble a system of equations relating the dry to the wet mole fractions and the system was solved by matrix inversion. It was found by Jones *et al.* (1992) that in order to avoid an over–specified problem, acetylene, whose concentration was not measured but which was assumed to be present in the sample in trace quantities, was included in the list of stable species, and thus the solution procedure gave the wet mole fractions of CO, CO_2, O_2, H_2O, N_2, H_2, CH_4, and C_2H_2, with the sum of the last two measured by the FID and referred to here as UHC. Typically, the calculated mole fraction of C_2H_2 was on the order of 0.005, so that its presence in the calculation procedure introduced negligible error in the calculations of the mole fractions of the other species.

For a limited number of measurements in premixed flames presented in Chapter 3 the hydrogen mole fraction could not be measured because the gas chromatograph was not available and the conversion from dry to wet samples was performed by the procedure outlined above, but with the assumption that the H_2 mole fraction was 0.65 times the CO mole fraction, as by Masri and Bilger (1986). A sensitivity analysis showed that the results were affected by a negligible amount when this proportionality factor changed by ±50%, due to the small percentage of CO in the sample mixture. The conclusions to be drawn from examination of measurements processed in this approximate way do not depend on the conversion procedure because they are based on trends observed in the *dried* measurements as well.

The (mean) mixture fraction, defined so as to have the value of unity in the fuel stream and zero in the air stream, was calculated based on carbon atom balance according to

$$F = \frac{Z_{sample}}{Z_{fuel}} , \qquad (2.4.2)$$

where Z is taken as the mean mass fraction of carbon atom and the subscripts have obvious meaning. The carbon atom mass fraction Z was calculated from the wet mole fractions of UHC, CO_2, and CO, and the calculation of the fuel carbon atom mass fraction allowed the possibility of dilution, so that

$$F = \frac{\left(\frac{12.011}{16.043}Y_{CH_4} + \frac{24.022}{26.038}Y_{C_2H_2} + \frac{12.011}{28.011}Y_{CO} + \frac{12.011}{44.011}Y_{CO_2}\right)_{sample}}{\left(\frac{12.011}{16.043}Y_{CH_4}\right)_{fuel}} , \qquad (2.4.3)$$

where Y refers to wet mass fractions, i.e. after processing.

The possibility of partial premixing of the fuel stream with air was accommodated by the term Y_{CH_4} in Eq. (2.4.3), as the mass fraction of the fuel in the fuel stream was smaller with partial premixing than without. The fuel mass fraction Y_{CH_4} is related to the air volume fraction in the fuel stream, X, by

$$Y_{CH_4} = (1 - X)\frac{16.043}{MW_{mix}} ,$$

where MW_{mix} is the fuel–air mixture molecular weight given by

$$MW_{mix} = (1 - X)\ 16.043 + X\ 28.82.$$

Note that the definition of mixture fraction in Eq. (2.4.2) is appropriate for the type of premixing used in this thesis, i.e. of the fuel stream with air, but is not appropriate for other types of premixing, for example of the air stream with fuel, or for diluted air streams by inerts. The reader is referred to Jones *et al.* (1992) for more details on the conversion of the measured dry to wet values, to Masri and Bilger (1986) for an alternative but more approximate conversion procedure, and to Stårner *et al.* (1992) for a comparison of alternative definitions of the mixture fraction.

2.4.4 Probes used

Two probes, both made of fused silica, were used for the species concentrations measurements and are shown in Fig 2.6: the probe shown in Fig. 2.6a was used previously by Milosavljevic (1993) and the water–cooled probe of Fig. 2.6b was manufactured for the present measurements. The basic requirements of a sampling probe are as follows: (i) to extract a representative sample from the flow without causing any disturbance, and (ii) to quench the reaction sufficiently rapidly so that subsequent gas analysis will correspond to the flow composition before the sample was extracted. In addition, since here on–line analysers were used, a further requirement was (iii) to provide enough sample flow rate for their operation.

To minimise the disturbance to the flow, the probe has to be small and isokinetic sampling is required, i.e. the velocity of the fluid entering the probe tip has to be equal to the flow velocity were the probe not there, but this is impossible to achieve in a turbulent flow (Becker, 1993). Insufficient quenching may give rise to higher CO_2 and smaller CO mole fractions (Schoenung and Hanson, 1981) and other factors that affect the measurement include probe orientation and sampling velocity (Attya, 1983). Becker (1993) in a recent and comprehensive review of probe designs and quenching criteria concluded that an important factor frequently overlooked in discussions about successful quenching of the chemical reaction is the radical destruction on the probe walls. Becker

(1993), in agreement with Colket *et al.* (1982), also argued that aerodynamic quench (the rapid cooling associated with the expansion from sonic to supersonic speed inside the probe after the choked probe tip) is usually not achieved with microprobes due to frictional losses, and therefore a realistic aim for a good design is to minimise the size of the sample passage and maximise its length so as to maximise radical destruction at the probe walls. In this spirit, the probe in Fig. 2.6b was designed to have a long, relatively straight section after the tip opening, which is beneficial for radical destruction, a water-cooling sleeve, which is beneficial for quenching, and a small tip diameter (0.3mm), to achieve both good resolution and efficient radical destruction.

2.4.5 Spatial averaging effects

Becker (1993) argued that the spatial resolution of a sampling probe is equal to the streamtube diameter d_{str} that contains the fluid to be aspirated into the probe and therefore depends on the local fluid velocity and density. The mass flow rate of the sample is $\dot{Q}_{samp}\,\rho_{samp}$ with $\dot{Q}_{samp}$ and ρ_{samp} being respectively the volume flow rate and density of the sample at the metering point (the rotameter in Fig. 2.4), and then conservation of mass gives

$$\rho_f\, U_f\, \frac{\pi d_{str}^2}{4} = \dot{Q}_{samp}\, \rho_{samp} \qquad (2.4.4)$$

where ρ_f and U_f are respectively the local density and velocity, averaged across the streamtube, of the fluid that enters the probe. Then the spatial resolution of the probe is given by (Becker, 1993)

$$d_{str} = \sqrt{\frac{4\ \dot{Q}_{samp}\,\rho_{samp}}{\pi\ \rho_f\ U_f}}\ . \qquad (2.4.5)$$

Equation (2.4.5) shows that d_{str} decreases as the fluid density and velocity increases, and as the sample flow rate decreases. Note that the resolution does *not* depend on the probe tip opening d_p directly; small d_p leads to good resolution because it increases the pressure drop across the probe tip for a given setting of the sampling pump thus leading to smaller $\dot{Q}_{samp}$ than big probes. For most of the measurements described in this thesis (Chapter 3), the probe in Fig. 2.6b was used which gave $\dot{Q}_{samp} \approx$ 1 l/min at regions of low temperatures and 0.5 l/min at high temperatures; $U_f = 2 - 4$ m/s for the flames studied here at the sampling locations; $\rho_{samp}/\rho_f \approx T_f/T_{amb}$ with $T_{amb} = 300$K and T_f is assumed equal to the maximum temperature across the flame in the range 1400 – 1900 K; then $d_{str} \approx 3 - 7$ mm corresponds to the estimated best and worst resolution. The measurements shown in Chapter 3 show that the maximum mean temperature is

found between the two jets and the width of the temperature profile is about 10mm, which is of comparable magnitude with the probe resolution. This raises a question as to the extent of spatial averaging produced by the finite probe resolution and this is discussed next.

Spatial averaging is caused by the fact that an analysis instrument (for example, the CO_2 meter) will read the concentration of the species *averaged over the fluid sample*, i.e. the measured concentration will be the average over d_{str}. Imagine that the mean concentration F_{true} of CO_2 depicted by the solid line in Fig. 2.7 needs to be measured as a function of cross–flame distance y. When the centreline of the probe is located at Y_p, because of the finite width of the streamtube reaching the probe, the measured value will represent the average in the interval $Y_p - w/2$ to $Y_p + w/2$ where w is the width of the streamtube (equal to d_{str}, but the use of d_{str} is restricted to denote the probe resolution in the experiments, as opposed to the hypothetical discussion to follow). The measured concentration will then be given by

$$F_{meas}(Y_p) = \frac{1}{w} \int_{Y_p-w/2}^{Y_p+w/2} F_{true}(y)\, dy \qquad (2.4.6)$$

where it has been assumed that the fluid velocity is constant across the streamtube. It can be shown from Eq. (2.4.6) that if $F_{true}(y)$ is linear in y, $F_{meas}(Y_p) = F_{true}(Y_p)$, i.e. no spatial averaging effects are present, but if the profile is non–linear, spatial averaging will be important, $F_{meas}(Y_p)$ can be larger or smaller than $F_{true}(Y_p)$ (e.g., Becker, 1993), and, in particular, when there is a peak in the profile of $F_{true}(y)$, the spatially–averaged measurement will be smaller than the real value.

As quantitative guidance to the magnitude of the possible spatial averaging effects, Eq. (2.4.6) can be evaluated numerically by assuming a functional form for $F_{true}(y)$ and comparing $F_{meas}(Y_p)$ with $F_{true}(Y_p)$. Figure 2.8 shows such calculations for $F_{true}(y) = \exp(-y^2/\delta^2)$, i.e. a gaussian curve normalised to give a maximum of unity and of characteristic width δ, and for different values of w/δ. To facilitate presentation, $\delta=1$ and then all lengthscales should be thought of as normalised by δ. Figure 2.8a shows that as w increases, the width of the measured profile increases and the peak value decreases, and Fig. 2.8b shows the latter trend in more detail. The ratio $F_{meas}(0)/F_{true}(0)$, i.e. the ratio of the peak values, decreases from unity at small w to about 0.6 at $w/\delta = 3$ and these values can be useful to estimate the order of magnitude of spatial averaging effects in the measurements. For example, $\delta \approx 5$mm in the counterflow flames (Chapter 3), $w \approx 7$mm at worst, and so the peak concentration of, say, CO_2 is expected to be smaller than the real value by at most 20%. This discussion is strictly valid for laminar flames but will be used below for estimating the relative

magnitude of spatial broadening effects for measurements in turbulent flames performed by the two probes described in Fig. 2.6a and 2.6b.

2.4.6 Comparison of the two probes and sample results

The measurements of species concentrations with the two probes described in Fig. 2.6 are expected to be different for two reasons: (i) the large probe (Fig. 2.6a) has a larger tip diameter and therefore worse spatial resolution because $\dot{Q}_{samp}$ is expected to be larger, and (ii) the small probe (Fig. 2.6b) is also water–cooled and therefore is expected to have better quenching characteristics.

Experience with the large probe showed that the flow rate of sample was about $\dot{Q}_{samp} \approx 2$ l/min, i.e. twice the volume flow rate of the small probe for the maximum capacity of the sampling pump. This means that d_{str} for the large probe was about 1.4 times the resolution of the small probe (Eq. 2.4.5) and so the peaks of measured profiles of species concentrations resembling Fig. 2.8 would be smaller with the large probe than with the small probe. Fig. 2.9a confirms this expectation because it shows that the CO and CO_2 mole fractions in a turbulent partially premixed counterflow *diffusion* flame are smaller when measured with the large probe than with the small probe. However, for twin *premixed* flames (Fig. 2.9b), the two probes measure similar concentrations; the reason is that for these flames, the CO and CO_2 profiles spread over a larger axial distance than in the diffusion flame of Fig. 2.9a, and so the averaging effect with either probe is expected to be small (because w/δ of Fig. 2.8b is closer to unity), and so the two probe measurements agree. Therefore, depending on the steepness of the concentration profiles to be measured, either probe may be appropriate because the spatial averaging effects may be small.

As mentioned in Section 2.4.4, insufficient quenching inside the probe could result in the conversion of CO to CO_2, and so the smaller mole fraction of CO measured by the large probe in Fig. 2.9a could also be explained by the fact that the small probe, which also includes water–cooling, stops the reaction, and therefore the generation of CO_2, faster than the large probe. However, the smaller CO_2 measured by the large probe cannot be explained by this argument, and so the difference in the measurements are attributed mostly to spatial averaging effects. The difference in quenching characteristics between the two probes cannot be ascertained at present, but, as discussed in Section 2.4.3, the small probe is expected to be more efficient in quenching the reaction because it has a more pronounced radical destruction rate at its walls due to the small diameter and also includes water cooling.

It was found that the present flames, which are only a few millimetres thick, would be visually disturbed by the presence of the large probe Fig. 2.6a , but less by the small probe. Although the 0.5mm probe could still be considered small for other applications of measurements in turbulent flames, it was imperative for the present

flames to have a probe with the smallest possible physical size, yet resulting in enough flow rate of the sample to operate the analysers. The small probe shown in Fig. 2.6b provided just enough sample flow rate, and gave the best compromise between minimal disturbance to the flames, spatial resolution, and compliance to the reaction–quenching criteria outlined by Becker (1993) and discussed in Section 2.4.4.

2.4.7 Uncertainties

Most of the measurements of species concentrations presented in this thesis were made with the small probe of Fig. 2.6b at a radial distance of 10mm under constant sampling pump setting (the control valve V7 in Fig. 2.4 was always fully open), with the probe axis always aligned in the radial direction, and constant cooling water flow rates, and so any errors due to spatial averaging and insufficient quenching are expected to be systematic. The error in positioning the probe was about ±0.5mm relative to the burner, and the distance between measurement points was accurate to within ±0.1mm during an axial traverse across the flow.

Whitelaw (1986) claimed that the aspiration–probe measurements are closer to Favre–averages than to time–averages, while Becker (1993) contradicted this and suggested that, for situations where $d_{str} < d_p$, as in the present measurements, lighter fluid parcels are preferentially sucked into the probe (Becker, quoting Bilger, 1977). Kennedy and Kent (1981) compared the mean mixture fraction measured by Mie scattering with that measured by aspiration probe in jet diffusion flames and concluded that the probe results fell between the time– and Favre–averages, and so the type of averaging performed by the probe measurements is not clear. In Chapter 3, the wet mole fractions calculated as described in Section 2.4.3 are presented and the mixture fraction is also presented with an estimated uncertainty of ±10% due mostly to the measurement uncertainties of less than ±0.01 mole fraction (Whitelaw, 1986). The conclusions to be drawn from comparisons between measurements made under different flow conditions are not affected by these uncertainties or systematic errors.

2.5 TEMPERATURE MEASUREMENTS

This Section starts with an overview of the thermocouple system and some details are then presented on the numerical processing of the measured data used to compensate for the thermocouple finite thermal inertia. Sample results are presented and estimates of the uncertainties involved in the measurements and in the numerical methods are also given. Developments more recent that the paper of Heitor *et al.* (1985), which contains an extensive review and literature survey of works concerning thermocouple measurements until 1985, are emphasised here.

2.5.1 Thermocouples

Temperatures were measured with Pt – Pt/13%Rh uncoated butt–welded thermocouples of 40μm (and, in a few cases, 25μm or 80μm) diameter wire; the thermocouples were attached to 0.3mm posts supported in twin–bore ceramic cladding and orientated horizontally to minimise the mean temperature gradient along their length (Heitor *et al.*, 1985). The ceramic tube was enclosed in a stainless–steel tube to provide a stronger support. The thermocouple was about 200 diameters long to avoid heat conduction along its length (Bradley and Mathews, 1968) and no radiation correction was attempted.

2.5.2 Data acquisition

The signal from the thermocouple was amplified by a custom–made amplifier and interfaced to a microcomputer through a 16–bit A/D card. Two systems were used in the measurements presented in this thesis: (i) amplifier with gain of 373 and a Data Translation DT2827 analogue–to–digital converting card, and (ii) amplifier with gain of 100 and an Analogic HSDAS card. The second system has been described in detail in an internal report (Mastorakos, 1992b) and also included the possibility of applying a heating pulse to the thermocouple and monitoring the subsequent decay so as to measure the time constant in the manner of Heitor *et al.* (1985), and both systems had two amplifiers to allow the simultaneous measurement at two points with two thermocouples (Section 2.5.6). The voltage from the thermocouple was translated into temperature through the use of curve–fits to tabulated data (Labfacility, 1982) with error at most ±0.5%, and the measured time series of temperature were saved on the hard disk of the IBM–PC compatible microcomputer for further processing.

2.5.3 Compensation

The thermal inertia of the thermocouple acts on the temperature to be measured like a first–order filter so that

$$T_g = T_w + \tau_{wire}\,(T_g,u)\,\frac{dT_w}{dt}\,, \qquad (2.5.1)$$

where T is the temperature, t the time, the subscripts 'g' and 'w' refer to the gas and the wire temperatures respectively, and τ_{wire} is the wire time constant that depends on the instantaneous gas temperature, the local velocity u, and wire properties (Heitor *et al.*, 1985; Katsuki *et al.*, 1987). For the evaluation of τ_{wire}, the expression of Collis and Williams (1959) was used to give

$$\tau_{wire} = \frac{\rho_w C_{pw} d_w^2}{4 k_g [0.24 + 0.56 Re_w^{0.45}]}, \qquad (2.5.2)$$

where ρ_w is the wire density (equal to 24545 kg/m^3), C_{pw} the wire heat capacity (equal to 146 J/kgK; Kaye and Laby, 1986), d_w the wire diameter, k_g the gas conductivity, and Re_w the Reynolds number based on the local velocity u, the gas kinematic viscosity ν_g, and the wire diameter; the above expression is valid in the range $0.02 < Re_w < 44$. Heitor *et al.* (1985) compared the time constant evaluated from Eq. (2.5.2) with that measured by monitoring the temperature decay after applying a heating pulse to the thermocouple and found good agreement, and the same conclusion is reached here in Section 2.5.4. It is evident from Eq. (2.5.2) that the time constant depends on the instantaneous velocity, composition, and temperature of the fluid around the thermocouple and the dependence of the time constant on these is considered next.

The time constant is small at large velocities and at high temperatures because Re_w increases with u, and because k_g increases with T, and it was found by evaluation of Eq. (2.5.2) that the largest dependence of τ_{wire} on the temperature is through the thermal conductivity, with the Reynolds number playing a smaller role. For the evaluation of Eq. (2.5.2), the following expressions were used to provide the air transport properties as a function of temperature to within about 2% from the tabulated values in Vargaftik (1975):

$$\rho = 1.29304 \ (0.2729 * 1000 / T), \qquad (2.5.3a)$$

$$\mu = 1.716 \times 10^{-5} \ (-0.51065 + 9.2361 \times 10^{-2} \sqrt{T}), \qquad (2.5.3b)$$

$$k = 2.414 \times 10^{-2} \ (-0.98554 + 0.11938 \sqrt{T}), \qquad (2.5.3c)$$

with T in K and the result in SI units[4]. Hence the calculation of the time constant when the fluid around the thermocouple is air is accurate. However, the transport properties that should be used in Eq. (2.5.2) depend also on the instantaneous *composition* and this cannot be inferred from the instantaneous temperature for a turbulent diffusion flame; therefore the transport properties upon which the evaluation of the time constant is based require consideration and are discussed next.

For a laminar diffusion flame, the ratio of the time constant of a 40μm wire at 1m/s, based on the transport properties taken from a calculation of the composition of a laminar counterflow diffusion flame of methane with a low strain rate (5 s^{-1}) by Jones and Lindstedt (1988), to that based on *air* properties at the same temperature (calculated from Eq. 2.5.3) does not vary monotonically with temperature, as Fig. 2.10 shows.

[4] The numerical values before the parantheses in the r.h.s. of Eqs. (2.5.3) correspond to the density, viscosity, and conductivity of air at 0 °C.

The true time constant is less than that based on air properties by up to 0.55 on the fuel side of the maximum temperature and by a factor of 0.75 at the location of maximum temperature. The ratio plotted in Fig. 2.10 is weakly sensitive to wire diameter and gas velocity because the difference in thermal conductivity dominates Eq. (2.5.2), and this finding explains the observation of Heitor *et al.* (1985) that direct use of time constants based on air properties led to over–compensation, i.e. the compensated temperature fell outside realistic upper and lower bounds, unless it was reduced by an empirically–determined factor of about 0.65.

In the measurements presented here for turbulent diffusion flames, the ratio plotted in Fig. 2.10 averaged over the temperature range was used, which resulted in

$$\tau_{wire} = 0.76\ \tau_{air}(T, u), \qquad (2.5.4)$$

i.e. the time constant used was 0.76 times that of Collis and Williams law evaluated with properties of air at the same temperature. For the present measurements, the velocity u used in the time–constant evaluation was taken as the mean velocity and estimated from the potential flow solution of the opposed jet flow, with the strain rate taken as $2U_o / H$. The temperature measurements were taken prior to the velocity measurements, and when the latter became available, it was found that the fluctuations of the time constant due to fluctuations of velocity in the measurement locations were only a few percent at large radii, but by up to 20% at the centreline because the small mean velocities close to the stagnation region resulted in a large sensitivity of τ_{wire} to velocity, unlike the case at large radii where the dominant radial velocity reduced the time constant *and* its sensitivity to velocity. The fluctuating temperatures presented in this thesis were taken at r = 10mm to ensure both a small time constant and with small variations. Finally, if the temperature sensitivity of the time constant is small, as found by evaluating Eq. (2.5.4) in the expected temperature range (say, at 300 and 2000K) and asserting that the difference is small, compensation with a time constant evaluated at the mean temperature $\langle T \rangle$ may be adequate.

2.5.4 Numerical methods

Compensation was performed by solving algebraically Eq. (2.5.1) for T_g, (i) with a constant value of τ_{wire}, or (ii) by allowing τ_{wire} to depend on gas temperature as in Eqs. (2.5.2 – 4) by an iterative procedure which converged to ±1K after two or three iterations. The time–derivative in Eq. (2.5.1) was evaluated with a three–point central difference. It will be shown later (Section 2.5.5) that the two methods yield similar results for the present flames, so it is sufficient for the purposes of discussing certain aspects of compensation to consider next only the situation where a constant value of τ_{wire} is adequate.

Taking the Fourier transform of Eq. (2.5.1) shows that

$$\hat{T}_g = (1 + j\,2\,\pi\,\tau_{wire}\,f\,)\,\hat{T}_w\,, \text{ or}$$

$$Re(\hat{T}_g) = Re(\hat{T}_w) - 2\,\pi\,\tau_{wire}\,f\,Im(\hat{T}_w) \qquad (2.5.5a)$$

and

$$Im(\hat{T}_g) = Im(\hat{T}_w) + 2\,\pi\,\tau_{wire}\,f\,Re(\hat{T}_w) \qquad (2.5.5b)$$

where f is the frequency, $j = \sqrt{-1}$, a caret denotes the Fourier transform, and Re and Im are the real and imaginary parts of the transform respectively. Alternatively to directly solving Eq. (2.5.1), numerical compensation can be performed by taking the Fourier Transform of the measured signal, evaluating Eq. (2.5.5) with a given τ_{wire}, and then inverting. It is evident from the second terms in the r.h.s. of Eqs. (2.5.5) that compensation amplifies the high frequencies and therefore will also amplify any noise present in the signal; to avoid this, low–pass filtering of the uncompensated temperature was performed before compensation (Press *et al.*, 1985). A related matter is that for the correct evaluation of the time derivative in Eq. (2.5.2), which is needed when compensation is done in the time–domain, good time resolution is required; Heitor *et al.* (1985) recommended a sampling rate about 5 times the fastest frequency that the thermocouple can resolve before the signal becomes indistinguishable from the background noise. However, high sampling rates allow more noise in the signal, and therefore the need for a noiseless signal becomes pressing, as has also been recognised by other researchers (Bradley *et al.*, 1989; Yoshida *et al.*,1989).

Based on these considerations, the compensation procedure for all temperature measurements in this thesis was as follows: (i) acquire the temperature time series; (ii) examine in the frequency spectrum of the measured signal the frequency $f_{cut-off}$ where the signal becomes indistinguishable from the noise; (iii) numerically low–pass filter the signal at $f_{cut-off}$; (iv) examine the sensitivity of the time constant to velocity and temperature at the measurement location by evaluating Eq (2.5.4); (v) based on (iv), decide on the suitability of using a constant $\tau_{wire} = f(\langle T\rangle,\langle u\rangle)$ or whether a variable $\tau_{wire} = f(T, \langle u\rangle)$ is more appropriate; and (vi) solve Eq. (2.5.1).

2.5.5 Sample results

This Section presents a few results of time constant measurements in air and typical temperature measurements in the counterflow flames stabilised in the burner of Fig. 2.1 to show the use of the compensation procedure described in the previous paragraph. The temperature measurements presented here are typical of those shown in Chapter 3.

Surface catalysis

It was found that catalytic effects took place on the wire surface under conditions of high partial premixing and resulted in an unreasonably high peak in the temperature probability density function (pdf) in the range 1200 – 1500 K. Fig. 2.11 shows a pdf of the compensated temperature (see Section 2.5.2 for the compensation procedure) for a counterflow flame with $X = 0.8$ at the fuel side of the maximum mean temperature and it is believed that the peak at about 1500K is not realistic. Fig. 2.11 is typical of measurements contaminated by catalytic effects and such pdfs were observed only on the fuel side of the flame, consistent with the visual observation that when traversing from the air to the fuel side, the wire remained red–hot even at cold locations of the flow in the fuel side of the flame. However, when the partial premixing was less than about 50%, the temperature pdf did not show any unusual peak and no hysteresis was observed and so the temperatures of diffusion flames presented in this thesis are limited to $X < 0.5$. Use of anti–catalytic coatings increases the time constant of the wire (Heitor *et al.*, 1985) and this is detrimental for the accuracy of measurement of temperature fluctuations and therefore was not tried.

Time constant

The time constant was measured by monitoring the temperature decay after applying to the wire a heating pulse of 0.5A current for a few microseconds (Mastorakos, 1992b; Laker, 1992). The wire was placed at the exit plane of one of the tubes shown in Fig. 2.1 with a flow of ambient air at a variable bulk velocity and, as presented in Chapter 3, the perforated plate produced a turbulence of about 0.085 times the bulk velocity for $H_p = 55$mm [5]. Five hundred measurements of the time constant were taken, and Table 2.2 shows the average and the r.m.s. value of the measured time constant for a 40μm wire; the scatter in the τ_{wire} measurement reflects partly the randomness in the velocity surrounding the wire, i.e. the fact that at the beginning of different realisations the velocity had different values, and partly the time variation of the velocity *during* the decay. During a temperature decay, which lasts about $5\,\tau_{wire}$ (i.e. close to 200ms), the velocity can change because the estimated integral velocity timescale is smaller than the duration of the decay and about 50ms for a mean velocity of 1 m/s and 16.7ms for a mean velocity of 3 m/s; therefore the fluctuating time constant during the decay period would result in a scatter in the measured τ_{wire} larger than that caused by a scatter in the velocity value alone. Table 2.2 also includes results at identical velocity and temperature conditions from a Monte–Carlo calculation of τ_{wire} based on Collis and Williams (1959) law (Eq. 2.5.2) with the velocity as a gaussian stochastic variable with

[5] Throughout the thesis, the lengthscale of the turbulence generated by the perforated plate is assumed to be equal to the plate hole diameter of 4mm. See also Section 3.2.3.

given mean and variance; the measured r.m.s. in τ_{wire} is larger than the calculated one and this is consistent with the argument concerning the varying time constant during the decay. The calculation based on Collis and Williams law over–predicts τ_{wire} in still air and this is expected since Eq. (2.5.2) is not valid for wire Reynolds numbers close to zero. The agreement between the measured and the calculated *mean* value is good at non–zero velocities and gives confidence in the use of Collis and Williams law for the evaluation of the time constant, a conclusion also reached by Heitor *et al.* (1985).

Table 2.2
Time constant measurements in isothermal turbulent air flow and Monte–Carlo calculations based on the expression of Collis and Williams (1959). The heating pulse was set at 0.5 A for the indicated duration.

$\langle U \rangle$ (m/s)	u' (m/s)	Heating pulse duration (ms)	$\langle \tau_{MEAS} \rangle$ (ms)	rms(τ_{MEAS}) (ms)	$\langle \tau_{CALC} \rangle$ (ms)	rms(τ_{CALC}) (ms)
0	0	45	102.5	3.7	252	0
1	0.085	65	50.7	3.1	49.9	1.2
2	0.17	85	41.9	2.5	41.6	1.4
3	0.255	105	36.7	2.3	35.6	1.3

Instantaneous temperature

A typical trace of the temperature measured with a 40μm wire in a diffusion flame stabilised between unpremixed fuel and air turbulent jets, under flow conditions typical of most measurement in this thesis, is shown in Fig. 2.12a by the heavy solid line. The spectrum of the uncompensated temperature is presented in Fig. 2.12c and it is evident that the signal becomes indistinguishable from the noise at about 500Hz and this is a typical cut–off frequency for the present flames, for 40μm wires, and for the electronic noise of the system which corresponded to about ±1K. The uncompensated time series was low–pass filtered at 500Hz and compensation was performed with two methods: (i) assuming a constant τ_{wire} determined by Eq. (2.5.4) evaluated at the mean temperature, and (ii) a τ_{wire} dependant on the instantaneous temperature, and for both methods, the mean velocity at the measurement point of about 2m/s was used. Table 2.3 compares the uncompensated and the compensated mean and r.m.s. values of temperature and Figs. 2.12a to c include the compensated temperature traces, probability density functions, and frequency spectra respectively. The following observations are made.

First, the mean compensated temperature is identical to the mean uncompensated temperature when an invariant time constant was used, but the latter is smaller by about

30K when compensation with a variable time constant was performed, in agreement with Ballantyne and Moss (1977). The small difference is typical for most measurement conditions and so mean temperatures based on uncompensated temperatures can be used with small error. Secondly, the r.m.s. values, the spectra, and the pdfs of the compensated temperatures are substantially different from the uncompensated ones, and, thirdly, the different types of compensation produce very similar temperature traces and pdfs. The shift of the low–temperature part of the pdfs to lower temperatures when the time constant depends on the temperature is due to the fact that at low temperatures the time constant is larger, and compensation more pronounced, and this observation agrees with the measured smaller *mean* value with $\tau_{wire} = f(T)$ in Table 2.3. Finally, the r.m.s. values are to within 10% with the two compensation methods.

It is concluded that with the present thermocouple system and compensation routine, most of the energy–containing region of the fluctuating temperature spectrum can be resolved, that the mean temperatures can be based on the uncompensated temperatures with small error, but also that the r.m.s. values depend on the value of the time constant, as also found by Heitor *et al.* (1985).

Table 2.3

Uncompensated, compensated with $\tau_{wire} = f(2,\langle T\rangle) = 19.7$ ms, and compensated with $\tau_{wire} = f(2,T)$ mean and r.m.s. temperatures.

Temperature	Uncompensated	$\tau_{wire} = 19.7$ ms	$\tau_{wire} =$ f(2m/s,T)
Mean	1071	1070	1041
r.m.s.	252.8	419.7	443.9

2.5.6 Two–point measurements

A limited number of two–point temperature measurements were taken in order to obtain insight in the spatial coherency of the flame. For these measurements, two identical thermocouples were located at different points in the flow and the signals from both were acquired by the two–channel system described in Section 2.5.2, and the time series corresponding to both channels were processed in the manner described previously. During the course of this work, it was found that the two wires could result in compensated r.m.s. values differing by up to 20% even when put in the same location in the flow, and that when located as close as possible (distant by a minimum of about 1mm), the correlation coefficient between the two compensated signals was not close to unity, as expected, but smaller. The problem was traced to the fact that sometimes

during the thermocouple welding, the bead could be larger or smaller than the wire diameter and so the effective d_w in the evaluation of the time constant in Eq. (2.5.2) was not equal to the nominal wire diameter. After this discovery, only thermocouples with bead diameter as close as possible to the wire diameter were used, as judged visually by examination under a microscope, and some previous measurements were repeated and confirmed.

2.5.7 Uncertainties

Radiation loss

The present thermocouples under–estimate the fluid temperature due to radiation heat loss and it is expected that the error would be about 10% at 1800K (Heitor, 1985) and that it increases with temperature. To confirm these expectations, preliminary measurements were performed with the thermocouples in laminar stoichiometric premixed flames stabilised in a flat–flame matrix burner (Powling burner; e.g. Gaydon and Wolfhard, 1960) and the temperature of the hot product side was registered at about 1950K; the adiabatic flame temperature of stoichiometric methane–air mixtures is about 2200K and hence it is concluded that the *maximum* under–estimation associated with 40μm wires used here amounts to about 250K at flame temperatures.

The effect of the radiation heat loss from the thermocouple is to shift the instantaneous temperature to lower values by an amount that is practically zero at room temperatures to 250K at flame temperatures. Assume that the real gas temperature is T_g and has a probability density function $p(T_g)$; the mean and variance will then be given by

$$\langle T \rangle_g = \int T_g \; p(T_g) \; dT_g \qquad (2.5.6a)$$

and

$$T'_g{}^2 = \int [T_g - \langle T \rangle_g]^2 \; p(T_g) \; dT_g \; . \qquad (2.5.6b)$$

The radiation loss from the thermocouple will make the wire temperature equal to

$$T_w = T_g - f_{RL}(T_g)$$

where $f_{RL}(T_g)$ describes the temperature under–estimation and is an increasing function of T_g. In reality, $f_{RL}(T_g)$ is a very non–linear function increasing quickly at high temperatures, but assume pessimistically (and for algebraic simplicity) that it is linear in T_g and increases from zero at 300K to 250K at 2200K, so that

$$T_w \approx C_1 \, T_g + C_2 \qquad (2.5.7a)$$

with

$$C_1 = (1 - \frac{250}{2200-300}) = 0.87 \qquad (2.5.7b)$$

and

$$C_2 = \frac{300}{2200-300} * 250 = 40\,K. \qquad (2.5.7c)$$

Then the mean and variance of the measured temperature will be

$$\langle T \rangle_w = C_1 \langle T \rangle_g + C_2 \qquad (2.5.8a)$$

and

$$T'_w{}^2 = C_1{}^2 \; T'_g{}^2. \qquad (2.5.8b)$$

Equation (2.5.8a) shows that the thermocouple under–estimates the mean temperature by about 90K at 1000K, 150K at 1400K, and 190K at 1800K, and that the effect on the r.m.s. values is to consistently under–estimate these by about 10%. These estimates are considered pessimistic because the radiation heat loss is smaller than Eq. (2.5.7) would suggest and so should be treated as upper bounds. Most of the mean temperatures presented in this thesis are time–averages of the uncompensated temperature and, as shown in Table 2.3, it is expected that this will over–estimate the real mean temperature by about 30K for most flames discussed here due to the variations of the time constant with temperature. The maximum mean temperatures are about 1400K for the diffusion flames in this thesis, and therefore a total systematic under–estimate of the reported mean temperature measurements of about 120K is expected.

Statistical and positional

The means of uncompensated temperatures were formed over 2048 values sampled at 200Hz, which was equivalent to about 1000 statistically independent samples (following the emphasis by Tennekes and Lumley, 1972), and this resulted in uncertainties of a maximum of 3% for $T'/\langle T \rangle = 0.5$ (Bendat and Piersol, 1971). For the compensated temperatures, the statistical error is about 5% for the mean and 10% for the r.m.s. values because the records used for their evaluation were briefer at about 300 integral–timescales long. Correlation coefficients between two signals are expected to be accurate to within ±0.1 and frequency spectra presented in later Chapters were calculated with Hanning windowing (Press *et al.*, 1986) and were based on 5 to 10 sets of 2048–point Fourier transforms which resulted in statistical uncertainties about ±20% (Bendat and Piersol, 1971). As for the aspiration probe, the thermocouple was located to within ±0.5mm relative to the burner and the uncertainty was ±0.1mm for the distance between measurement points in the same traverse. To minimise errors, when points across a profile are reported only measurements from the same traverse and the same

thermocouple are shown. The thermocouple statistics are expected to represent real time–averages, unweighted by density changes.

Uncertainties due to the time constant

The discussion in Section 2.5.3 highlighted that the biggest source of uncertainty in the fluctuating temperature measurements is the chosen value of the time constant, especially because the latter depends on the unknown instantaneous fluid composition around the wire. The reported r.m.s. are estimated to be accurate to within ±15% of the real values, but it is noted that the *qualitative* shape of the probability density functions of the temperature, which will be emphasised more than the r.m.s. themselves as discussed in Chapter 3, does not change if the time constant is systematically varied from the used value (Eq. 2.5.4) to within 20%, and does not depend on the compensation procedure (Section 2.5.5; Fig. 2.12). The conclusions to be drawn from the fluctuating temperature measurements are not affected by this uncertainty.

2.6 VELOCITY MEASUREMENTS

Mean and fluctuating velocities and, in a few cases, the associated probability density functions, were measured with a one–component forward–scatter laser–Doppler velocimeter and because all the presented measurements could not be taken at the same time, two systems were used with different transmitting optics.

2.6.1 LDV systems

The first system, with principal characteristics given in Table 2.4a, included an optical unit (DISA Model 55X7) fitted with a single Bragg cell to give an optical frequency shift of 40MHz while the receiving optics comprised a 150mm focal–length lens which focused the forward–scattered light from the seed onto a 350μm pinhole in front of a photomultiplier (Hamamatsu R1477). After electronic downshifting, resulting in an effective frequency shift of 4 MHz, the Doppler frequency was measured by a custom–made counter controlled by an 8–bit microcomputer (Heitor *et al.*, 1984), operated with "5/8" validation at 0.19% tolerance. For measurements in inert flows, silicone oil seed from a air–blast atomiser was used, and reacting flows were seeded with aluminium oxide particles of nominal diameter 1μm (Milosavljevic, 1993) introduced in the flow with a reverse–cyclone feeder.

The second system had principal characteristics given in Table 2.4b, and was different in that an optical unit with a rotating grating, a photodiode with a pinhole of 200μm diameter instead of a photomultiplier, and an IBM–PC microcomputer were used (Fujibayashi, 1992), but the same counter, laser, and seed, and similar frequency shifts

were employed. The first system was used for the measurement of the initial conditions and for a few inert flow measurements and the second system for most of the measurements presented in Chapter 3.

2.6.2 Uncertainties

The amount of frequency shift was always large compared to the velocities to be measured so that direction ambiguity was resolved and the "cone of acceptance" included all possible velocity components (Durst *et al.*, 1976). It was found in preliminary measurements that the ensemble–averaged mean and r.m.s. velocities close to the stagnation region depended on the unevenness of the seeding concentration in the two jets (see Section 3.2.4 for a more detailed discussion) and the seeding rates in the two jets was kept as close as possible in the measurements reported here. This was not an easy task because the reverse–cyclone feeders, necessary for the measurements in reacting flow, did not provide a very uniform seeding rate, but it was possible to keep the valid signal data rate in the inlet planes of the two jets equal to within 10% and constant during a traverse across the flow, so that the uncertainty in the measurements due to unequal seeding rates was made small.

No significant gradient broadening effects in the measurements are expected because, for axial velocity measurements, the long dimension of the probe volume was aligned with the radial direction and the radial gradient of the mean axial velocity was zero, and because, for radial velocity measurements, the long probe dimension was aligned normally to the radius so that the mean radial velocity variation along the probe was negligible due to the axisymmetry of the flow. The reported mean and r.m.s. velocities are expected to be closer to Favre–averages than to time–averages because of the tendency to record preferentially velocities associated with high densities as these contained more seeding particles.

A minimum of 2000 measurements were taken at each point resulting in a statistical uncertainty in the reported values of mean and r.m.s. velocity of at most 2 % and 4 % respectively to within 95% confidence level (Yanta and Smith, 1978), and the probability density functions were based on 5000 samples to achieve better statistical convergence. The data rate was about 100 – 200 Hz so that the samples were separated in time by a delay of the same order as the estimated integral timescale (see Section 3.4.1) giving hence truly statistical independent samples. The optical components were mounted on a bench which was attached to a three–directional traversing mechanism from a milling machine to locate the control volume to within ±0.5mm relative to the burner and the uncertainties in the steps along a traverse were ±0.1mm in the horizontal directions and ±0.2mm in the vertical direction.

Table 2.4a
Principal characteristics of the laser–doppler velocimeter with the DISA optical unit

35mW (nominal) He–Ne laser : wavelength	632.8nm
Beam diameter at e^{-2} intensity	1.2mm
Focal length of lens	310mm
Measured half–angle of intersection	5.92°
Fringe spacing	3.067μm
Calculated dimensions of measuring volume at e^{-2} intensity (major and minor axes of ellipsoid)	2.01; 0.20 mm
Calculated number of fringes within e^{-2} intensity level	67
Focal length of collecting lens	150mm
Velocimeter transfer constant	0.326 MHz/(ms^{-1})
Frequency shift (MHz)	4.00

Table 2.4b
Principal characteristics of the laser–doppler velocimeter with the rotating grating optical unit

35mW (nominal) He–Ne laser : wavelength	632.8nm
Beam diameter at e^{-2} intensity	1.2mm
Focal length of lens	450mm
Measured half–angle of intersection	4.14°
Fringe spacing	4.385μm
Calculated dimensions of measuring volume at e^{-2} intensity (major and minor axes of ellipsoid)	1.11; 0.081 mm
Calculated number of fringes within e^{-2} intensity level	18
Focal length of collecting lens	150mm
Velocimeter transfer constant	0.228 MHz/(ms^{-1})
Frequency shift (MHz)	4.38

2.7 SUMMARY OF CHAPTER 2

The flow configuration and the methods followed for photographing the flames and for measuring the mean species concentrations, and the instantaneous temperatures and velocities were presented in this Chapter. The burner comprised two vertically–aligned assemblies of straight tubes of 25.4mm diameter fitted with turbulence–promoting perforated plates and surrounded by annular tubes. The fuel used was natural gas,. consisting practically only of methane, air was delivered by shop compressors, the co–flow was nitrogen, and unpremixed and partially–premixed diffusion and fully premixed flames were stabilised by varying the compositions of the inner tube reactants streams with flow rates measured by calibrated rotameters.

The mean mole fractions of CO, CO_2, O_2, H_2, and unburnt hydrocarbons (UHC) were measured by extracting samples from the flame with a fused silica water–cooled probe of 0.3mm tip diameter and subsequent drying and on–line analysis. The operation of most of the analysers was straightforward, but special methods were developed for the correction of the indication of the Flame Ionisation Detector (FID) used to measure the mole fraction of UHC because of the non–linear response of the instrument between small and large UHC concentrations. The species concentrations measurements were processed to give the wet mole fractions and the mean mixture fraction was also calculated based on carbon atom mass fraction.

The instantaneous temperature was measured by 40μm–wire thermocouples numerically–compensated for their thermal inertia. It was found that the wire time constant depended on the velocity, temperature, and composition of the fluid around the wire and, the last dependence in particular, introduced large uncertainties in the value of the time constant that should be used for compensation, but calculations based on the composition of laminar diffusion flames reduced these uncertainties. Finally, velocities were measured with a one–component laser–doppler velocimeter operating in forward scatter. The expected uncertainties in the measurements of flow rates, species mole fractions, temperatures, and velocities that are presented in Chapter 3 are given in the respective sections of this Chapter and are expected to be small enough so that they do not affect the conclusions to be drawn in later Chapters.

Figures for Chapter 2

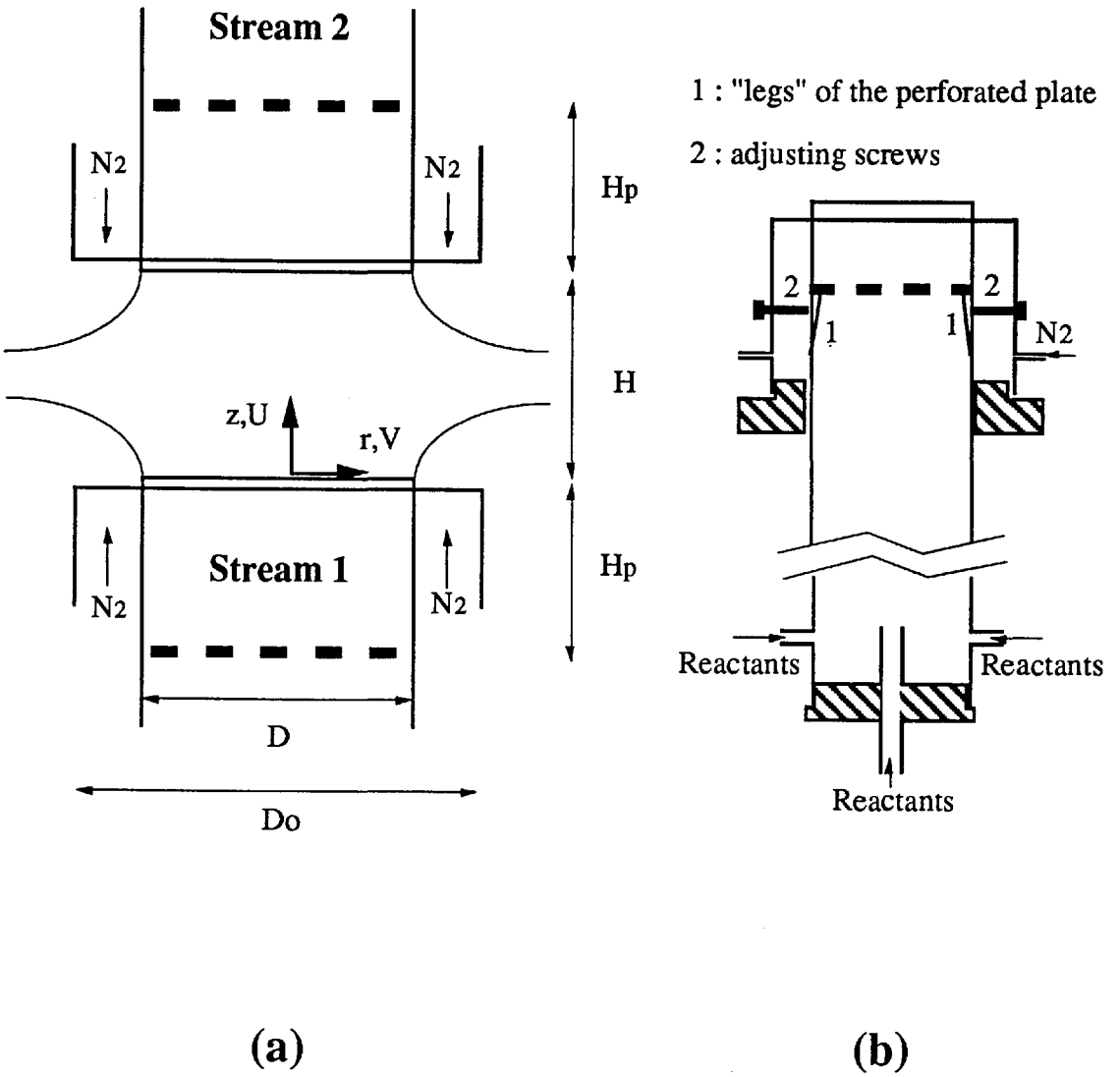


Figure 2.1 (a) The burner arrangement used for most of the measurements in this thesis. Included are the coordinate system and the definitions of lengths used to describe the flow parameters like the jet separation and the location of the perforated plate from the tube exit plane. (b) More details of the rear part of the burner showing the way the reactants are fed.

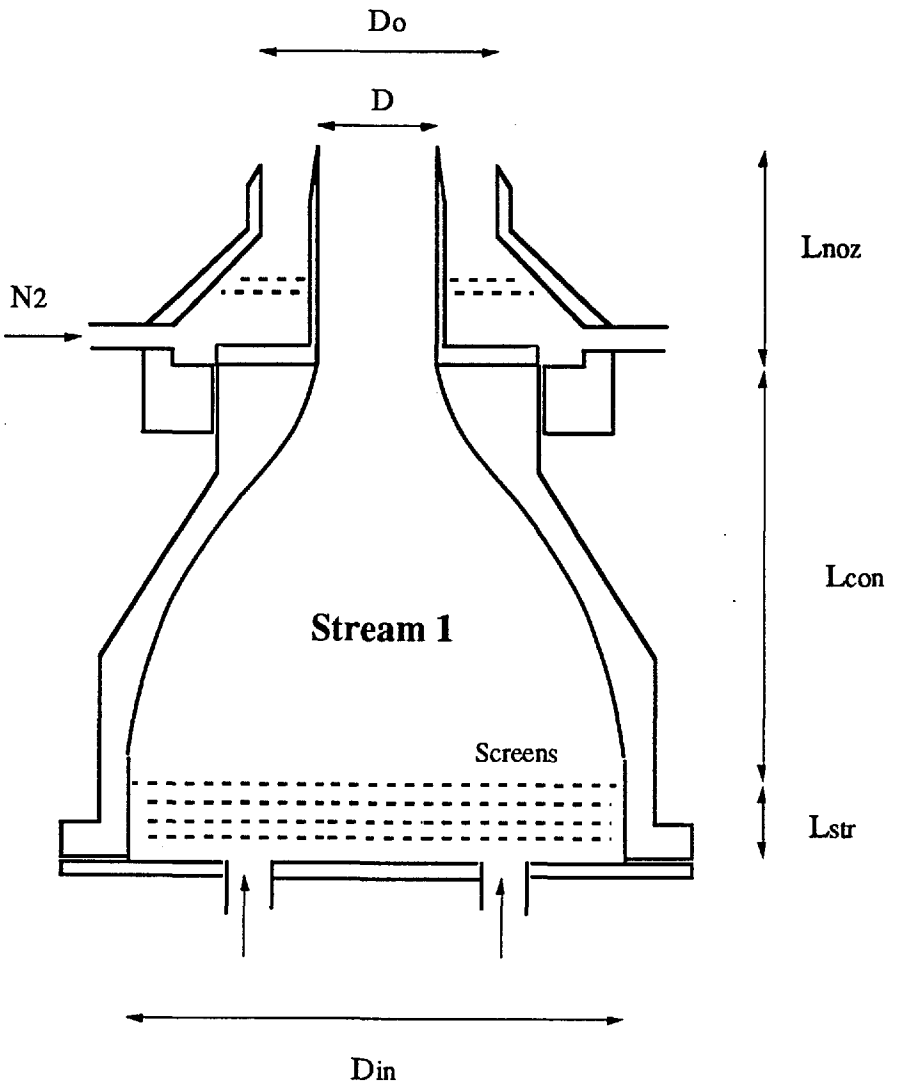


Figure 2.2 One of the contractions used for stabilising laminar counterflow flames. The burner consists of two such identical assemblies.

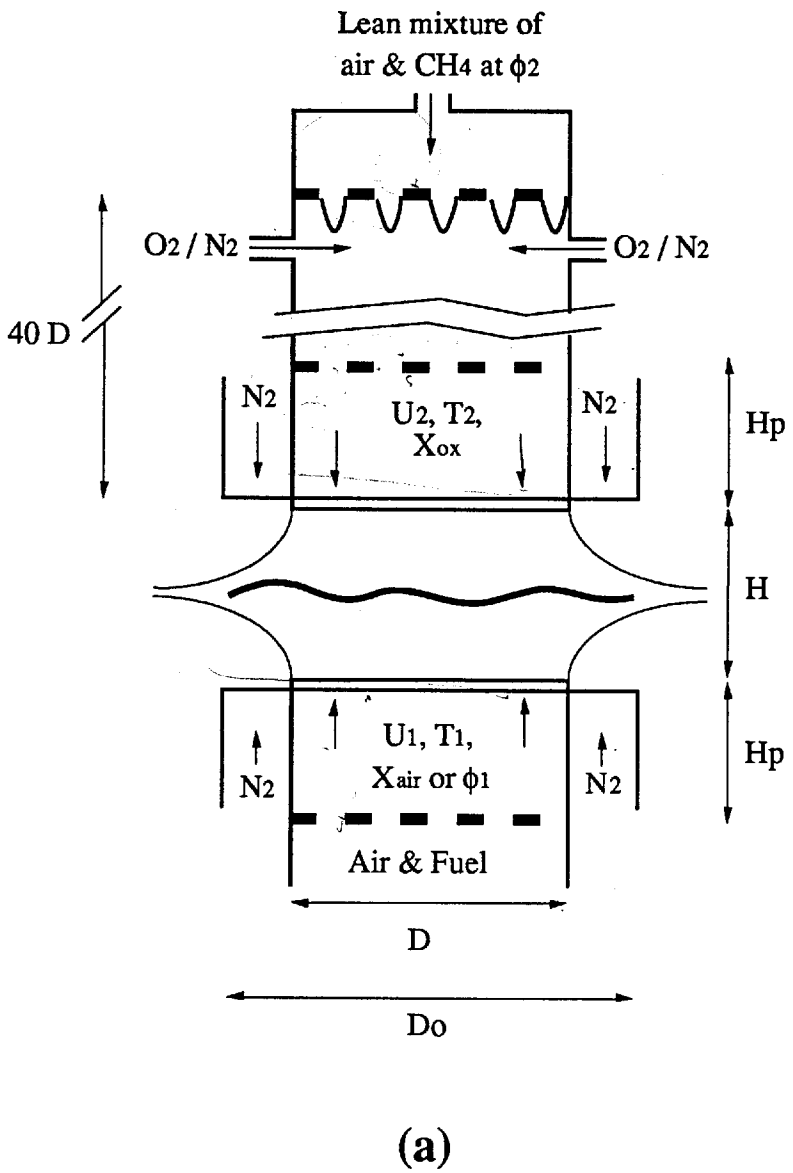


Figure 2.3 (a) The burner used for the experiments with air diluted by hot products, termed vitiated air, in some extinction experiments in Chapter 4. A laminar, premixed flame that supplies the hot products is ignited on a perforated plate inside the upper tube. (b) The arrangement used to achieve higher temperatures that those reached in (a) due to the close proximity of the "supply" flame to the exit plane.

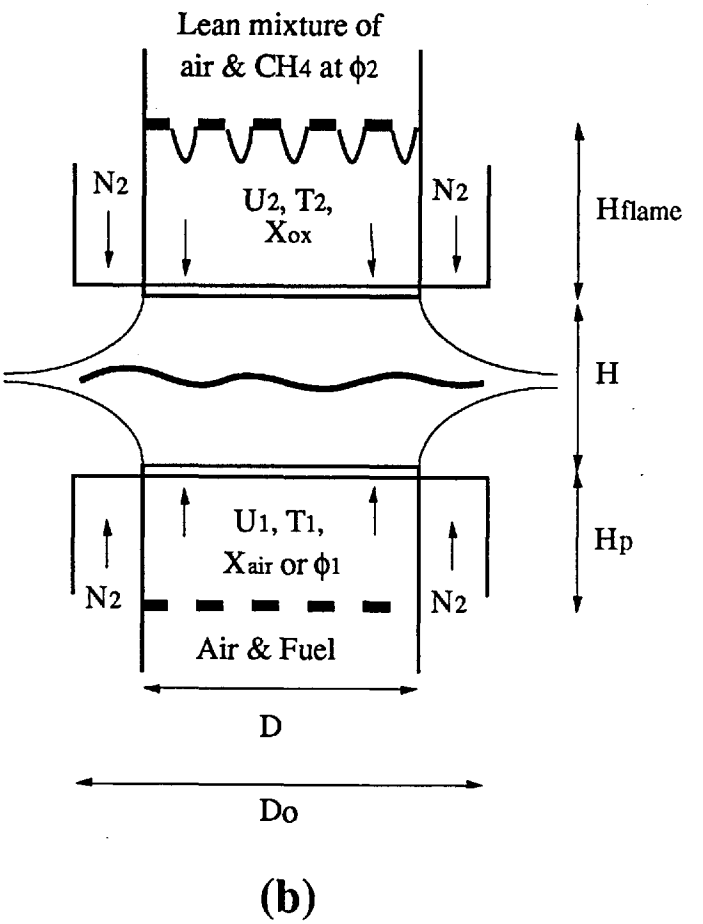


Figure 2.3 Continued and concluded.

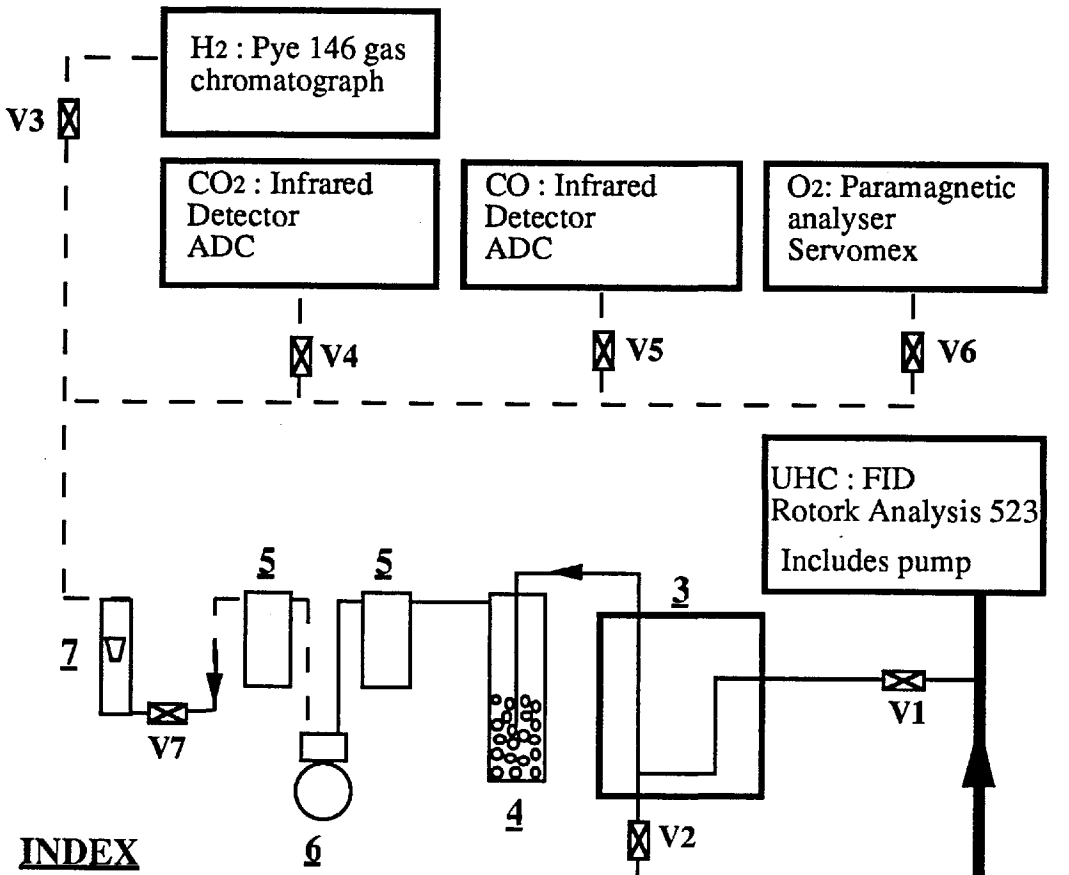


Figure 2.4 Outline of the sampling circuit showing the various drying and filtering stages, valves, and analysers.

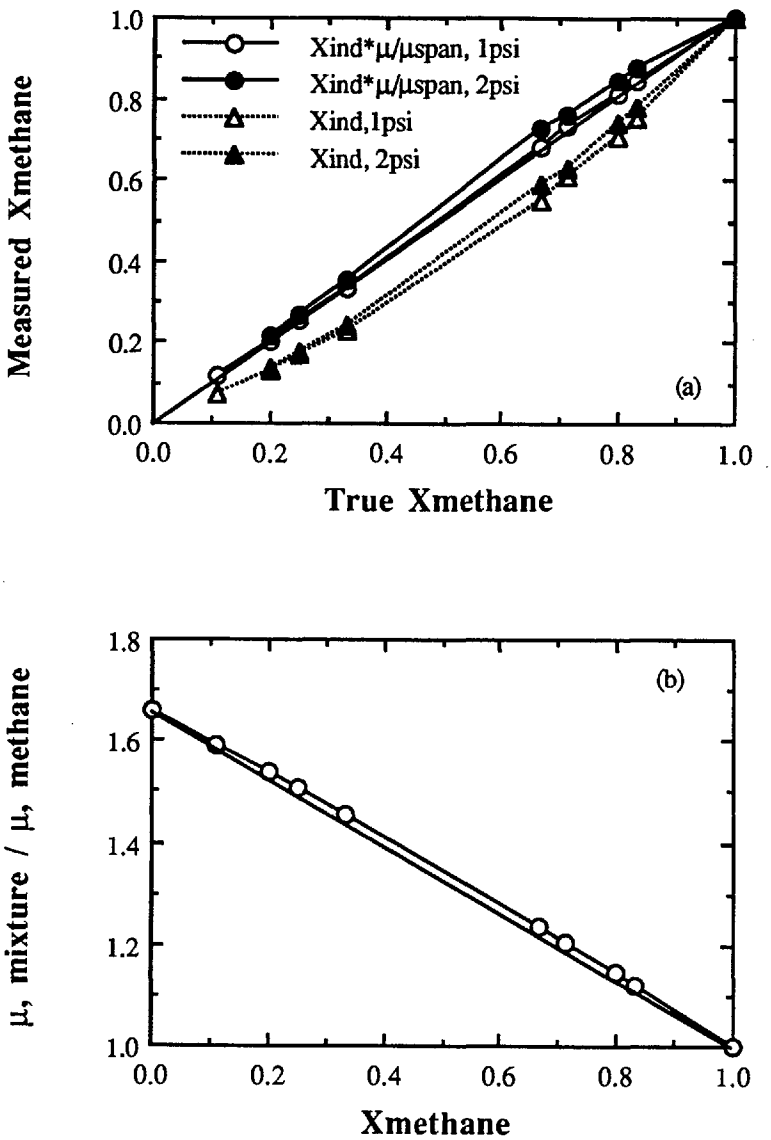


Figure 2.5 (a) The mole fraction of methane in methane–air mixtures measured by the FID without (triangles) and with (circles) subsequent correction using Eq. (2.4.1) for two different pressure settings. The horizontal axis represents the known mole fraction of methane in the mixture to within ±7.5%. The FID was calibrated with 100% methane. (b) The ratio of methane–air mixture viscosity to the viscosity of pure methane as a function of the methane volume fraction. The straight line was drawn to emphasise that the relationship is slightly non–linear.

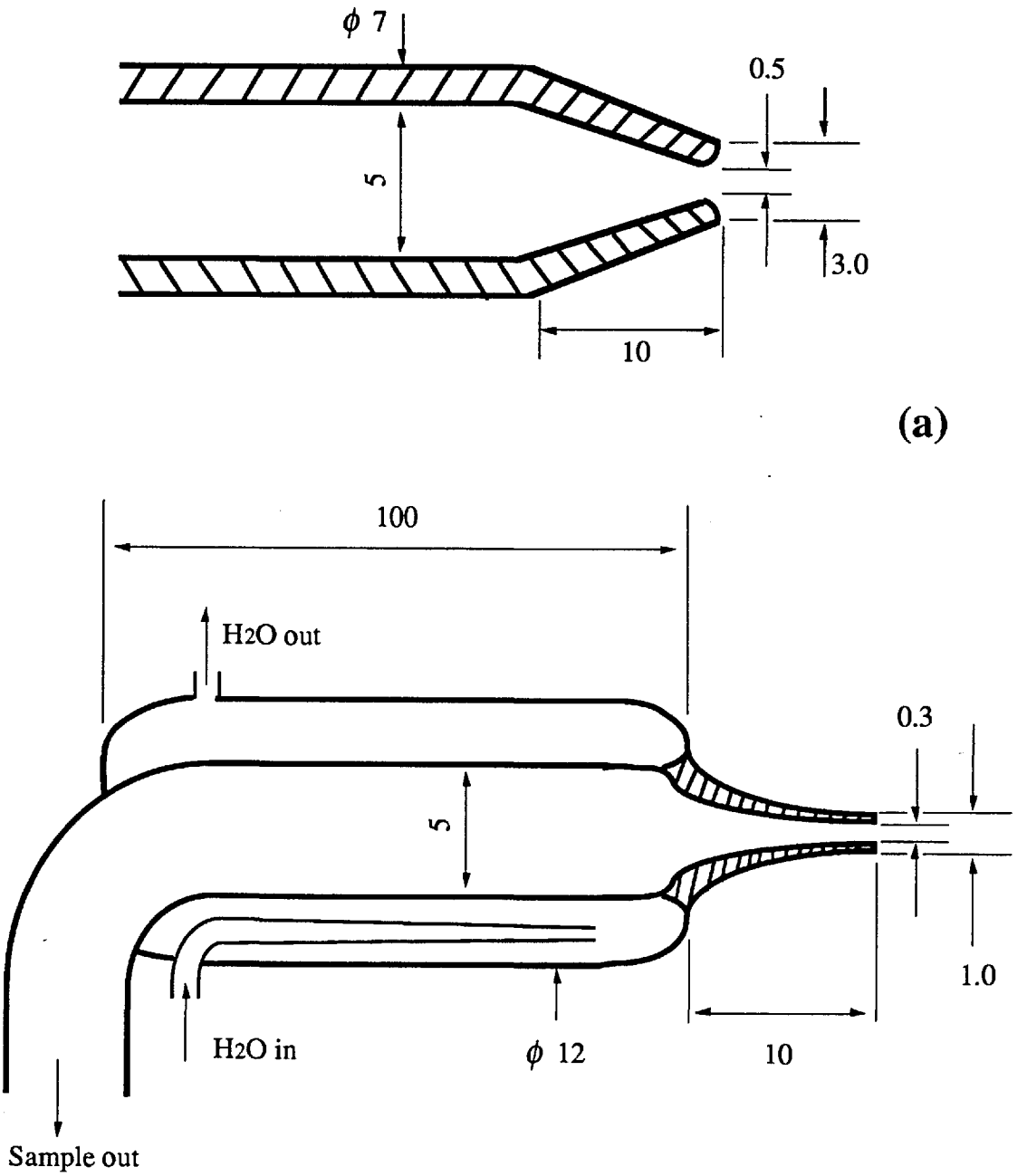


Figure 2.6 Sketches of the probes used for extracting samples from the flames. The probe in (b) was used for most of the measurements presented in this thesis.

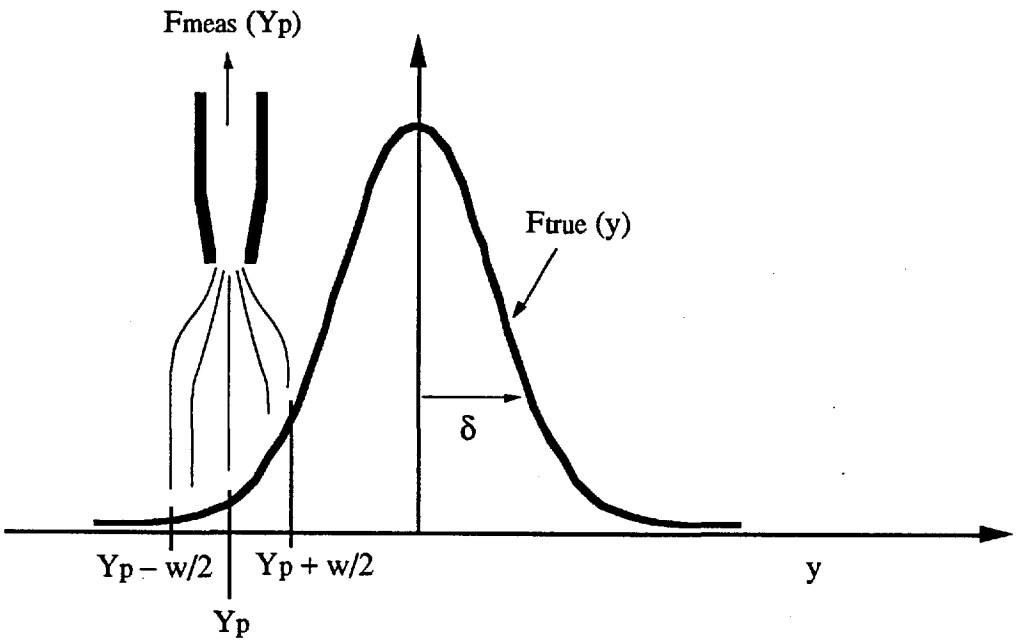


Figure 2.7 A hypothetical profile of mole fraction, F_{true}, as a function of a coordinate y. The profile has a characteristic width δ. The extracted sample from the probe at Y_p occupies a region of width w centred at Y_p and subsequent analysis of the sample is, in fact, the average over w, which leads to "spatial averaging".

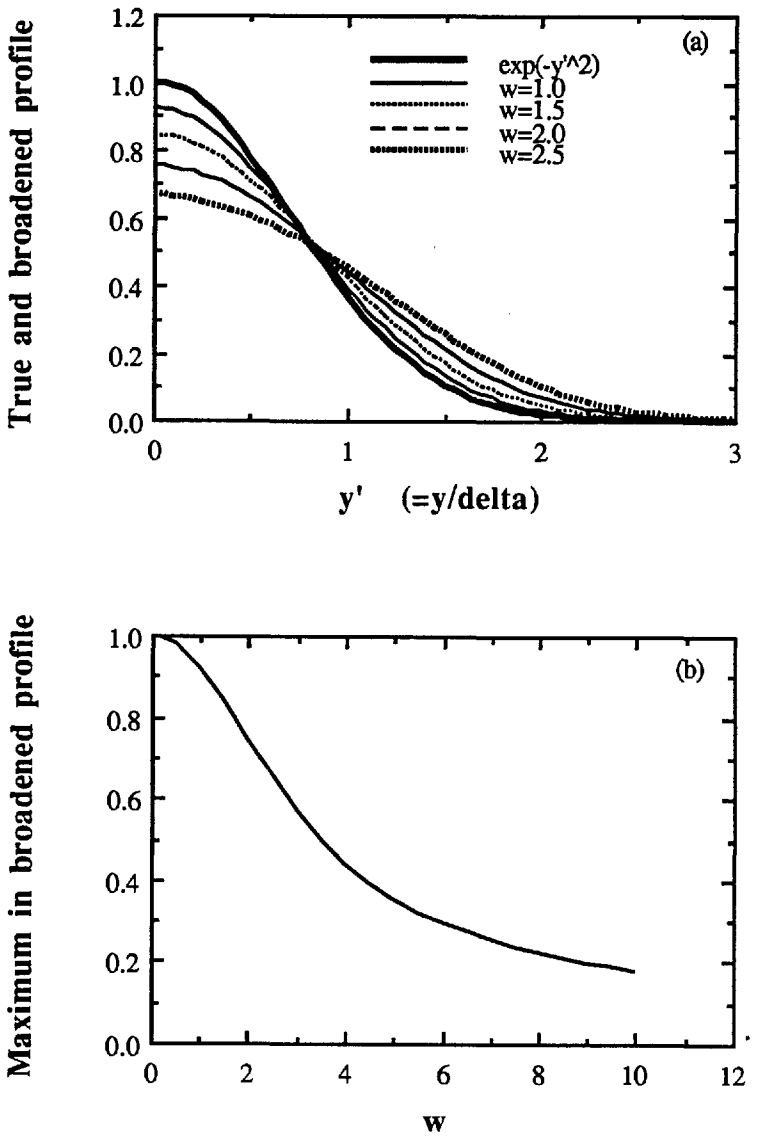


Figure 2.8 (a) Broadening of gaussian profiles $F(y')=\exp(-y'^2)$, $y'=y/\delta$, for different values of the averaging width w/δ. The broadened curves were calculated with Eq. (2.4.6) and, for simplicity, $\delta=1$. (b) The peak value of F_{meas}/F_{true} from profiles such as (a) plotted as a function of w.

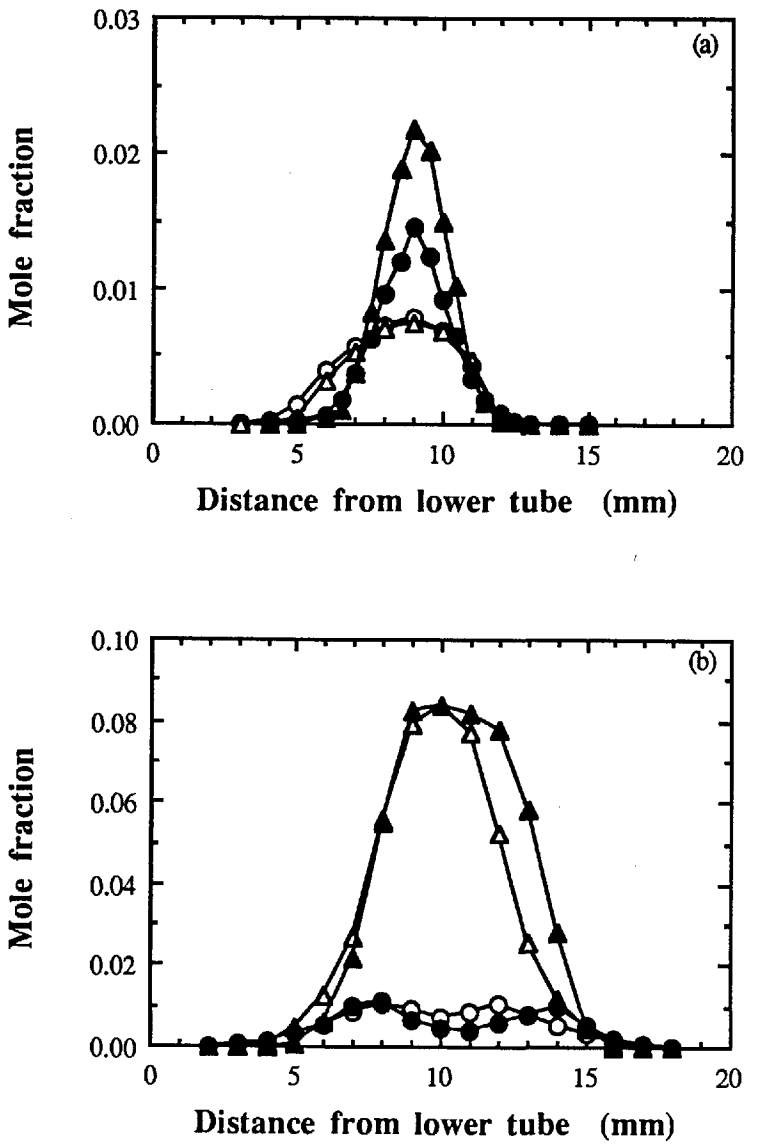


Figure 2.9 (a) The mole fractions of CO (circles) and CO_2 (triangles) in axial traverses of counterflow diffusion flames with X=0.5, H=20mm, H_p=55mm, U_1=1.91m/s, U_2=1.64m/s; the flow rates were selected such that $\rho_1 U_1^2 = \rho_2 U_2^2$ and these conditions are typical of the partially–premixed diffusion flames examined in this thesis. The open symbols correspond to measurements with the probe of Fig. 2.7a and the blocked symbols to measurements with the smaller probe of Fig. 2.7b. (b) Comparison of the measured CO and CO_2 with the two probes as in (a), but for twin premixed flames with $U_1=U_2$=1.64m/s and $\phi_1=\phi_2$=0.9. Symbols as in (a).

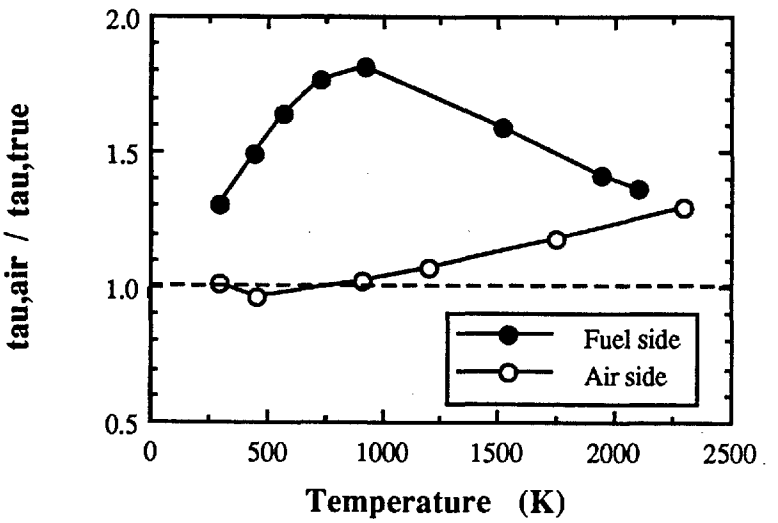


Figure 2.10 The ratio of the time constant of a 40μm wire at 1m/s based on air properties (Eq. 2.5.2 with Eq. 2.5.3) to that based on the local properties across a laminar counterflow diffusion flame calculated by Jones and Lindstedt (1988). This curve is typical for other velocities and wire diameters because the difference is mostly due to the thermal conductivity (Eq. 2.5.2), and the average value of the ratio over the temperature range from 300 to 2200K resulted in Eq. (2.5.4).

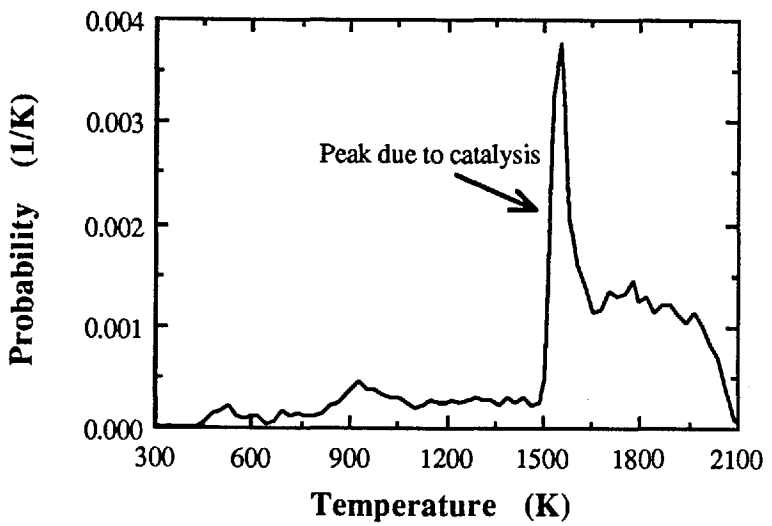


Figure 2.11 Typical probability density function (pdf) of compensated temperature at conditions of high partial premixing of the fuel stream with air (X=0.8) that shows signal contamination by catalytic effects on the wire surface. Note the unreasonable high peak at about 1500K. No surface catalysis was observed for X<0.5.

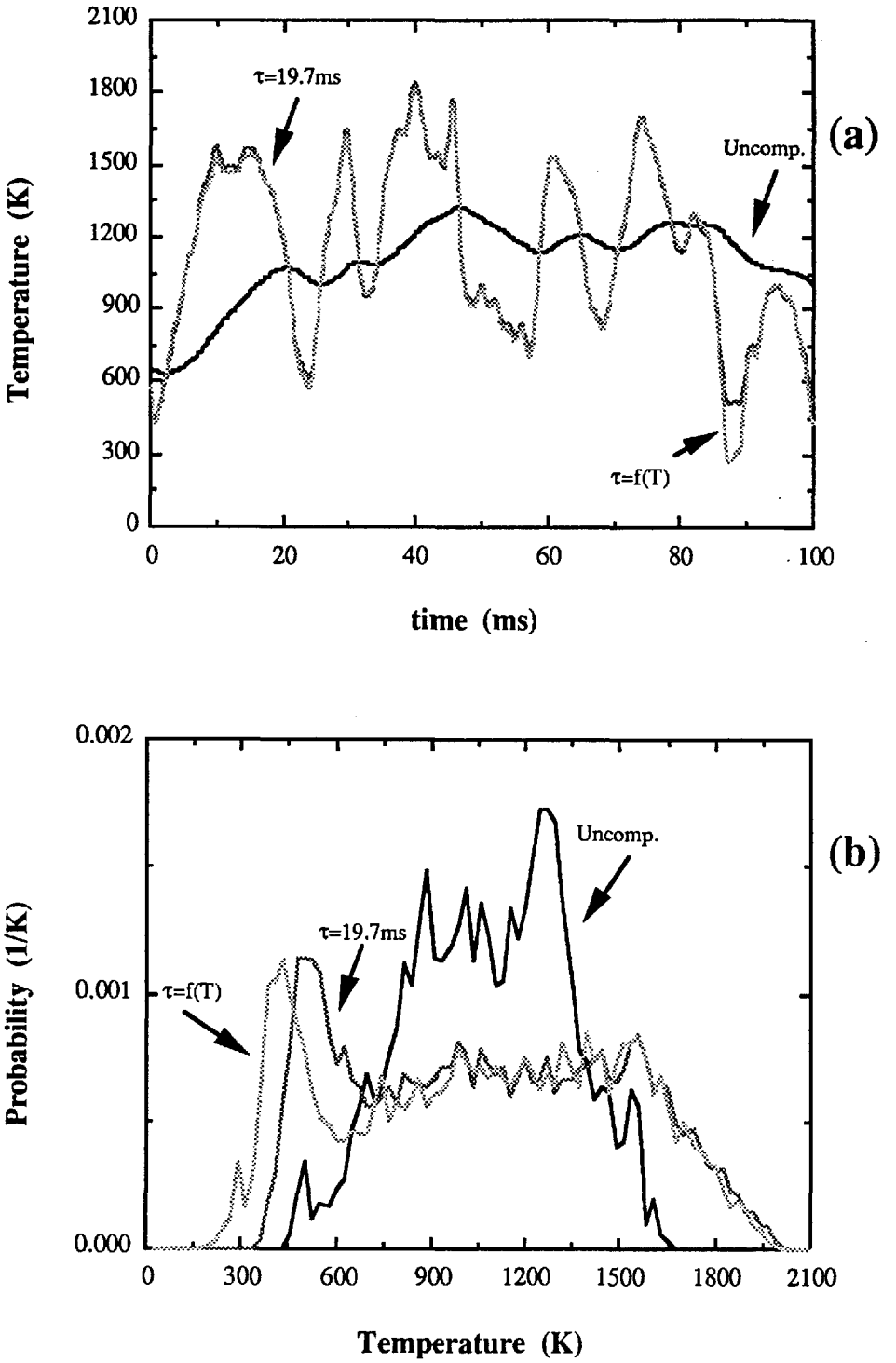


Figure 2.12 For caption see next page.

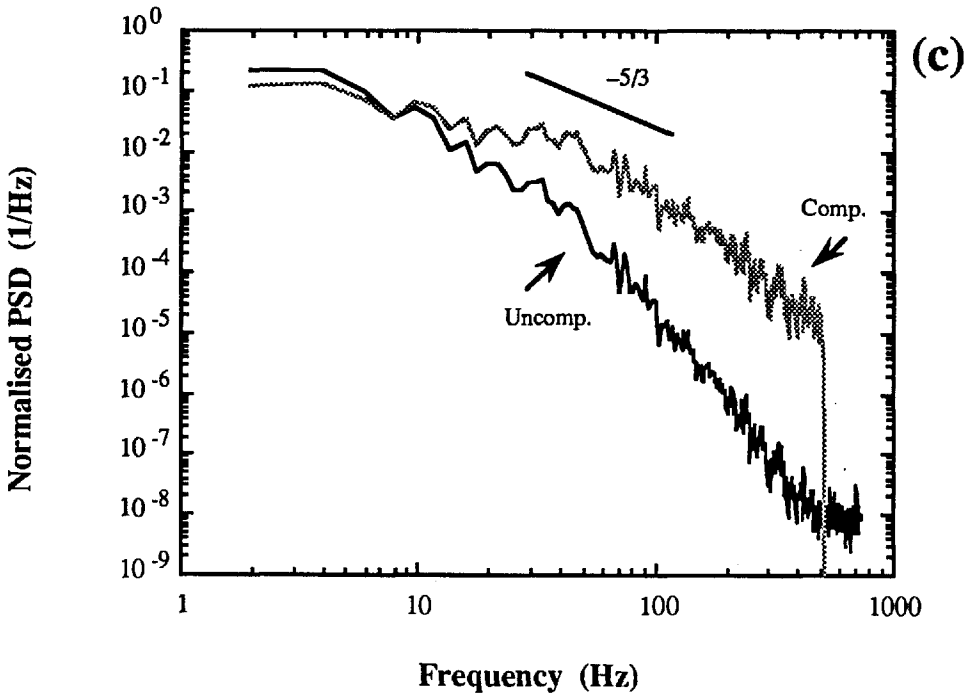


Figure 2.12 Typical temperatures measured, compensated with a constant τ_{wire} evaluated at the mean local velocity and temperature, and compensated with $\tau_{wire}=f(T)$, at the location of maximum temperature across a counterflow diffusion flame with X=0.0, H=20mm, H_p=55mm, U_1=1.34m/s, and U_2=1.0m/s at r=13mm. These measurements are typical of the temperature measurements in Chapter 3. In (a), traces of the temperatures are shown, with the associated probability density functions in (b) and frequency spectra in (c). Note that the spectrum of the compensated time series with variable time constant is not shown in (c) because it was almost indistinguishable from the spectrum corresponding to the compensated temperatures with a constant τ_{wire}.

Chapter 3. The structure of opposed jet turbulent flames

3.1 INTRODUCTION

3.1.1 The structure of this Chapter

Detailed measurements are presented in this Chapter that reveal certain unexplored features of inert and reacting opposed jet flows. In inert flows, the mixing between the two jets was examined by heating one of the jets and measuring the temperature which acted as a passive scalar (and so was a measure of the mixture fraction), and in reacting flows, the mean mixture fraction was determined by point measurements with an aspirated probe of the mean mole fractions of stable species and subsequent processing. For both inert and reacting flows, the velocity distributions were measured and the temperature was also examined in flames. These measurements provide information on the structure of opposed jet inert flows and diffusion and premixed flames and were performed for various conditions of jet separation, strength of the turbulence, bulk velocity, and for inert flows and for pure diffusion, partially premixed diffusion, and premixed flames.

In the following Section, the flow conditions used for the measurements are summarised, and in the next Sections the measurements are presented and discussed. The Chapter closes with a summary of the main findings.

3.1.2 Flow conditions and nomenclature

Varying and constant parameters

The way the present opposed jet flows are characterised was described in detail in Section 2.2 and here, the conditions for the measurements presented in this Chapter are given. The parameters that were varied are the following (with the uncertainty in the reported values in parentheses; Chapter 2): (a) the bulk velocity of each stream, U_1 for the lower (fuel) stream and U_2 for the upper (air) stream (±5%); (b) the jet separation H (±0.5mm); (c) the distance of the perforated plate form the tube exit, H_p (±1mm); and (d) the composition of the fuel stream. When the air volume fraction in the fuel stream, X, was less than 0.86, the flame was deemed "diffusion" and was characterised by X (±7.5%), and when X≥0.86, the flame was deemed "premixed" and characterised by the equivalence ratio ϕ (±0.03).

The conditions that were kept constant for all measurements are: (a) equal momentum flow rates of the two streams, i.e. $\rho_1 U_1^2 = \rho_2 U_2^2$ where ρ_1 and ρ_2 are respectively the densities of the lower and upper streams; (b) both jets were at room

temperature (293K), apart from the mixing measurements in the inert flow where the upper stream was preheated to 450K; and (c) the co–flow of nitrogen was at a bulk velocity of 0.3m/s for premixed flames and 0.5m/s for diffusion flames. For the inert measurements, air was used as co–flow at 0.3m/s (all to within ±5%).

Nomenclature and normalisations

Velocities have been normalised by the velocity U_o which was equal to the upper stream velocity, U_2. The corresponding lower stream bulk velocity was determined by the momentum flow rate balance after calculating the density ratio of the two streams. Therefore, *by definition* $U_2=U_o$, for flames $U_1=\sqrt{\rho_2/\rho_1}\,U_o$, and for inert flows $U_1=U_o$. In inert flow temperature measurements, the mixture fraction f is defined as the normalised temperature $(T_2–T)/(T_2–T_1)$ so that it is equal to unity in the cold (lower) stream and zero in the hot (upper) stream. This facilitates comparisons with the mixture fraction measured in the reacting flows. Finally, the axial coordinate z is measured from the exit of the lower jet (to within ±0.1mm relative to the first point along a traverse; ±0.5mm relative to the jet exit) and has been normalised by H when comparisons between measurements from different jet separations are made.

3.1.3 Correspondence between measurements

The location of the stagnation point, as found from repeating axial velocity traverses, had an uncertainty of about ±1mm and similar tolerances on reproducibility exist for the location of the peak temperature and CO_2 mole fraction in the flames, and for the location of the point where the mean mixture fraction takes the value 0.5 in both inert and reacting flow measurements. The origin of the uncertainty in the location of the stagnation point and the flame is traced to the uncertainties in flow metering, and has also been observed by Kostiuk (1991) and Smooke *et al.* (1986), and can be understood by using the analytical results of Seshadri and Williams (1978), who predicted that, with the nomenclature of this thesis,

$$\frac{Z_{st}}{H} = \frac{1}{1+U_2/U_1}, \qquad (3.1.1)$$

where Z_{st} is the location of the stagnation point in laminar impinging streams of equal densities measured from the stream of velocity U_1. Taking the derivative of Z_{st} with respect to velocity, say that of the upper stream U_2, suggests that a 5% increase in the bulk velocity can shift the stagnation point by about 0.3mm for a jet separation of 20mm, which is of comparable magnitude to the observed irreproducibility of the stagnation point location in the present experiments. It has been found, however, that the profiles of the species mole fractions and temperature, of the mixture fraction, and of the

velocities, are *identical* to within experimental error if *shifted* in the axial direction by a small amount (of the order of 1mm) so as to make the location of the profile peak, or the location of $\langle F \rangle$=0.5, or the stagnation point respectively coincide. Therefore, to facilitate graphical presentation, in many instances a reduced axial coordinate z^* has been defined as $z^* = z - Z_{st}$ for the velocity measurements, or $z^* = z - Z_{half}$ for the species measurements, where Z_{st} is the axial coordinate where U=0 and Z_{half} is the axial coordinate where $\langle F \rangle$=0.5.

The correspondence between the measurements of velocity, temperature, and species concentrations is as follows. For inert flows, velocity was measured only for opposed jets of equal temperature and symmetry suggests that stagnation occurs where $\langle F \rangle$=0.5, although there might be small differences between Z_{st} and Z_{half} in the measurements of mixing because of the different temperature, and therefore density, of the upper stream. Simultaneous measurements of species and temperature in reacting flows, made by placing a thermocouple in front of the sampling probe tip to within ±0.5mm in the axial direction, showed that the axial location of the peak temperature coincided with the location of the peak concentration of CO_2 and with the centre of the visible flame brush, whose position was judged by eye to within ±0.5mm and has been marked in the velocity traverses presented here[1].

The conclusions that will be drawn from the measurements are not affected by the uncertainty in the flame location because emphasis is placed on the peak value of quantities like temperature and species mole fractions which are not affected by the flame location, and because comparing flames under different bulk flow velocities is done only for differences in these velocities larger than the measurement errors. Finally, the exact flame location is unimportant for certain conclusions because they are based on aspects of the measurements that do not refer to their spatial distributions, for example by plotting the mean species concentrations against mean mixture fraction or by examining the qualitative shape of the scalar probability density functions of temperature.

[1] Researchers who might want to use the data for comparison with theoretical or numerical results should keep in mind the uncertainty in the stagnation point location in the present experiment.

3.2 INERT OPPOSED JET FLOWS

3.2.1 Background and structure of this Section

The flow of two inert turbulent impinging jets has been examined by Kostiuk *et al.* (1993a) and Mounaïm–Rousselle and Gökalp (1993) who presented a few velocity measurements but restricted attention to jet separations larger than a jet diameter; in contrast, emphasis is placed here on jet separations close to or smaller than one diameter and so the present *velocity* measurements complement those performed by other authors. The reason for the present interest is that small jet separations minimise both buoyancy effects in flames and the phenomenon of "bouncing", a term used by Kostiuk (1991) to describe an unsteady axial motion of the stagnation region that can interfere with the correct interpretation of the measurements (Kostiuk *et al.*, 1993a).

No measurements of *mixing* in impinging jets are known to the author and are needed to help interpret reacting flow measurements, and so mixing is examined here analytically and experimentally. In the next Section, the initial conditions of velocity are presented, followed by the presentation of axial traverses. Then, a theoretical model for mixing between the jets is described (Section 3.2.5), measurements of the mixture fraction are given, and the Section closes with a comparison between the theory and the experiment (Section 3.2.7).

3.2.2 Visualisation

The photograph of the light scattered from alumina particles illuminated by a laser sheet, Fig. 3.2.1, was obtained with the upper jet seeded with particles, and so the illuminated area identifies the spatial extent of the fluid originating from the seeded jet. It can be seen that the jet turns radially outwards immediately from the tube exit and that the interface between the two jets is wrinkled, with small indentations of one jet into the other (the "curl", a few mm right of the symmetry axis in the photograph). It is also evident that the lengthscale of the wrinkling is larger in the radial than in the axial direction, which is consistent with expectations of the shape of the turbulent eddies in stagnating flows (for example, Lee, 1989, and Wei and Miau, 1992, and references therein), and that a vortex is formed in the region outside the burner as the radially moving fluid entrains ambient air. The measurements to be presented later are, however, restricted to variations along the centreline and to radii less than about a jet radius, and so any influences of the co–flow or the ambient flow patterns are avoided.

3.2.3 Initial conditions

Single jet

Figure 3.2.2 shows that the mean axial velocity measured at the exit plane of a single jet (without the opposed flow) is approximately uniform for about 75% of the pipe radius with a boundary layer close to the wall of about 2mm, and that the corresponding axial turbulence intensities are uniform in the central part of the pipe and increase towards the walls, as expected[2]. The smaller intensities for the larger distance of the perforated plate (blocked triangles) indicate that the normalised turbulence intensity without the opposed flow is a function of H_p, and suggests that while keeping the bulk velocity constant, the turbulence intensity at the stagnation plane can be altered by moving the perforated plate. The turbulence intensity at the tube exit at the centreline was measured for different bulk velocities and locations of the perforated plate and Fig. 3.2.3 shows that the normalised turbulent kinetic energy

$$C_q = q' / U_o = \sqrt{(u'^2 + 2v'^2)/3} / U_o \qquad (3.2.1)$$

is largely independent of the bulk velocity for $H_p = 120$mm, while it changes by about 20% for $H_p = 55$mm from $U_o = 1$m/s to 3m/s, which are velocities typical of the experiments described here. The ratio of axial to radial intensities was about 1.1 for all the conditions measured (Fig. 3.2.4a), and Fig. 3.2.4b shows in more detail how C_q decreases with increasing distance of the perforated plate from the tube exit. In view of the much larger variation of C_q with H_p than with bulk velocity, for estimates of the turbulence under different conditions, C_q is approximated as independent of U_o and given by

$$C_q = 0.085 \text{ for } H_p = 55\text{mm, and}$$
$$C_q = 0.045 \text{ for } H_p = 120\text{mm.} \qquad (3.2.2)$$

and these values will be used throughout the thesis for making estimates of turbulence timescales and other quantities (Section 3.4.1) without resorting to the detailed measurements.

The turbulence lengthscale has not been measured, but following Kostiuk *et al.* (1989) and Cho *et al.* (1988), will be taken as the size of the hole of the perforated plate and equal to L_{turb}=4.0mm. It will be assumed that the lengthscale is the same for all flow conditions of velocity and perforated plate location based on the lengthscale

[2] The angle of the laser beams relative to the axis of symmetry of the burner for axial velocity measurements was such that the LDV control volume could not approach closer than 2mm to the exit plane of the jet.

measurements of Cho *et al.* (1988) who found small variations, but the validity of this assumption for the present flow awaits experimental verification.

Opposed jets

The mean axial velocity across the jet is not uniform when the two jets oppose each other with the velocity increasing towards the jet edge peaking close to the wall, Fig. 3.2.5, in contrast to the velocity profile in unopposed jets. This finding is consistent with measurements of Rolon *et al.* (1991) in *laminar* opposed jet flows at small jet separations and profiles like those of Fig. 3.2.5 are typical for all velocities and H_p, but not for all jet separations. Figure 3.2.6 includes radial traverses of the axial velocity at the exit plane of jets opposed at H=25mm, a separation larger than the 20mm for the data of Fig. 3.2.5, and shows that the velocity profile is more uniform, i.e. approaches that of the single jet flow. The fact that the axial velocity increases towards the jet edges as the stagnation point is approached is also evident, but not discussed, in the measurements of Kostiuk (1991; Fig. 5.9). A possible explanation for this non–uniformity is that the adverse pressure gradient along the centreline is larger than at finite radii because of the negative radial pressure gradient and so the flow along the centreline is decelerated by a larger amount; at small jet separations, the adverse pressure gradient affects the flow *inside* the tubes and so the exit velocity profile is non–uniform.

The r.m.s. values at the exit of the opposed jets are higher than at the single jet by about 20%, Fig. 3.2.5, partly due to production due to shear associated with the velocity gradients in the non–uniform axial velocity profiles, and partly due to the stretching associated with the stagnation, since the axial velocity profiles have a non–zero axial gradient even at the jet exit (see below).

3.2.4 Velocity traverses

Measurements of the mean and r.m.s. velocities in inert opposed jet flows are presented in this Section to show the effects of the stagnation on the turbulence and on the mean flow field. The mean axial velocities follow, to a certain extent, their radial distributions at the exit plane of the jet at all subsequent axial locations and the axial r.m.s. velocities are uniform across the jet, Fig. 3.2.6. Although the mean axial velocity may not be uniform across the whole of the jet, depending on the jet separation, it is uniform for a small region around the centreline, and thus emphasis is placed below on centreline variations, in accordance with theoretical analyses of opposed jet flows.

The mean axial velocity along the centreline, Fig. 3.2.7a, decreases to zero at a point half–way between the two jets, as expected, and the bulk velocity gradient is not far from the value estimated by the potential flow model, i.e. $2U_o/H$, but curvature exists in the profile so that the axial velocity gradient is not uniform across the flow, in agreement with the theoretical prediction of Champion and Libby (1993). It is also

evident that the mean velocity is not affected by the turbulence because the two velocity profiles in Fig. 3.2.7a are almost identical, although they correspond to different turbulence intensities (H_p=55mm : high, H_p=120mm: low turbulence; Eq. 3.2.2). Figure 3.2.7b shows that the axial velocity fluctuations are higher for H_p=55mm for all axial locations, as expected from the measurements of initial conditions in the single jet (Fig. 3.2.4), and also shows that the turbulence intensity peaks at the stagnation region. The axial velocity is close to zero at all radii at the stagnation region (Fig. 3.2.8a) and the radial velocity increases linearly with radius, and the corresponding r.m.s. values (Fig. 3.2.8b) are uniform with radius. Therefore in the discussion of the turbulence intensities in the opposed jet flow it is sufficient to consider only the centreline variations.

The turbulence increases from its value at the jet exit (Figs. 3.2.7b and 3.2.9b) and this is consistent with expectations from arguments of vortex stretching (for example, Tennekes and Lumley, 1972; Britter *et al.*, 1979) in the straining field of the opposed jet flow. The independence of the mean flow from the turbulence suggested in Fig. 3.2.7 implies that the mean and the turbulent field can be described independently, for example by assuming a mean flow field and considering the turbulence evolving in it without influence of the latter on the former, as done, for example in one of the models in Bray *et al.* (1991).

The effect of the jet separation on the mean and r.m.s. velocities is presented in Fig. 3.2.9. Centreline traverses of axial velocity for H=20, 25, and 30mm are plotted against the normalised axial coordinate $\zeta = 2\,(z - Z_{st})/H$, which thus takes the value -1 in one jet, zero at the stagnation point, and 1 in the other jet, to facilitate comparison with the theoretical predictions of Champion and Libby (1993). These authors predicted that the axial velocity along the centreline varies as

$$U/U_o = 2\,\zeta\,(1 - 0.5\,\zeta) \qquad (3.2.3)$$

after assuming that the velocity of the flow exiting the jets was radially uniform and equal to U_o ("plug flow"). The fact that there is close agreement between the measurements and the prediction for H=25mm, but less so for H=20mm, indicates that approximating the flow at the jet exit as plug flow is valid for jet separations about equal to the jet diameter, and is consistent with the radial variations of axial velocity at the different jet separations (Figs. 3.2.5 and 3.2.6) that showed that the centreline velocity may be smaller than the bulk velocity for small H.

Both the axial and radial r.m.s. velocities increase as the stagnation point is approached, peak there, and the turbulence is very anisotropic with the axial r.m.s. about twice as the radial values, Fig. 3.2.9b. Opposite trends are found with jet separation for the two components: the axial r.m.s. values are higher at H=30mm than at 20mm, but the radial are smaller at the large separation, the latter trend consistent with the

expectation that the turbulence intensity increases with the bulk flow stretch rate. It is possible, therefore, that the axial fluctuations respond not only to stretching, but are affected by another mechanism as well, and a possibility that would give rise to high measurements of the axial turbulence component is examined next.

The velocity measurements presented so far were performed with both jets seeded with LDV scattering particles. Figure 3.2.10 shows that the measured mean and r.m.s. axial velocities are smaller close to the stagnation point when only one jet has been seeded, while the r.m.s. *radial* velocity is identical with both types of seeding[3]. This implies that the measured increase in the axial turbulence is, in addition to the stretching, partly due to sampling fluid from either jet but with mean velocities of opposite sign; this effect is not present in the radial r.m.s. velocities because both fluids (upper and lower) have identical mean radial velocities (which is equal to zero along the centreline). The corresponding probability density functions (pdf) for the axial and radial velocities at a location just before the stagnation point are presented in Fig. 3.2.11, which shows that the radial velocity pdfs are identical with either type of seed, but that the axial velocity pdf is broader with both jets seeded. The finding that part of the measured axial r.m.s. is due to conditional sampling of fluid from the two jets, and not only due to stretching, implies that care is needed in estimating the stretch rates that flames experience in the opposed jet flow from velocity measurements.

The present results are consistent in most respects with those of Kostiuk *et al.* (1993a) and Mounaïm–Rousselle and Gökalp (1993) and extend these to small jet separations. An important difference is that small jet separations introduce a non–uniform axial velocity profile at the jet exit and so the flow there does not resemble plug flow, as most theoretical models conveniently assume, and a way to overcome possible difficulties associated with this departure from plug flow will be discussed in Section 3.4.5.

3.2.5 Mixing – Theoretical results

In this Section an analysis for the mean mixture fraction, F, and its r.m.s. fluctuations, f', along the centerline of the stagnation flow geometry is presented. The analysis is used for predicting the mixing layer width as a function of the bulk velocity, turbulence intensity, and jet separation, and the corresponding f' which are needed for interpreting reacting flow measurements. An additional usefulness of this analysis is that it leads to estimates of the mean turbulent scalar dissipation rate, χ, which is an important quantity for determining the mean reaction rates in turbulent diffusion flames (Bilger,

[3] Of course, for the case of one jet seed, measurements could be made only so far from the seeded jet exit because there was no observable LDV signal inside the unseeded jet.

1980) and also flame structure and extinction, as will be discussed in Sections 3.4.1, 3.4.5, and 4.3.4.

Formulation

The governing equations for the mean mixture fraction F and for its fluctuations f are given for axisymmetric, constant density flow as

$$V\frac{\partial F}{\partial r} + U\frac{\partial F}{\partial z} = D_{mol}\nabla^2 F - [\frac{\partial \langle u_r f\rangle}{\partial r} + \frac{\langle u_r f\rangle}{r} + \frac{\partial \langle u_z f\rangle}{\partial z}], \quad (3.2.4)$$

$$\begin{aligned} V\frac{\partial \langle f^2\rangle}{\partial r} + U\frac{\partial \langle f^2\rangle}{\partial z} &= D_{mol}\nabla^2\langle f^2\rangle \\ &\quad - 2[\langle u_r f\rangle\frac{\partial F}{\partial r} + \langle u_z f\rangle\frac{\partial F}{\partial z}] \\ &\quad - [\frac{\partial \langle u_r f^2\rangle}{\partial r} + \frac{\langle u_r f^2\rangle}{r} + \frac{\partial \langle u_z f^2\rangle}{\partial z}] \\ &\quad - \chi, \end{aligned} \quad (3.2.5)$$

where $\nabla^2 = \partial^2/\partial r^2 + 1/r\,\partial/\partial r + \partial^2/\partial z^2$, D_{mol} is the molecular diffusion coefficient, z is measured from, and in the direction normal to, the stagnation (symmetry) plane[4], r is the radial coordinate, $\langle\ \rangle$ denote time–averaged quantities, and χ is the mean turbulent scalar dissipation rate, defined by $2\,D_{mol}\langle\partial f/\partial x_i\rangle^2$.

The molecular diffusion terms are ignored and a gradient–transport model is employed for the turbulent fluxes of the mixture fraction and for the third–order correlations in the fluctuations equations, so that

$$\begin{aligned} \langle u_r f\rangle &= -\frac{\nu_t}{\sigma_f}\frac{\partial F}{\partial r}, \\ \langle u_z f\rangle &= -\frac{\nu_t}{\sigma_f}\frac{\partial F}{\partial z}, \\ \langle u_r f^2\rangle &= -\frac{\nu_t}{\sigma_f}\frac{\partial \langle f^2\rangle}{\partial r}, \text{ and} \\ \langle u_z f^2\rangle &= -\frac{\nu_t}{\sigma_f}\frac{\partial \langle f^2\rangle}{\partial z}, \end{aligned} \quad (3.2.6)$$

where σ_f is the turbulent Schmidt number and the eddy viscosity ν_t is taken to be equal to

$$\nu_t = C_\mu\, q'\, L_{turb}, \quad (3.2.7)$$

[4] Only for this Section; for the rest of the thesis, z is measured from the exit of the lower jet.

with q' being the r.m.s. turbulence intensity and L_{turb} a characteristic turbulent lengthscale. The mean scalar dissipation rate is modelled as

$$\chi = 2 \frac{q'}{L_{turb}} f'^2 , \qquad (3.2.8)$$

where f' is the r.m.s. value of the mixture fraction fluctuations (= $\langle f^2 \rangle^{1/2}$) (Jones and Whitelaw, 1982). Equations (3.2.4) and (3.2.5), together with the models in Eqs. (3.2.6 – 3.2.8) and suitable boundary conditions for F and f', form a closed system which requires external input about the mean axial and radial velocities and for the eddy viscosity from a solution of, or appropriate assumptions about, the velocity field.

Following Bray *et al.* (1991), the mean velocities are approximated for constant density stagnation point flow by the potential flow solution which gives

$$U = -2 S z , \qquad (3.2.9)$$

$$V = S r , \qquad (3.2.10)$$

where S is one half of the bulk strain rate, uniform everywhere. It is also assumed that q' and L_{turb} are approximately constant and depend on the turbulence external to the mixing layer formed between the two opposed flows, and so the eddy viscosity is assumed to be constant throughout the mixing layer. The bulk flow strain rate is determined from the bulk velocity, U_o, and the separation between the two nozzles, H, and is given by

$$S = U_o / H. \qquad (3.2.11)$$

The assumptions in Eqs. (3.2.9), (3.2.10), and (3.2.11) for the mean velocities and the assumption of a constant eddy viscosity are not substantiated by the velocity measurements presented in Section 3.2.4 which show that the bulk strain rate is not uniform and that the turbulence intensity changes from its value at the jet exit; they facilitate, however, the analysis of the mean mixing field and the r.m.s. of the mixture fraction without resorting to a detailed calculation of the velocity field, and are accurate if the mixing layer is relatively thin, because close to the stagnation plane, around which the mixing layer is located, the strain rate and turbulent intensities do not change much. More discussion on the justification of these assumptions is given in Section 3.2.7.

With these simplifications, the governing equations for the mean mixture fraction and its fluctuations along the stagnation streamline reduce to ordinary differential equations and become

$$\frac{\nu_t}{\sigma_f}\frac{d^2F}{dz^2} + 2\,S\,z\frac{dF}{dz} = 0\,, \tag{3.2.12}$$

and

$$\frac{\nu_t}{\sigma_f}\frac{d^2(f'^2)}{dz^2} + 2\,S\,z\frac{d(f'^2)}{dz} + 2\frac{\nu_t}{\sigma_f}\left(\frac{dF}{dz}\right)^2 - 2\,\frac{q'}{L_{turb}}\,f'^2 = 0\,. \tag{3.2.13}$$

The axial coordinate is normalised by a reference lengthscale, Z^*, which is characteristic of the mixing layer width and given by

$$Z^* = \left(\frac{\nu_t/\sigma_f}{S}\right)^{1/2}, \tag{3.2.14}$$

which results naturally in Eq. (3.2.12) after dividing both terms by (ν_t/σ_f). A non–dimensional distance from the stagnation point is defined by

$$\eta = z/Z^* \tag{3.2.15}$$

and also let

$$g = \frac{1}{2}\,f'^2\,. \tag{3.2.16}$$

Then Eqs. (3.2.12) and (3.2.13) become

$$\frac{d^2F}{d\eta^2} + 2\,\eta\frac{dF}{d\eta} = 0 \tag{3.2.17}$$

and

$$\frac{d^2g}{d\eta^2} + 2\,\eta\frac{dg}{d\eta} + \left(\frac{dF}{d\eta}\right)^2 - \alpha\,g = 0\,, \tag{3.2.18}$$

where

$$\alpha = \frac{2\,q'}{L_{turb}S} = 2\frac{q'}{U}\frac{H}{L_{turb}}\,. \tag{3.2.19}$$

The parameter α can be interpreted as the ratio of the large–eddy turbulent to the bulk flow strain rate or, equivalently, as the ratio of the mean flow timescale to the turbulent

timescale, and plays a crucial role in determining the r.m.s. of the mixture fraction, as will be shown below. The boundary conditions for Eq. (3.2.17) are

$$F(-\infty) = 1, \text{ and}$$
$$F(\infty) = 0 , \qquad (3.2.20)$$

and for Eq. (3.2.18),

$$g(\infty) = g(-\infty) = 0 . \qquad (3.2.21)$$

Equation (3.2.17) subject to boundary conditions (3.2.20) is identical to that describing mixing in laminar opposed jet flow, but with a turbulent transport coefficient instead of a molecular one appearing in the reference length used for normalising the axial coordinate, Eq. (3.2.14). It has been solved by Spalding (1961) (see also Liñan, 1974) to give

$$F(\eta) = \frac{1}{2} [\, 1 - \mathrm{erf}(\eta) \,] , \qquad (3.2.22)$$

plotted in Fig. 3.2.12a, which shows that a measure of the width of the mixing layer, defined as the axial distance between F=0.01 and F=0.99, is about 3 reference lengthscales Z^*. From Eqs. (3.2.7), (3.2.14) and (3.2.19),

$$\frac{Z^*}{L_{turb}} = \sqrt{C_\mu / 2\sigma_f}\ \ \alpha^{1/2} , \qquad (3.2.23)$$

which shows that the mixing layer width depends *only* on the turbulence lengthscale and on the parameter α. The latter parameter can be interpreted as the ratio of the turbulent strain rate to the mean flow strain rate and so Eq. (3.2.23) shows that, consistent with our intuition, intense turbulence increases the mixing layer width and a high mean strain rate decreases it. Equations (3.2.22) and (3.2.23) are the first important results of this analysis and describe the mean mixture fraction profile across the mixing layer in the opposed jet flow and give the dependence of the layer width on the flow conditions through the value of the parameter α. In addition, the solution for the mean mixture fraction is necessary for evaluating the production term in the fluctuations equation.

Using Eq. (3.2.22) to evaluate $dF/d\eta$ and substituting in Eq. (3.2.18), the final form of the modelled equation for the mixture fraction fluctuations becomes

$$\frac{d^2g}{d\eta^2} + 2\eta \frac{dg}{d\eta} + \frac{1}{\pi} \exp(-2\eta^2) - \alpha\, g = 0 , \qquad (3.2.24)$$

subject to the boundary conditions expressed by Eq. (3.2.21). Before continuing with the description of the solution of this equation, note that it depends *only* on the parameter α. This is the second important result of the present analysis and shows that the mixture fraction fluctuations will depend on the flow conditions only through the value of the ratio of the turbulent strain rate to the mean flow strain rate, Eq. (3.2.19), and therefore with appropriate choice of initial turbulence intensity and lengthscale and of the bulk strain rate, f' in the opposed jet flow can be controlled.

Physical intuition suggests that solutions for g have to be symmetric in η in view of the symmetry of the production term and of the mean flow, and of the decay of g on both sides of the mixing layer. Therefore for the numerical results presented in the next Section, integration of Eq. (3.2.24) started at $\eta = 0$ where $dg/d\eta$ was set equal to zero, and terminated at a large, but finite, value of η where g was set equal to 0. Numerical solution of Eq. (3.2.24) was performed by an adjustable step size, fifth–order Runge–Kutta routine from the MATLAB software package on an Apple Macintosh.

Numerical results

Here, results obtained from solving Eq. (3.2.24) for different values of α are presented. Figure 3.2.12b shows that the solutions obtained for different values of α decay towards zero at large η, as required, and that the value of f' at $\eta = 0$, i.e. the plane of symmetry, decreases with increasing α, and Fig. 3.2.13a shows the latter trend in more detail. The limiting case of $\alpha = 0$ refers to an unrealistic situation without any scalar dissipation and there the scalar fluctuations obtain their maximum possible value. The magnitudes of the diffusion, convection, production, and dissipation terms in Eq. (3.2.24) are plotted against η in Fig. 3.2.14; it is evident that for large α the production of f' is mostly balanced by the dissipation with the diffusion and convective terms being relatively small, while for small α the dissipation term becomes negligible, and this explains the increase in f' with decreasing α in Fig. 3.2.13a.

The scalar dissipation rate can also be written as

$$\chi = S \alpha f'^2 , \qquad (3.2.25)$$

by combining Eqs. (3.2.8) and (3.2.19), and Fig. 3.2.13b shows that the maximum value of the scalar dissipation rate across the mixing layer (at $\eta = 0$) made dimensionless with the bulk flow strain rate increases with α and approaches the value of the production rate at large α. The mean scalar dissipation rate therefore increases with an increase in the *turbulent* strain rate q'/L_{turb}, as seen from Eq. (3.2.8), and with an increase in the *bulk* strain rate U_o/H (Eq. 3.2.25), provided the turbulence intensity q' is proportional to U_o, which is an experimentally confirmed expectation (Fig. 3.2.3). A

physical justification is that as U_o increases, q' increases proportionately and thus χ increases, and also that as H decreases, the mean mixture fraction gradient increases hence increasing f'; Eq. (3.2.8) then shows that the scalar dissipation rate increases.

These results will be used in Chapter 4 to estimate the scalar dissipation rate under extinction conditions of diffusion flames and the results for F and f' will be compared in Section 3.2.7 with measurements, to be presented next.

3.2.6 Mixing – Experimental results

Temperature measurements were performed with numerically–compensated 25μm–diameter thermocouples in the inert opposed jet flow of cold air impinging on air preheated at a temperature $T_2 = 450K$ to examine the mean and fluctuations of the temperature, which "tags" one of the jets and thus gives information on the mixing of the two jets. The flow rates of the two jets were balanced so that the momentum flow rates were equal, i.e. $U_1=\sqrt{\rho_2/\rho_1}\,U_2$, so that $U_1 \approx 0.80\,U_2$. In most graphs shown below, the measured temperatures have been normalised so as to give the mixture fraction $f = (T_2–T)/(T_2–T_1)$ as unity in the cold jet and zero in the hot jet.

Contours of the mean temperature across the flow, Figure 3.2.15, show that the mean temperature is uniform in the radial direction for all axial locations for $r \leq 14mm$ and so the mean mixture fraction depends only on the axial location, at least for radii smaller than the jet radius; it is sufficient therefore to consider the axial variations of mixture fraction along the centreline. This finding also justifies the assumption in theoretical descriptions of opposed jet flows (Section 3.2.5; Bray *et al.*, 1991) that the radial variations of scalar quantities are negligible, and suggests that measurements of scalar quantities in flames (Section 3.3) may be performed off–axis.

Figure 3.2.16a shows that, under conditions of equal momentum flow rates of the two jets, the temperature rise from cold to hot occurs closer to the symmetry plane (z=10mm) than under conditions of equal velocity because in the latter case the hot stream has a lower density. However, if these profiles are shifted by their respective distance from the point where the mixture fraction is equal to 0.5 (i.e. the mid–point of the temperature rise), they become almost indistinguishable (Fig. 3.2.16b). Since even such large misbalances between the two flow rates as when the densities are unequal and the velocities equal do not have any effect on the mixing layer except for its position, it may be concluded that comparisons between mixing layers under different flow conditions can be done by shifting the profiles in the axial direction without loss of accuracy.

The width of the mixing layer increases with jet separation and decreases as the turbulence weakens (Figure 3.2.17), and the r.m.s. values peak at the location of $\langle F\rangle=0.5$, also the location of the steepest mean gradient, decrease on both sides of the

mixing layer, and are smaller for the weak initial turbulence. Note that the measurement uncertainty involved in the mean values is negligible, while for the r.m.s. is about ±15% (Section 2.5.7). Other measurements (not shown here) show that the mixing layer width does not depend on the bulk flow velocity for the same H_p, and these results for the mean mixture fraction are in agreement with the theoretical predictions of Section 3.2.5[5].

The probability density functions associated with the measurements of Fig. 3.2.17 are presented in Figs. 3.2.18 and 3.2.19 for strong and weak initial turbulence respectively. For both cases (and for all other conditions measured), the pdfs across the mixing layer were bimodal with peaks corresponding to the initial cold and hot temperatures and with the relative heights of the peaks changing with axial location, so that the mean values depended on which peak was highest. The bimodality of the pdfs is consistent with the structure of the time trace of the mixture fraction (Fig. 3.2.20a), which shows sharp transitions between cold and hot values, with the temperature spending little time at intermediate values. The frequency of these transitions is higher for the case with H_p=55mm (strong turbulence) than for weak turbulence, and examination of the associated frequency spectra (Fig. 3.2.20b), which are flat initially and decay with a slope close to –5/3 after a roll–off frequency that is smaller for weaker turbulence, also implies that the frequency of these transitions follows the turbulence intensity.

In more detail, Fig. 3.2.21b shows that the frequency, Ω_{cross}, of crossing the value f=0.5, found from examining time series as in Fig. 3.2.20a measured in the axial location corresponding to $\langle F \rangle$=0.5, is higher for strong turbulence than for weak turbulence by a factor of about two, which is close to the ratio between the initial q'/U_o for the two perforated plate locations (Eq. 3.2.2; Fig. 3.2.3). Therefore, the crossing frequency follows the inverse of the turbulence timescale. Also, Fig. 3.2.21 shows that Ω_{cross} increases with radius and that the corresponding r.m.s. values of the mixture fraction remain unchanged with radius and for the two turbulence conditions (Fig. 3.2.21a). Contours of f' and Ω_{cross} (Fig. 3.2.22) show that although the mean and r.m.s. values are uniform with radius, the crossing frequency is not; recall that the axial and radial turbulence intensities did not vary with radius (Figs. 3.2.6 and 3.2.8), and therefore the frequency of occurrence of the transitions between cold and hot temperatures does not depend only on the turbulence, but on the radial location as well.

A possible physical description, motivated by the results presented in the previous paragraphs concerning the almost square–wave structure of the mixture fraction time trace and the correspondence between the scalar and the velocity timescales, suggests that the two jets mix on the molecular level at thin interfaces that are randomly

[5] It will be shown in Section 3.4.2 that the mixing under reacting and inert conditions is identical and that under reacting flow conditions the mixing layer is not affected by the bulk velocity, giving thus further evidence for the agreement between theory and experiment.

convected by the turbulence past the measurement point and that these interfaces always separate fluids with temperatures equal to those of the two jets. It is expected that these interfaces, if allowed enough time in the flow, will wrinkle and "roll–over" (see the "curl" in Fig. 3.2.1) so that at large radii, the frequency of encountering these interfaces will increase, and so the measurements in Figs. 3.2.22 are explained. In Section 3.4.6 a more extensive discussion of this conceptual picture of mixing is given that includes the implications of the present mixing measurements for modelling.

3.2.7 Mixing – Comparison of experiment with theory

The measurements in Fig. 3.2.17 indicated that the width of the mixing layer is independent of bulk velocity but decreases with decreasing turbulence intensity; both these trends are predicted by Eq. (3.2.22) in conjunction with the measured (and assumed) independence of q'/U_o on U_o, and so the model performs well in predicting the qualitative dependence of the mean scalar field on the flow conditions. However, the agreement is less satisfactory for the fluctuations. Equations (3.2.24) shows that f' depends *only* on the parameter α and numerical solutions showed that f' decreases with increasing α because the scalar dissipation rate (the last term in the l.h.s. of Eq. 3.2.24) increases with α while the other terms (production, diffusion, and convection) do not. In the context of the experiments presented here, α depends on H_p (because this affects q'/U_o), on H, and on L_{turb}. For a jet separation of H=20mm, H_p=55mm has α=0.85 (because q'/U_o=0.085; Eq. 3.2.2) and H_p=120mm has α=0.45, so that the theoretical model predicts that the r.m.s. fluctuations increase with decreasing turbulence intensity (Fig. 3.2.12), contrary to the experiment (Fig. 3.2.17; but note that the measurement uncertainty in Fig. 3.2.17b is almost as large as the difference in the curves). Finally, the model predicts slightly higher values of f' than the experiment for the most common case used in this thesis (H=20mm, H_p=55mm, giving α=0.85), and some possible reasons for these discrepancies are explored below.

The velocity measurements showed that q'/U_o changes from its assumed value at the exit plane of the jet to a larger value around the stagnation region, but it is also evident that the variation of q'/U_o around the mixing layer is not large; therefore the mixing layer could be adequately characterised by a *constant* eddy viscosity, albeit a higher one than assumed in the model. This would mean that the "effective" α in the mixing region is higher than the assumed one, but spatially invariant, and this explains why the model works well for the mean quantities and why it predicts higher f' than the experiment. However, the reason why the predicted *dependence* of the r.m.s. fluctuations on turbulence intensity is contrary to the measurements is not clear at this stage, and this discrepancy will be discussed again in Section 3.4.6. The mean mixture fraction profiles from different jet separations and turbulence intensities collapse on the same curve if plotted against the reduced coordinate η (Eqs. 3.2.15, 3.2.23), Fig.

3.2.23. But it is also evident that this curve is less steep than the theoretical prediction, and this is consistent with the fact that the effective α in the experiment is larger than the values given by Eq. (3.2.19).

The model of Champion and Libby (1993), which was based on a Reynolds–stress description of the velocity and scalar field and thus might be expected to perform better than the eddy–viscosity model of Section 3.2.5, predicts the same qualitative dependence of the mean mixing layer width on flow parameters as the simpler model. However, slightly different dependencies are predicted for the scalar fluctuations on flow conditions, and it would hence be interesting to compare Champion and Libby's (1993) model against the present scalar data.

Finally, it is interesting to note that the values of α in the present experiments (in the range 0.45 to 0.85 for H=20mm) are smaller than unity, which suggests that the bulk stretch rate is larger than the large–eddy strain rate of the turbulence. Another interpretation of the same observation is that a mean residence time in the flow is smaller than the eddy turn–over time, and this has important implications for mixing and its modelling, as discussed in Section 3.4.6.

3.3 REACTING OPPOSED JET FLOWS

3.3.1 Background and structure of this Section

As discussed in the introduction to the thesis, very few measurements exist for turbulent counterflow flames. Kostiuk *et al.* (1993b) and Mounaïm–Rousselle and Gökalp (1993) presented measurements of velocity in *twin premixed* flames, and Kostiuk (1991) also analysed results from tomographic images of the reaction progress variable to find the integral scalar lengthscale and the frequency at which the reaction zone crosses contours of the mean progress variable, parameters that are used in flamelet models for turbulent premixed combustion (Bray and Cant, 1991). However, no measurements exist for *single premixed* and for *diffusion* counterflow flames, and the aim of this Section is to show the structure of these flames through measurements of the scalar and velocity fields and to show the changes in the flow patterns with approach to extinction.

Velocity, temperature, and mean species mole fractions in flames stabilised in the opposed jet flow are presented in this Section. Velocities were measured along the centreline and at r=10mm, temperatures at r=0 and r=10mm, and species concentrations at r=10mm because the presence of the sampling probe at the centreline disturbed the flow, but in view of the finding in Figs. 3.2.15 and 3.2.22 that the mean and r.m.s. of the mixture fraction do not depend on the radial distance, it is sound to use scalar measurements at off–axis locations to represent centreline variations. Photographs of the flames established in the present opposed jet flow are first shown, followed by the presentation of scalars and velocity measurements separately for diffusion and premixed flames. The results are discussed in Section 3.4 in their own right and in conjunction with the inert flow measurements of the previous Section.

3.3.2 Visualisation

Pure diffusion flames

Figure 3.3.1 is a photograph of a typical counterflow non–premixed flame and shows that the flame is blue, flat, located about mid–way between the two burners, and extends in the radial direction up to about the radius of the annular tube. The flame is quenched there by dilution with the co–flowing nitrogen and if this quenching is inadequate (for example, by an insufficient nitrogen flow rate), the unburnt fuel gives rise to uninteresting, but inconvenient for the integrity of the upper burner, flame fragments outside the stagnation region. Altering the strain rate did not change the general features of flame appearance.

Partially premixed diffusion flames

With air premixed with the fuel, but at volume fractions X less than 0.86, which corresponds to the limit for premixed flame propagation, the flames are still of diffusional nature and have appearance similar to that in Fig. 3.3.1, with a single, blue, and flat reaction zone. In contrast, *laminar* partially premixed flames, stabilised in a counterflow burner without perforated plates (Fig. 2.2), may have *two* reaction zones instead of one, Fig. 3.3.2, with the lower reaction zone having the characteristics of a premixed flame and the other those of a diffusion flame (Yamaoka and Tsuji, 1974, 1976). The presence of these "double structures" is a function of the equivalence ratio and the strain rate (Yamaoka and Tsuji, 1974; Stårner *et al.*, 1990) with the "double structures" merging at high stretch rates and equivalence ratios. This result suggests that single reaction zones should be expected in *turbulent* partially premixed flames, where the strain rates are high because of the small scale motions.

Figure 3.3.3a is a photograph of a partially premixed flame, where the air stream has been seeded with alumina particles and illuminated by a laser sheet, which shows that the luminous zone touches the laser–illuminated area, so that the flame lies on the interface between the air and the fuel jets. This is expected because air from the upper stream is necessary for combustion of the lower stream, even if the latter is partially premixed with air, but this behaviour changes when the fuel/air mixture corresponds to that of a premixed flame, as shown below.

Premixed flames

The flame zone is well separated from the upper air stream for lean single premixed flames, which are established when a reactant stream impinges on an air stream, and so the oxygen in the upper stream does not participate in combustion, but serves only to stagnate the reactant stream[6], Fig. 3.3.3b. These single premixed flames therefore are expected to be similar to the stagnating premixed flames with the reactant jets impinging on solid plates (Cho *et al.*, 1986, 1988; Liu and Lenze, 1988).

When two identical reactant mixtures impinge on each other, two premixed flames are stabilised (Fig. 3.3.4), one on each side of the stagnation plane, and it is evident that these flames are also flat and each similar to the single premixed flame of Fig. 3.3.3b. The region between the two flames contains hot products and becomes thinner with decreasing jet separation or increasing the jet velocity (not shown). Therefore the flame location depends on the strain rate (Bray *et al.*, 1991) and the two flames come close together at high strain rates, i.e. as extinction is approached.

---

[6] It will be shown, however, in Section 4.3.2 that the extinction limits of these single premixed flames depends on the temperature of the opposing stream because this affects the heat loss from the flame.

3.3.3 Scalar fields – diffusion flames

Temperature measurements

Contours of mean and r.m.s. temperatures in a typical counterflow turbulent diffusion flame (Fig. 3.3.5) show that the flame is located between the two jets and that both the mean and the r.m.s. values are radially uniform and depend only on axial distance, so that, as in the inert flows, variations along the centreline or any other radius smaller than the tube radius may only be examined. Distributions of mean temperature along the axial coordinate at r=10mm for pure and partially premixed diffusion flames have the same shape and Fig. 3.3.6 shows such distributions for H=10 and 20mm. The mean temperature changes from room temperature to a maximum value of around 1400K and then decreases again over distances of about 4mm and 8mm for the small and large jet separations respectively, in agreement with the expectations from the mixing measurements in Section 3.2.6 that the mixing layer width increases with jet separation. The r.m.s. values increase from zero at both sides of the flame to high values peaking at about 450K at two locations, on either side of the maximum temperature. The r.m.s. values are slightly lower at the location of the maximum mean temperature, and this is so for both jet separations (Fig. 3.3.6a & b) and for the two perforated plate locations (Fig. 3.3.6b) examined. Recall from Section 3.2.3 that H_p=120mm has a lower initial turbulence intensity than the case with H_p=55mm, and then Fig. 3.3.6b shows that the mean temperature in the low turbulence case is higher than in the high turbulence case and that the width of the profile smaller.

The mean temperature profiles across pure diffusion flames are similar for all jet velocities and jet separations and the temperature does not depend on the bulk velocity for the same H, but the maximum mean temperature decreases slightly with increasing jet separation, Fig. 3.3.7. The latter variation is shown in more detail in Figure 3.3.8, which shows that $\langle T \rangle_{max}$ decreases with H from 1350K to 1250K for separations of 10 to 25mm respectively[7]. This result indicates the small dependence of the maximum mean temperature on flow conditions and that $\langle T \rangle_{max}$ increases with a decrease in tube separation. It will be shown in Chapter 4 that a small tube separation leads to extinction, and so the temperature measurements in Fig. 3.3.8 suggest that the measured $\langle T \rangle_{max}$ in the counterflow non–premixed flame *increases* as extinction is approached. This result is in contrast to expectations, to the measurements of Masri and Bilger (1986) and Masri *et al.* (1990) in a piloted turbulent jet flame, and to predictions in laminar counterflow diffusion flames (for example, Jones and Lindstedt, 1988); an explanation is provided in the following paragraph by examining the temperature fluctuations.

---

[7] The measurements in Fig. 3.3.8 were taken with an 80μm thermocouple and so are systematically lower than all the other temperature measurements due to the larger radiation loss from the bigger wire.

The probability density functions corresponding to the r.m.s. values shown in Fig. 3.3.6 and Figs. 3.3.9 to 3.3.13 show a maximum at about 350K which becomes progressively smaller as the location of maximum mean temperature is approached and where the pdf is almost bimodal with a high temperature broad peak at about 1800K. This bimodality is not as pronounced as in premixed flames (see Fig. 3.3.30 and, for an example of premixed flames in other geometries, Heitor *et al.*, 1985), in which the low– and high–temperature peaks are much narrower than here. Towards the fuel and the air sides of the maximum temperature, the pdfs have long tails towards high temperatures and this explains the high r.m.s. values of Fig. 3.3.6. The shape of the pdfs is broad, particularly in the region of maximum mean temperature, and this was typical of the flame under all flow conditions. Hence, even if a *part* of the high temperature portion of the pdf was attenuated or depressed by a few hundred degrees as extinction was approached, the net effect on the first and the second moments would be small, and this is consistent with the small dependence of the maximum mean temperature on strain rate. Comparison of the pdfs at small and large jet separations shows that the peak at low temperatures in the location of $\langle T \rangle_{max}$ is less pronounced as the jet separations decreases (Fig. 3.3.9 and 3.3.12) and as the turbulence intensity decreases (Figs. 3.3.10 and 3.3.11) and therefore the higher low–temperature peak at high H explains the decreasing trend of $\langle T \rangle_{max}$ with jet separation shown in Fig. 3.3.8.

The turbulent nature of the flame was investigated by measuring the frequency spectra of the compensated temperature and Fig. 3.3.14 shows two typical spectra at the location of maximum mean temperature for weak and strong turbulence (conditions corresponding to those of Fig. 3.3.6b). Both spectra have a small region with a slope of –5/3, characteristic of isotropic, high Reynolds number turbulence, and decay from about 100 Hz (earlier for the weak turbulence) up to the cut–off frequency with a constant slope of about –4. This result is consistent with measurements in a turbulent jet diffusion flame with an estimated Re_t ($\equiv q'L_{turb}/\nu$, with ν based on cold air properties) of about 900 (Ballantyne and Moss, 1977) and with measurements in a premixed flame stabilised on a bunsen burner with Re_t about 200 (Chandran *et al.*, 1985), which had a decay faster than –5/3. The present flames had a turbulence Reynolds number of $20 \leq Re_t \leq 60$ which is lower than that of the above experiments, but the similarity of the temperature spectra suggests that the present flame is turbulent (see also Section 3.4.1). Finally, the fact that under conditions of weak turbulence the roll–off frequency is lower than for the high turbulence case is consistent with the similar finding in the inert flow mixing measurements (Fig. 3.2.20), which hence suggests that there is a close correspondence between the inert and the reacting flow in that the velocity field affects the frequency of the scalar fluctuations in the same way. This conclusion is further substantiated by the measurements of *velocity* spectra in an inert opposed jet flow by

Mounaïm–Rousselle and Gökalp (1993) which showed a decay faster than –5/3, similar to the temperature spectra measured here.

Species concentrations measurements

The axial distributions of the mean mole fractions of O_2, unburnt hydrocarbons (UHC), CO_2, CO, and H_2, after processing in the manner described in Section 2.4.3 to convert the measured mole fractions in the *dried* specimens to *wet* mole fractions, are presented in a series of graphs in Figs. 3.3.15 to 3.3.20. The axial coordinate in each graph has been shifted by the indicated value of Z_{half}, which is the axial location where the mean mixture fraction based on the species measurements, defined by Eq. (2.4.3), is equal to 0.5. This way, the spatial extent of the profiles at different flow conditions can be compared easily and the location of the peaks relative to the mixture fraction can be ascertained (more discussion on the latter will be given in Section 3.4.5).

Figures 3.3.15, 3.3.16, and 3.3.17 show the axial distributions of the species mole fractions for different bulk velocities for X=0.0, 0.5, and 0.8 respectively. It is evident that the peak concentration of CO_2 is found towards the air side of the peak of CO and H_2, and that the peak values decrease with increasing velocity for all conditions of premixedness; because the mixture fraction fluctuations did not change with velocity (Section 3.2.5 and 3.2.6), this is considered as evidence for finite–rate chemical kinetics, and will be discussed in Section 3.4.5. As partial premixing increases, there is no large change in the reaction products mole fractions with air premixedness from X=0.0 up to X=0.8, but there is a large increase as the flame approaches the rich flammability limit (X=0.86), Fig. 3.3.18. Finally, results for a different jet separation and turbulence intensity are presented in Figs. 3.3.19 and 3.3.20 respectively in order to complete a data set and, more importantly, to provide more information on the changes in the species mole fractions with approach to extinction. The discussion of the species concentration measurements is postponed until Sections 3.4.2, 3.4.3, and 3.4.5.

3.3.4 Velocity fields – diffusion flames

In this Section, velocity traverses along the centreline of diffusion flames are presented and compared for different jet separations, turbulence intensities, premixedness, and bulk velocities. Results are shown for the mean and r.m.s. axial and radial velocities normalised by the air stream velocity, U_o.

Initial conditions

The axial velocity profile in a diffusion flame at the exit plane of the jet is not uniform, Fig. 3.3.21, but increases towards the jet edge and the centreline axial velocity is about 0.8 times the jet bulk velocity, as in the inert flow (Fig. 3.2.5). This result is characteristic of all flames at H=20mm and is also similar to the initial conditions of

premixed flames (Fig. 3.3.33) and so the initial conditions across the jet exit depend *only* on the jet separation and *not* on the velocity, turbulence intensity, or type of the flame, and are similar for inert and reacting flows.

Centreline variations

The axial distributions of mean axial and r.m.s. axial and radial velocities are presented in Fig. 3.3.22 for two jet separations and for flames with X=0.0 (Fig. 3.3.22a &b), X=0.5 (c & d), and X=0.8 (e & f). In these figures, the axial coordinate has been normalised by the jet separation and the visible flame brush location (judged by eye to within approximately ±0.5mm) has been marked on the graphs. The mean velocity decreases from its value in the fuel jet (which is higher than U_o by a factor $\sqrt{\rho_2/\rho_1}$) to zero at the stagnation region and then assumes the (negative) value of the air jet, and at the smaller separation and for all X, the velocity closest to both jet exits is smaller in magnitude than at the higher separation, consistent with the observation that the centreline axial velocity at the jet exit is smaller than the bulk velocity for H=20mm, but closer to it for H=25mm (Figs. 3.2.5, 3.2.6, 3.3.21).

Contrary to the monotonic inert flow centreline traverses presented in Fig. 3.2.9, the reacting flow profile shows a "hump" that is smaller as the premixedness increases. In addition, for pure diffusion flames (X=0.0), the flame brush is located in the region of negative axial velocities (i.e. towards the air side of the stagnation point), while for partially premixed flames with X=0.8, the flame brush is located symmetrically around the stagnation point, and at an intermediate location for flames with X=0.5. This observation is explained by the fact that partially premixed flames have a higher stoichiometric mixture fraction than pure diffusion flames and hence are located closer to the fuel jet; for X=0.8, f_{st}=0.458 (Eq. 2.2.1) and so the stoichiometric mixture fraction lies very close to the symmetry plane of the two jets. For pure diffusion flames, f_{st}=0.055 and then there is a region between the flame zone and the stagnation region which can accommodate the expansion associated with the heat release, giving rise to the axial acceleration observed. Similar results for *laminar* counterflow diffusion flames of unpremixed fuel have been found experimentally (Tsuji, 1982; Chelliah *et al.*, 1990; Durst *et al.*, 1992) and theoretically (Bloor *et al.*, 1986; Kim *et al.*, 1992) and it is expected that laminar flames with partial premixing will show the same behaviour in their velocity field as the turbulent flames examined here.

The r.m.s. velocities increase from their values at the jet exit, as in the inert flow, but differences arise between the two turbulence components. The radial fluctuations are symmetric about the stagnation point, increase monotonically from their initial value, and peak at the stagnation region, while the normalised v'/U_o are higher than the

corresponding values of the inert flow (Fig. 3.2.9) and slightly lower for the large jet separation, consistent with the expectation that the stretch rate increases the turbulence.

The axial turbulence is higher than the radial, and thus the turbulence is anisotropic as in the inert flow, but the axial distribution of the axial r.m.s. is not monotonic. For flames with X=0.0, u'/U_o on the fuel side increases monotonically to the peak at the stagnation point for both jet separations; in the air side however, u'/U_o increases at first, decreases just before the flame brush, and then increases again through the flame brush until the peak at the stagnation point is reached. For flames with partial premixing, the r.m.s. acquires this non–monotonic behaviour on both sides of the flame, and for the flame with X=0.8, which is the closest to the stagnation point of the diffusion flames examined, the flow is approximately symmetric with u'/U_o showing the same variation on both sides of the flame. Note that the region of decreasing axial turbulence corresponds to the preheat zone of the flames with the maximum temperature being located approximately at the centre of the visible flame brush and that this non–monotonic increase in the axial turbulence is characteristic of all flames examined in the present experiments. Such variations of u'/U_o are also evident in certain measurements in twin *premixed* flames close to extinction by Kostiuk (1991; Fig. 6.13) and here in Fig. 3.3.38, which both show a slight tendency in the axial velocity r.m.s. to decrease just before the flames and the subsequent stagnation region peak.

Figure 3.3.23 shows that the mean velocity in diffusion flames does not change much with increasing initial turbulence, except that the spatial extent of the region occupied by the "hump" in the profile is smaller in the weak turbulence case, consistent with the previous finding that the width of the scalar profiles is smaller at low turbulence intensities (Figs. 3.2.17, 3.3.6, 3.3.20). The fluctuations throughout the flow are lower for the weak turbulence case and the shape of the profiles is similar for both cases, which suggests that the turbulence does not affect the mean flow field but that the mean flow straining acts in an one–way manner on the turbulence so as to increase it above its initial value, as also concluded in the inert flow velocity measurements (Fig. 3.2.7).

The differences between pure and partially premixed flames are more easily shown from Fig. 3.3.24 in which the data from Fig. 3.3.22 for one jet separation are re–plotted for clarity. The "hump" in the mean axial velocity is smaller for partially premixed than for pure diffusion flames, and the velocity gradient at the stagnation point is higher for X=0.0 than for the other flames, which also gives rise to higher fluctuations for both the axial and radial velocity components than for the partially premixed flames. For flames with X=0.8, the flow is close to the inert flow with the exception of the non–monotonic u'/U_o profiles. Finally, increasing the bulk velocity does not have an appreciable effect on the normalised mean and fluctuating velocities in the flames, Fig. 3.3.25. In Fig. 3.3.25b and c, the r.m.s. values for the high velocity case are slightly

lower than for the low velocity case and this is probably due to the fact that the initial normalised turbulence decreases slightly with the bulk velocity (Fig. 3.2.3).

Off-axis variations

Along the centreline the mean radial velocity is zero, but this is not so for radii larger than zero. Figure 3.3.26 shows that the axial mean and r.m.s. velocities at r=10mm are almost indistinguishable from the traverses at r=0 for partially premixed flames, and this result is typical for flames with and without premixing. However, the radial fluctuations are greater than their value at the centreline by a factor of about two and are higher than the axial fluctuations, and hence the anisotropy is reversed at large radii, contrary to the inert flow (Fig. 3.2.8) where the turbulence did not change with radius. Note that the increase in the radial turbulence at r=10mm is not evident at all axial locations, but is concentrated around the stagnation region, and so is probably related to the heat release associated with the flame that lies there.

The mean radial velocities at r=10mm for the flow conditions of the centreline traverses of Fig. 3.3.22 are presented in Fig. 3.3.27 which shows that the mean radial velocity peaks at the stagnation point (see Fig. 3.3.25a) and with magnitude that increases with the axial velocity gradient, as expected from mass continuity. The radial fluctuations have similar magnitudes for all premixedness (Fig. 3.3.27), and are higher than the values in the inert flow, Fig. 3.3.28b. The mean radial velocity in both reacting and the inert flows increases approximately linearly with radius along the stagnation plane, faster for the reacting flow, and the fluctuations continuously increase with increasing radial distance away from the centreline, as shown in Fig. 3.3.28. Straight lines have been fitted to profiles such as these at several axial locations to find the bulk stretch rate, which is defined as the radial gradient of radial velocity and such measurements are presented and discussed in Section 3.4.5.

This concludes the presentation of the measurements for turbulent counterflow diffusion flames. In the next two Sections, the scalar and velocity data for premixed flames are presented, and a discussion of all results follows in Section 3.4.

3.3.5 Scalar fields – premixed flames

In this Section, results of the temperature and mean species concentrations in single and twin premixed flames are presented. Emphasis is placed on single flames because these have not been studied before, and only aspects of the present twin flames that are different from, or complement, those examined by Kostiuk *et al.* (1993b) are shown. Due to the smaller amount of data for premixed than for diffusion flames, discussion of some results will be given alongside their presentation.

Temperature measurements

The mean and r.m.s. values of the temperature across a single lean premixed flame are shown in Fig. 3.3.29. The mean temperature increases from 300K in the reactants side of the flame to temperatures close to the adiabatic flame temperature expected for flames of this equivalence ratio, and in the post–flame region the temperature drops again due to mixing with the opposing cold air stream. The r.m.s. values are high where the mean temperature gradient is high, are low in both the reactants and air streams, and are also low in the immediate post–flame region which contains mostly hot reaction products. The corresponding pdfs (Fig. 3.3.30) show a bimodal structure, with peaks at room and flame temperatures and small, but not negligible, probabilities at intermediate values, in the location of the flame zone, and the subsequent mixing with air eventually reduces the peak at the flame temperature and increases the probability of intermediates. The bimodal structure of the temperature pdfs is consistent with the Bray–Moss–Libby flamelet model of premixed flames (see, for example, Bray and Libby, 1990 for a recent review) and suggests that theoretical predictions of the present counterflow flames may be based on the BML model, and the applicability of this model for the present flames is discussed further in Section 3.4.1.

Species concentrations measurements

The mean mole fractions of O_2, UHC, CO_2, and CO are presented for single premixed flames in Figs. 3.3.31 and 3.3.32. Figure 3.3.31 shows that the peak concentration of CO_2 across the flame is found downstream from the peak CO and that the UHC mole fraction decreases to zero before the CO_2 takes its maximum value. At higher bulk velocities, however, the maximum mole fraction of CO_2 is smaller (Fig. 3.3.31b), as in the diffusion flames examined in Section 3.3.3, and the UHC mole fraction slightly higher at the location of maximum CO_2. These results suggest that the approach to extinction, which is brought about by increasing the velocity (Chapter 4), is accompanied by a decrease in the mole fractions of reaction products, and this finding is consistent with the measurements of diffusion flames presented previously.

Rich premixed flames give rise to higher CO and lower CO_2 mole fractions than the lean premixed flames just described at the same bulk velocity (Fig. 3.3.32) and as the equivalence ratio increases, the flame eventually enters the diffusion flame regime; the flames in Fig. 3.3.32b and 3.3.18b bracket the nominal limit for premixed flame propagation (ϕ=1.6 or X=0.86) and the transition from diffusion to premixed flames will be discussed in Section 3.4.3.

Finally, lean *twin* premixed flames also show reductions in the mole fractions of CO_2 with increasing bulk velocity (Fig. 3.3.33), as for the single premixed flames and consistent with the visualisation in Fig. 3.3.4 and the theoretical prediction of Bray *et al.* (1991), and show appreciable CO in the post–flame region which indicates that

combustion in not complete. At high velocities, there is a finite concentration of unburnt hydrocarbons in the region between the two flames, which also suggests incomplete combustion through the flame. Close to extinction therefore the present twin flames show incomplete combustion, and this is consistent with the suggestion of Law (1988) that laminar lean methane–air twin premixed flames have a Lewis number greater than unity, and so cannot extinguish with stretch alone; increasing the bulk velocity brings the two flames to a point where they touch and therefore extinction is caused by incomplete combustion. This behaviour at extinction is qualitatively different in twin flames with Le<1 which may extinguish due to stretch alone (Law, 1988). If the flames of Kostiuk *et al.* (1993b), which are lean propane–air flames with Le<1, do not show evidence of unburnt hydrocarbons between the flames as in the present experiment, it may be surmised that non–unity values of the Lewis number affect *turbulent* flames in the same way as for *laminar* flames, and so may not be overlooked, as is usually the case in theoretical models of turbulent combustion (but see Bradley *et al.*, 1992).

3.3.6 Velocity fields – premixed flames

Initial conditions

The axial velocity radial variation across the jet exit (at z=2mm) has a similar non–uniformity to that measured in inert flows and diffusion flames (Fig. 3.3.34), but both the axial and the radial fluctuations are approximately uniform with radius. The radial velocity radial gradient is non–zero, which shows that the jet is already spreading radially close to the exit of the jet, and these measurements are typical and can be used as the boundary conditions for theoretical models for this flow.

Centreline variations

The axial velocity in single lean premixed flames, Fig. 3.3.35, decreases from the reactants jet to a minimum, then increases to a maximum due to the expansion associated with the heat release, and the flow eventually stagnates as it impinges on the opposing air flow and the air stream velocity variation resembles that of the inert flows. The radial fluctuations in the premixed flames are similar to those in the diffusion flames, but large differences are evident for the axial fluctuations. As the flame is approached from the reactants side, the axial r.m.s. increases sharply through the flame, drops in the post–flame region, increases again at the stagnation point between the hot products created by the flame and the opposing air flow, and then decreases from the peak corresponding to the stagnation point to the value at the jet exit. Note the slight tendency for the axial r.m.s. to decrease just before the hot region in the air flow and that the axial fluctuations are higher than both inert flows and diffusion flames.

Selected probability density functions of axial and radial velocity have been included in Fig. 3.3.35 which shows that the radial pdfs are unimodal and that the axial

velocity pdfs have a bimodal structure with peaks probably corresponding to reactants and products at locations in the flame brush; the large increase in the axial fluctuations and the mean velocity is due to the velocity probe sampling cold (slow) and hot (fast) fluid. The so–called "slip velocity" of the BML model, where the reactants and the products have different mean velocities, is approximately the difference between the peaks in the pdfs as in Fig. 3.3.35 and hence the present flames have a structure that can be described by this combustion model, as also concluded from the temperature measurements of Fig. 3.3.30.

The measurements in Fig. 3.3.35 are similar to those of Cho *et al.* (1986) and Liu and Lenze (1988) in stagnating premixed flames impinging on solid plates, rather than an opposing jet, in that there was a local minimum in the axial velocity before the acceleration through the flames zone, which also resulted in increased axial fluctuations and bimodal pdfs. A comparison between the present single flames and the twin flames of Kostiuk *et al.* (1993b) will be discussed shortly.

Figure 3.3.36 shows that increasing the equivalence ratio of single premixed flames away from stoichiometric conditions makes the peak associated with the expansion through the flame less pronounced and the velocity profile is indistinguishable from that of partially premixed diffusion flames for a flame bordering the rich flammability limit. The axial fluctuations are high when there is a pronounced "hump" in the mean velocity, but become low and close to those in diffusion flames when the profile is smoother. It seems, therefore, that an important condition for the existence of the axial acceleration is that the flame is located away from the stagnation plane: for vigorous premixed and pure diffusion flames the reaction zone is inside the reactant and the air stream respectively, but for weak premixed and partially premixed flames the reaction zone is located close to the stagnation plane and the acceleration is not manifested in the axial velocity measurements.

Figure 3.3.37 allows a comparison of the inert opposed jet flow, the single premixed flame of Fig. 3.3.35, and twin premixed flames at the same equivalence ratio. It is evident that each of the twin flames has a structure similar to that of the single flame, but the presence of the second flame implies that the mean axial velocity profile has two maxima and the axial fluctuations have three. The axial turbulence is higher than the inert flow turbulence, partly due to the production through the flame and partly due to the higher axial velocity gradient associated with the fast hot–product flows fed from each flame to the stagnation point. The radial fluctuations are similar for both flames, and higher than the corresponding r.m.s. in the inert flow, and this is again consistent with the observation that the axial velocity gradient is higher in the reacting flows than in the inert flows.

The twin premixed flames of Fig. 3.3.38 have a less pronounced acceleration at high bulk velocities with the flames closer to the stagnation point and the axial

fluctuations reduce from their low–velocity values, while the radial fluctuations have similar profiles and slightly smaller magnitudes at high velocities. Note that the normalised axial velocity gradient at the stagnation point decreases with increasing bulk stretching because the local velocity gradient depends on the velocity maximum of the post–flame regions; a large maximum, as when the flames are farther apart in the low velocity case, suggests a larger velocity drop to the symmetric value at the maximum in the products region of the twin flame and so the gradient is higher.

The present measurements in twin flames are different from those of Kostiuk *et al.* (1993b) who did not observe acceleration through the flame, with the axial velocity profile almost indistinguishable from the inert flow. This difference is attributed to two reasons. First, the present measurements were done with jet separations smaller than a jet diameter and so were less than those of Kostiuk *et al.*, and this implies that the phenomenon of "bouncing" is less pronounced, where the term was used by Kostiuk *et al.* to denote a large–scale unsteady axial motion of the flames which was eliminated when the jet separation was smaller than about two jet diameters (see also Mounaïm–Rousselle and Gökalp, 1993). This type of motion would smear out the structure associated with the flame in the ensemble averages of the measured velocities, and this is avoided in the present data. Secondly, the present experiments were performed with flames farther from extinction than those of Kostiuk *et al.* and this suggests that the flames were more vigorous and hence gave rise to higher accelerations.

Off–axis variations

The axial velocity profile at r=10mm, Fig. 3.3.39, is identical to that along the centreline and the axial fluctuations are similar, while the mean radial velocity peaks close to the stagnation region and the radial fluctuations are higher than their centreline values, results similar to those in diffusion flames (Fig. 3.3.26). The radial fluctuations of Fig. 3.3.40 increase with radial distance, but, as for the diffusion flames in Fig. 3.3.27, only for axial locations where the temperature is higher than the initial temperature of the reactants. Therefore the presence of the flame increases the radial turbulence at large radii for both premixed and diffusion flames.

Finally, Fig. 3.3.34a shows that the mean radial velocity increases with radius faster at the stagnation region than at the jet exit, also expected from examination of the corresponding mean axial velocity gradient which increases towards the stagnation region, and so the bulk stretching in the flow is not constant. More discussion of the bulk stretching is given in Section 3.4.5.

This concludes the presentation of results for both difusion and premixed flames. A discussion follows in the next Section.

3.4 DISCUSSION

3.4.1 Scale estimates and combustion regimes

Turbulent combustion regimes

Some recent theoretical models of turbulent combustion treat turbulent flames as ensembles of laminar–like small–scale reaction zones so that quantities of interest, like the mean reaction rate, can be calculated as the ensemble over all possible laminar flamelets. Based on results presented in the previous Sections, estimates are made here of certain parameters that help classify the present turbulent flames into the appropriate regimes of turbulent combustion, and it will be shown below that both the diffusion and premixed flames described in this thesis may be treated by laminar flamelet concepts.

The validity of laminar flamelet models has been discussed by various authors, for example Peters (1986) and Bilger (1988) for diffusion, and Peters (1986), Bray and Cant (1991), and Poinsot *et al.* (1991) for premixed flames. For both types of flames, it is generally believed that flamelets exist when the reaction zone thickness is smaller than the smallest scales of turbulence, but the proposed quantitative criteria for flamelet existence are different for the different types of flames because the laminar reaction zone thickness depends on the type of flame, as argued next.

For diffusion flames, the laminar diffusion layers embedded in the turbulent flow have a thickness of the order of the Kolmogorov lengthscale, η_K (Gibson, 1968; Bilger, 1988; Section 3.4.6), and reaction occurs in these layers at mixture fractions close to the stoichiometric, but with a finite thickness that depends mostly on the nature of the reactants. For example, for CH_4–air diffusion flames the reaction rates have non–zero values over mixture fractions between about 0.025 and 0.085, bracketing the stoichiometric value of 0.055, and so reaction occurs across a mixture fraction scale, $\Delta f_R \approx 0.06$ (Bilger, 1988). The corresponding *spatial* thickness of the reaction zone is determined by Δf_R and by the local mixture fraction spatial gradient, and by relating the latter to the turbulent scalar dissipation rate, it can be shown that the mixture fraction variation varies by an amount $\Sigma_f \approx (\chi\, \tau_K)^{1/2}$ across a Kolmogorov lengthscale, where Σ_f is interpreted as a scale denoting the smallest possible scalar variation for which molecular effects are unimportant, χ is the mean turbulent scalar dissipation rate, and τ_K the Kolmogorov timescale. Bilger (1988) suggested that laminar diffusion flamelets exist if $\Delta f_R < \Sigma_f$, and using the model for χ in Eq. (3.2.8), the resulting criterion was that

$$\Delta f_R < \sqrt{2}\, f'\, Re_t^{-1/4} \qquad (3.4.1)$$

for a turbulent flame to be described by laminar flamelets. Large scalar dissipation rates, large fluctuations of the mixture fraction, and small turbulent Reynolds numbers ($Re_t=q'L_{turb}/\nu$) therefore suggest applicability of flamelet concepts.

For premixed flames, laminar flamelets exist when the thickness of the reaction zone is smaller than the Kolmogorov lengthscale (Peters, 1986), i.e.

$$\delta_L < Re_t^{-3/4} L_{turb} , \qquad (3.4.2)$$

where δ_L is the laminar flame thickness, defined by $\delta_L = \tau_{chem} S_L$, with S_L the laminar flame speed and τ_{chem} a reaction timescale. The chemical timescale can also be written as ν / S_L^2 and is close to 0.1ms for stoichiometric CH_4–air flames that have $S_L \approx$ 0.4m/s, and therefore $\delta_L \approx$ 0.04mm. Below, estimates of Eqs. (3.4.1) and (3.4.2) are made for typical diffusion and premixed flames examined in this Chapter.

Scale estimates

In Table 3.1, estimates for *diffusion* flames are summarised. Typical conditions are H=20mm, H_p=55mm, U_o= 1.5 m/s, X=0 to 0.8, and the turbulence conditions at the exit of the jet are used (Eq. 3.2.2), so that $q'/U_o = 0.085$ and L_{turb}=4mm. The r.m.s. of the mixture fraction at the position of the mean stoichiometric mixture fraction, f'_{st}, is taken from the eddy–viscosity analysis (Fig. 3.3.12) and is close to the measured values (Fig. 3.2.17). It is clear that the pure diffusion flames are in the flamelet regime, since Δf_R is smaller than Σ_f, and that partial premixing results in flames into the non–flamelet regime as defined by Eq. (3.4.1), because the reaction zone thickness in mixture fraction space increases. However, because of the approximate nature of the present discussion and the large number of assumptions behind Eq. (3.4.1), it is concluded that all the present diffusion flames may probably be described by flamelet concepts since $\Delta f_R/\Sigma_f$ is on the order of unity.

Table 3.1
Estimates for diffusion flames with different degrees of partial premixing. For all estimates, q'/U_o=0.085, U_o=1.5m/s, and L_{turb}=4mm, giving Re_t=33. The values for Δf_R were taken from Stårner *et al.* (1990).

X	f_{st}	f'_{st}	Δf_R	Σ_f	$\Delta f_R/\Sigma_f$
0.0	0.055	0.25	0.06	0.15	0.4
0.5	0.153	0.30	not available	0.18	–
0.8	0.458	0.45	0.55	0.27	2.0

Table 3.2

Estimates for premixed flames at different velocities. For all, q'/U_o=0.085, L_{turb}=4mm, $\tau_{chem} = \nu/S_L^2$, $\delta_L = \tau_{chem} S_L$, $\tau_K = Re_t^{-1/2} L_{turb}/q'$, and $\eta_K = Re_t^{-3/4} L_{turb}$.

ϕ	S_L	U_o	q'/S_L	η_K/δ_L	τ_{chem}/τ_K
0.9	0.36	2.0	0.47	5.5	0.033
0.8	0.33	2.0	0.52	5.1	0.040
0.9	0.36	3.0	0.71	3.8	0.062

Similar estimates for *premixed* flames under typical conditions are shown in Table 3.2 and it is again evident that Eq. (3.4.2) is satisfied and so the present flames fall into the flamelet regime of turbulent premixed combustion, as also suggested by the temperature and velocity measurements presented in Figs. 3.3.40 and 3.3.35 respectively.

3.4.2 Comparison of reacting with inert flow

Velocities

The velocity measurements showed many common aspects between the reacting and inert flows and important differences. The mean axial velocity profile across the centreline showed non–monotonic variations under reacting conditions, with acceleration of the axial velocity through the flame zone under conditions where the flame was located away from the stagnation point, while it varied monotonically and close to the theoretical prediction of Champion and Libby (1993) for inert flows. For both reacting and inert flows, the axial and radial fluctuations increased from the jet exit and peaked at the stagnation point at values that increased with the initial turbulence intensities at the jet exit, which depended mostly on the characteristics of the turbulence generator, and the normalised v'/U_o acquired values that were lower with increasing jet separation, and therefore bulk stretching rates, consistent with our expectations. The axial fluctuations, however, showed different behaviour under reacting and inert conditions. Depending on the flame location relative to the stagnation point, the axial distributions of the axial fluctuations showed peaks also at axial locations away from the stagnation region; for both single and twin premixed flames, there was a large increase in u'/U_o through the flame if the flame was under low bulk stretch or of equivalence ratio close to stoichiometric. For diffusion flames, the axial fluctuations decreased with increasing premixedness, probably through the influence of the latter on the flame position.

The mean and r.m.s. axial velocities did not vary with radius for both inert and reacting flows, while the radial turbulence increased with radius at the flame locations for all flames examined here, in contrast to the inert flow, and a possible explanation for this observation follows. The pressure at the stagnation point of the inert opposed jet flow is expected to be larger than atmospheric by an amount on the order of $\frac{1}{2}\rho_o U_o^2$, and this results in a negative (favourable) pressure gradient in the radial direction. If this pressure gradient acted on cold gases as in the inert flow, it would accelerate the radial flow by a amount smaller than in the flame, and so the radial velocity axial gradient (Fig. 3.2.27) are expected to be greater in the flame, leading hence to larger radial fluctuations.

For both inert and reacting flows, there was no appreciable difference in the mean velocity profiles under conditions of weak and strong turbulence, which suggests that the turbulence can be treated independently from the mean flow by considering the turbulence evolving in the straining opposed jet flow. This finding suggests that approaches like that of Rapid Distortion Theory are applicable in this flow, and this suggestion is strengthened by the observation that mean residence times in the flow are smaller than typical estimated eddy turnover times (see Section 3.2.7), which is the criterion of validity of Rapid Distortion Theory (RDT).

Britter *et al.* (1979) found favourable comparisons between RDT predictions and experimental measurements of isotropic homogeneous turbulence stagnating on a solid surface and found that the axial and radial fluctuations increase in the straining field, as found in the present opposed jet flow. Lee (1989) predicted that in homogeneous isotropic turbulent flows with decreasing mean velocity, a condition appropriate for the opposed jet flow, typical eddies of, say, a spherical shape, become elongated in the radial direction and compressed in the axial direction, consistent with the experimental data of Wei and Miau (1992). These results suggest that the velocity anisotropy increases at the stagnation plane and that the lengthscales may also become highly anisotropic, and this implies that theoretical predictions of the opposed jet flow should probably be based on second–order closures and that models like the k–ε model, which assume isotropic turbulence, are not expected to perform well for inert or reacting opposed jet flows.

Mixing

The mean mixing field in the opposed jet flow is identical under reacting and inert conditions (Fig. 3.4.1). Figure 3.4.1a shows that the mixing layer width for H_p=120mm (weak turbulence) is smaller than for strong turbulence, for both inert flows and diffusion flames, and depends *only* on H_p for the same jet separation, as the bulk velocity does not affect it (Fig. 3.4.1b). Note that the mixture fraction is defined for each type of flame so as to be unity in the fuel stream and zero in the air stream and that

the mixture fraction profile is identical for all flame types. These results show that, if the mixing is brought about by the action of a turbulent diffusivity that scales with the turbulence intensity and the turbulence lengthscale, the same diffusivity exists for inert and reacting flows and the collapse of the data from different bulk velocities in Fig. 3.4.1b also suggests that the turbulent diffusivity scales with the bulk velocity for both inert and combusting flows, as also suggested by Eq. (3.2.7) and the measured and assumed independence of q'/U_o from U_o.

If the eddy diffusivity is the same in reacting and inert flows, the eddy diffusivity must be a function of density, because the lengthscales are expected to be unaffected by heat release but the velocity fluctuations are found to be higher in the flames than the inert flows, so that the decreasing density in the flame must decrease the diffusivity to compensate for the increase in turbulence. Various functional forms have been used in a k–ε model by Bray *et al.* (1991) for mixing in counterflow premixed flames, and so the present data can quantify this dependence of the eddy diffusion coefficient on density.

3.4.3 Transition from diffusion to premixed flames

The appearance of pure and partially premixed diffusion turbulent flames is similar with a single reaction zone (flame brush), unlike for partially premixed *laminar* flames in which two reaction zones may be visible at low strain rates and high premixedness (Fig. 3.3.2), and the difference is attributed to the high strain rates associated with the turbulent flow, which cause the two reaction zones to merge (Stårner *et al.*, 1990; Smooke *et al.*, 1988). The existence of two reaction zones in partially premixed counterflow flames can be understood by making an analogy with an aerated bunsen burner flame, i.e. with some air entrained in the fuel stream, in which the inner cone is a premixed flame but without enough oxygen to complete combustion. The products of this flame are hot, consist of intermediates like CO and H_2, and will react with the next available oxygen in a diffusion flame; in bunsen flames, this is found at outer regions of the jet but, if the flame is enclosed so that air entrainment is precluded, the second reaction zone will be located away from the premixed flame where the enclosure ends (Gaydon and Wolfhard, 1960). In counterflow flames (Fig. 3.3.2; Yamaoka and Tsuji, 1974), the inner reaction zone is located inside the fuel–air stream and the outer reaction zone is located at the region where diffusion with the opposing oxygen stream, and hence combustion, is possible.

The inner zone of partially premixed flames in Fig. 3.3.2 is green / cyan while the outer zone is definitely blue with no hint of green, and this is consistent with the expectation that the outer zone is similar to a $CO/H_2/N_2$ flames "fed" by the inner flame which then mostly acts so as to break down the hydrocarbon molecule (Yamaoka and Tsuji, 1974). This structure is also that of rich *premixed* flames and therefore there is no clear distinction between rich premixed flames and diffusion flames with partial

premixing and so the physical significance of the rich limit for premixed flame propagation, which is invariably based on experiments concerning propagation of a rich flame in a tube (e.g. Kuo, 1986), is vague when applied to flows where diffusion of oxygen in the flame is possible, like in the counterflow flames.

Examination of the data presented in Section 3.3 for turbulent partially premixed and rich premixed flames shows the following aspects of the transition between diffusion (X<0.86) to premixed (X>0.86) flames. First, as oxygen is progressively added to the fuel stream in a diffusion flame, less oxygen from the upper stream is necessary, the stoichiometric mixture fraction increases, the flame location shifts towards the fuel jet and is close to the stagnation point, and this results in a different axial acceleration of the axial velocity through the flame for X=0.0 to X=0.8. From about X=0.8 to ϕ=1.3 (Fig. 3.3.24 and 3.3.35), the flames have approximately the same velocity field because they are close to the stagnation point. Secondly, the mean concentrations of CO and CO_2 increase as the partial premixing increases from X=0.8 (Fig. 3.3.17) to 0.83 (Fig. 3.3.18a), 0.85 (Fig. 3.3.18b), past the nominal limit of ϕ=1.6 to premixed flames with ϕ=1.43 (Fig. 3.3.32b) and ϕ=1.2 (Fig. 3.3.32a), and the spatial separation between the peak in CO and CO_2 increases in premixed flames. These results show that the transition between diffusion and premixed counterflow flames is smooth, without any clear distinction around the rich flammability limit, but the reason why the reaction products mole fractions increase is not clear at present[8]. Finally, Fig. 3.4.2 shows that the mean mixture fraction profile is the same for *all* flames in the opposed jet flow, for both diffusion and single premixed flames, and so no large difference in the mixing patterns between the fuel (or reactant) jet and the opposing air jet is expected. Note that the mixture fraction in premixed flames denotes the concentration of fluid originating from the reactants jet but is not related with the flame location, in contrast to diffusion flames. The collapse of the data in Fig. 3.4.2 shows that irrespective of the location of the flame, the mixing between the two jets is similar and this then implies that the mixing measurements presented previously can also be applied to premixed flames as well, for example for determining the mixing of the premixed flame products with the opposing air stream and thus examining the heat loss from the flame.

Theoretical analyses of turbulent diffusion and premixed flames are usually based on different approaches, for example theories based on laminar flamelet approaches are different for premixed and diffusion flames (Peters, 1986). Recently, Peters (1993a) attempted to unify the two turbulent flame idealisations of a pure diffusion flame and a

---

[8] The smooth transition between diffusion flames and premixed flames is also reflected in the extinction measurements presented and discussed in Chapter 4. It was shown in Section 3.3 that the approach to extinction reduces the mole fractions of reaction products for both diffusion and premixed flames, but this reduction is smaller than the difference in CO_2 between diffusion and premixed flames and so the latter is not due to the different degree of approach to extinction of the different flames. See also Section 3.4.5.

fully premixed flame, motivated by the fact that in practice most flames have characteristics of both, and produced an approximate laminar flamelet description of partially premixed flames that aims to cover the whole spectrum of flames from pure diffusion, partially premixed, and fully premixed flames. The present data show a continuation between diffusion and premixed turbulent flames and so can also be useful for validating predictions based on this new theory.

3.4.4 Flame motion

In this Section, the diffusion flame temperature measurements presented in Section 3.3.3 are examined again with the aim of identifying the turbulent motions of the flame that result in the measured probability density functions, and two–point measurements are presented to identify the spatial coherence of the flame and to yield inferences about the turbulent eddy lengthscales and shapes around the stagnation region in opposed jet flows.

Frequency content

It was mentioned in Section 3.3.3 that the wide temperature probability density function made the evidence of localised temperature reductions due to high strain rates and possible localised extinctions, as with increasing bulk velocity, less obvious than expected. Therefore an explanation for the initially surprising finding that the maximum mean temperature increased even as extinction was approached, was attributed to the different pdfs of temperature at different jet separations. Here, the flame motions that would give rise to these pdfs are discussed at greater length.

Far from the location of the maximum mean temperature, the temperature pdfs had a maximum at about 350K, with long tails towards high temperatures and were bimodal at the location of the maximum mean temperature. In general, for turbulent diffusion flames, in the absence of localised extinction the temperature pdf should follow the pdf of the mixture fraction; bimodal temperature pdfs *have* been observed, however, where local extinction occurs in turbulent jet diffusion flames, in contrast to those of mixture fraction (Masri *et al.*, 1990). The reason for the bimodality was the existence of fluid which had been quenched by excessive straining and therefore, although it was potentially reactive in terms of composition, the temperature was low. Also, turbulent mixing of the quenched fluid suggested that low–temperature elements were not associated with any particular range of frequencies.

The probability density function at the fuel side of a pure diffusion flame loses its low–temperature peak and tail after digital high–pass filtering at 20Hz and the bimodal pdf at the location of the maximum mean temperature becomes near–Gaussian, Fig. 3.4.3. The effect of high–pass filtering at various frequencies is more evident from Fig. 3.4.4, which shows that the r.m.s. of the filtered temperature is less than the r.m.s.

of the unfiltered and that the skewness of the pdfs decreases as the high–pass filter frequency increases, and this is consistent with the observations from the filtered pdf shapes shown in Fig. 3.4.3. Therefore, the presence of high–temperature fluid at the fuel and air side of $\langle T \rangle_{max}$ and the presence of low–temperature fluid at the location of $\langle T \rangle_{max}$ is associated with the low–frequency motions of the flame and not with localised extinctions as in Masri *et al.* (1990). The slight increase of $\langle T \rangle_{max}$ with decreasing tube separation, Fig. 3.3.8, is due to the smaller probability of low–temperature fluid at low separations than at large separations (Figs. 3.3.9 and 3.3.12) and this suggests that the lengthscale of this low–frequency motion is smaller for small tube separations, as expected.

The previous paragraph implies that there is a low–frequency motion of the flame past the temperature probe that gives rise to the wide temperature pdfs observed. It is important to realise that this motion is not associated with any particular frequency, as there is no peak in the frequency spectrum (Fig. 3.3.14) of the flame; it is only concluded that the motion is contained in the low frequencies, and so more information is needed to infer the turbulent lengthscales, and such information may be provided by two–point measurements.

Two–point measurements

Two–point temperature measurements have been performed in diffusion flames to examine the extent of spatial correlation that the flames exhibit. Figure 3.4.5a shows that the correlation coefficient between temperature fluctuations at the axial location of $\langle T \rangle_{max}$ extends over larger radial separations at r=13mm than at the centreline. If a lengthscale is defined based on the first point where the correlation coefficient is zero, then the radial lengthscale is about 7mm at the centreline and about twice that value at r=13mm. These magnitudes, and their relative size, are consistent with the predictions of eddy shape of Lee (1989), also discussed in Section 3.4.2, who used Rapid Distortion Theory to predict that the radial dimension of eddies will be extended and their axial lengthscale reduced in initially isotropic turbulence with decreasing mean velocity, a situation similar to the stagnating turbulent jets examined here.

The axial lengthscale was measured in the flames by placing two thermocouples in the same radial location and varying their axial separation. The correlation coefficient is *negative* when the two measuring point bracket, symmetrically, the location of $\langle T \rangle_{max}$ and reduces to zero at large axial separations, as shown in Fig. 3.4.5b. It was not possible to place the thermocouples closer together than about 2mm, but an extrapolation joining the measurement at the smallest axial separation and the point of ρ_{12}=1 on the ordinate of the graph, corresponding by definition to the case of zero separation, would show the probable approximate shape of the correlation coefficient curve for small separations. If, as for the radial lengthscale, a lengthscale is defined by the axial

separation where the correlation coefficient first becomes zero, it is evident that the axial lengthscale of temperature fluctuations is of the order of 2mm, smaller than the radial lengthscale and smaller than the estimated *velocity* lengthscale at the exit plane of the jet of L_{turb}=4mm.

The negative portion of the correlation coefficient will be discussed in more detail shortly, but it is timely to state that the lengthscale anisotropy predicted for rapidly decelerating flows and discussed in Section 3.4.1 is substantiated in the present two–point measurements and is also consistent with the observation in Fig. 3.2.1 (Section 3.2.2) that the interface between two inert jets shows a "waviness" of larger scale in the radial than in the axial direction. Imagine now that this interface, depicted in Fig. 3.2.1, is between fuel and air and that a diffusion flame lies along it. The turbulence will strain and convect this interface randomly and one may imagine an instantaneous temperature profile "pegged" on the interface and moving with it; the temperature fluctuations registered by the thermocouples in Fig. 3.4.6b correspond to how far these are from the moving interface. If, as in Fig. 3.4.5b, the thermocouples bracket the interface, an axial motion of the flame means that when the temperature at one probe increases, it decreases at the other, and so the resulting correlation coefficient is negative.

This description is approximate in that it neglects the convolutions and the possible "curls" of the interface (see Fig. 3.2.1) that would invalidate the correlation between the sign of the temperature fluctuations at the two measuring points in the previous paragraph. However, the finding that the correlation coefficient is indeed negative, the finding in Section 3.2.6 that the probability of intermediate mixture fraction was small, and the observation that a residence time in the flow is small compared to an estimated eddy turnover time which is necessary for "curls" to develop (Section 3.2.7 and 3.4.1), suggest that this description is appropriate for explaining measurements in the opposed jet flow under inert and reacting conditions and will be further discussed and developed in Section 3.4.6.

3.4.5 The approach to extinction and the strain rate on the flame

It will be shown in Chapter 4 that both diffusion and premixed flames extinguish at high bulk velocities and with strong turbulence, and a phenomenological correlation based on the estimated total bulk stretch rate that the flame experiences has been proposed for twin premixed flames by Kostiuk *et al.* (1989). In Chapter 4, a similar correlation is proposed for *diffusion* flames which approximately extinguish when the total stretch rate

$$S_{total} = 2\,U_o / H + Re_t^{1/2}\, q'/L_{turb} \qquad (3.4.1)$$

exceeds a certain value, with the first term in the r.h.s. of Eq. (3.4.1) being a measure of the bulk stretch rate on the flame, and the second equal to the inverse of the Kolmogorov timescale, and thus a measure of the small–scale turbulent stretch rate. Both these estimates, however, are approximations and here, the velocity measurements are discussed in order to facilitate estimates of the bulk and the turbulent stretch rates acting on the flame. First, the behaviour of the flame far from, and close to, extinction is discussed in terms of its chemical structure.

Species concentrations

The mean mixture fraction in diffusion flames can be calculated from the measurements of species mole fractions by Eq. (2.4.3), and in Fig. 3.4.6 measurements of the mole fractions of UHC, O_2, CO_2, CO, and H_2 are plotted against the mixture fraction. Results are included from a numerical calculation of a laminar counterflow diffusion flame at low and high strain rates (Lindstedt, 1992) to allow comparison between the structure of the laminar and the turbulent flames. The following points are noted. The mole fractions of O_2 and UHC do not change much as the bulk velocity increases and are higher than those predicted in the laminar flame, but the mole fractions of CO_2, CO, and H_2 decrease with strain rate in the laminar flame and the same trend is found in the turbulent flame (Fig. 3.4.6c,d, & e), which also has mole fractions lower than those of the laminar flame. Finally, the peaks of the reaction products mole fractions in the turbulent flame are located at mean mixture fractions about 0.2 to 0.4, although those of the laminar flame are located very close to the stoichiometric value of 0.055.

The lowering of the mean mole fractions from their laminar flame values is expected due to the existence of mixture fraction fluctuations (Bilger, 1980) that also cause a shift in the location of the measured peak into richer values of the mixture fraction. However, the mixture fraction fluctuations in the opposed jet flow do not depend on the bulk velocity for given turbulence intensity and jet separation (see Sections 3.2.5 and 3.2.6 for theoretical and experimental evidence respectively). So the effect of the fluctuations on graphs of mole fractions against mixture fraction are expected to be independent of bulk velocity, and hence the separation of the curves of the mole fractions of reaction products with different bulk velocities in Figs. 3.4.6 constitute evidence for finite chemical kinetic effects on the flames.

The flame farthest from extinction (the one at the lowest velocity) gives a peak in the CO_2 profile closest to the stoichiometric mixture fraction and as the velocity increases, the peak lowers and is shifted towards richer values. Very similar profiles of mean mole fractions *vs.* mixture fraction were observed by Masri and Bilger (1986) in measurements by aspiration probe in turbulent jet diffusion flames and these were also attributed to finite kinetics, with validation of this explanation given by Raman scattering

measurements later in Masri *et al.* (1990). However, the fact that the sampling probe measurements involve significant spatial averaging effects (Secion 2.4.5), that also cause a lowering of the peaks and their shifting to richer values, should not be disregarded and may be another reason for the observed shifting in the peak towards rich mixture fractions.

In anticipation of the results of Chapter 4, it is stated here that extinction of turbulent counterflow diffusion flames occurs at a critical value of the mean turbulent scalar dissipation rate, χ, defined in Section 3.2.5 and modelled by Eq. (3.2.8). It is reasonable then to describe the approach to extinction by the ratio χ/χ_{ext}, where χ_{ext} is the critical value at extinction, found experimentally, which depends only on the amount of premixedness in the fuel stream (Section 4.3.4). For pure diffusion flames, it is shown in Chapter 4 (Fig. 4.16) that $\chi_{ext} = 2.3\ s^{-1}$, for flames with X=0.5, $\chi_{ext} = 6.8\ s^{-1}$, and for flames with X=0.8, $\chi_{ext} = 17.4\ s^{-1}$; for each flame in Figs. 3.3.18 to 3.3.20, the scalar dissipation rate was estimated by evaluating $\chi = 2\ q'/L_{turb}\ f'^2$, with $q' = C_q\ U_o$ and with C_q given from Eq. (3.2.2), with L_{turb}=4mm, and f' found from numerical calculations as of Fig. 3.2.12b with the α corresponding to the jet separation and initial turbulence intensity of each flame (Eq. 3.2.19). The ratio χ/χ_{ext} for all flames was thus formed and the maximum mole fraction of CO_2, CO, and H_2 across the flame was plotted as a function of χ/χ_{ext} in Fig. 3.4.7.

It is evident from Fig. 3.4.7 that the mole fractions decrease slightly as χ/χ_{ext} approaches unity and that, more importantly, the points from flames of different H and H_p fall on the same, relatively smooth, curve for each premixedness examined. Therefore the ratio χ/χ_{ext} is appropriate for describing the approach to extinction of diffusion flames, and this result emphasises the importance of the mean turbulent scalar dissipation rate in turbulent diffusion flames. Furthermore, since the points along the curves in Fig. 3.4.7 contain points at the same U_o but different H and H_p (and therefore different f') *and* points at the same H and H_p but different U_o (and therefore same f'), the mean turbulent scalar dissipation rate qualitatively encompasses both the effects of unmixedness (high f' and so low mean mole fractions) and of finite kinetics (low mole fractions at all f').

Other points in connexion with Fig. 3.4.7 are that the mole fraction of CO_2 is almost the same for all premixedness, in contrast to the H_2 and CO concentrations that decrease as the premixedness increases for the same "distance" from extinction. As, however, the flame goes into the premixed flame regime, the CO and CO_2 mole fractions increase sharply (Section 3.4.3). It is difficult at present to discuss further these results because no laminar flame data, like those included in Fig. 3.4.6, exist for partially premixed counterflow diffusion flames, and so a comparison between turbulent and laminar flames is impossible. Note that the mixture fraction fluctuations at the location of the mean stoichiometric mixture fraction increase with partial premixing (Table 3.1), and

so reductions in the reaction products due to unmixedness are expected, but similar decreases should occur for *both* CO and CO_2 in contrast to the trends depicted in Fig. 3.4.7, and so one may conclude, awaiting confirmation, that mole fractions in laminar counterflow flames will show the same dependence on premixedness as in the turbulent diffusion flames studied here.

Temperatures

It was mentioned in Section 3.3.3 that the maximum mean temperature did not decrease as extinction was approached, either through increasing the bulk velocity or decreasing the jet separation, and emphasis was placed in explaining this observation by examining the temperature fluctuations. It was found, however, in the previous paragraph that the present diffusion flames do display evidence of finite kinetic effects in the reaction product mole fraction measurements. This apparent inconsistency is resolved by referring to the discussion in Section 3.3.3 on the temperature pdfs, where it was explained why small jet separations may lead to higher mean temperatures, and also by noting that it is experimentally difficult to locate accurately the peak value in a profile as steep as that of temperature; recall that the species measurements involve spatial averaging effects and so the measurement of, say, CO_2, results in smoother profiles than those of temperature, and thus in smaller error in determining the maximum values. It is believed therefore that the species measurements discussed in the previous paragraphs are more reliable for identifying chemical kinetic effects than the temperature measurements in the present counterflow diffusion flames.

Bulk stretch rate

The bulk stretch rate in the flow is important because it may lead to extinction of the flame, as shown both for twin premixed flames by Kostiuk *et al.* (1989) and for diffusion and single premixed flames in Chapter 4, and hence measurements of the bulk stretch rate are presented here. The bulk stretch rate in axisymmetric flow is defined as twice the mean radial velocity radial gradient, $\partial V/\partial r$, (Dixon–Lewis, 1990) and measurements of the radial velocity around the centreline are processed to find the bulk stretch rates presented in this Section. The radial velocity increases linearly with radius for both diffusion and premixed flames (Figs. 3.3.28 & 3.3.39), and so straight–line regression to the radial velocity profiles was used with negligible error to give the gradient $\partial V/\partial r$, and the axial velocity axial gradient, $\partial U/\partial z$, was also calculated by employing central differences to the measured profiles such as those of Figs. 3.3.22, and both gradients are discussed below.

Figures 3.4.8 and 3.4.9 show that $\partial V/\partial r$ increases from the jet exits to a peak at around the flame location, while the axial velocity gradient $-0.5\ \partial U/\partial z$ shows larger variations. For axisymmetric flow, continuity requires that

$$\frac{\partial V}{\partial r} = -0.5 \frac{1}{\rho} \frac{\partial(\rho U)}{\partial z},$$

which reduces to

$$\frac{\partial V}{\partial r} = -0.5 \frac{\partial U}{\partial z} \qquad (3.4.4)$$

for constant–density flow. Far from the flame therefore, where the temperature is at its initial value, the two curves in Fig. 3.4.8 coincide, but in the flame, the density variations imply that the two mean velocity gradients in Eq. (3.4.4) are different, and this is reflected in the graphs. The bulk stretch rate at the flame is almost the same for flames with and without partial premixing and is smaller for large jet separations (Fig. 3.4.9); the normalised stretch rate $(\partial V/\partial r)/(U_o/H)$ should be equal to unity, if the estimate used in Eq. (3.4.1) (and in Chapter 4 and by Kostiuk *et al.*, 1989) was correct, and Fig. 3.4.10 shows that the measured stretch rate on the flame is higher than the estimated one by a factor of about two, but also that this factor does not depend much on the jet separation and flame type. The estimate of $2U_o/H$ therefore underestimates the actual stretch rate on the flame, but by an approximately constant factor.

Similar results have been found for laminar (Rolon *et al.*, 1991; Dixon–Lewis, 1990) and for turbulent counterflow premixed flames (Kostiuk *et al.*, 1993b) and suggest that detailed velocity measurements, such as those presented here, should be performed if an accurate determination of the stretch rate on the flame is required. The data of stretch rate in Figs. 3.4.8 and 3.4.9 will assist the evaluation of theoretical modelling of the present flames, since most analyses of the velocity field concentrate on variations along the centreline and thus solve for the stretch rate (Dixon–Lewis, 1990). If the flow exiting from the jets resembles a plug flow, the boundary conditions at the jets are well–characterised, but difficulties in the modelling may arise if the exit flows are not uniform, as in the present experiments, and these difficulties can be overcome by referring to the measurements of stretch rate, such as those shown here, as boundary conditions.

A final point, based on the profiles of $-\partial U/\partial z$, is that these show *identical* axial variations with the axial r.m.s. fluctuations (for example, Figs. 3.4.8 and 3.3.22b, d, & f), and so the axial turbulence in the measurements is increased over its initial value by the action of the velocity gradient in the axial direction. The turbulence therefore in the present flows is dominated by production through normal stress – normal strain, without any shear effects, confirming thus the conclusion reached in Section 3.4.2 that the evolution of the turbulence depends mostly on the mean flow gradients.

Turbulent stretch rate

The small–scale turbulent stretch rate on the flame has been shown to affect extinction and it is important to consider how this quantity may be estimated in the light of the present velocity measurements. It has been shown both here (Fig. 3.2.10 & 3.2.11) and by Kostiuk *et al.* (1993a) that part of the measured *axial* fluctuations around the stagnation point in opposed jet flows is due to sampling fluid from either jet and hence with different mean velocities, giving thus rise to high r.m.s. values. It is not clear then how the measured fluctuations are related to the actual small–scale stretch rate. It is more appropriate, therefore, in estimates of the small–scale stretch rate to use the measured values of the *radial* turbulence which have not been affected by this phenomenon of unsteady motion of the jet stagnation point.

It is recommended that simultaneous measurements of axial and radial velocity and temperature, processed to give the r.m.s. velocities conditional on a high temperature, are a more accurate determination of the velocity fluctuations that the *flame* experiences, which are the fluctuations pertinent to the flame behaviour. Such measurements would also result in the determination of flux, which would be interesting in their own right.

3.4.6 Mixing in opposed jet flows

In this Section the findings concerning the instantaneous structure of the mixture fraction (Figs. 3.2.18, 3.2.20) in the inert opposed jet flows are discussed in more detail. Although only the *mean* mixture fraction between inert and reacting flows has been compared, it is expected that the fluctuations as found in the inert flow experiments are similar to the mixture fraction fluctuations under reacting conditions and so the issues raised below for mixing in inert flows are applicable to counterflow diffusion flames as well. It was mentioned in Section 3.2.5 that the theoretical predictions of f' depend on the parameter α which is proportional to the ratio of the mean flow timescale (H/U_o) to the large–eddy turbulent timescale (L_{turb}/q'). Based on assumptions about the turbulence lengthscale and measurements of the turbulence intensity, α was estimated to lie in the range 0.45 to 1.1. The fact that this value is of the order of unity, or less, implies that a mean residence time in the flow is smaller than the large–eddy turnover time, and the implication of this observation for the velocities and turbulent eddy shapes were discussed in Sections 3.4.2 and 3.4.4 respectively by introducing results from Rapid Distortion Theory, which is applicable for this flow precisely because the bulk flow strain rates are high compared to the turbulent strain rates. The implications for mixing of this disparity in timescales are now discussed.

Short residence times

Stapountzis *et al.* (1986) measured the statistics of temperature released into decaying wind–tunnel turbulence by heating a wire, so that the experiment simulated the diffusion from a line source in homogeneous turbulence. It was found that far downstream of the source, the scalar pdfs were approximately Gaussian, but that close to the source the pdfs were bimodal with peaks at hot and cold temperatures, similar to the pdfs measured in the present experiments. Close to the line source in the experiment of Stapountzis *et al.* (1986), the time–of–flight was short compared with an eddy timescale, and so the thermal plume released from the source kept its coherence; the scalar fluctuations were mostly due to the plume "meandering", as these authors called it, in the cross–stream direction. Bimodal pdfs of passive scalars have also been observed by Eswaran and Pope (1988) in direct numerical simulations of turbulence into which "blobs" of a passive scalar were introduced at a certain time. At times from the scalar's release shorter than about one large–eddy timescale, the pdfs of the scalar were bimodal and this bimodality became less pronounced as time passed with the pdfs becoming eventually unimodal at long times, results consistent with those of Stapountzis *et al.* (1986). It is then not surprising that in the opposed jet flow, where residence times are short, the probability density functions of the mixture fraction are bimodal with small probabilities of intermediate values. It is also consistent with these results and those of Eswaran and Pope (1988) and Stapountzis *at al.* (1986) to consider that, analogous to a coherent meandering plume, molecular mixing in the opposed jet flow occurs in the thin interfaces separating the two jets, as also mentioned in Section 3.2.6 and 3.4.2, and such a description is discussed next.

Instantaneous scalar structure

A conceptual model of mixing in the opposed jet flow may be based on the finding in Fig. 3.2.20a that the scalar fluctuations are characterised by well–defined transitions between cold and hot values, and that the frequency of these transitions scales with the velocity timescales. At the centreline of the opposed flow, the two jets impinge and with an instantaneous interface which can be viewed as a laminar diffusion layer strained in an unsteady manner by the turbulent field that separates the two jets. The instantaneous mixture fraction profile in a direction normal to the interface can be described by an error function from zero to unity, similar to that expected from a laminar counterflow, and the thickness of this profile would be on the order of the Kolmogorov lengthscale (Gibson, 1968). The layer would be convected in the axial and radial directions by the turbulence and because an eddy turnover time is long compared with the residence time in the flow, the interface will not have enough time to wrinkle, as would be the case if the mean flow was slow compared to the turbulence (Dimotakis, 1989). Therefore these unsteady laminar diffusion layers, which separate the two jets, retain

their identity, with the instantaneous zero–fluid side being *always* towards, and at the temperature of, the cold jet, and with the instantaneous unity–fluid side of the interface *always* towards, and at the temperature of, the hot jet. This suggests that the measured scalar fluctuations are due to the movement of laminar diffusion layers, always separating zero– and unity–fluid, and would depend on the lengthscale of this movement and on the thicknesses of these layers.

Flapping Model for inert mixing

The ideas behind the conceptual picture in the previous paragraph are elaborated in the Flapping Model of scalar turbulence (Kerstein, 1991). In the context of this model, the randomness in the scalar is due to the randomness in positioning an invariant scalar profile relative to the measuring location, and the ensemble–averaged mean and r.m.s. of the scalar are given by the convolution of the profile shape with the probability of profile displacements. Kerstein (1991) used this model to predict the scalar statistics in turbulent shear flows by considering profiles of thickness of the order of the mean flow width flapping in the cross–stream direction, and Verravalli and Warhaft (1990) (see also the references in that paper) predicted many of the features of their scalar measurements of thermal dispersion from a line source in wind–tunnel turbulence using similar concepts. Here, these ideas are used for interpreting the large–scale scalar fluctuations based on the movement of the small–scale diffusion layers separating the opposed jets; note that such a picture of scalar fluctuations has already been used successfully in explaining the observation that the correlation coefficient between the temperature fluctuations in diffusion flames at two points bracketing the flame in the axial direction is negative (Fig. 3.4.5b; Section 3.4.4). Below, quantitative predictions from the Flapping Model are presented and compared with the measurements in Section 3.2.6.

Consider a scalar profile resembling an error function between zero and unity of characteristic width w and whose centre is at a distance y from the (arbitrarily set) origin (Fig. 3.4.11). Consider now that the distance y is a random variable with mean Y and r.m.s. y' and that, for simplicity, obeys a Gaussian distribution. Then, the resulting scalar statistics at the origin would depend on the profile shape and on the relative magnitude of the profile displacements, y', to the profile width, and quantitative results can be made by performing a Monte–Carlo simulation, i.e. by choosing numerically from a random number generator the quantity y to be normally distributed with mean Y and r.m.s. y', locating the profile at y, and calculating the scalar value at the origin.

Figure 3.4.12 shows that the mean and r.m.s. values found by such simulations depend on the quantity y'/w, denoted by β, so that for large β, the scalar is spread over larger distances than for small β, and the r.m.s. values are larger and also spread over larger distances. Note that all lengths have been made dimensionless with w, so that β

is the only parameter of the simulation[9]. Figure 3.4.13a shows that the maximum scalar fluctuations (at the location where $\langle F \rangle$=0.5, i.e. the origin) increase with β and reach a plateau at about $f' \approx 0.45$ at about $\beta \approx 3$, i.e. the r.m.s. of profile displacements being three times the profile width, and Fig. 3.4.13b shows that the corresponding probability density functions of the scalar predicted at the origin for different β are unimodal for small β and later become bimodal for β larger than about one.

The qualitative correspondence of these predictions with the mixing measurements in the opposed jet flow is as follows. The mean scalar width decreases with decreasing β, and so small β corresponds to measurements with large H_p (i.e. small q') or small jet separation; the r.m.s. values decrease with decreasing β, and this also corresponds to large H_p (Fig. 3.2.17b); finally, the scalar pdfs at $\langle F \rangle$=0.5 become bimodal after about $\beta \approx 1$, and so the measurements of bimodal scalar mixture fraction pdf (Fig. 3.2.18) correspond to $\beta > 1$. Note also that the evolution of the pdfs shown in Fig. 3.4.13b is very similar to the evolution of the scalar pdfs from bimodal to unimodal shape with increasing time from the release of the scalar in direct numerical simulations (Eswaran and Pope, 1988) and so increasing β corresponds to decreasing residence time. It is clear that the Flapping Model reproduces important features of the measured statistics of the passive scalar in inert opposed jet flows and below, an effort is made to examine the temperature fluctuation measurements in *flames* with the aid of this model in order to extend the validity of the proposed concepts.

Flapping Model for flames

Consider in Fig. 3.4.11 a Gaussian scalar profile of height of unity and consider again the distance of this profile from the measuring point as a random variable of given mean and variance. This situation is meant to approximate the profile of temperature or, say, CO_2, across a laminar diffusion flamelet that is, in turn, convected by the turbulence. Figure 3.4.14 shows that the mean values decrease as β increases, i.e. as the r.m.s. of the profile displacements increase relative to the profile width, and that the r.m.s. of the scalar fluctuations increase. The pdfs at the origin (the location of maximum mean value) have a peak at unity but with progressively increasing probabilities of smaller values, and eventually a peak at zero, as β increases (Fig. 3.4.15a). Finally, Fig. 3.4.15b shows that the correlation coefficient between two points symmetrically placed about the origin is positive at small separations, but becomes negative at separations larger than about a profile width, because an increasing scalar fluctuation registered at one side of the maximum corresponds always to a decreasing fluctuation at the other side.

---

[9] In the numerical calculations described here, the profile has been defined by $f = 0.5\,[\,1 - \mathrm{erf}((y-Y)/w)]$.

The qualitative correspondence with the temperature measurements of Section 3.3.3 is unexpectedly good and remarkable. As β increases, the maximum mean scalar decreases and in the experiment, the mean temperature decreases as H increases, Fig. 3.3.8, and as H_p decreases, Fig. 3.3.6. As β increases, the mean profile is spread over a larger distance while in the measurements, the mean temperature is spread over a larger distance as H increases and at small H_p, Fig. 3.3.6. Also, as β increases, the height of low–value peak in the pdf at the location of the maximum mean scalar increases and the same is observed in temperature measurements at large H and small H_p; Figs. 3.3.9 to 3.3.12, and finally, the correlation coefficient between the temperature fluctuations at two points across the flame has the same qualitative shape in the Flapping Model predictions and the measurements (Fig. 3.4.5).

Discussion on the Flapping Model

The conceptual picture of the Flapping Model reproduces accurately the qualitative dependencies of the scalar fluctuations in inert and reacting flows. In the previous two sub–sections it was identified that increasing β corresponds to large jet separations and small turbulence intensities; it is possible that increasing the jet separation corresponds to increasing the r.m.s. of the profile displacements, while decreasing the turbulence intensity corresponds to increasing the profile thickness, suggested by the fact that the laminar strained interfaces separating the two jets are thicker, with weaker turbulence, because the Kolmogorov lengthscale, which is close to the thickness of these layers, increases as the turbulence decreases.

The Flapping Model does not contain any information about the *timescale* associated with the interface motions or about the thickness and shape of the interface, because it is based on the conjecture that if an appropriate invariant small–scale profile can be found, then the ensemble averages can be approximately predicted. Therefore the Flapping Model cannot provide any information for processes associated with the unsteady nature of the turbulence, but insight about the *mean* values associated with certain small–scale motions *can* be obtained. For example, the spatial gradient in the strained diffusion layers between the two opposed jets corresponds to the scalar dissipation rate (Section 3.2.5), and so the dissipation rate associated with the error–function profile depicted in Fig. 3.4.11a is represented by Fig. 3.4.11b. As the diffusion layer in Fig. 3.4.11a flaps, the scalar dissipation rate is determined by the flapping of Fig. 3.4.11b, and so the *mean* turbulent scalar dissipation rate, χ, changes with β in the manner shown in Fig. 3.4.14a. Therefore the mean turbulent scalar dissipation rate decreases as β increases, which suggests that in the opposed jet flow, the mean scalar dissipation rate is expected to decrease with increasing jet separation and decreasing turbulence intensity. This trend is consistent with the results of Section 3.2.5 from the eddy–viscosity model for the mixture fraction fluctuations f' and the model for

χ (Eq. 3.2.8); note, however, that the Flapping Model predicts that f' increases with β, and that the eddy–viscosity model predicts that f' *decreases* with increasing H, and the discrepancy suggests that Eq. (3.2.8) does not accurately model the scalar dissipation rate, which may, in turn, result in the erroneous prediction of f' in the eddy–viscosity model, and a possible reason for the inadequacy of Eq. (3.2.8) is explored next.

The scalar dissipation rate

It has been emphasised that the existence of invariant scalar profiles attached to the interfaces separating the jets, which motivated the Flapping Model predictions presented previously, is permitted by the fact that in the present opposed jet flows there is no time available to the turbulence to convolute appreciably the interfaces before these are swept radially outwards by the action of the high bulk stretch rate. It was shown in Section 3.4.5 and will be shown in Chapter 4 that the scalar dissipation rate in diffusion flames correlates the approach of these flames to extinction and their extinction limits, and so the implications of short residence times for the prediction of the mean turbulent scalar dissipation rate are discussed below.

A standard modelling assumption for the mean scalar dissipation rate, χ, is that the thermal and mechanical dissipation timescales are in a constant ratio (the factor 2 in Eq. 3.2.8), so that

$$\chi = 2 f'^2 / (\text{mechanical timescale}), \qquad (3.4.5)$$

(Jones and Whitelaw, 1982). Warhaft and Lumley (1978) found experimentally that the timescale ratio depended on the scale at which the scalar was introduced into their homogeneous turbulent flow (i.e. the ratio of the integral scalar to velocity lengthscale), so that the timescale ratio varied by up to an additional factor of two from its commonly accepted value. Eswaran and Pope (1988) calculated the scalar dissipation rate in direct numerical simulations and found that at short times from the release of the scalar, χ was larger than the standard model would suggest by a factor of about three. At times longer than about one eddy turnover time however, χ became close to the estimate from Eq. (3.4.5). Therefore the scalar dissipation rate depends on the time elapsed from the release of the scalar, and so questions arise about the applicability of the model of Eq. (3.4.5) for opposed jet flows where residence times are short. In conjunction with the discrepancies between the predictions of the eddy–viscosity formulation and the measurements discussed in Section 3.2.7, it is clear that models for opposed jet flows should account for the observation that the scalar turbulence is "young" compared with the velocity turbulence.

3.4 SUMMARY OF CHAPTER 3

Flat, blue, axisymmetric, pure and partially premixed diffusion and fully premixed turbulent flames have been stabilised in the opposed jet flow from two identical straight pipes fitted with perforated plates to promote turbulence in the jet flows. Photographs of these flames and measurements of velocity, temperature, and species mole fractions in inert and reacting flows have been presented and discussed in this Chapter and the following conclusions were reached.

The straining involved in the decelerating flow of inert opposed jets increased the turbulence along the stagnation streamline from its initial value, that was determined by the characteristics of the perforated plate, by up to a factor of two at the stagnation point, but part of the measured high axial fluctuations were due to intermittent sampling of fluid originating from either jet and thus having mean velocities of different sign.

The mixing between two inert jets was analysed theoretically, by formulating an eddy–viscosity description for the mean mixture fraction and its fluctuations, and experimentally, by heating one jet and measuring the instantaneous temperature in the mixing region. The analysis assumed radial uniformity, and the experiment confirmed this for radii up to about one jet radius, and both the analysis and the experiment showed that the axial width of the mixing layer increased with jet separation and with increasing turbulence intensity, but was independent of the bulk flow velocity, U_o, because the eddy diffusivity was proportional to it. The r.m.s. fluctuations, f', were predicted to depend only on the ratio $\alpha=2q'H/(U_oL_{turb})$, which is interpreted as the ratio of the mean flow timescale to the turbulent turn–over time, and numerical solutions of the modelled equation for f' showed that f' decreased as α increased, in disagreement with the data which showed the opposite trend. The discrepancy was attributed to the inadequate modelling of the scalar dissipation rate, χ, because the widely–used models found in the literature for χ do not account for the observation that in the present opposed jet flows the residence times are short compared to the turbulent timescales, which has been known to have a profound effect on χ. The instantaneous mixture fraction, defined as a normalised temperature to take the value of zero in one stream and unity in the other, showed a structure resembling a square wave, with sharp transitions from zero to unity, which thus resulted in bimodal probability density functions, and it is therefore not clear whether the standard modelling approaches for the dissipation rate used in the analysis are appropriate for such a scalar behaviour.

These measurements motivated the following physical model for mixing: the jets are separated by thin strained interfaces across which molecular diffusion is important and which are randomly convected by the turbulence, but retain the property of always

separating regions occupied solely by fluid originating from the respective jet. Predictions with techniques used in the Flapping Model of scalar turbulence for shear flows and assumptions pertinent to the statistics of the interface displacements and to the scalar profile across these small–scale interfaces, yielded results for the mean, r.m.s. fluctuations, and pdfs of the mixture fraction in qualitative agreement with the measurements. This physical model is warranted mostly because the bulk radial flow is fast enough to transport these interfaces outwards before these are convoluted by the turbulence, and therefore its success emphasises that models for the scalar field in opposed jet flows should account for the observation that the scalar and the velocity turbulence evolve according to different timescales.

The axial mean velocities in flames showed qualitatively different axial distributions in pure diffusion, partially premixed, or fully premixed flames, and for the latter type, also depended on the equivalence ratio. Pure diffusion flames were located in the air side of the stagnation plane and induced an acceleration of the flow, which was qualitatively similar, but of smaller magnitude, to the acceleration observed through lean premixed flames burning away from the stagnation plane. In contrast, partially premixed diffusion flames and weak premixed flames, that were found close to the stagnation plane, could not accommodate the axial expansion and so the axial velocity profile was smoother and closer to that of the inert flow. The axial velocity fluctuations followed the axial velocity gradient, so that these increased where the latter increased and hence the presence of the flame, which might alter the axial velocity gradients, also altered the axial turbulence distribution accordingly. In contrast, the radial fluctuations increased to a peak at the stagnation point for all types of flames, and the mean radial velocity gradient $\partial V/\partial r$ also peaked there.

The data are consistent with the notion that the straining flow increases the turbulence levels and also show that the turbulence does not influence the mean field, so that approaches like Rapid Distortion Theory, which track the evolution of turbulence in a prescribed mean field, may be appropriate for the opposed jet flow. In addition, the measurements show a large anisotropy in the two turbulence components that reverses at large radii with the radial being larger than the axial turbulence at the flame location, and this anisotropy should not be neglected in theoretical models.

Measurements of the mean mole fractions of stable species showed that the concentrations of reaction products decreased as the bulk velocity increased in both diffusion and premixed flames, and for diffusion flames, plots of these mole fractions against the mean mixture fraction calculated from the reacting flow measurements showed behaviour characteristic of finite chemical kinetic rates. The approach of unpremixed and partially premixed diffusion flames to extinction was quantified by the

ratio χ/χ_{ext}, where χ_{ext} is the mean turbulent scalar dissipation rate at the extinction of the particular type of flame, found experimentally in Chapter 4, and as this ratio increased, the mean mole fractions of reaction products decreased along unique curves for each value of X. Therefore, irrespective to whether the mean mole fractions of products in counterflow diffusion flames decrease due to unmixedness or due to finite rate kinetics, the mean scalar dissipation rate captures both effects.

The widths of the mean mixing layer in inert and reacting flows were identical, as found from comparisons of respective measurements, and this implies that the measurements of the fluctuations of the mixture fraction performed in the inert flow are appropriate for the reacting flow as well. The measured temperature fluctuations in diffusion flames showed wide probability density functions, with dependencies on jet separation and turbulence intensity captured successfully by the Flapping Model, and two–point measurements showed that the lengthscale in the radial direction was larger than in the axial direction, in agreement with other measurements of turbulent eddy shape in stagnating flows, and this lengthscale anisotropy further questions the use of standard modelling approaches for the opposed jet flow.

Figures for Chapter 3, Section 3.2

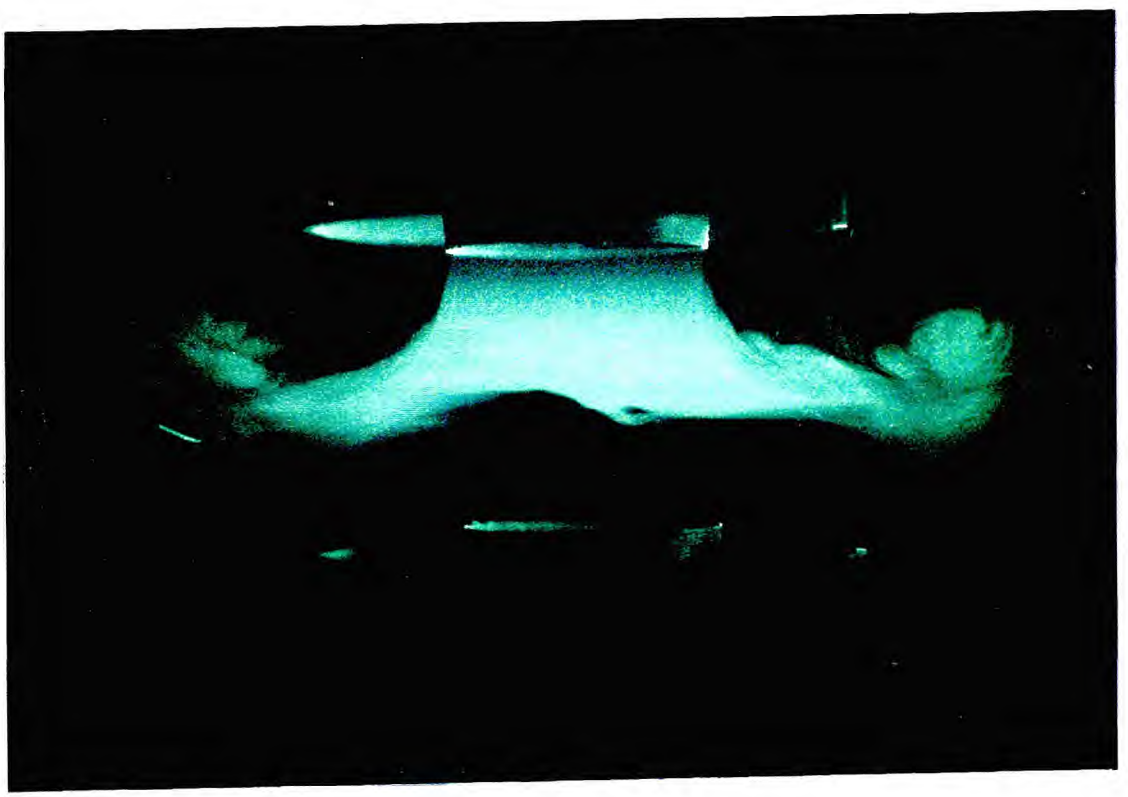


Figure 3.2.1 Photograph of the light scattered from alumina particles seeded in the upper jet of an inert opposed jet flow with H=25mm, H_p=55mm, and U_1=U_2=3.0m/s. Illumination is provided by a laser sheet of thickness about 1mm. Note the "waviness" in the interface between the two jets and the "curls" towards the right of the symmetry axis. Note also the vortex created at large radii outside the burner, but only the region along centreline and at about r=10mm (i.e. inside of the radius of the inner jet) are examined in this thesis.

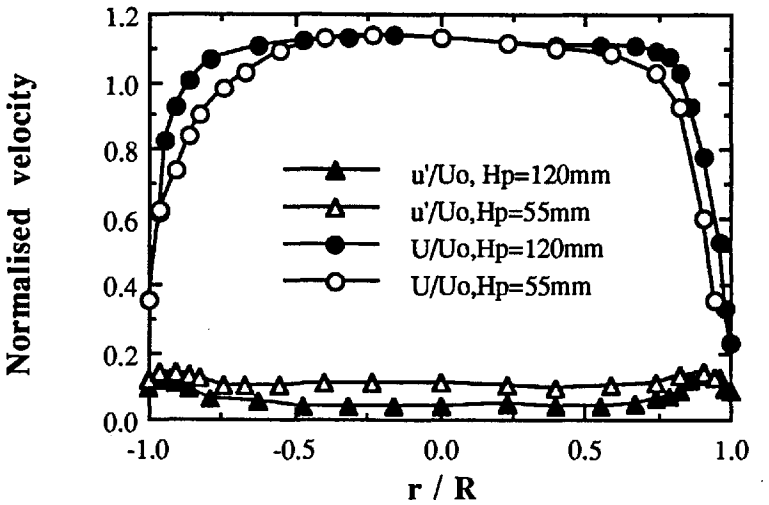


Figure 3.2.2 Mean and r.m.s. axial velocity radial variation across the exit plane of a single jet (z/D=0.08) for two locations of the perforated plate, H_p. The bulk velocity for the data with H_p=120mm was 3.13m/s and for H_p=55mm, U_o=2.0m/s.

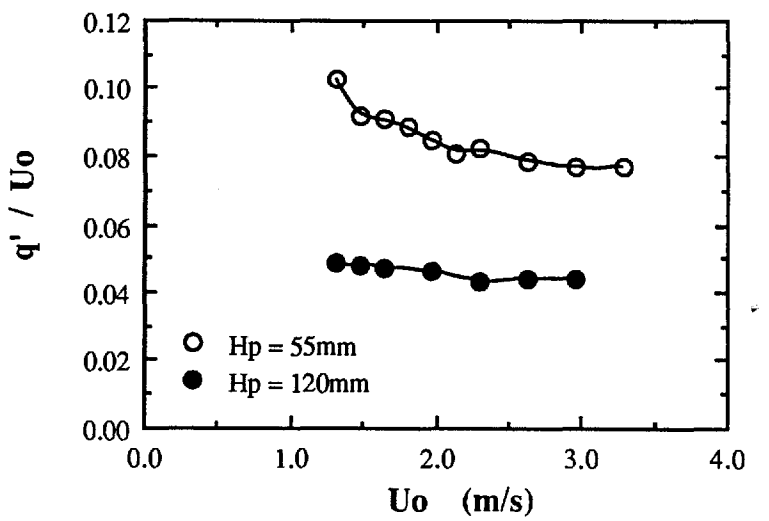


Figure 3.2.3 Variation of the turbulence intensity q' (Eq. 3.2.1) at r=0 at the exit of a single jet with bulk velocity for different locations of the perforated plate.

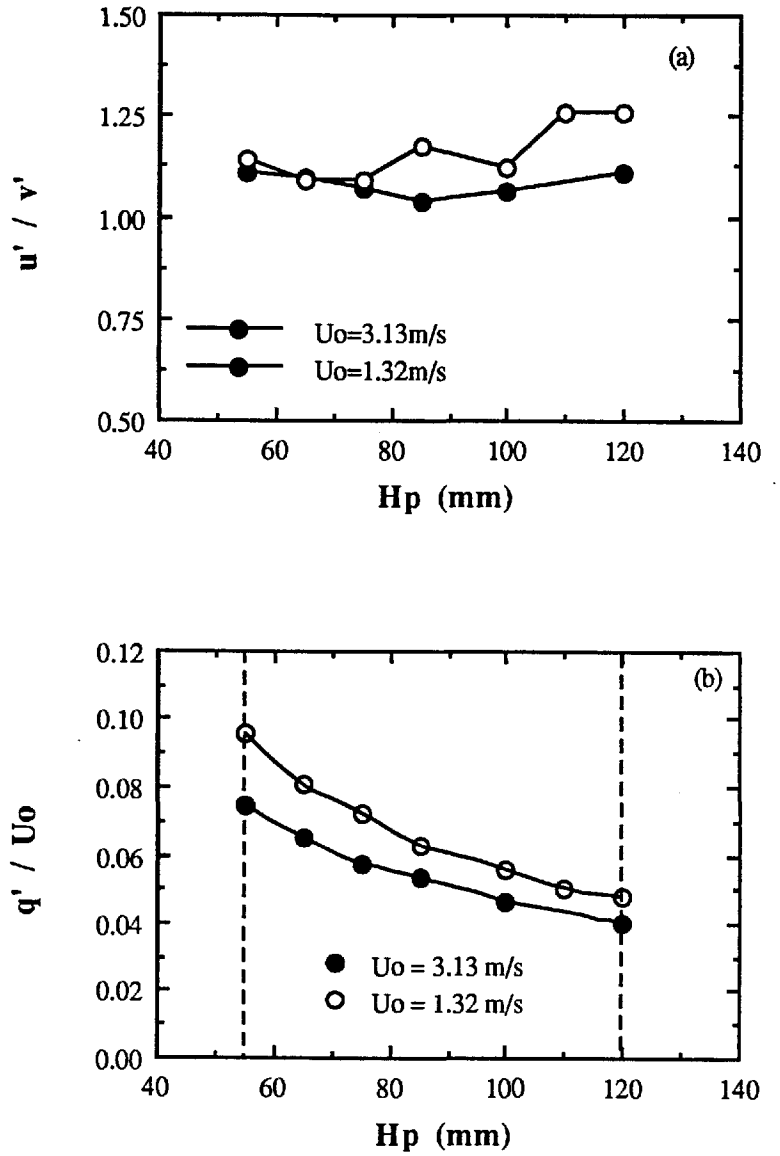


Figure 3.2.4 Variation of the anisotropy and the turbulence intensity (Eq. 3.2.1) at r=0 at the exit of a single jet with H_p for different bulk velocities. The dashed lines in (b) indicate the perforated plate locations used in most experiments in the thesis.

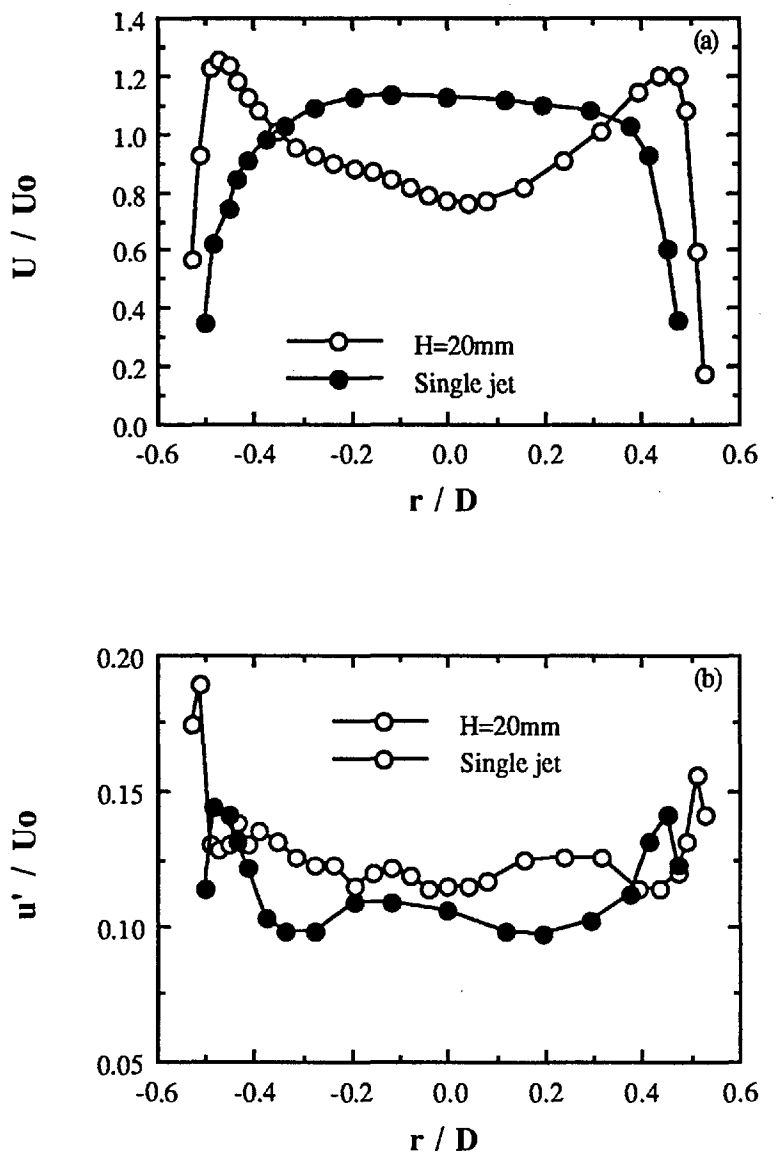


Figure 3.2.5 Comparison of the axial velocity radial variation at z=2mm in the jet exit of the single and the opposed jets with H=20mm. U_o=2.0m/s and H_p=55mm.

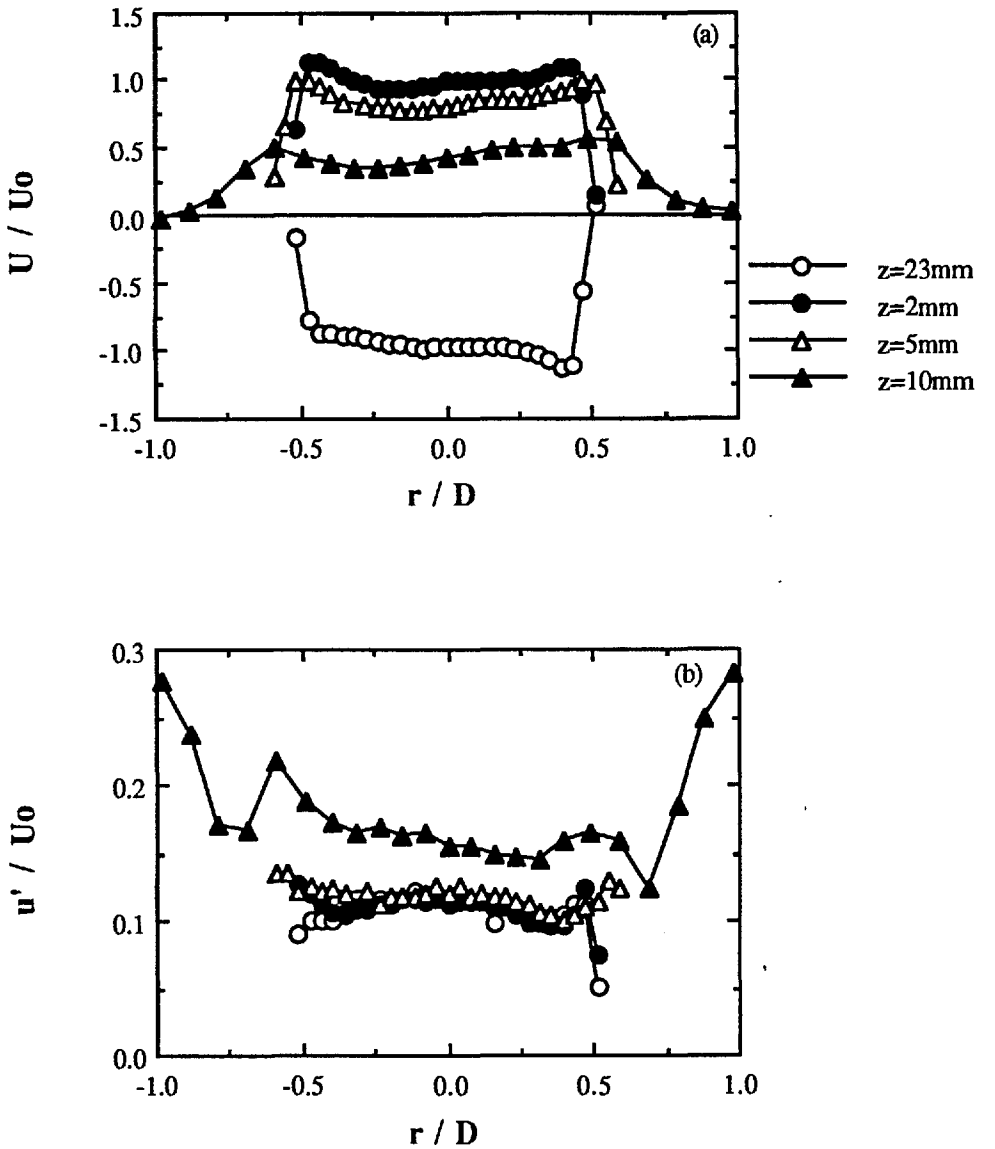


Figure 3.2.6 Radial variation of the mean and r.m.s. axial velocity at different axial locations for the inert opposed jet flow with H=25mm, U_o=1.62m/s, and H_p=55mm.

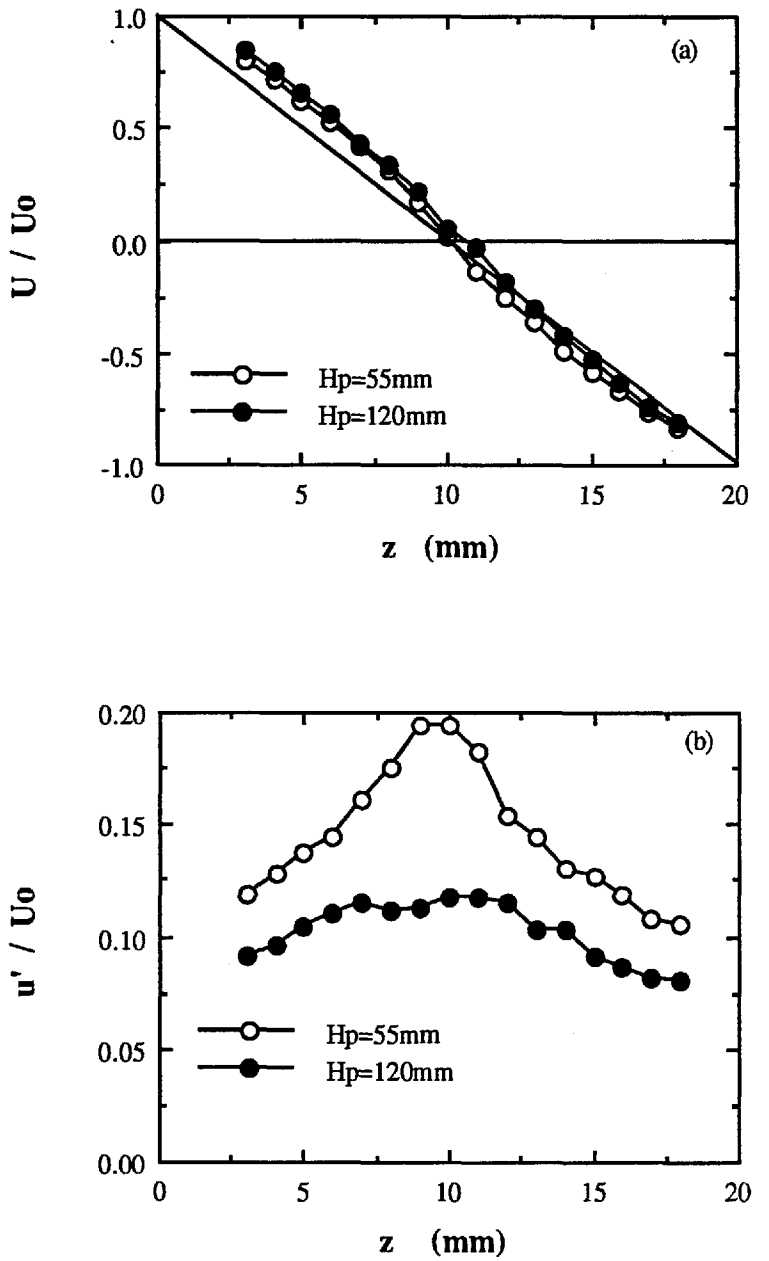


Figure 3.2.7 Axial traverses along the centreline of the inert opposed jet flow with H=20mm and U_o=1.64m/s for different H_p. A straight line in (a) depicts the potential flow model $U = -(2U_o/H)\ (z-Z_{st})$ where Z_{st} corresponds to the axial location of the stagnation point.

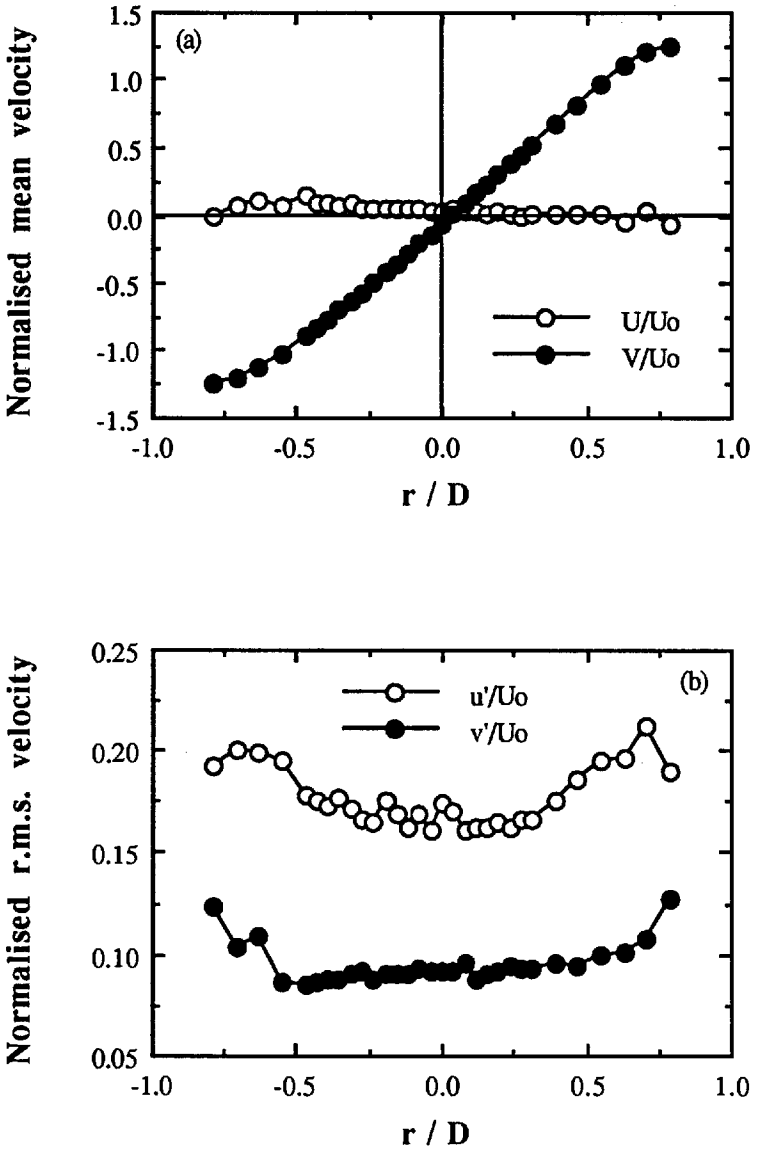


Figure 3.2.8 Radial variation close to the stagnation plane (z=10mm) of the axial and radial mean and r.m.s. velocity for the inert opposed jet flow with H=20mm, U_o=2.0m/s, and H_p=55mm.

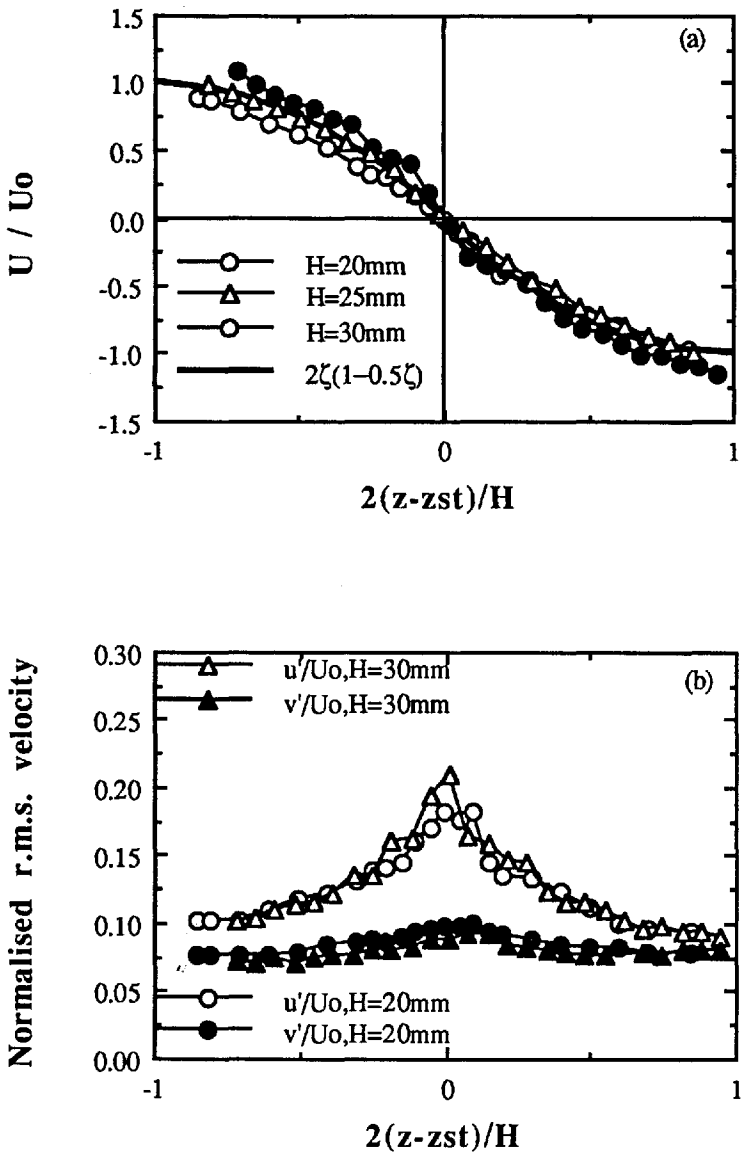


Figure 3.2.9 Centreline variation of the mean axial and r.m.s. axial and radial velocities for the inert flow with H_p=55mm and U_o=1.64m/s for different jet separations. In (a), the solid line depicts the theoretical prediction of Champion and Libby (1993) that $U/U_o=2\zeta(1-0.5\zeta)$ (Eq. 3.2.3) with $\zeta=2(z-Z_{st})/H$, z being measured from the exit plane of one jet, and Z_{st} being the axial coordinate of the stagnation point.

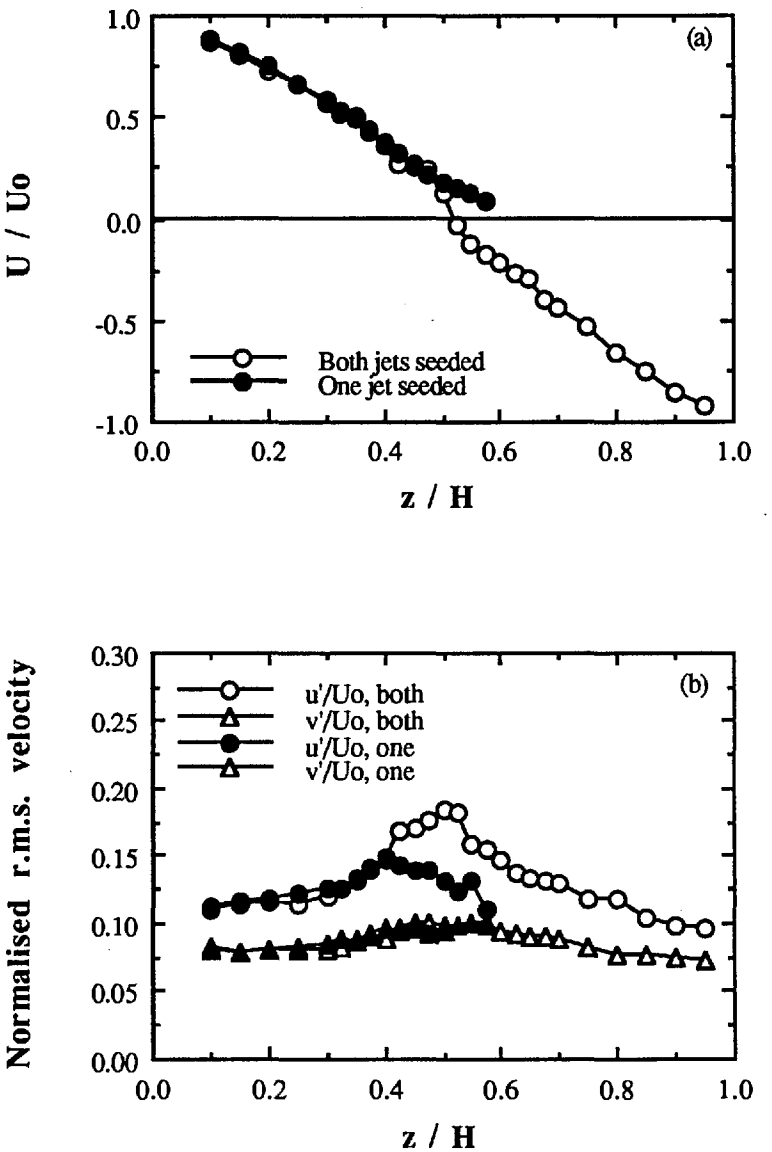


Figure 3.2.10 Centreline traverses in the opposed jet flow with H=20mm, U_o=1.64m/s, and H_p=55mm comparing jets when both and when only one of the jets are seeded with LDV scattering particles.

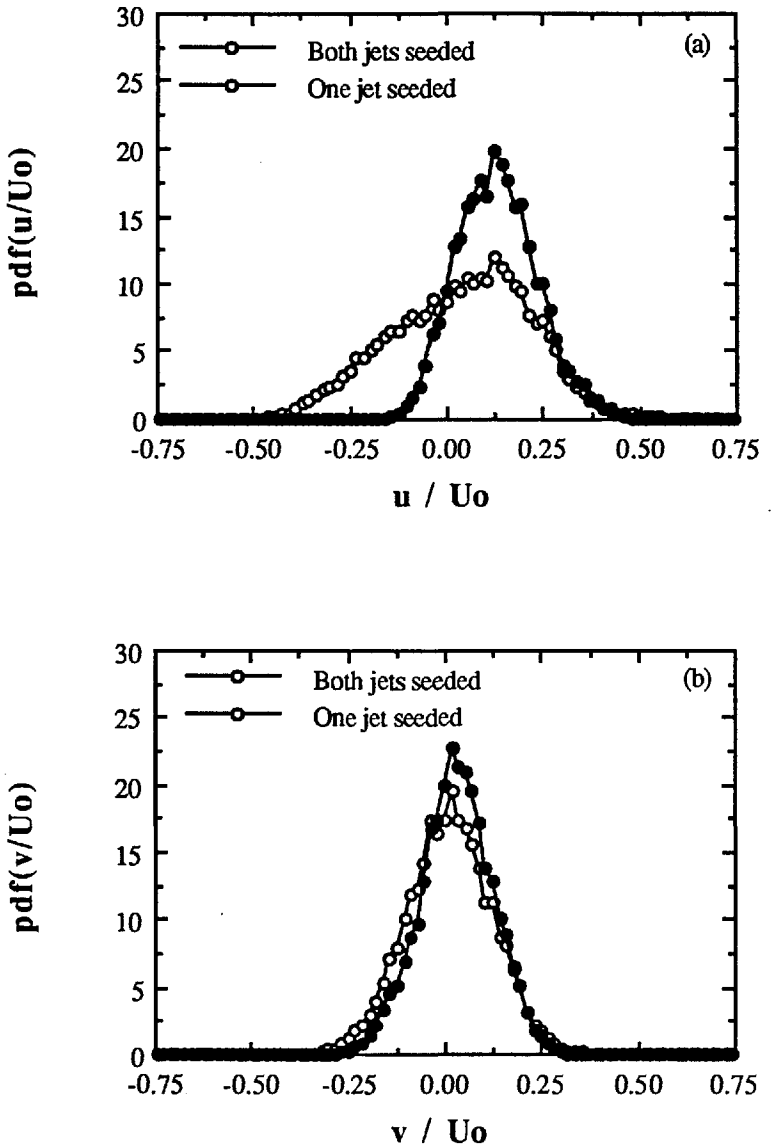


Figure 3.2.11 Probability density functions of axial and radial velocities close to the stagnation point at r=0 in an inert flow with H=20mm, U_o=1.64m/s, and H_p=55mm (same flow as in Fig. 3.2.9) with both and one jet seeded.

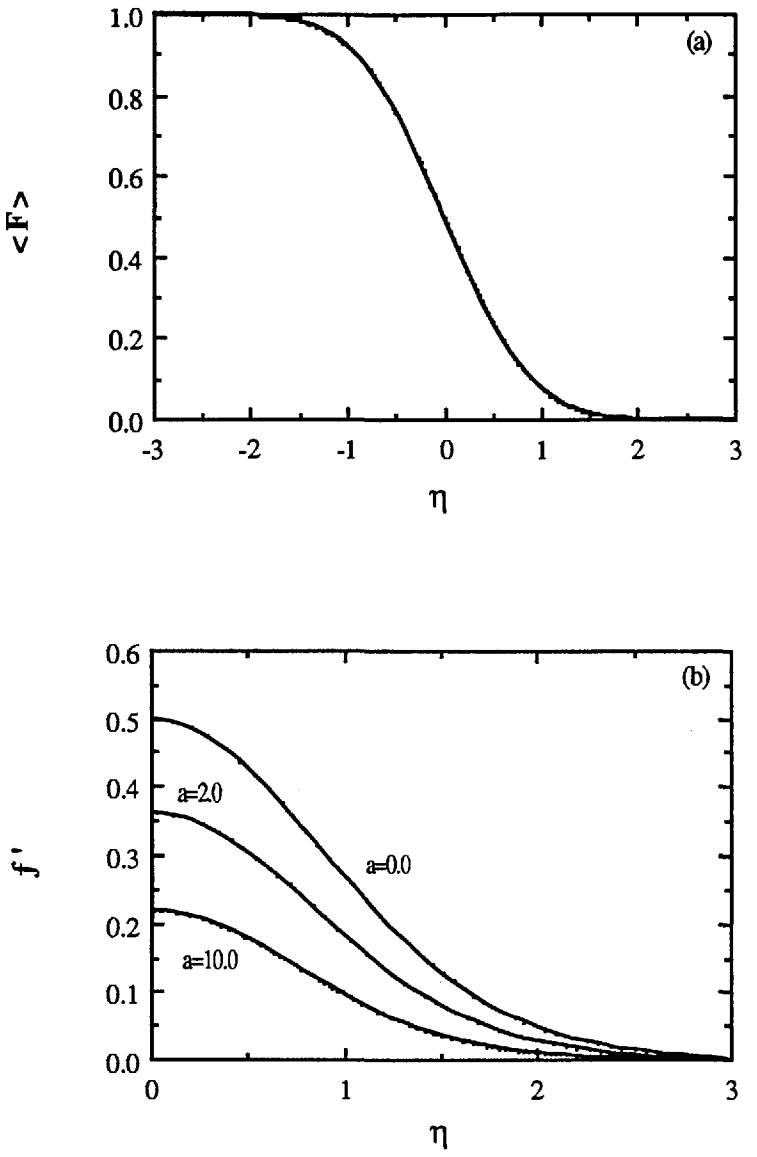


Figure 3.2.12 Mean and r.m.s. fluctuations of the mixture fraction across the mixing layer. In (a), Eq. (3.2.22) is plotted, and in (b), numerical solutions of Eq. (3.2.24) for different values of α (α=2 [q'/U] [H/L_{turb}]) are shown.

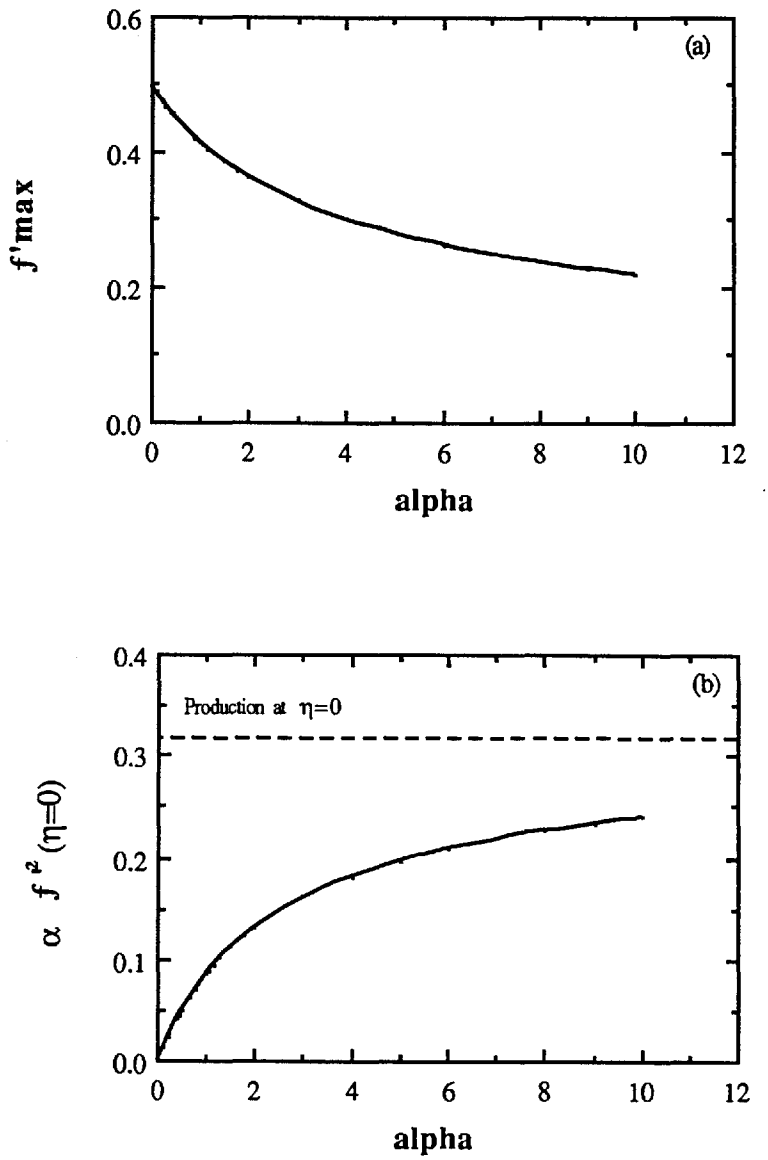


Figure 3.2.13 Variation of (a) the mixture fraction fluctuations at $\eta=0$ and (b) of one half of the dissipation rate, normalised by the bulk strain rate ($\chi=2\alpha f'^2 S$, Eq. 3.2.25), as a function of α.

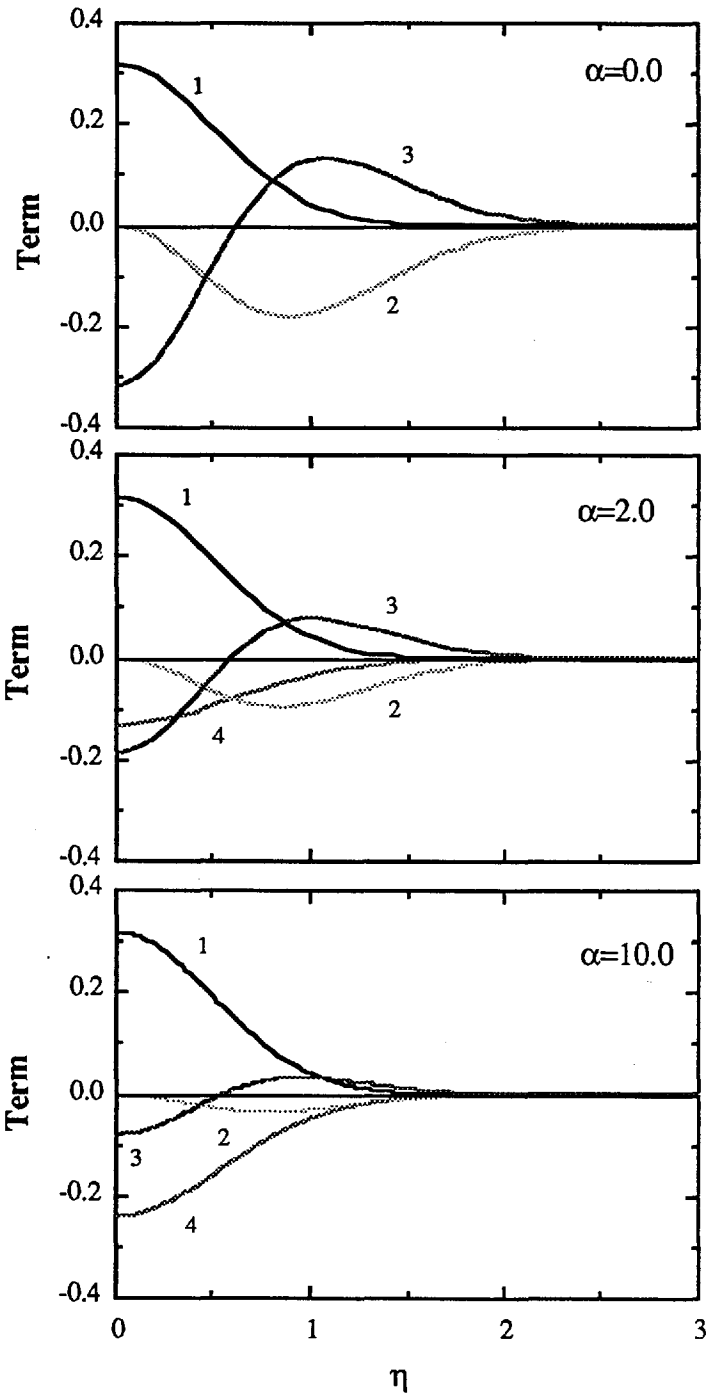


Figure 3.2.14 Axial variations of the production (1), convection (2), diffusion (3), and dissipation (4) terms in Eq. (3.2.24) for different values of α. A positive value in the y–axis denotes gain.

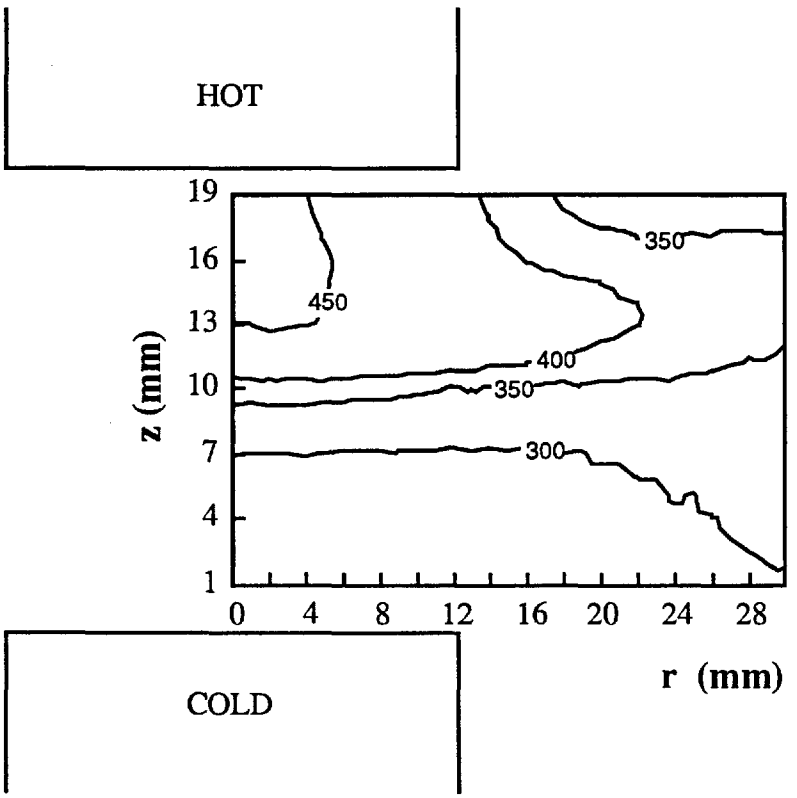


Figure 3.2.15 Contours of the mean temperature in the inert opposed jet flow with H=20mm, T_2=450K, U_1=1.88m/s and U_2=2.3m/s (so that the momentum flow rates were equal), and H_p=55mm. These contours were assembled from measurements in a square grid with 30 radial, spaced by one 1mm, and 25 axial points, spaced by 0.5mm at locations of steep changes and by 1mm elsewhere.

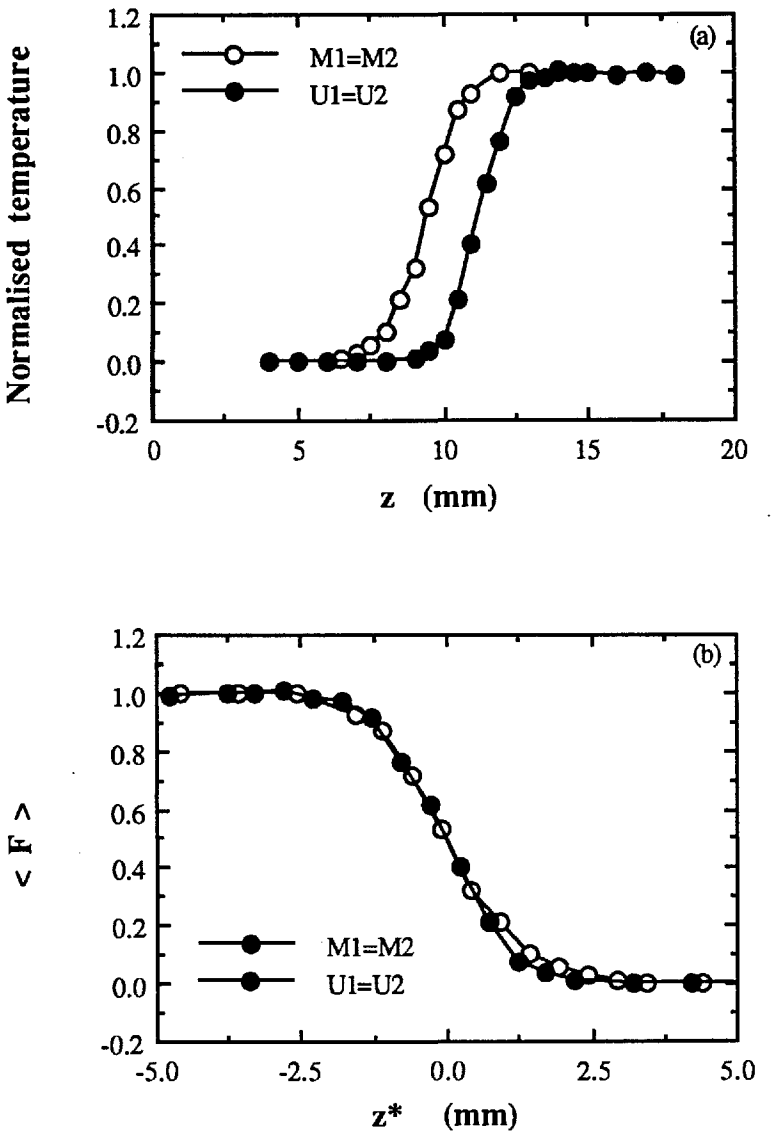


Figure 3.2.16 (a) Mean centreline normalised temperature $(T-T_1)/(T_2-T_1)$, with T_2=450K, H=20mm, H_p=55mm, in the inert opposed jet flow as a function of axial distance measured from the cold jet. (b) The same data, but plotted against z*, which is defined as z minus the distance from the point where $\langle F \rangle$=0.5 and with F being defined as $(T_2 - T)/(T_2-T_1)$ so as to be unity in the lower ("fuel" stream) and zero in the upper ("air" stream) and hence be compatible with the theoretical predictions of Section 3.2.5 and the measurements of Section 3.3.2. Two conditions, with the velocities of the two jets, $U_1=U_2$=2.3m/s being equal, and the momentum flow rates $\dot{M}_1=\rho_1 U_1^2$ and $\rho_2 U_2^2=\dot{M}_2$, with U_2=2.3m/s, being equal are shown.

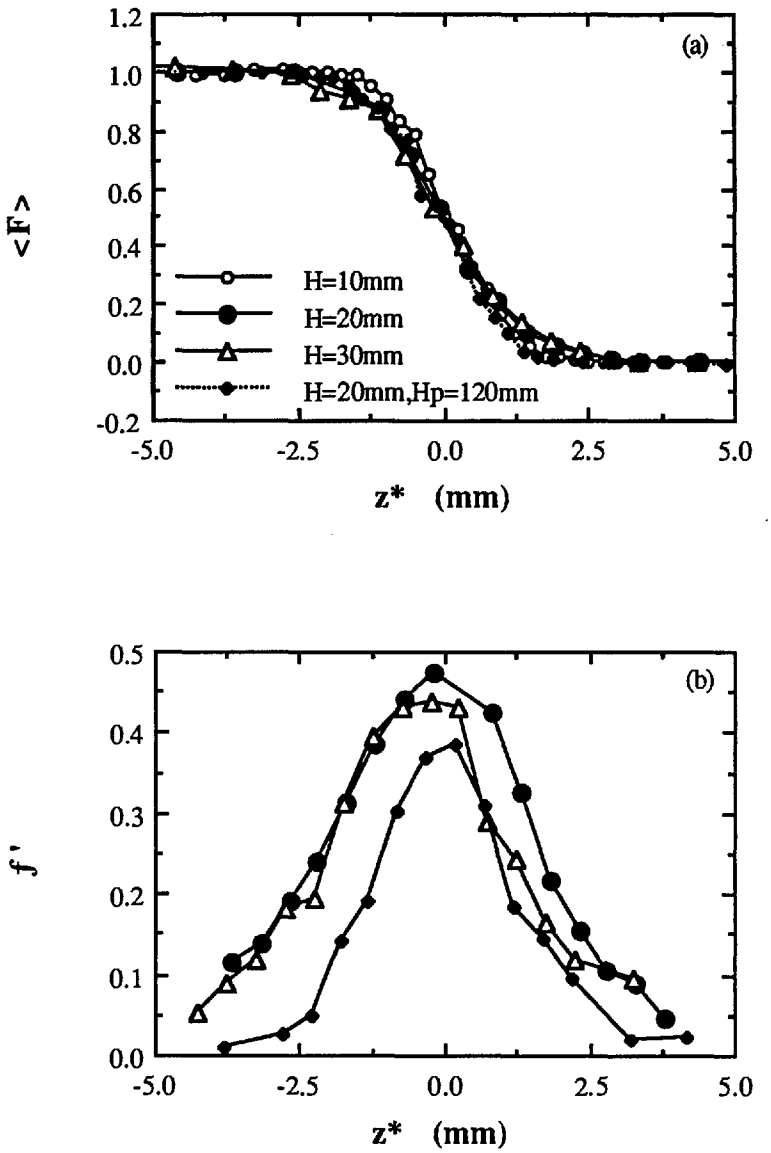


Figure 3.2.17 Centreline variations of the mean (a) and r.m.s. (b) mixture fraction for different jet separations and perforated plate locations. Where not mentioned, H_p=55mm. For all data, T_2=450K, and U_1=1.88m/s and U_2=2.3m/s.

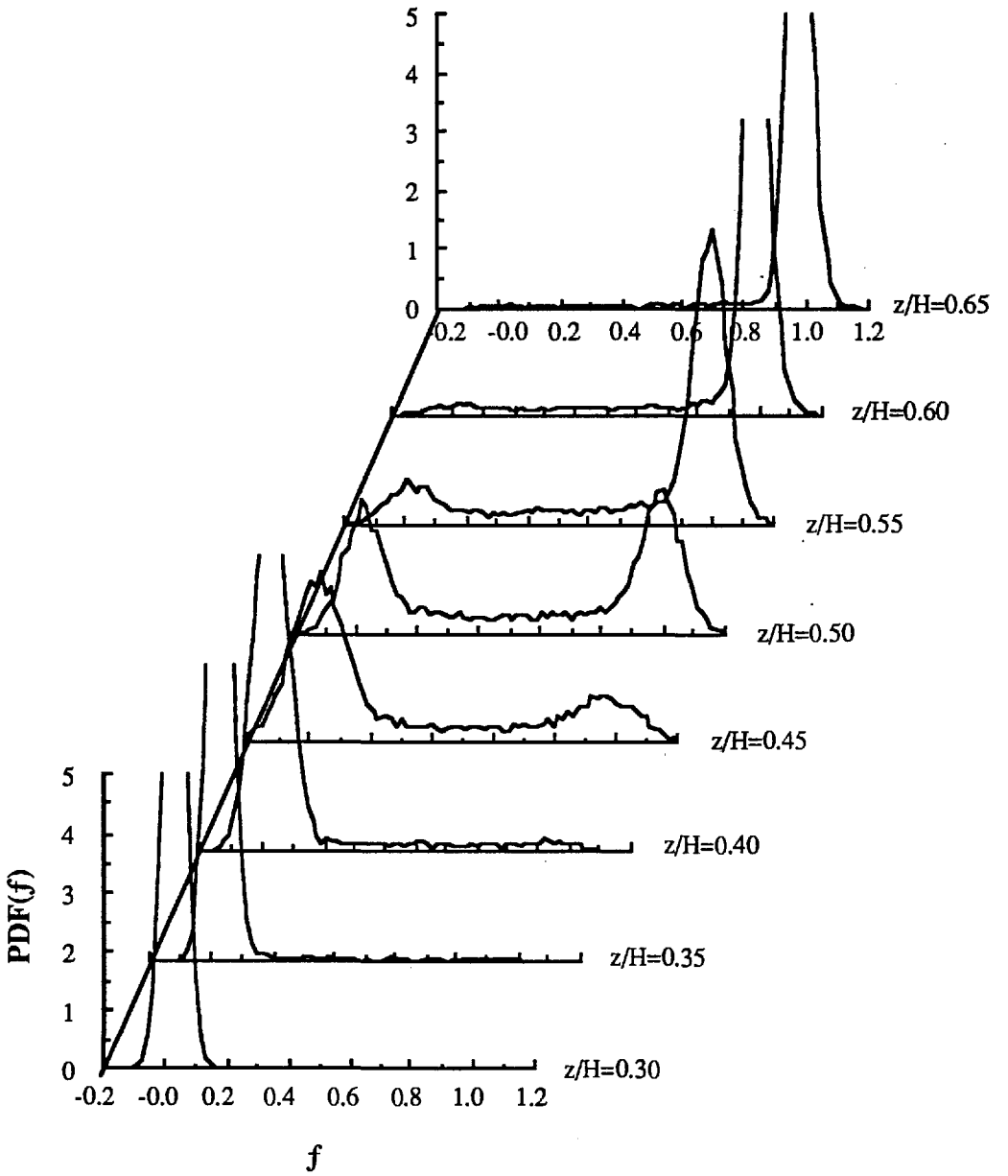


Figure 3.2.18 Probability density functions (pdf) of the normalised temperature $(T-T_1)/(T_2-T_1)$ along the centreline of the inert opposed jet flow with H=20mm, H_p=55mm, and U_1=1.88m/s and U_2=2.3m/s.

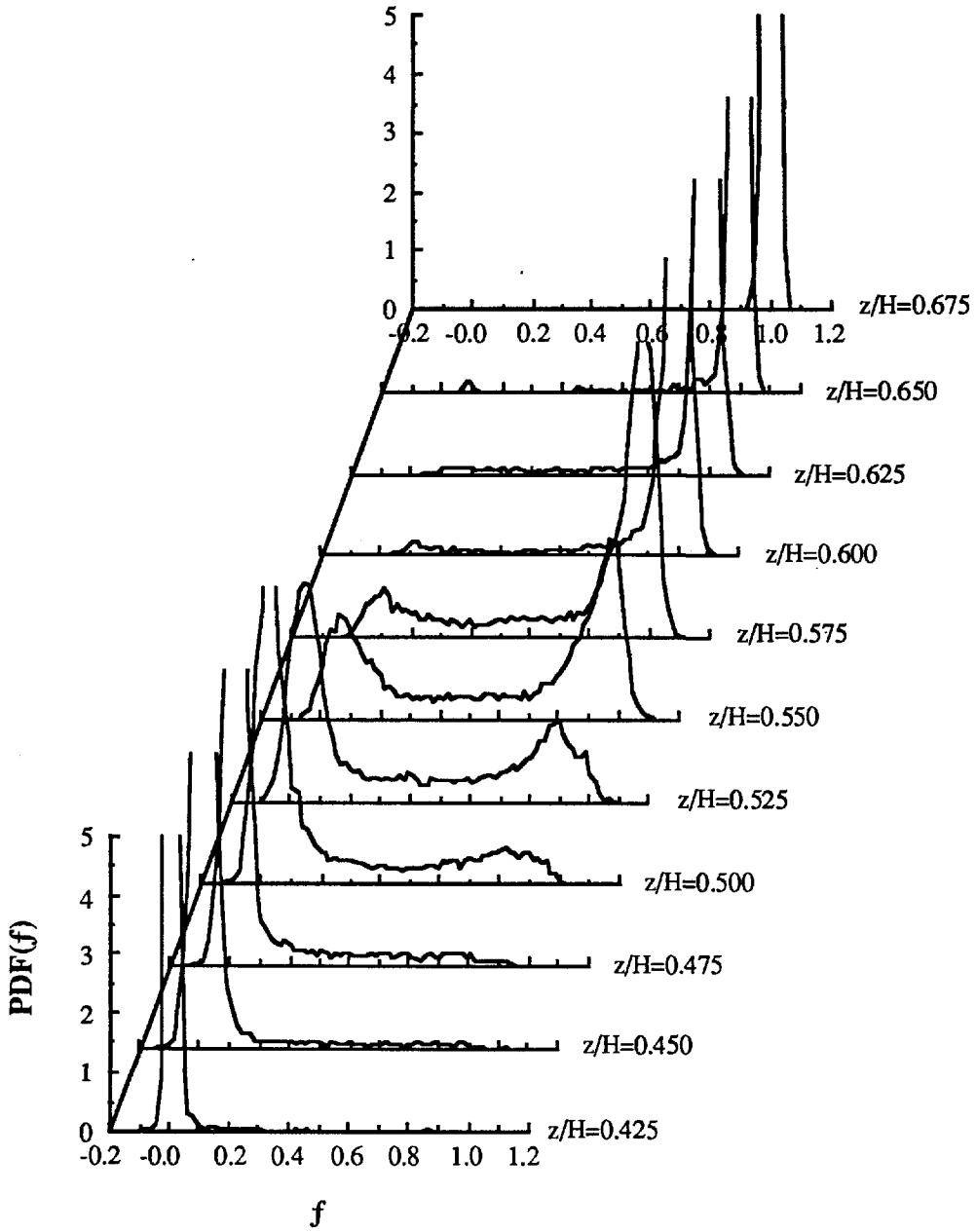
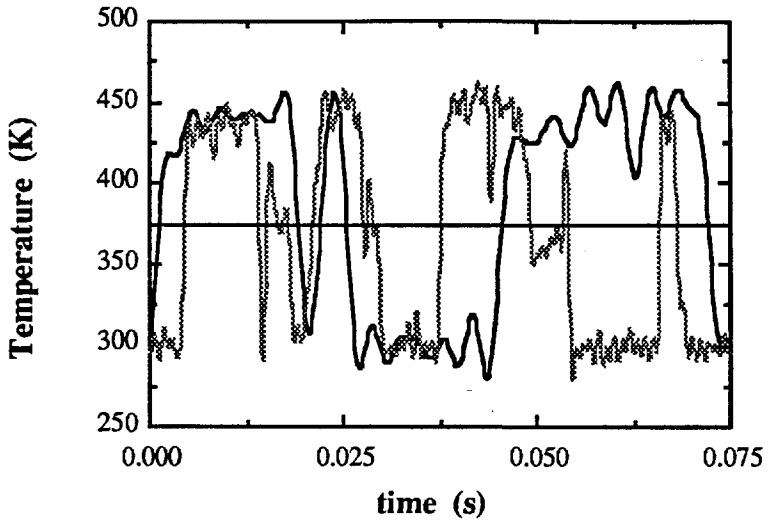
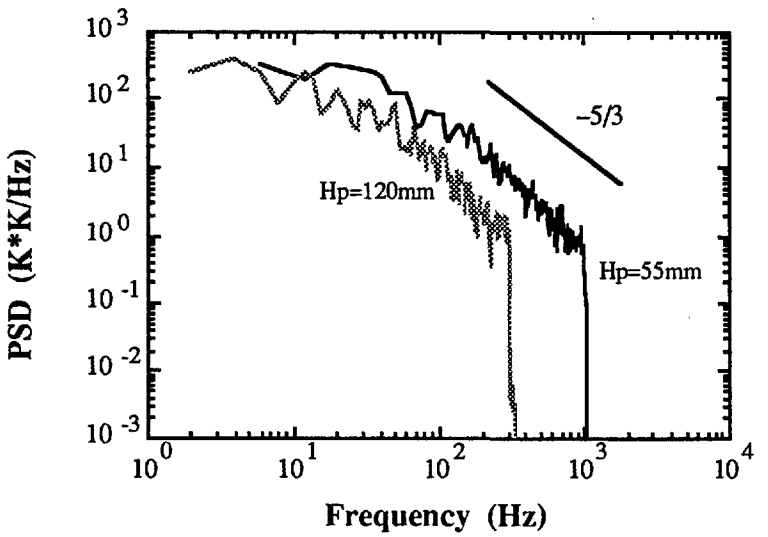


Figure 3.2.19 Probability density functions (pdf) of the normalised temperature $(T-T_1)/(T_2-T_1)$ along the centreline of the inert opposed jet flow with H=20mm, H_p=120mm, and U_1=1.88m/s and U_2=2.3m/s.



(a)



(b)

Figure 3.2.20 (a) Representative portions of the measured temperature at the centreline and the axial location of $\langle F \rangle$=0.5 for the flow conditions of Fig. 3.2.17 for H=20mm, and H_p=55mm (dashed line) and 120mm (solid line). (b) The corresponding frequency spectra. Conditions as marked.

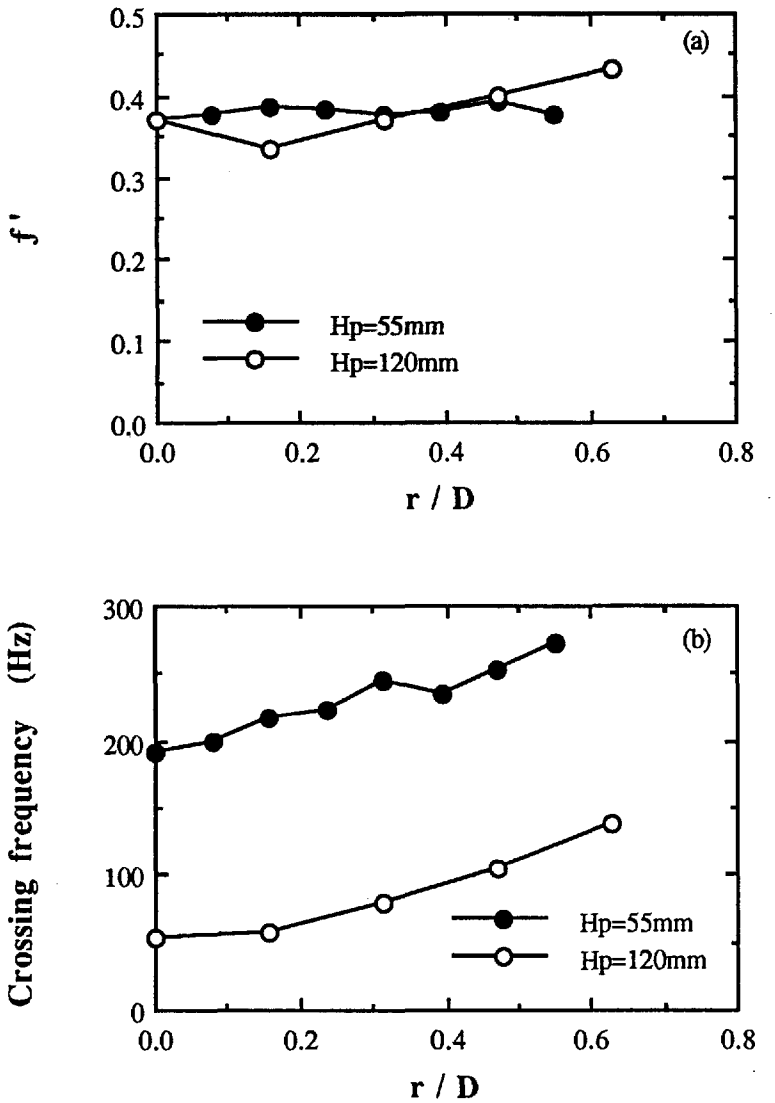


Figure 3.2.21 (a) Radial variation of the r.m.s. mixture fraction fluctuations at the axial location where $\langle F \rangle$=0.5 for H=20mm, T_2=450K, U_1=1.88m/s and U_2=2.3m/s, for strong and weak turbulence. (b) The corresponding frequency of crossing the value f=0.5, as found from time series as in Fig. 3.2.20.

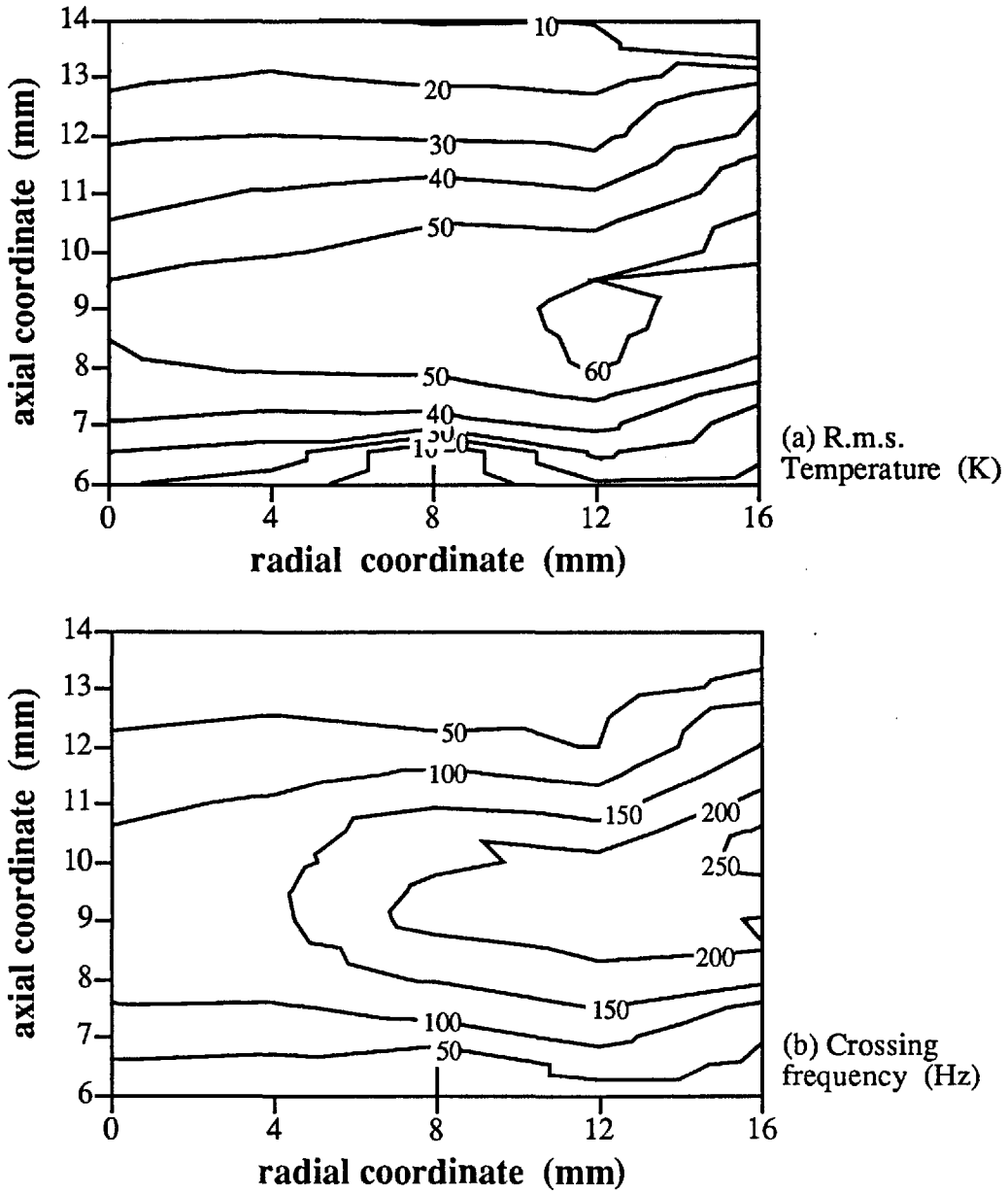


Figure 3.2.22 Contours of r.m.s. temperature (a) and crossing frequency of the value corresponding to ⟨F⟩=0.5 (370K) (b) for the flow conditions of Fig. 3.2.21: H=20mm, H_p=55mm, T_2=450K, and U_1=1.88m/s and U_2=2.3m/s. These contours were assembled from measurements spaced by 4mm in the radial and 1mm in the axial direction.

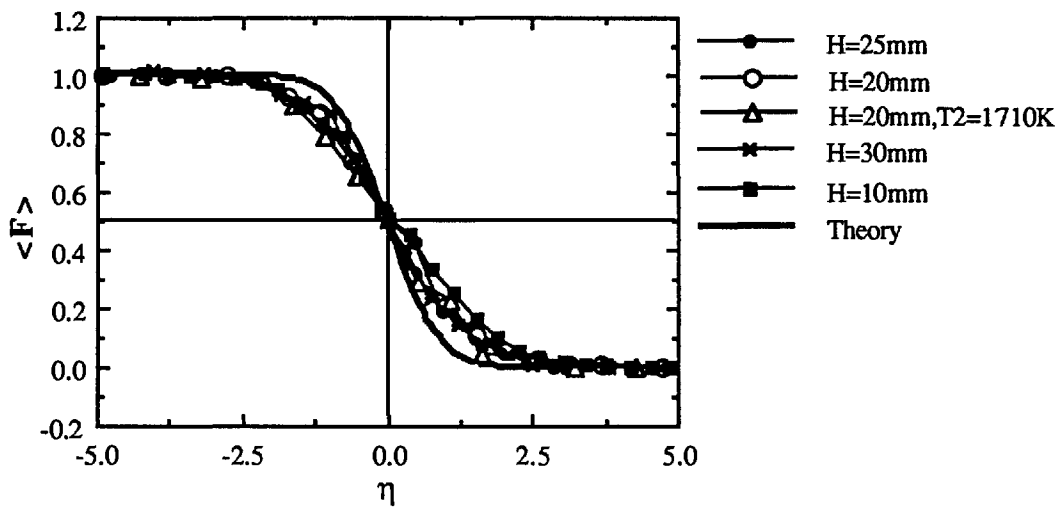


Figure 3.2.23 Centreline variation of the measured mixture fraction compared with the predictions from Eq. (3.2.22). For the data, the axial coordinate z* (i.e. z shifted so that $\langle F \rangle$=0.5 corresponds to z*=0) has been normalised by the lengthscale Z^* from Eq. (3.2.23), assuming in Eq. (3.2.23) the standard values C_μ=0.09 and σ_f=0.7, to create the non–dimensional coordinate η (Eq. 3.2.15). The flow rates are as in Fig. 3.2.22 and H_p=55mm. The graph also includes measurements in the opposed flow of a cold jet to a jet of hot combustion products, a flow used in Chapter 4 to examine extinction of flames impinging on hot reaction products, to show that the same mean mixing field is measured at all temperatures of the heated stream.

Figures for Chapter 3, Section 3.3



Figure 3.3.1 Photograph of a pure diffusion turbulent counterflow flame with H=20mm, H_p=55mm, U_o=1.0m/s, and the fuel stream velocity equal to 1.34 U_o so that the momentum flow rates of the two jets are equal. The flame extends in the radial direction up to the radius of the outer tube and is half–way between the jets. The appearance of the flame under different strain rates and premixedness is similar.

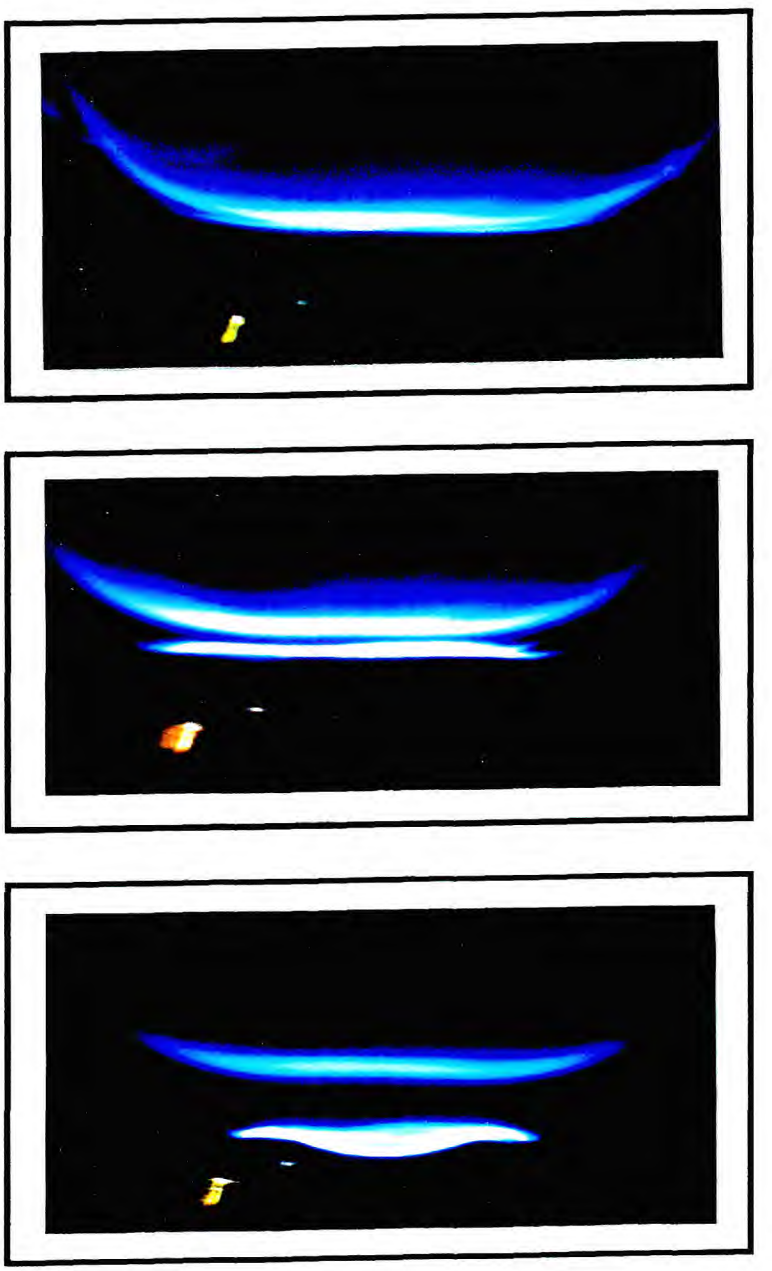
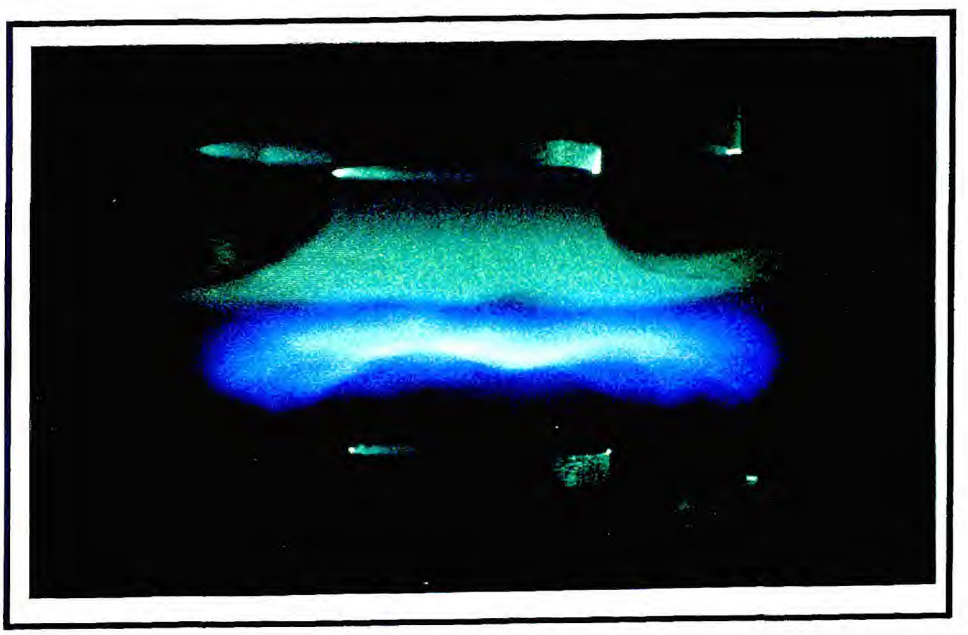


Figure 3.3.2 Photographs of *laminar* counterflow partially premixed diffusion and rich premixed flames stabilised in the burner of Fig. 2.2 for H=15mm, U_o=0.45m/s, and (a) ϕ=1.75 (or X_1=0.84), (b) ϕ=1.45, and (c) ϕ=1.25. The "double structure" is visible in (a) which shows a flame still in the diffusion flame regime.



(a)



(b)

Figure 3.3.3 Photographs of (a) partially premixed diffusion flame with H=40mm, X=0.5, and H_p=55mm, and U_o=1.5m/s, and (b) a single premixed flame with H=25mm, H_p=55mm, U_o=2.0m/s, and ϕ=0.8. For both photographs, the air stream has been seeded with alumina particles and illuminated with a laser sheet to show that the diffusion flame is located at the interface between the air and the fuel jets, but that the premixed flame is located to the reactants side of the stagnation plane. Note that the jet separation in (a) is larger than the typical value of 20mm used in most experiments described here.

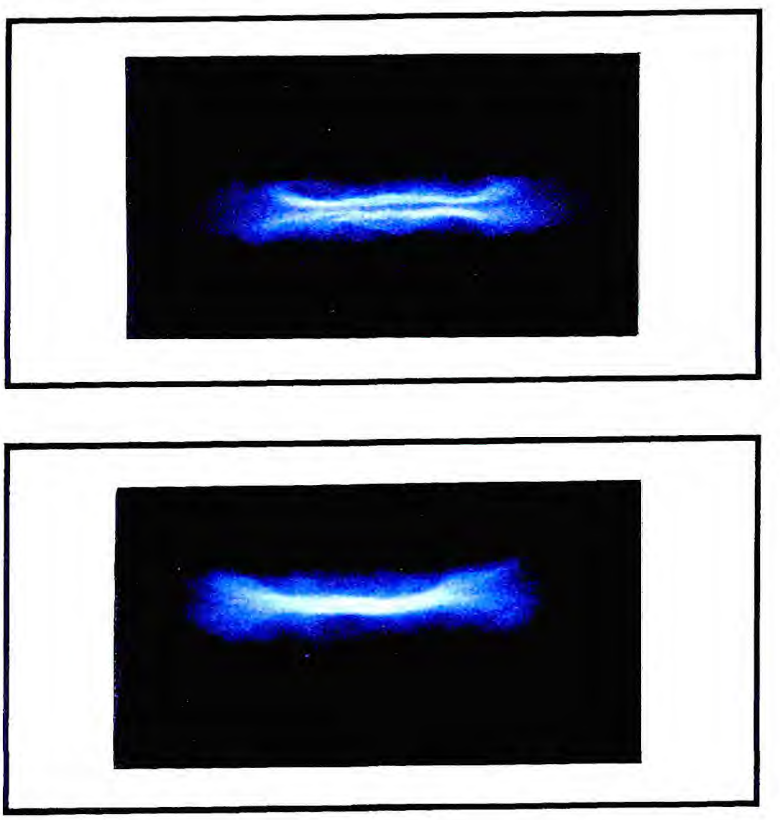


Figure 3.3.4 Photographs of twin premixed flames. Conditions are $\phi_1=\phi_2=0.7$, $U_1=U_2=2.0$m/s, and (a) H=20mm and (b) H=10mm. The flame shown in (b) is close to extinction.

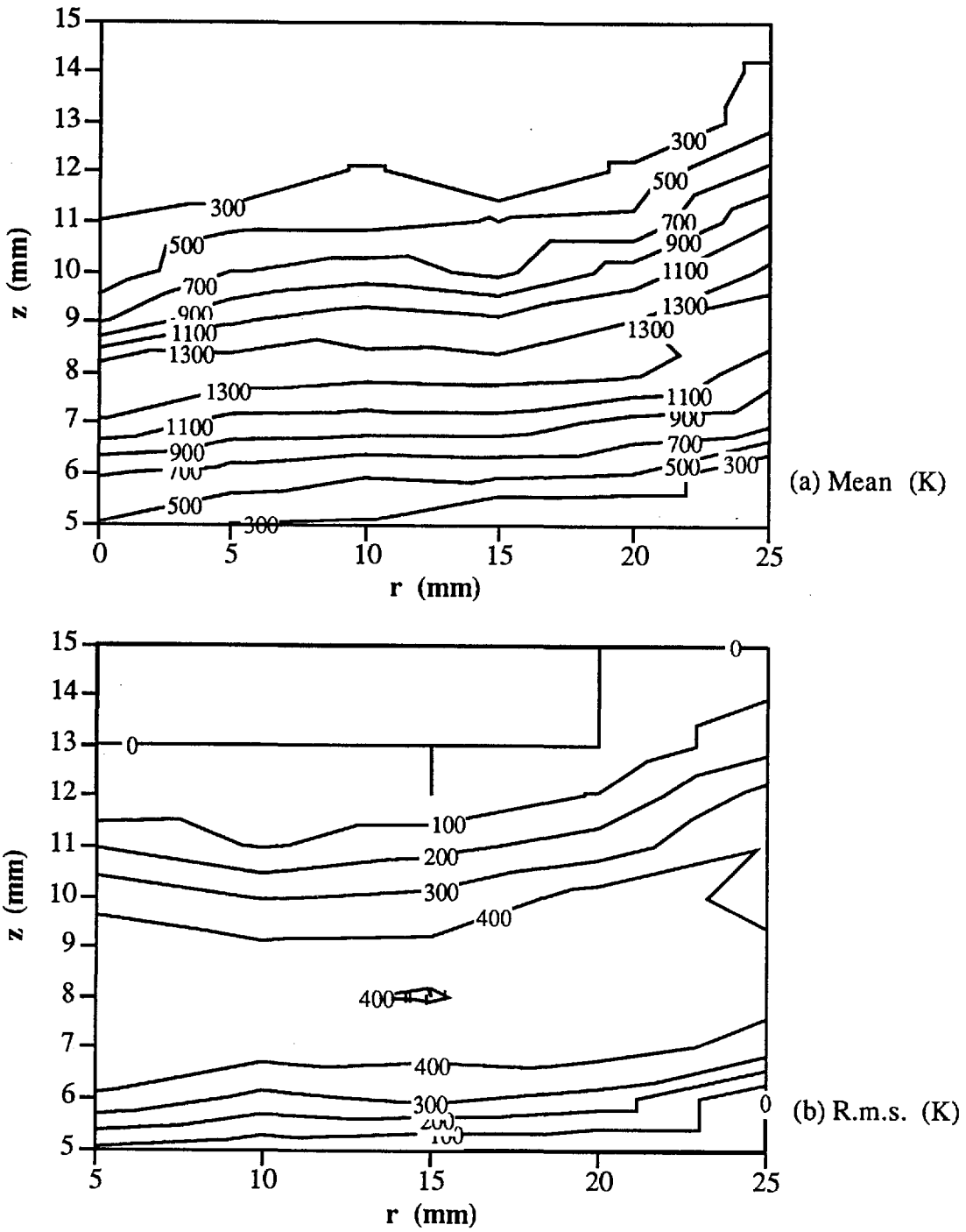


Figure 3.3.5 Mean (a) and r.m.s. (b) temperature contours in a diffusion flame with H=20mm, H_p=55mm, X=0.0, U_1=1.34m/s, and U_2=1.0m/s (condition described also as U_o=1.0m/s). This flame is the flame most commonly used in measurements presented here. The contours were assembled from measurements spaced by 0.5mm in the axial direction and by 5mm in the radial direction.

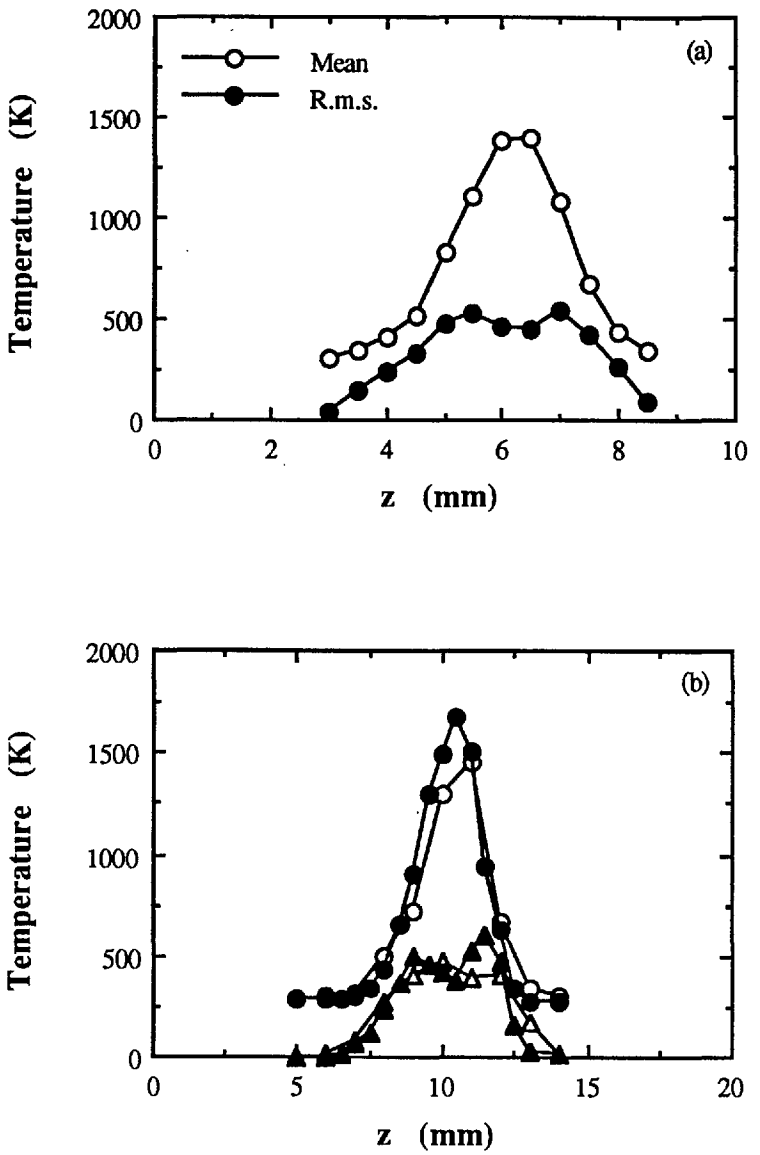


Figure 3.3.6 Mean and r.m.s. temperature at r=10mm for a diffusion flame with X=0.0, U_1=1.34m/s, U_2=1.0m/s, and (a) H=10mm and H_p=55mm, and (b) H=20mm, and H_p=55mm (open symbols) and H_p=120mm (blocked symbols). For (b), the circles correspond to the mean and the triangles to the r.m.s. temperature. The axial coordinate z is measured from the exit plane of the fuel jet.

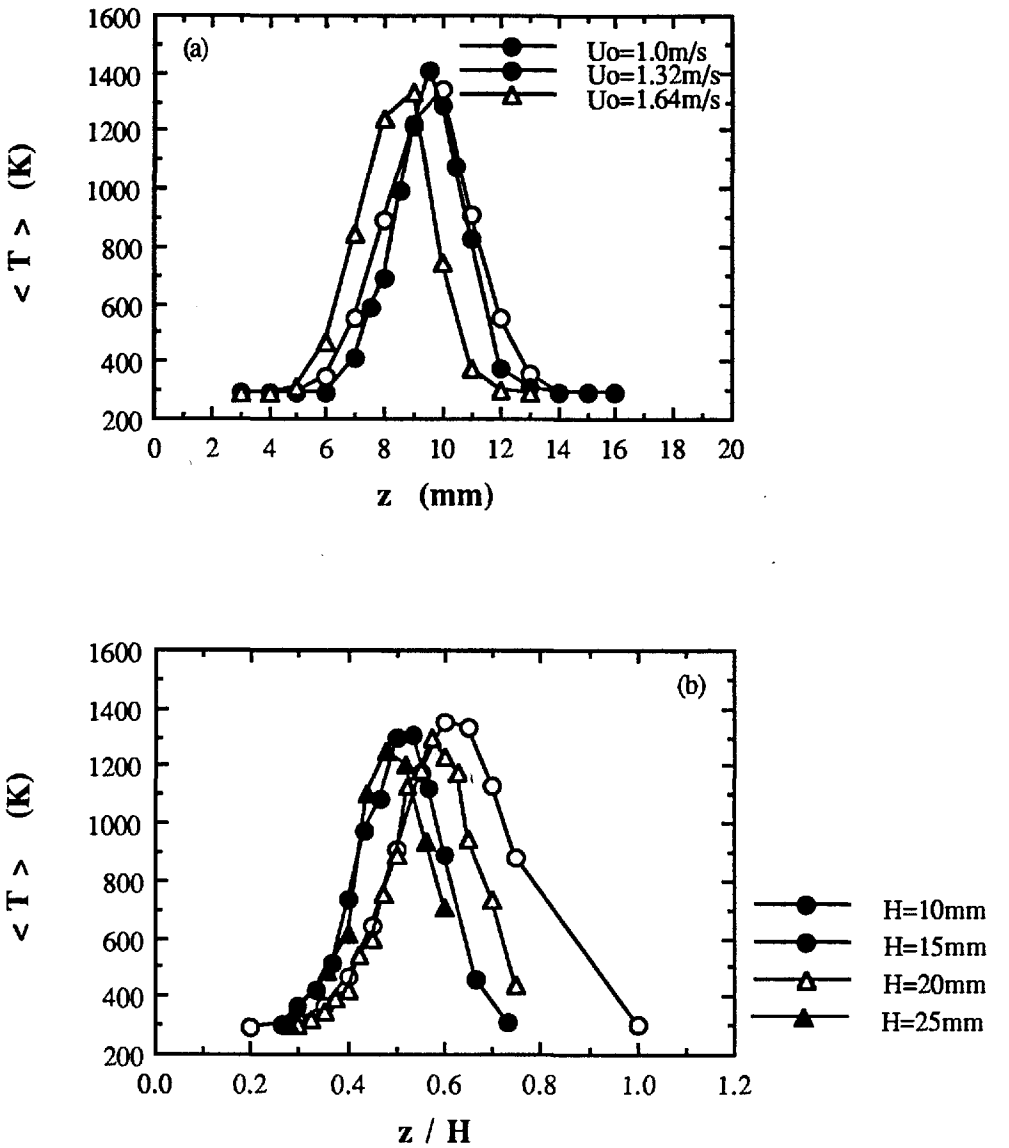


Figure 3.3.7 Mean temperature profiles along the centreline of diffusion flames with X=0.0 and H_p=55mm for (a) different velocities and H=20mm, and (b) U_1=1.34m/s, U_2=1.0m/s and different H. The velocity U_o is equal to the air velocity U_2 and the fuel and air momentum flow rates were always equal.

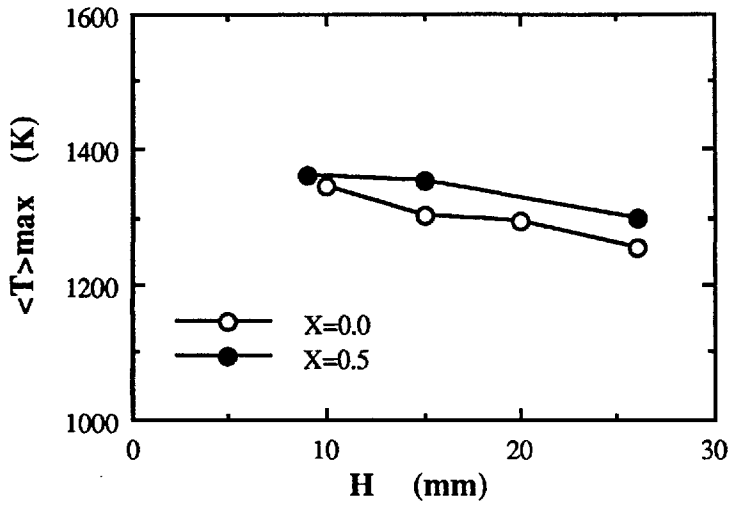


Figure 3.3.8 The maximum mean temperature at diffusion flames with U_o=1.0m/s (i.e. U_2=1.0m/s and U_1 so as to keep the momentum flow rates of the two jets equal) for X=0.0 and 0.5 as a function of jet separation.

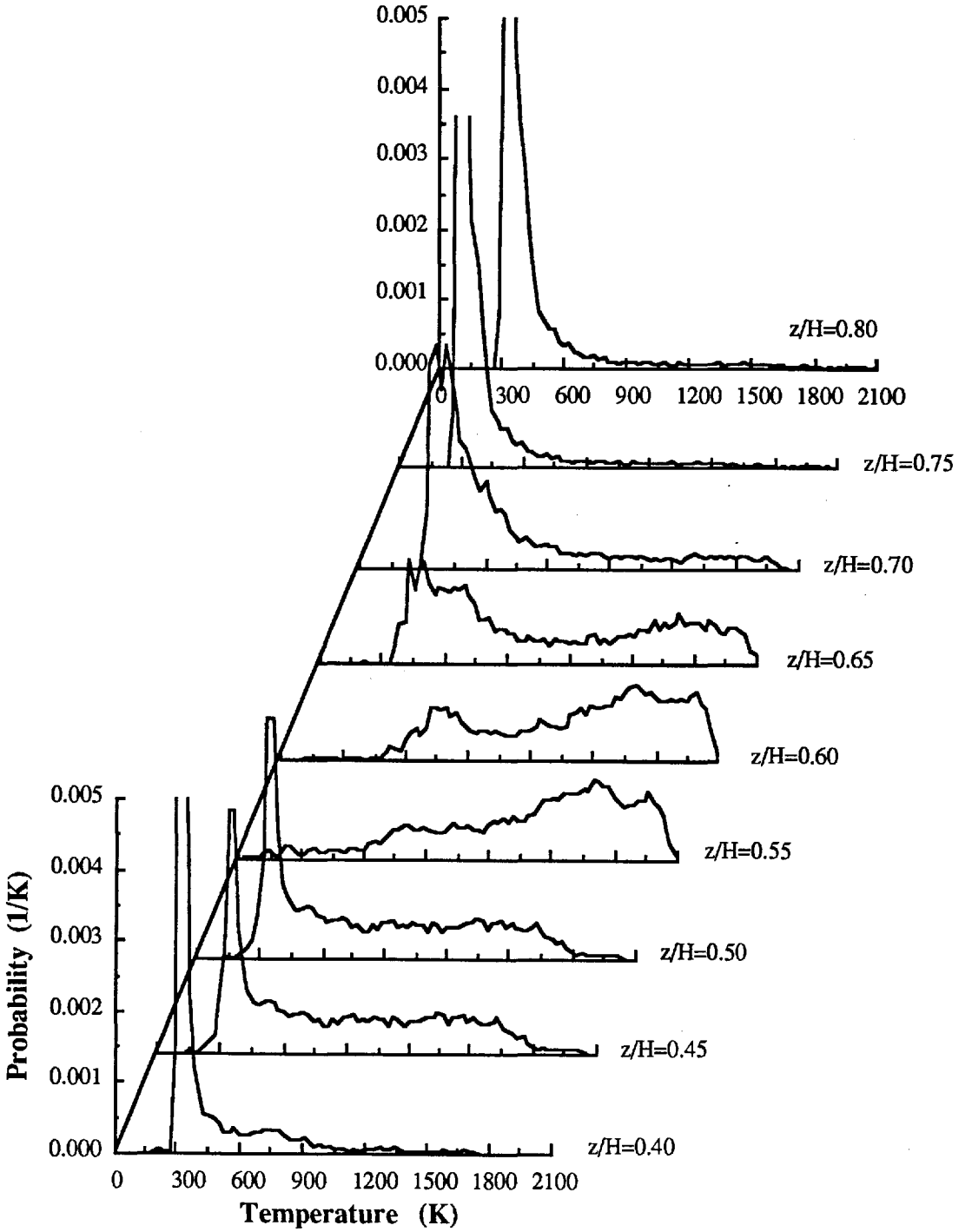


Figure 3.3.9 Probability density functions of the temperature measurements of Fig. 3.3.6a. H=10mm.

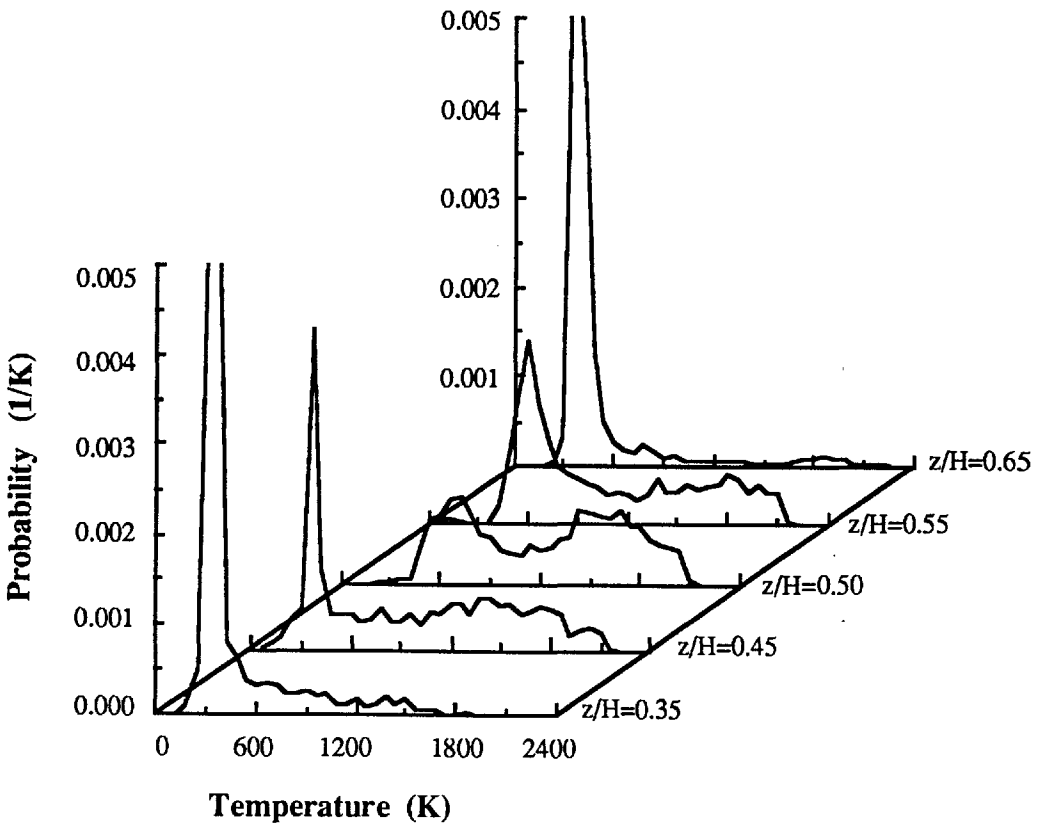


Figure 3.3.10 Probability density functions of the temperature measurements of Fig. 3.3.6b with H=20mm, H_p=55mm.

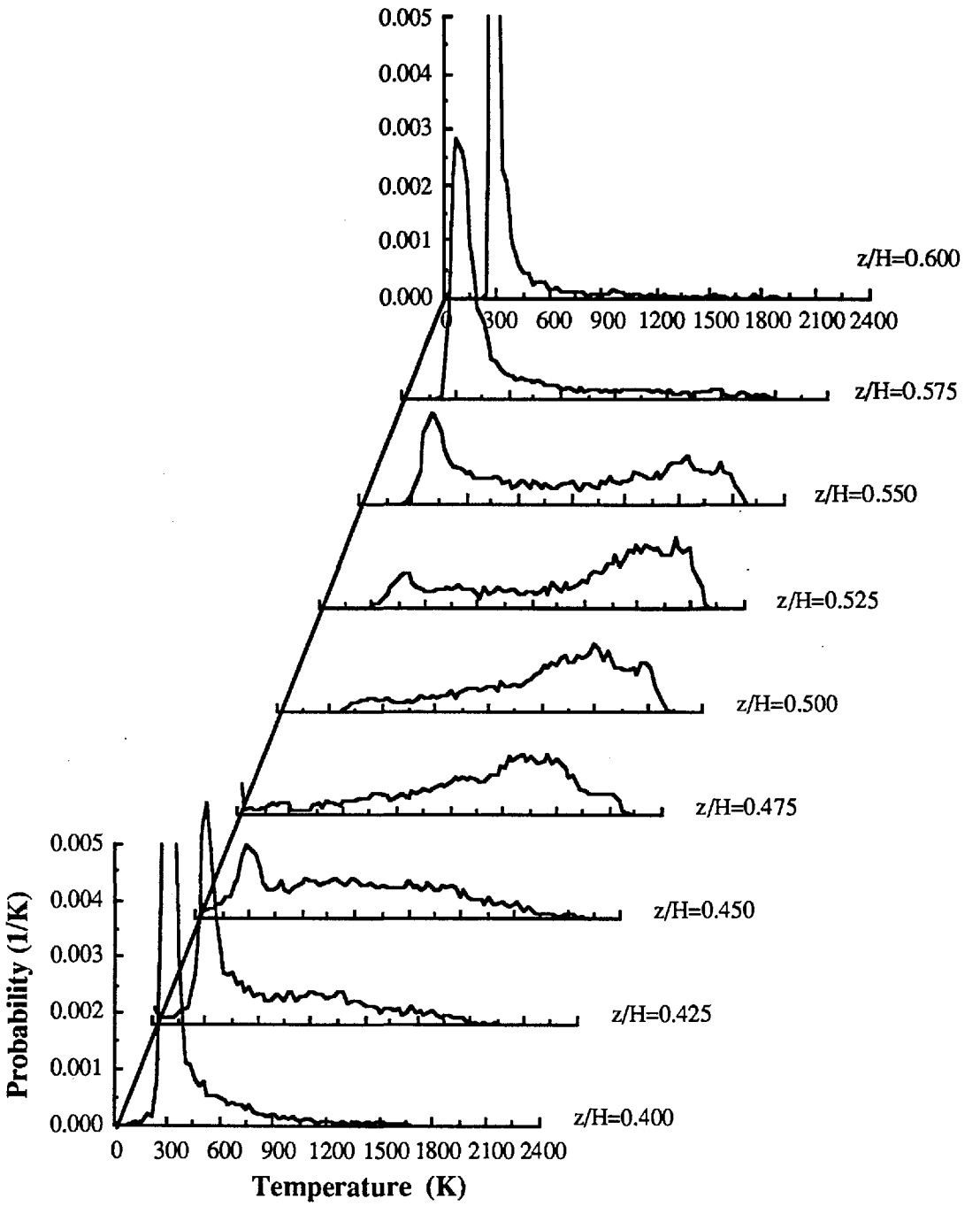


Figure 3.3.11 Probability density functions of the temperature measurements of Fig. 3.3.6b with H=20mm, H_p=120mm.

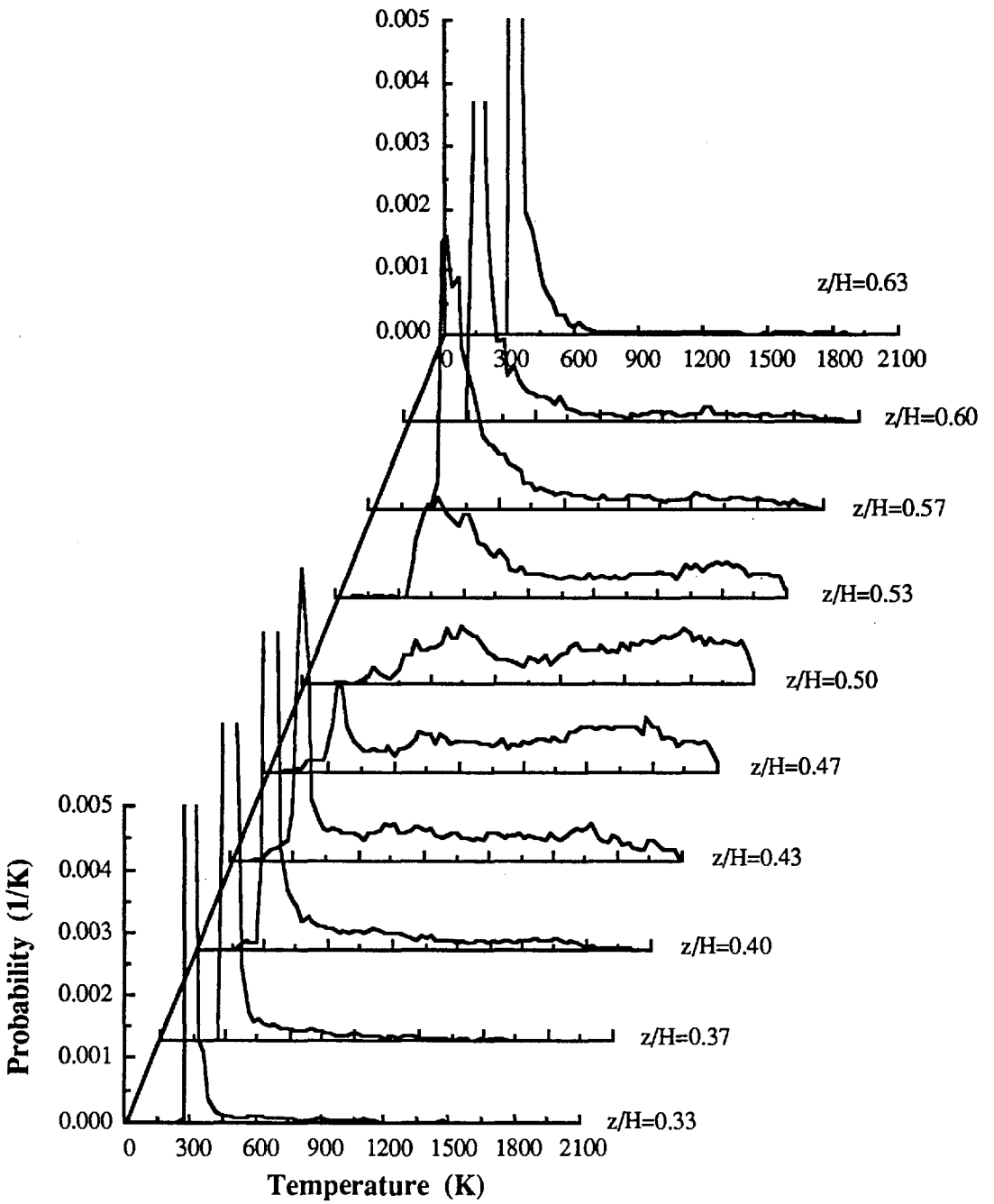


Figure 3.3.12 Probability density functions at r=10mm for a diffusion flame with the velocity conditions of Fig. 3.3.6 but at H=30mm.

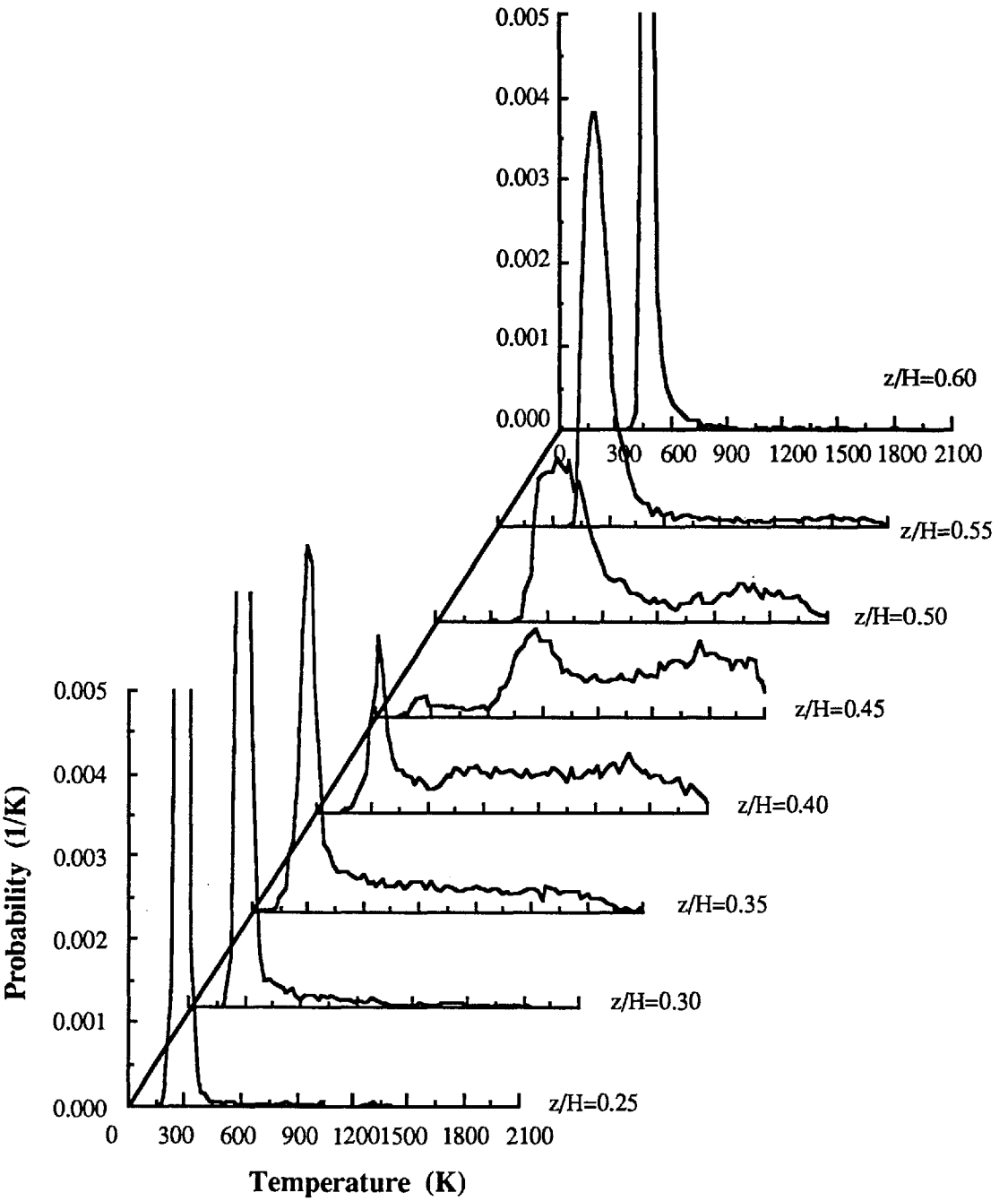


Figure 3.3.13 Probability density functions of the temperature at r=10mm of a diffusion flame with H=20mm, X=0.0, H_p=55mm, and U_1=2.60m/s, U_2=2.33m/s. The air stream has been preheated to 420K for examining the increase in the flame extinction limits (Section 4.3.5) and note that the cold temperature peak in the pdf corresponds to room temperature at the fuel side of the flame but at about 450K in the air side, and that both peaks at 300 and 450K are evident at the location of maximum temperature (z/H=0.45).

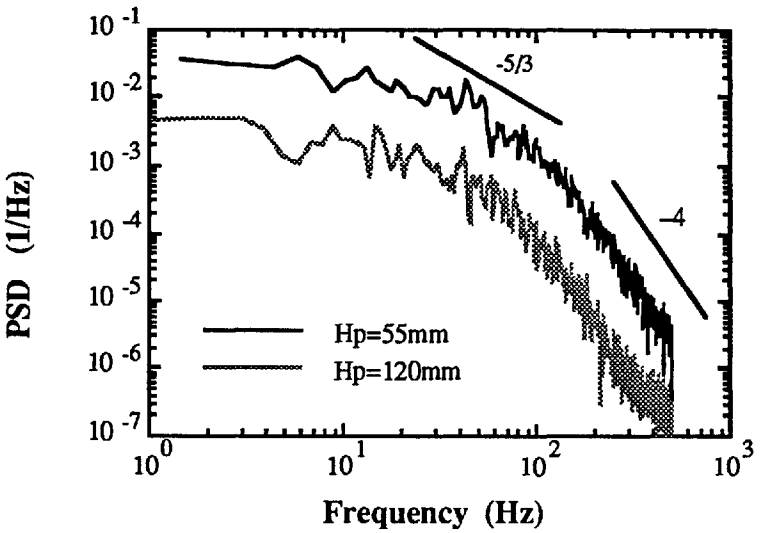


Figure 3.3.14 Frequency spectra at the location of maximum mean temperature for the pure diffusion flames of Fig. 3.3.6b. The spectrum corresponding to H_p=120mm has been shifted by one decade along the direction of decreasing PSD which has been normalised by the variance so that the integral of PSD over the frequency range gives unity.

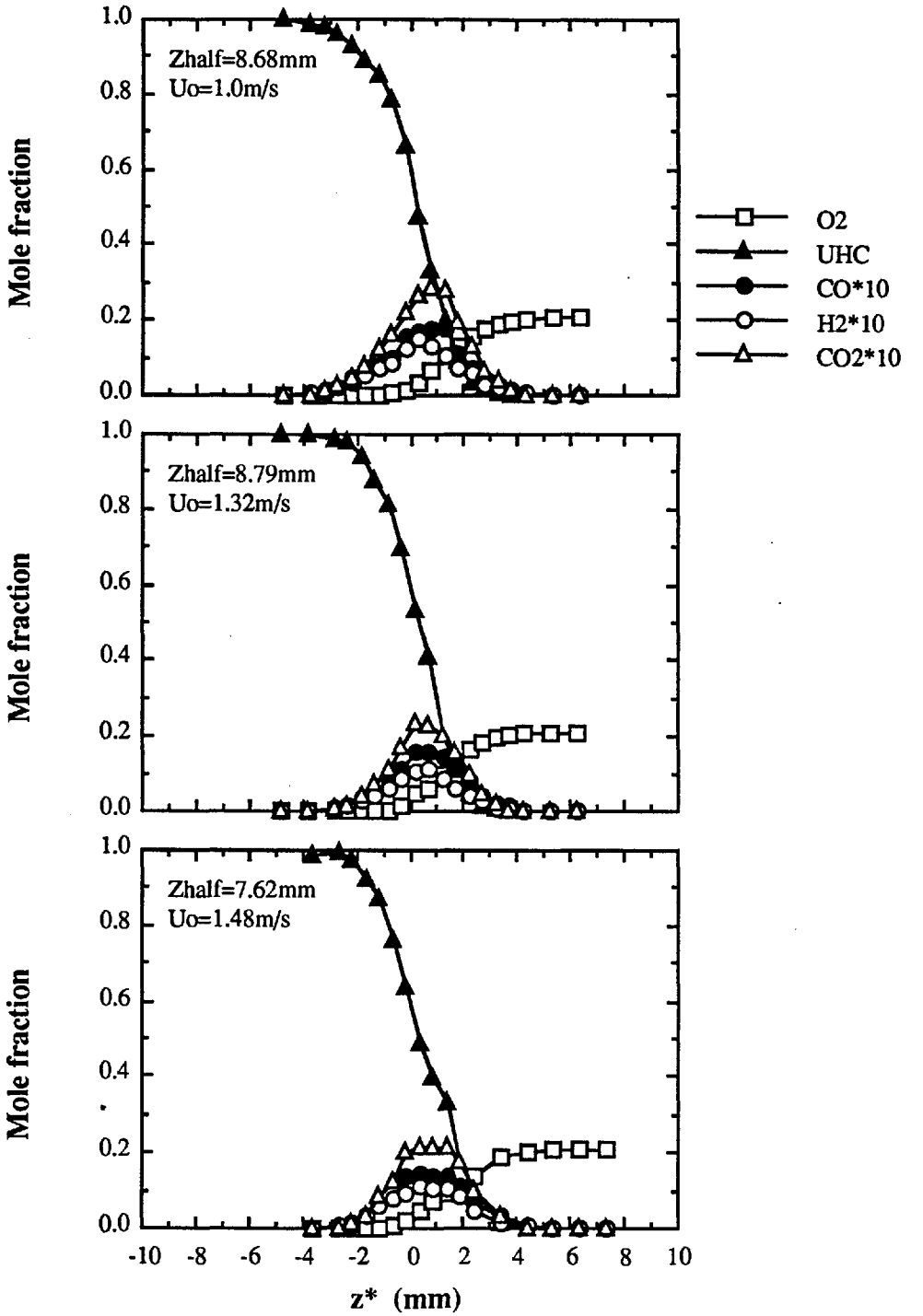


Figure 3.3.15 Mean species concentrations for diffusion flames with H=20mm, H_p=55mm, and X=0.0 at the indicated air bulk velocity. The fuel velocity was adjusted to give equal momentum flow rates in the two jets and the axial coordinate z* has been defined so that $z^*=z-Z_{half}$, where Z_{half} corresponds to the axial location where the mixture fraction is equal to 0.5 and was found by interpolating between data in the axial profile of the mixture fraction. See Fig. 3.4.1 for a typical mixture fraction axial variation.

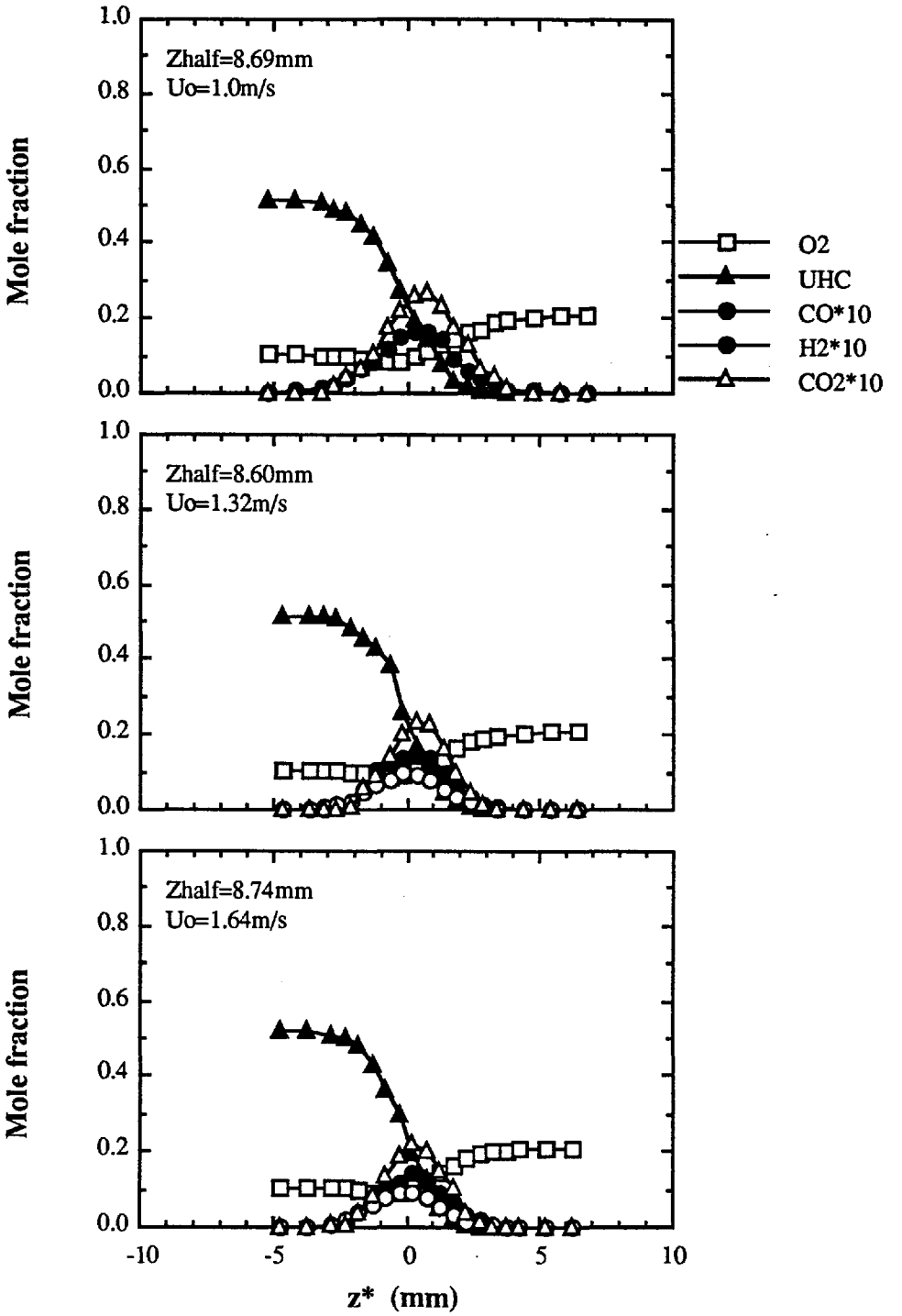


Figure 3.3.16 Mean species concentrations for diffusion flames with H=20mm, H_p=55mm, and X=0.5 at the indicated air bulk velocity. The fuel velocity was adjusted to give equal momentum flow rates in the two jets and the axial coordinate z* has been defined so that $z^*=z-Z_{half}$, where Z_{half} corresponds to the axial location where the mixture fraction is equal to 0.5.

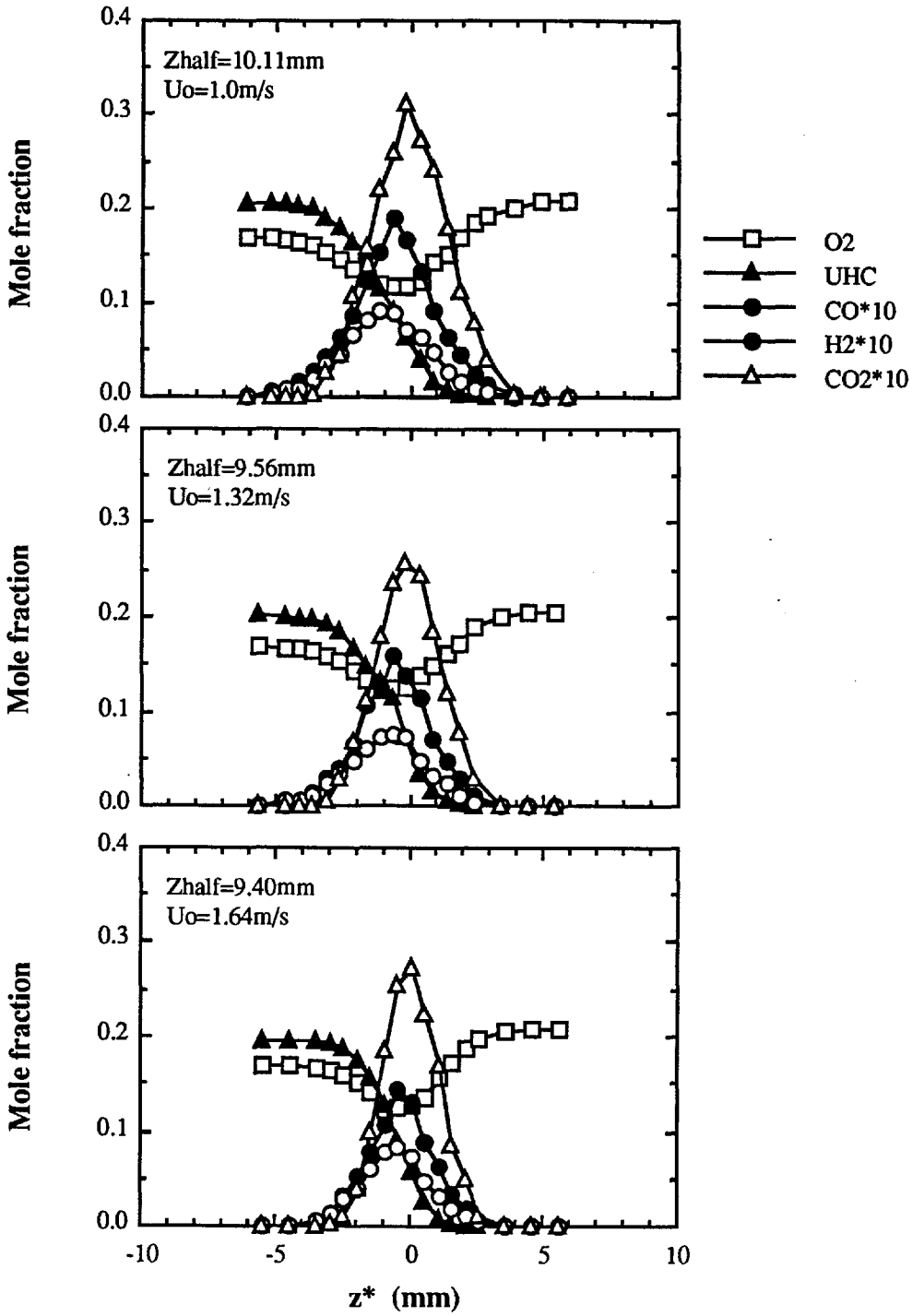


Figure 3.3.17 Mean species concentrations for diffusion flames with H=20mm, H_p=55mm, and X=0.8 at the indicated air bulk velocity. The fuel velocity was adjusted to give equal momentum flow rates in the two jets and the axial coordinate z* has been defined so that $z^*=z-Z_{half}$, where Z_{half} corresponds to the axial location where the mixture fraction is equal to 0.5.

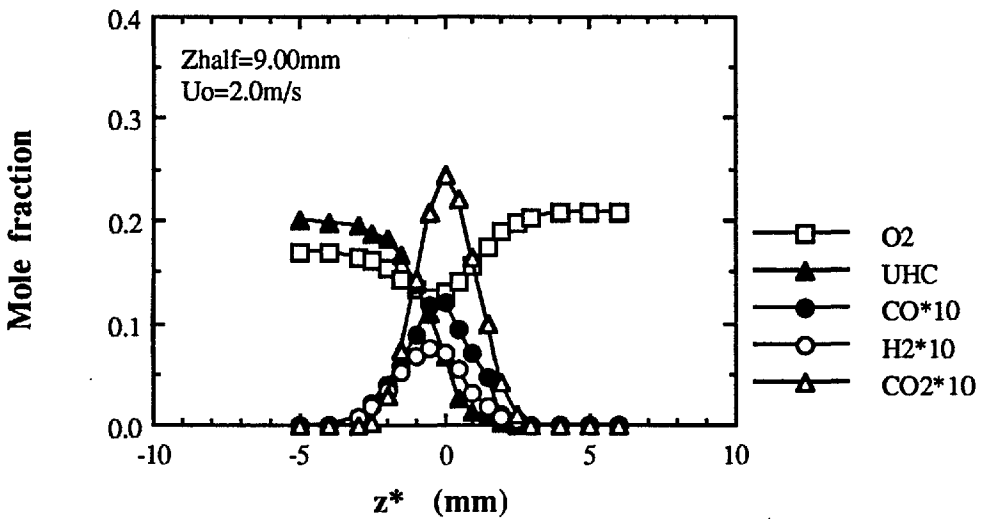


Figure 3.3.17 Continued and concluded.

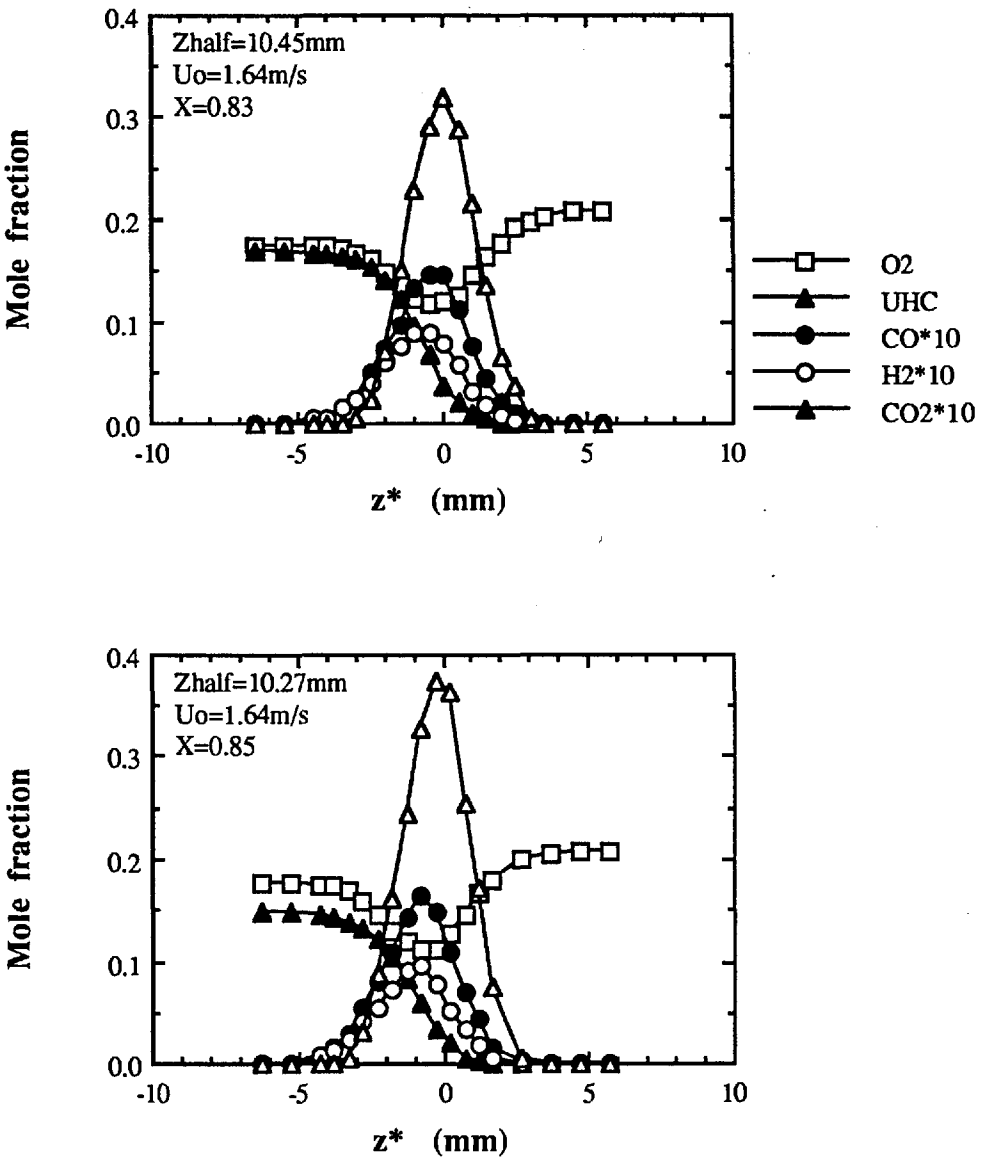


Figure 3.3.18 Mean species concentrations for partially premixed diffusion flames with H=20mm, H_p=55mm, U_o=1.64m/s, and at the indicated air volume fraction in the fuel stream. The axial coordinate $z^*=z-Z_{half}$, where Z_{half} corresponds to the axial locatin where the mixture fraction is equal to 0.5.

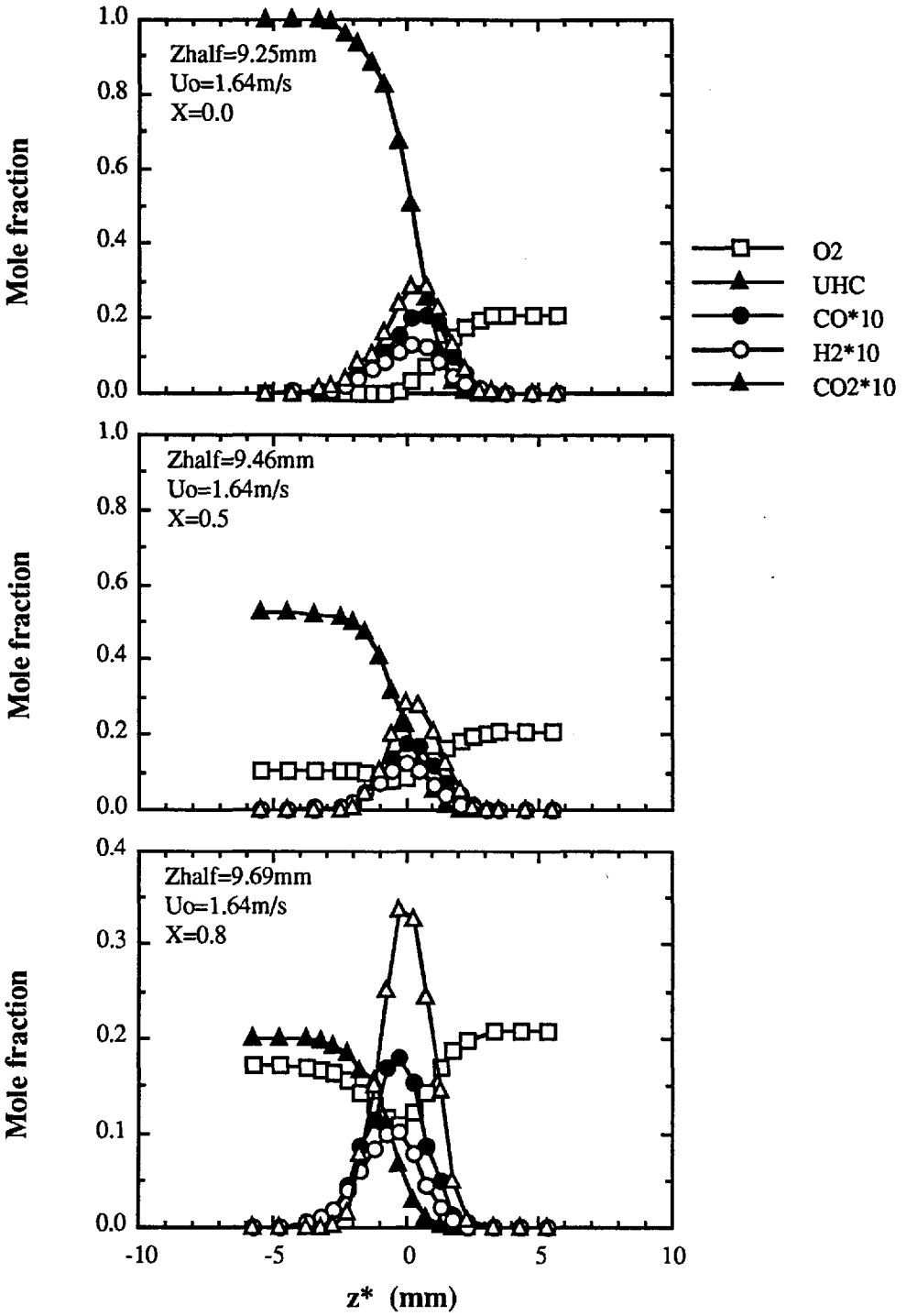


Figure 3.3.19 Mean species concentrations for pure and partially premixed diffusion flames with H=20mm, H_p=120mm, U_o=1.64m/s, and the indicated air volume fraction in the fuel stream.

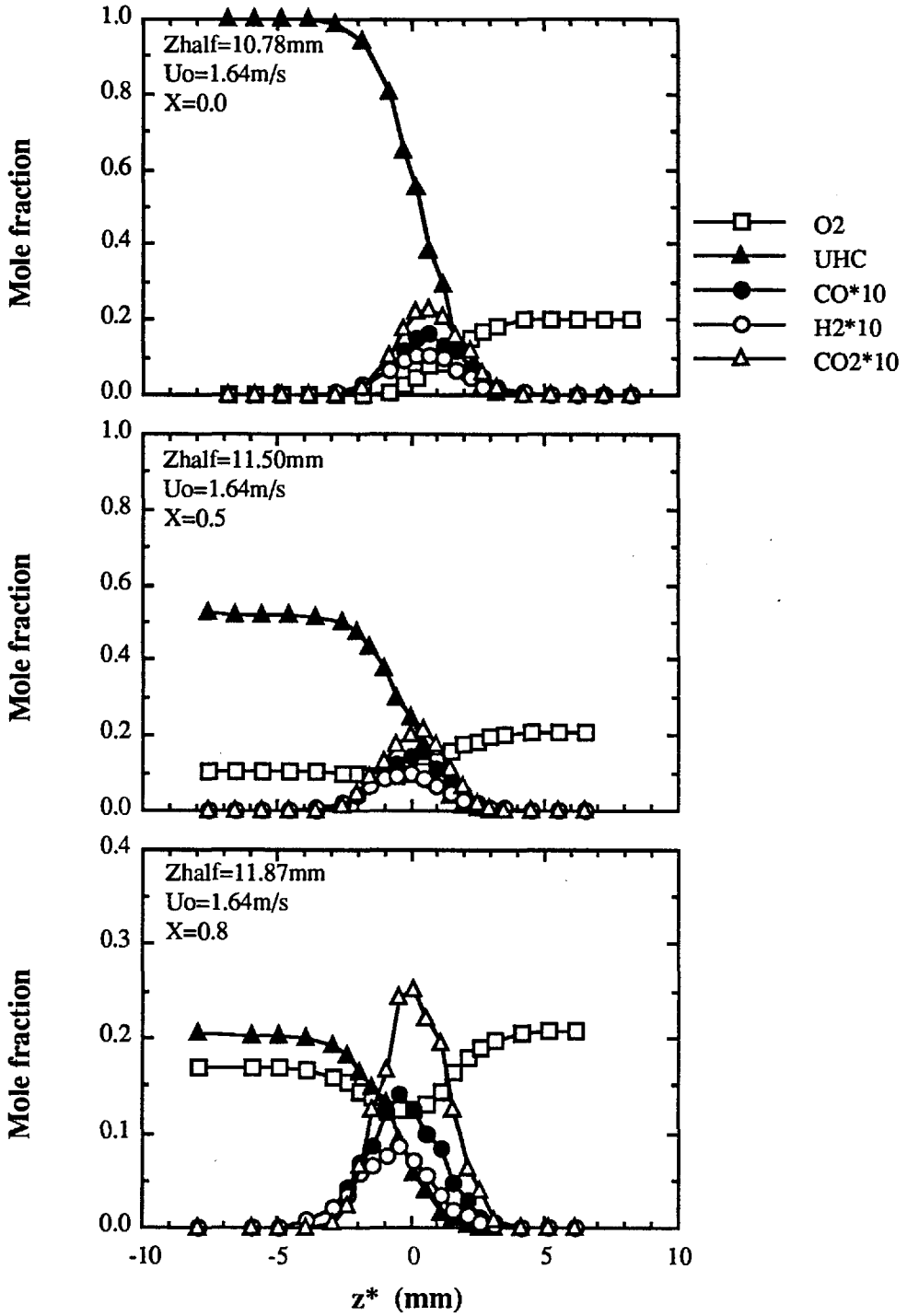


Figure 3.3.20 Mean species concentrations for pure and partially diffusion flames with H=25mm, H_p=55mm, U_o=1.64m/s, and the indicated air volume fraction in the fuel stream.

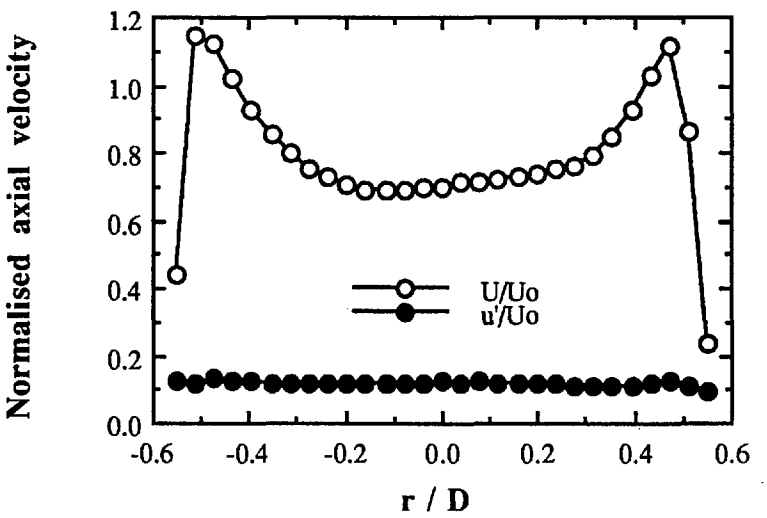


Figure 3.3.21 Mean and r.m.s. axial velocity radial variation at z=2mm for a diffusion flame with H=20mm, H_p=55mm, X=0.8, and U_o=2.0m/s. This radial profile is typical of the axial velocity initial condition at the jet exit for H=20mm for all flames.

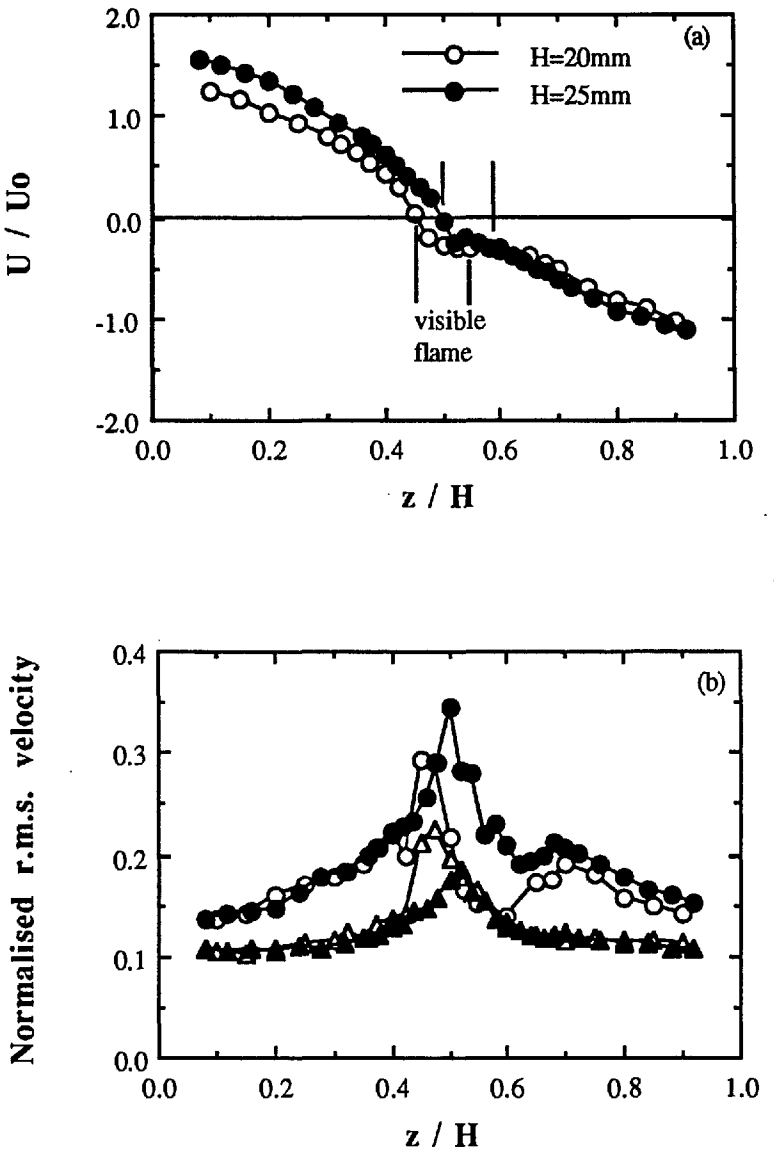


Figure 3.3.22 Mean axial and r.m.s. axial (circles) and radial (triangles) velocities along the centreline for diffusion flames with H=20mm (open symbols) and H=25mm (blocked symbols). (a, b) : X=0.0; (c, d) : X=0.5; and (e, f) : X=0.8. For all data, U_o=1.32m/s (the air bulk velocity) and the fuel stream velocity was adjusted so as to keep the momentum flow rates of the two jets equal.

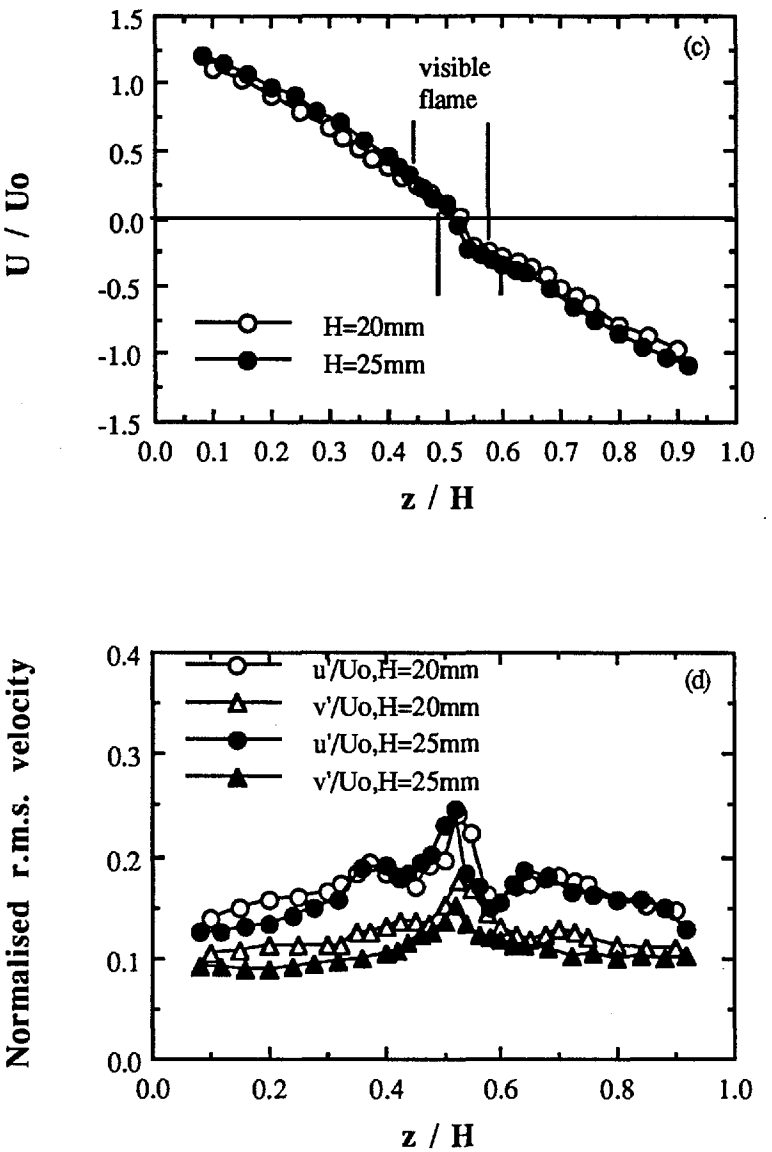


Figure 3.3.22 Cont'd.

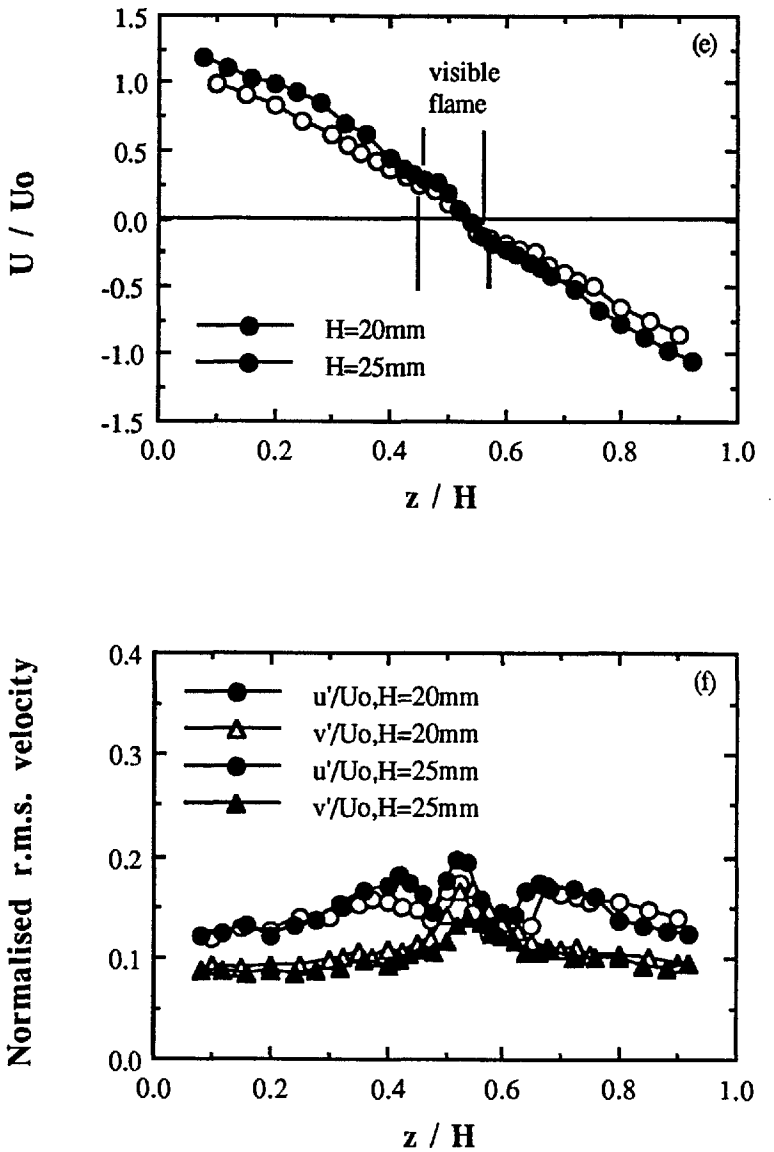


Figure 3.3.22 Concluded.

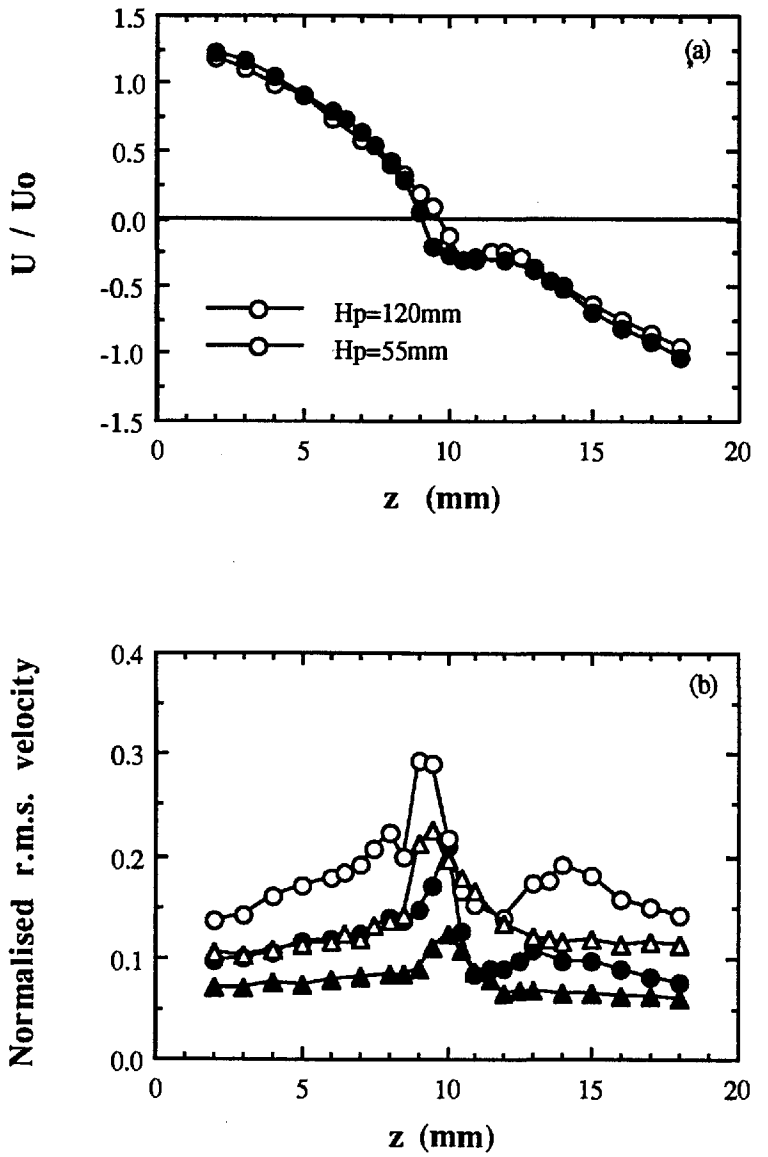


Figure 3.3.23 Mean axial (a) and r.m.s. axial and radial (b) velocities along the centreline of a diffusion flame with H=20mm and X=0.0 for H_p=55mm and 120mm. For H_p=55mm (open symbols), U_o=1.32m/s and for H_p=120mm (blocked symbols), U_o=1.64m/s. For (b), circles correspond to the axial and triangles to the radial velocities.

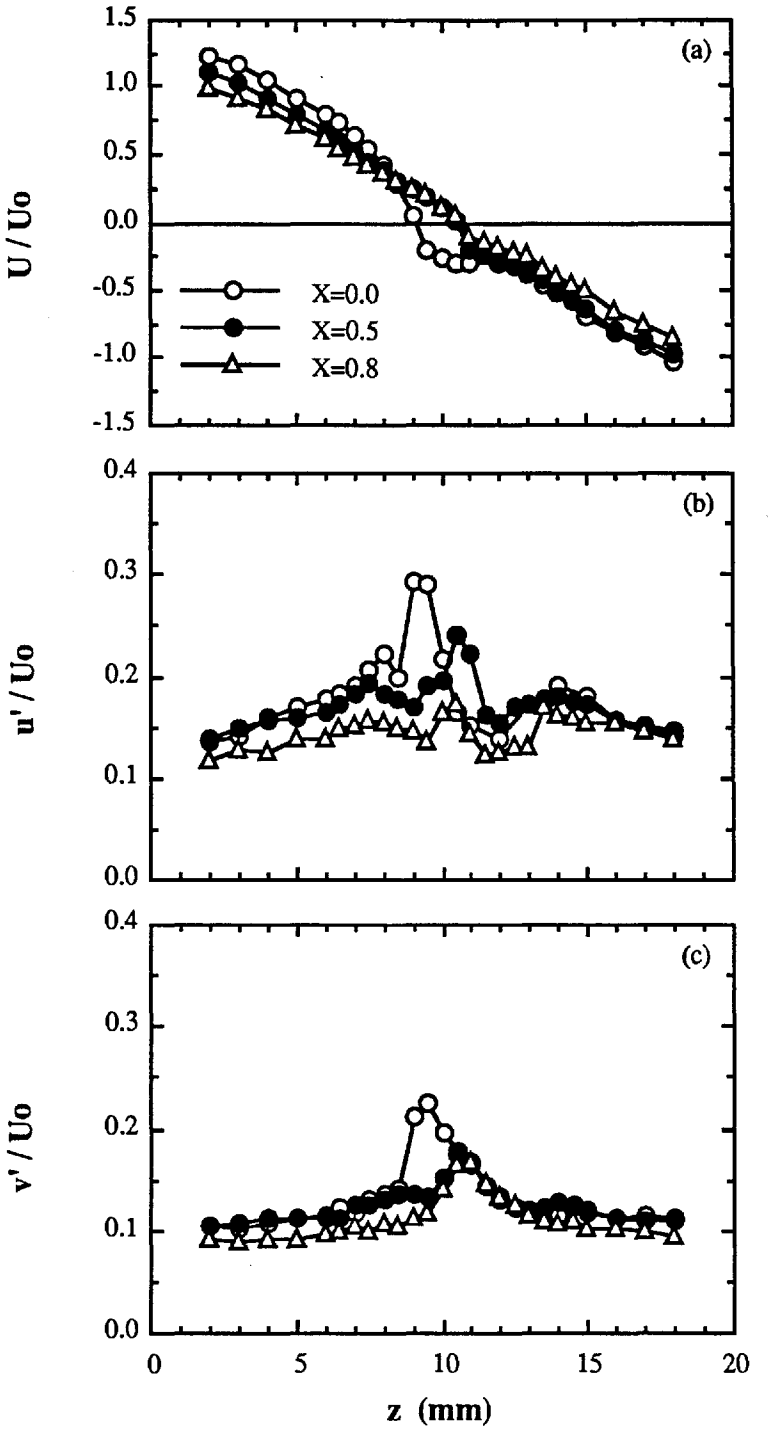


Figure 3.3.24 The data of Fig. 3.3.22 replotted in order to show more clearly the differences in the axial mean velocity and the turbulence with partial premixing. For all data, H=20mm, H_p=55mm, and U_o=1.32m/s.

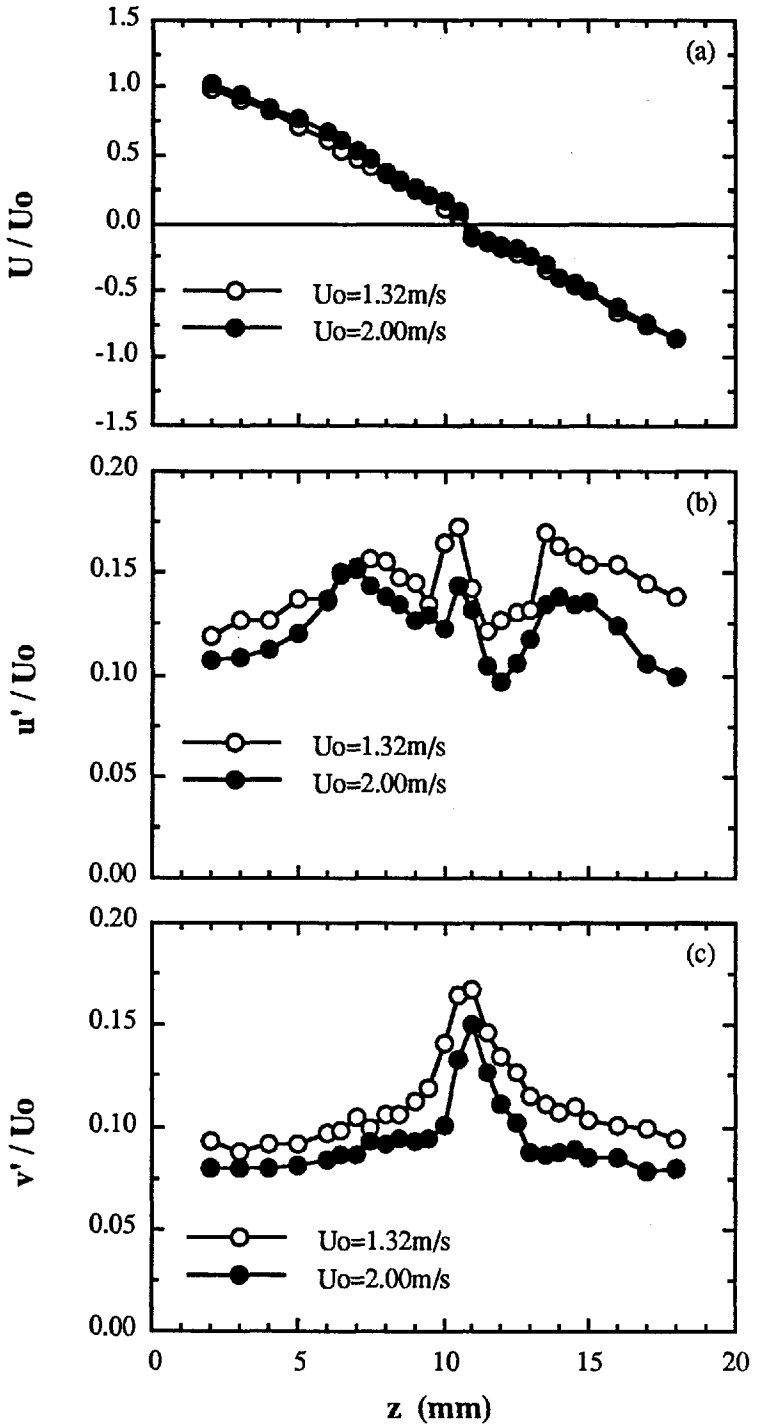


Figure 3.3.25 Centreline variations of axial mean (a), axial r.m.s. (b), and radial r.m.s. (c) velocities for partially premixed diffusion flames with H=20mm, H_p=55mm, and X=0.8 for two bulk velocities.

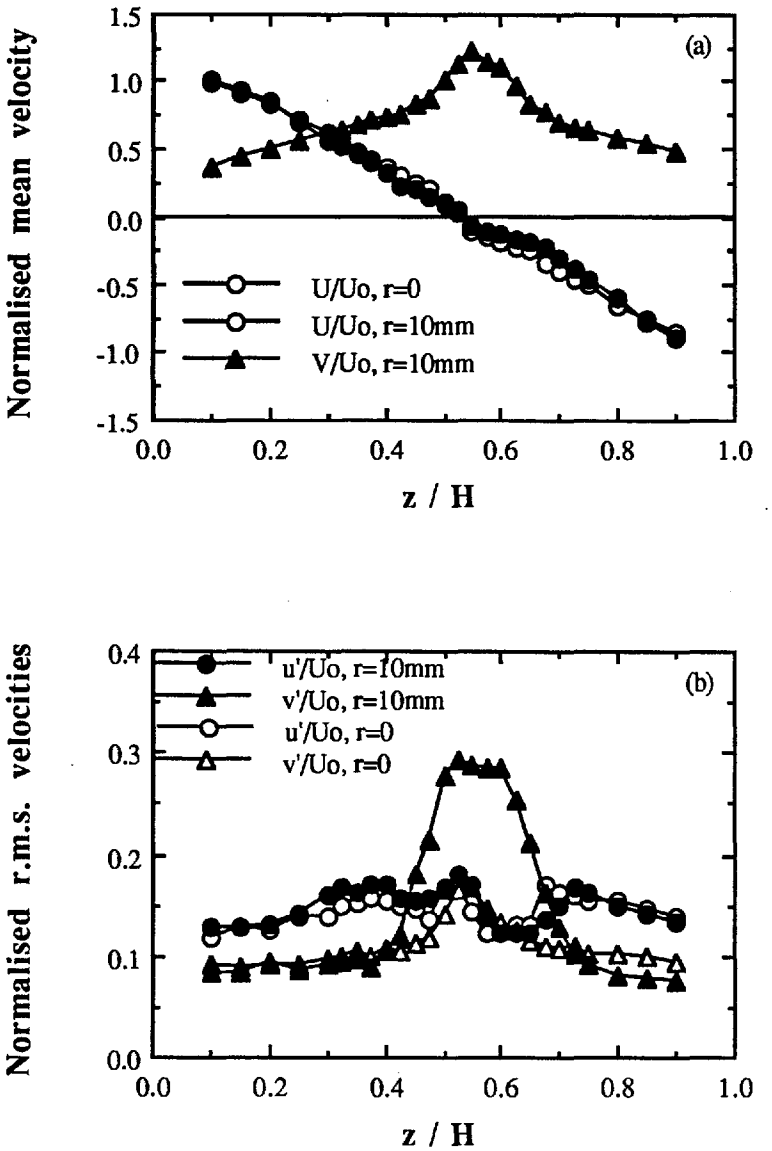


Figure 3.3.26 Comparison between axial traverses of the axial and radial velocities at r=0 and r=10mm for a diffusion flame with X=0.8, H=20mm, H_p=55mm, and U_o=1.32m/s.

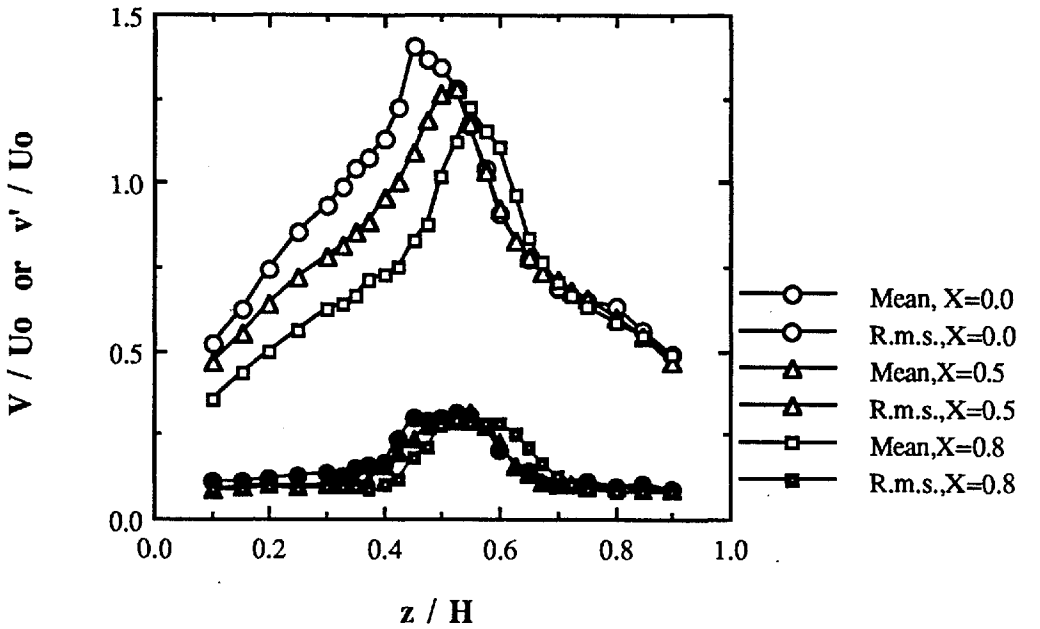


Figure 3.3.27 Axial traverses of radial velocity at r=10mm in diffusion flames with H=20mm, H_p=55mm, and U_o=1.32m/s for X=0.0, X=0.5, and X=0.8. These measurements correspond to the centreline measurements of Fig. 3.2.22.

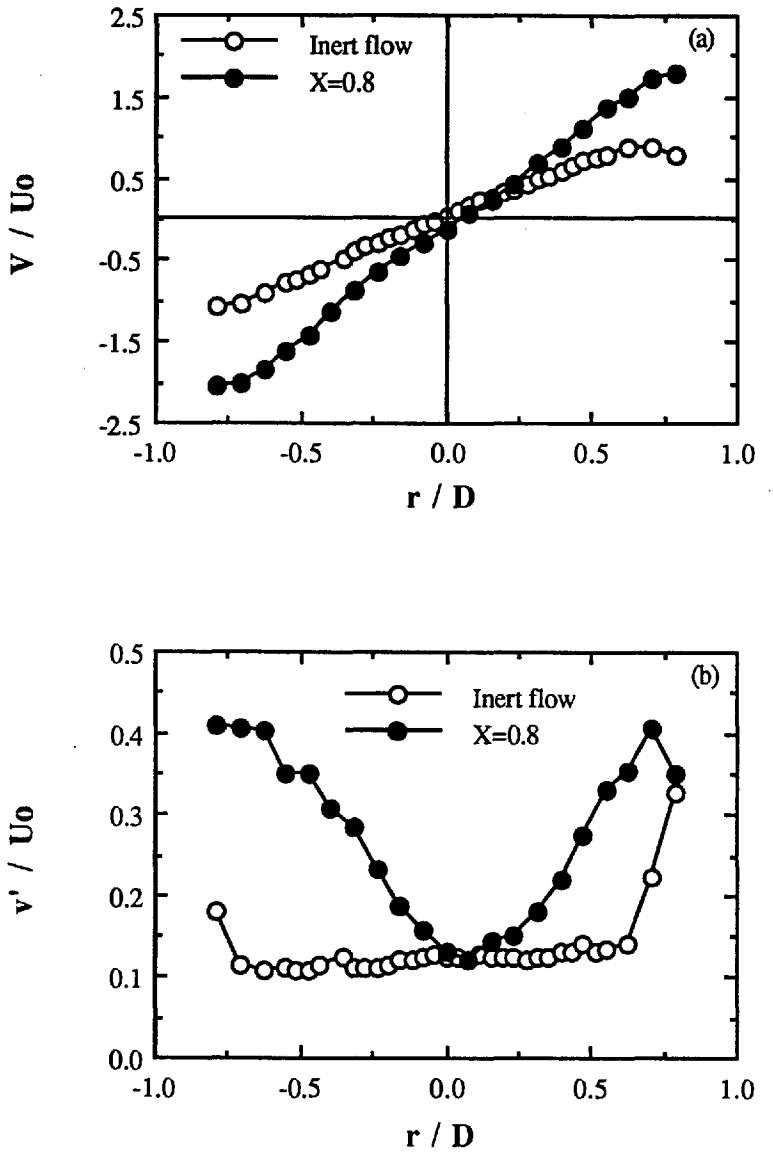


Figure 3.3.28 Radial variations at z=10mm of the radial mean (a) and r.m.s. velocity (b) for a diffusion flame with H=20mm, H_p=55mm, X=0.8, and U_o=1.64m/s, and for the inert flow for identical geometry and velocity conditions.

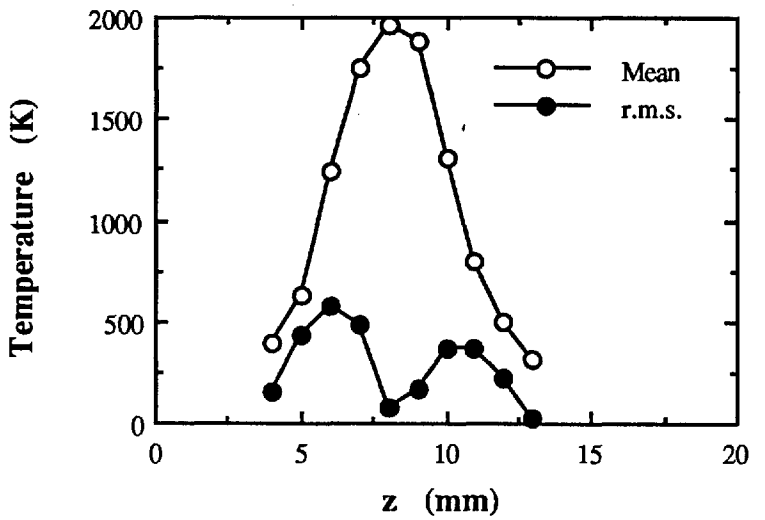


Figure 3.3.29 The mean and r.m.s. temperature at r=10mm for a single premixed flame with U_o=2.0m/s, H=20mm, H_p=55mm, and ϕ=0.8.

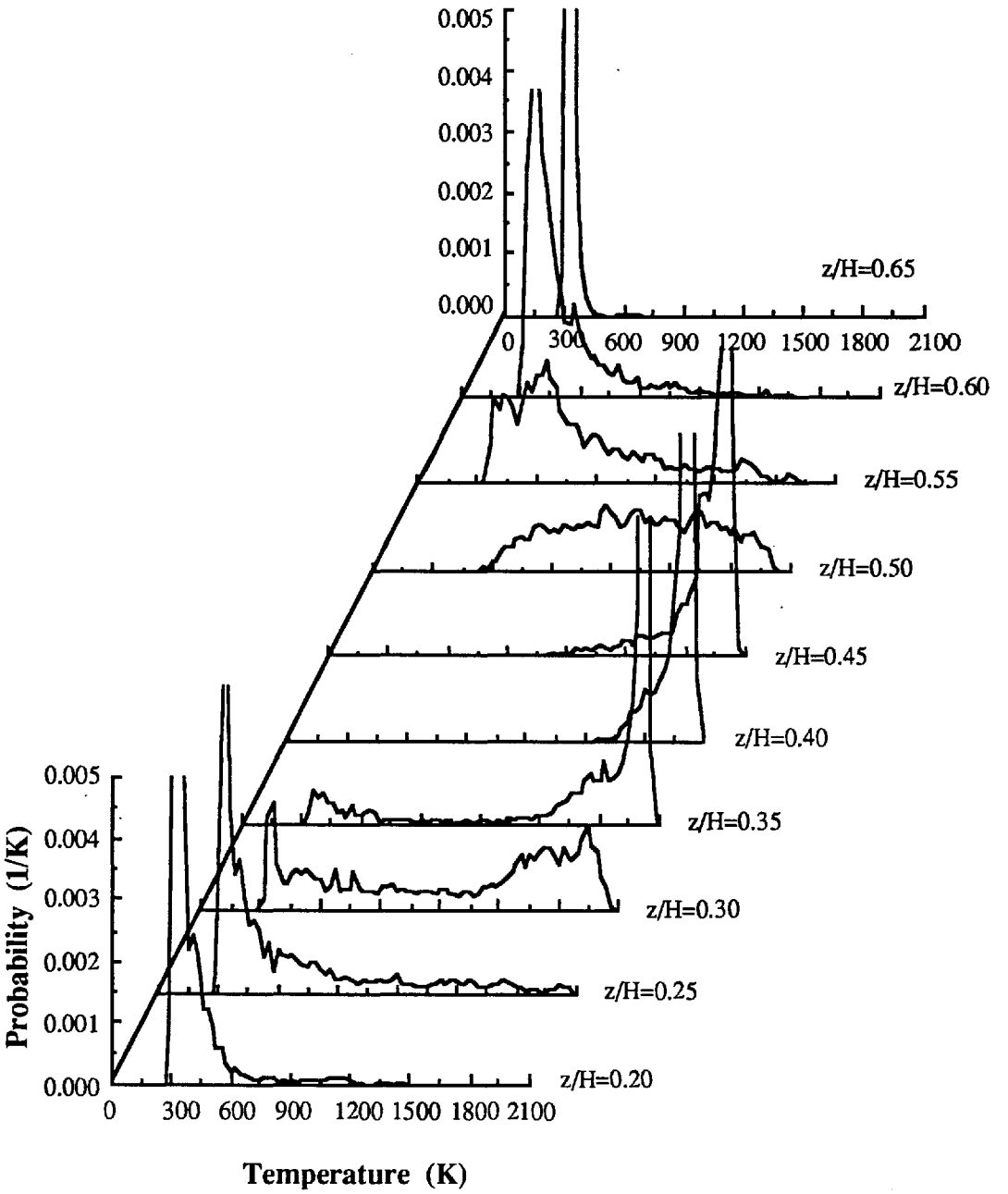


Figure 3.3.30 The probability density functions of the temperature measurements of Fig. 3.3.29.

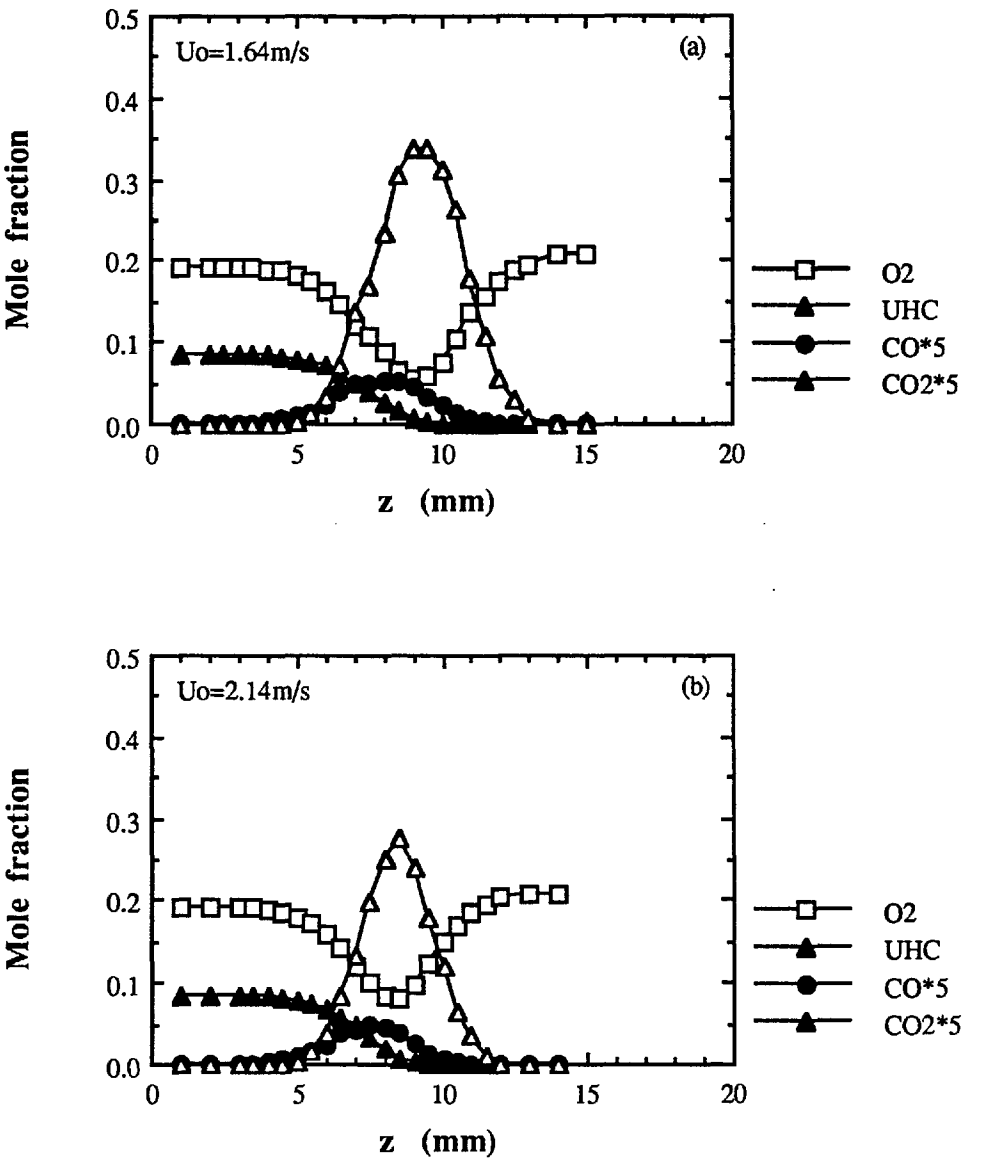


Figure 3.3.31 Mean species concentrations of single lean premixed flames with H=20mm, H_p=55mm, ϕ=0.9, and the indicated bulk velocity : U_o=1.64m/s for (a) and 2.13m/s for (b). The hydrogen concentration was not measured because the gas chromatograph was not available. The conversion from the dry measurements to the wet mole fractions presented here was made in the way described in Section 2.4.3.

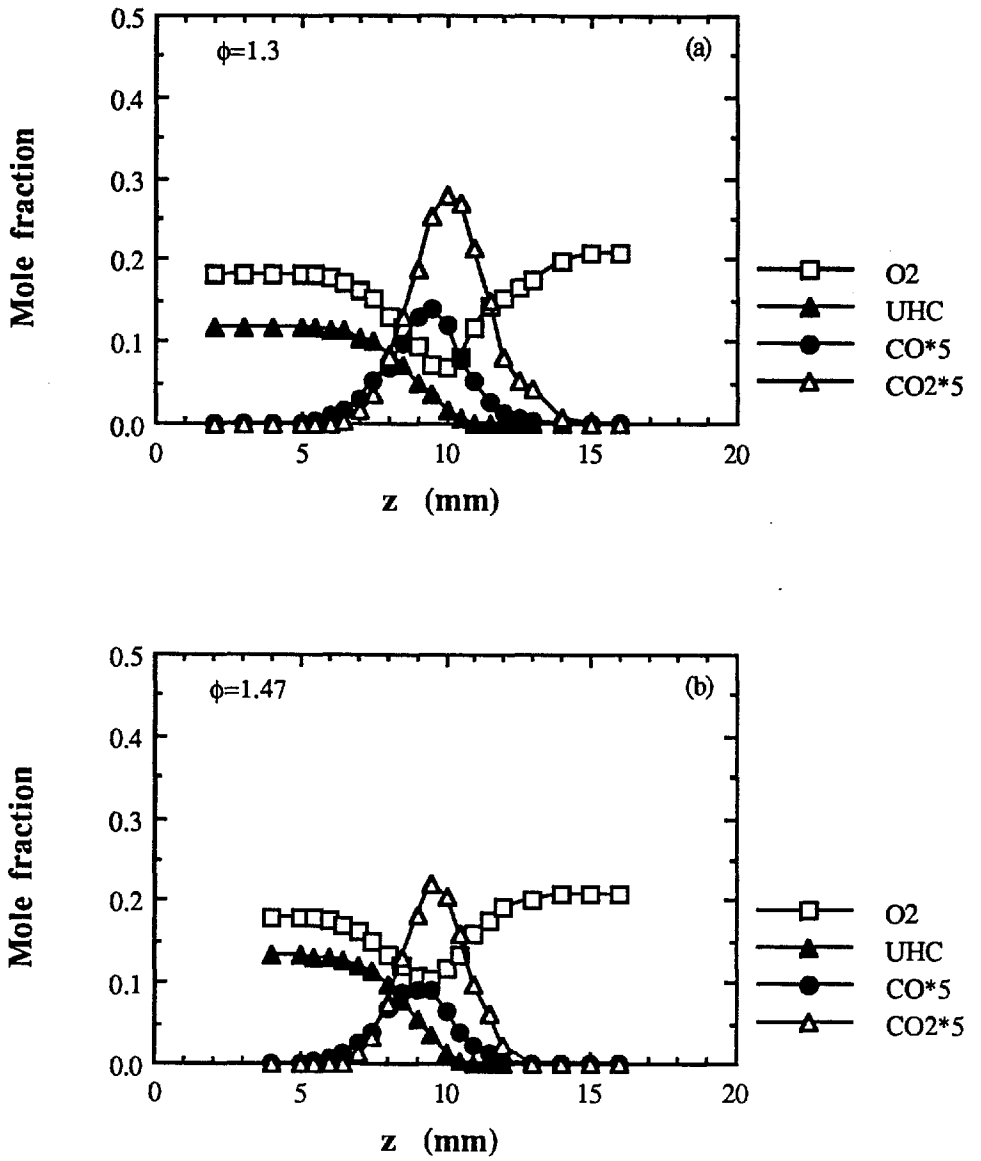


Figure 3.3.32 Mean species concentrations of single rich premixed flames with H=20mm, H_p=55mm, U_o=1.64m/s, and ϕ=1.2 for (a) and ϕ=1.47 for (b). The hydrogen concentration was not measured because the gas chromatograph was not available. The conversion from the dry measurements to the wet mole fractions presented here was made in the way described in Section 2.4.3.

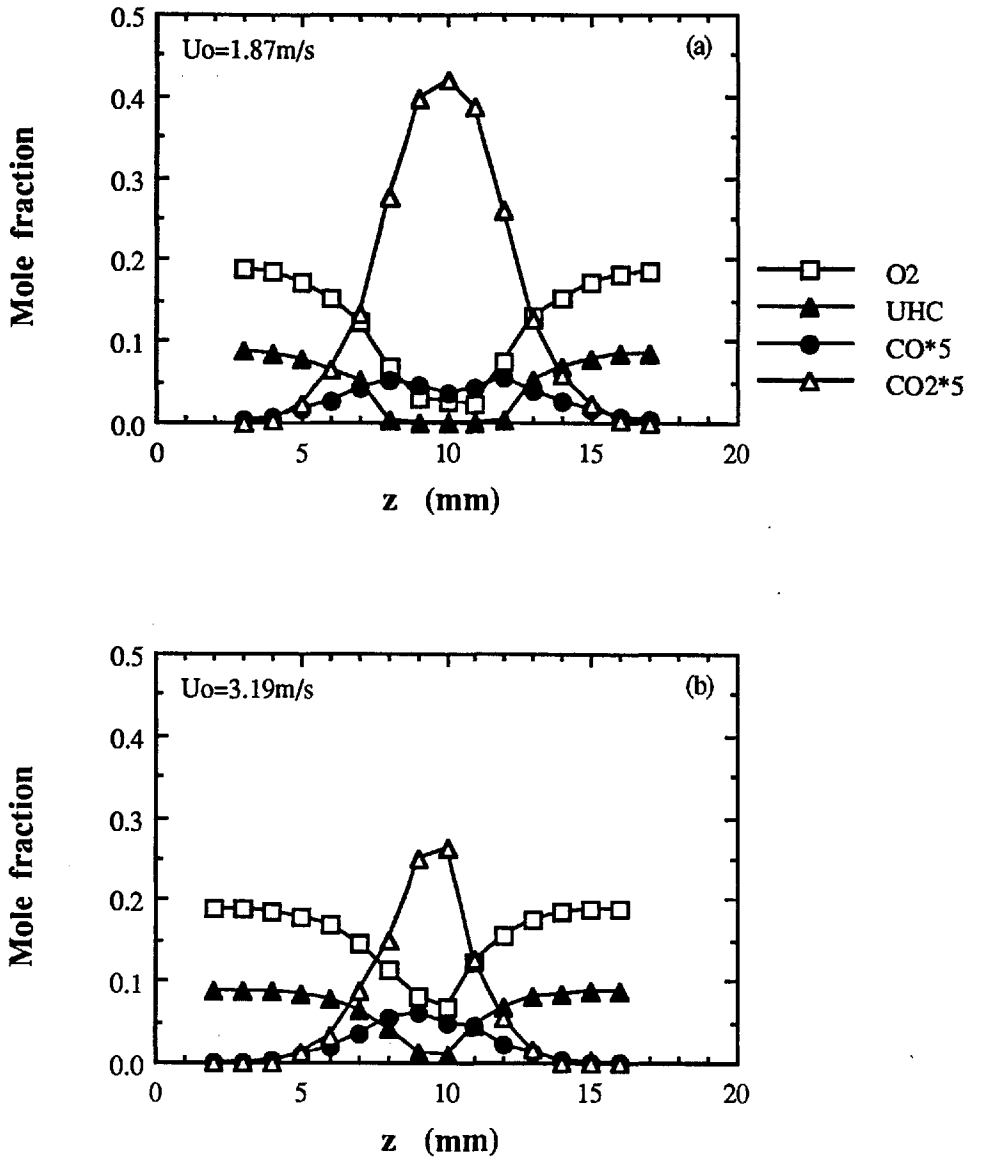


Figure 3.3.33 Mean species concentrations of twin lean premixed flames with H=20mm, H_p=55mm, ϕ=0.9, and for U_o=1.87 (a) and 3.19m/s (b). The hydrogen concentration was not measured because the gas chromatograph was not available. The conversion from the dry measurements to the wet mole fractions presented here was made in the way described in Section 2.4.3. These measurements were taken with the large sampling probe (see Sections 2.4.4, 2.4.5 and 2.4.6).

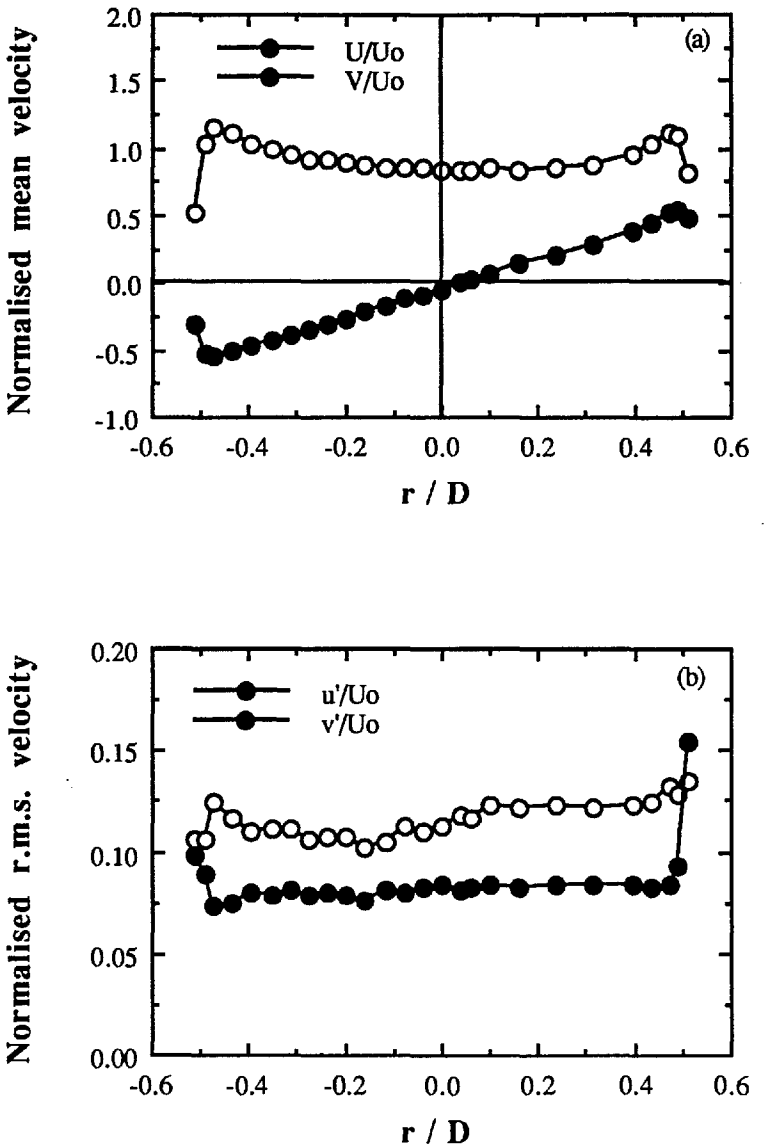


Figure 3.3.34 Mean axial (a) and (b) r.m.s. axial and radial velocities radial variation at z=2mm for a single premixed flame with H=20mm, H_p=55mm, ϕ=0.9, and U_o=1.64m/s.

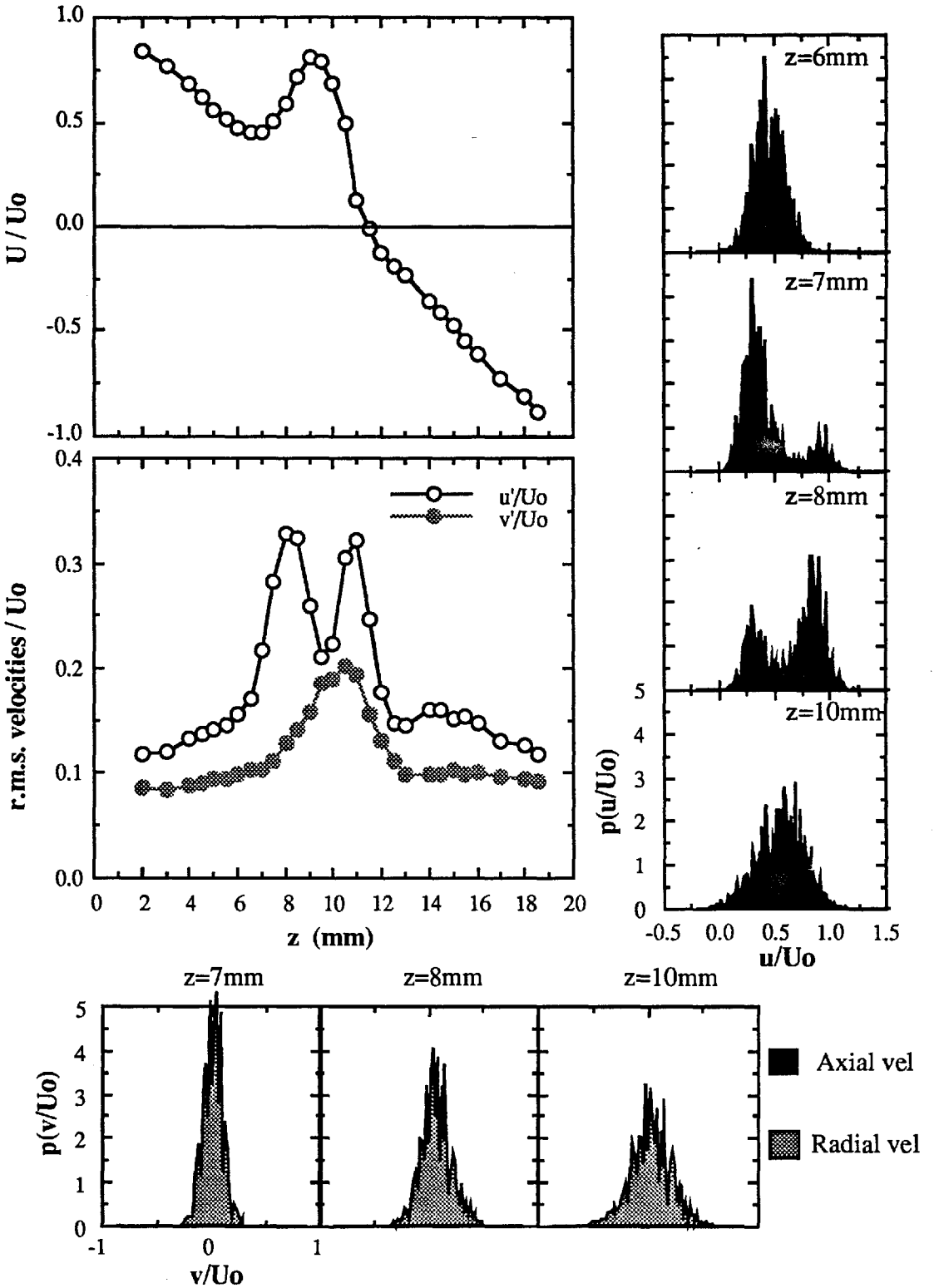


Figure 3.3.35 Centreline variation of the mean axial and r.m.s. axial and radial velocities for a single premixed flame with H=20mm, H_p=55mm, U_o=1.64m/s, ϕ=0.9. The probability density functions at a few locations are also shown.

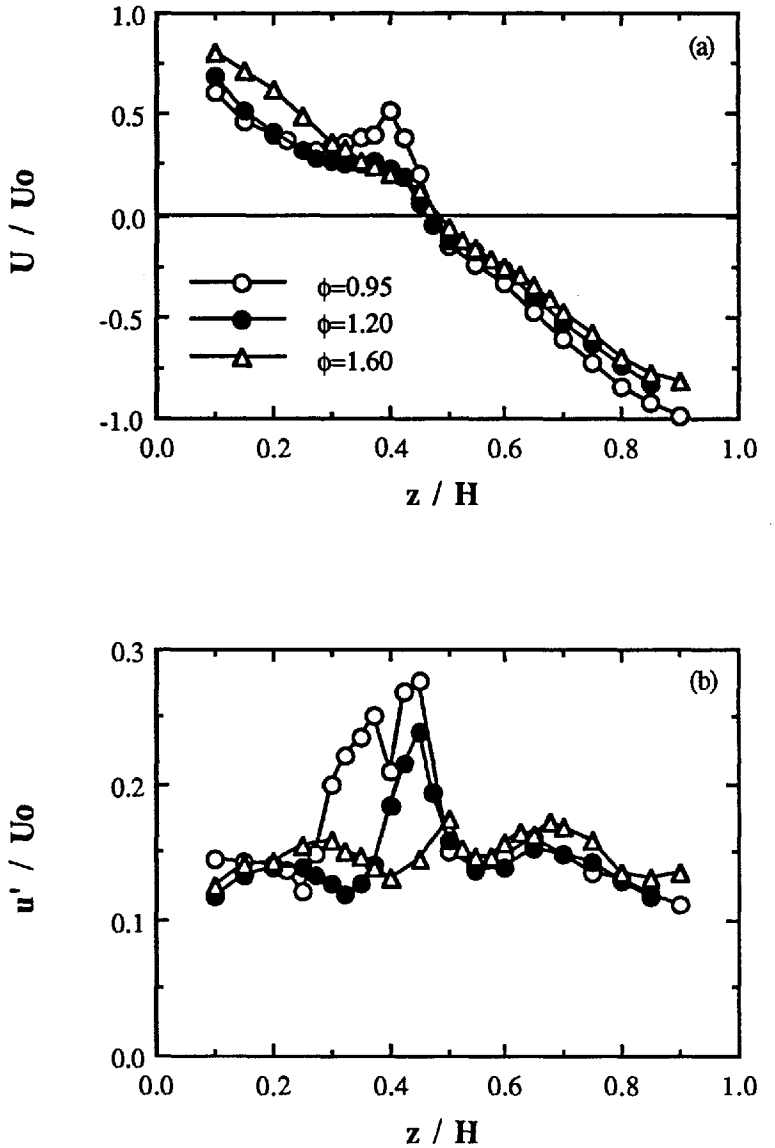


Figure 3.3.36 Centreline traverses of the axial mean (a) and r.m.s. (b) velocities in single premixed flames with H=20mm, H_p=55mm, and U_o=2.0m/s for different equivalence ratios.

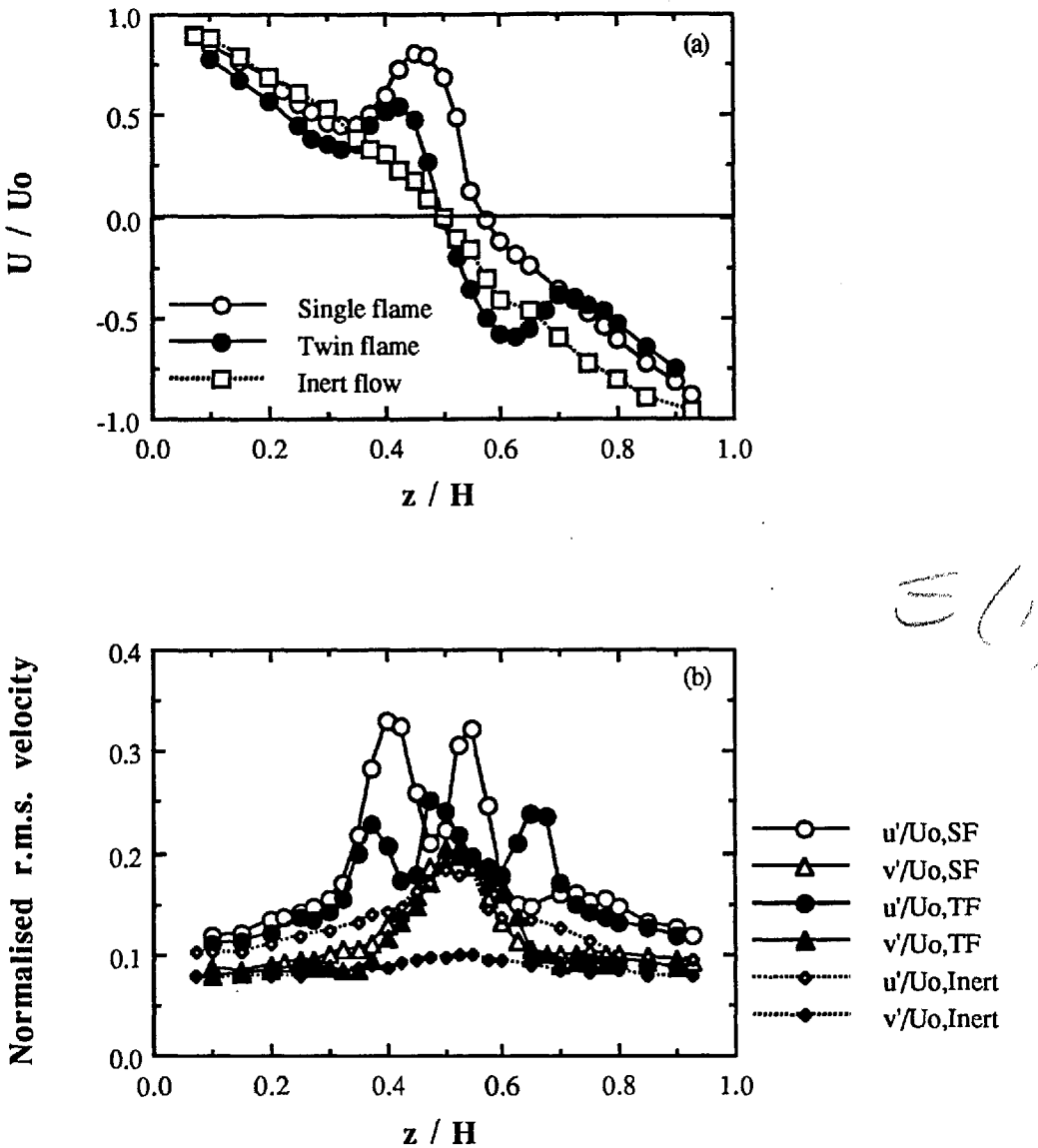


Figure 3.3.37 Centreline traverses of axial mean (a) and r.m.s. axial and radial (b) velocities in single (SF) and twin (TF) premixed flames and in the inert flow with H=20mm, H_p=55mm. For the single flame, ϕ=0.9, U_o=1.64m/s (same as Fig. 3.3.35); for the twin flames, $\phi_1=\phi_2$=0.9 and U_o=1.87m/s, and for the inert flow, U_o=1.64m/s.

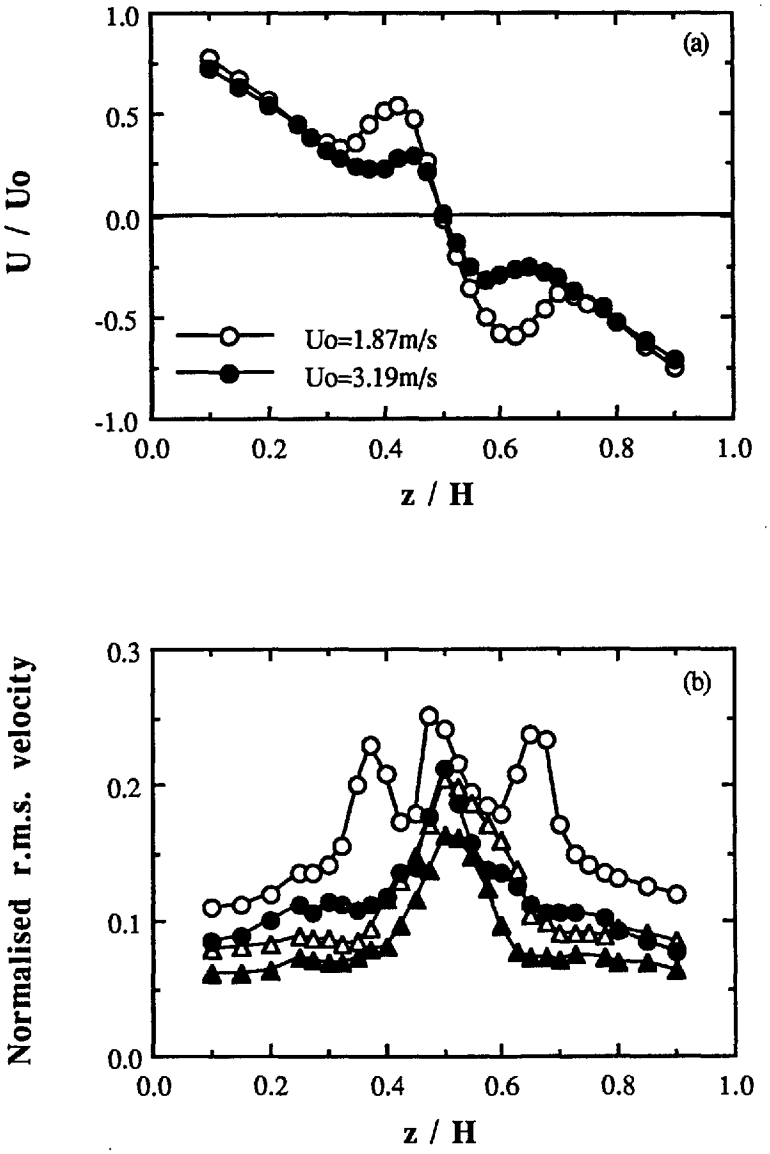


Figure 3.3.38 Centreline traverses of mean (a) and r.m.s. axial and radial (b) velocities in twin premixed flames with H=20mm, H_p=55mm, ϕ=0.9, and U_o=1.87m/s (open symbols) and 3.19m/s (blocked symbols). For (b), the circles correspond to the axial and the triangles to the radial fluctuations.

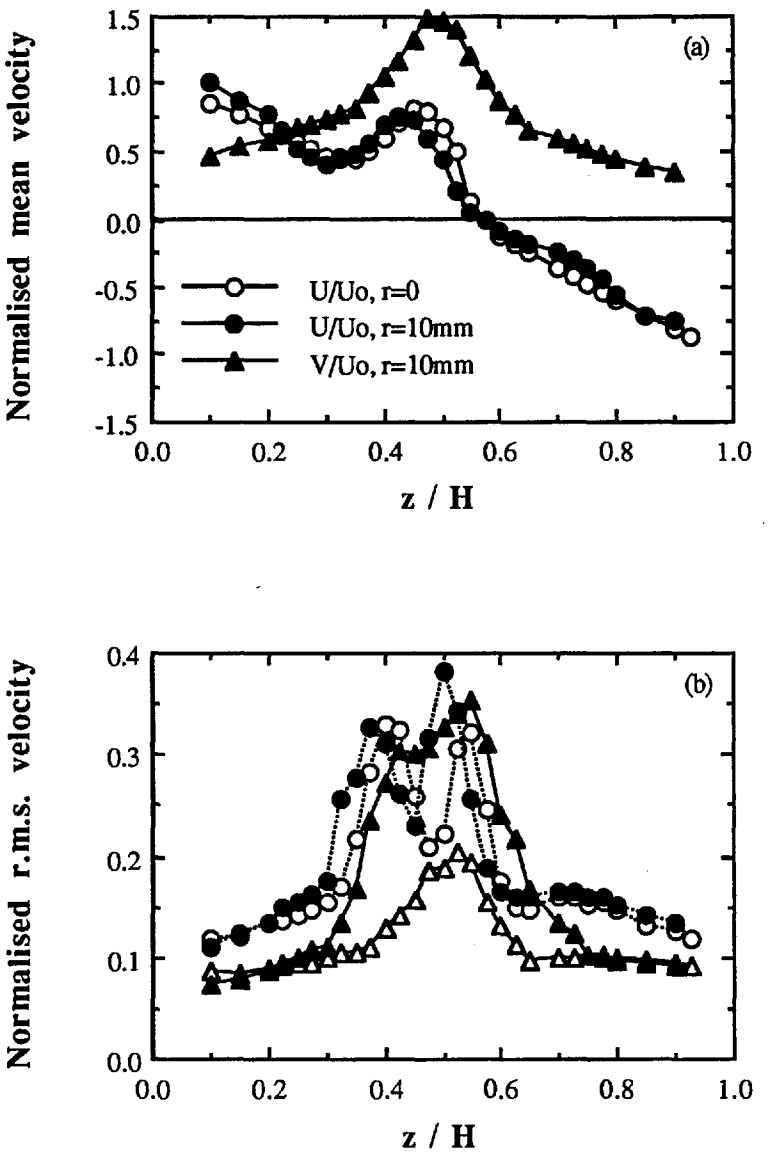


Figure 3.3.39 Axial variations of the axial and radial velocities at r=0 and r=10mm in single premixed flames with H=20mm, H_p=55mm, U_o=1.64m/s, and ϕ=0.9. For (b), open symbols correspond to r=0, blocked symbols to r=10mm, and the axial and radial fluctuations are represented by the circles and triangles respectively.

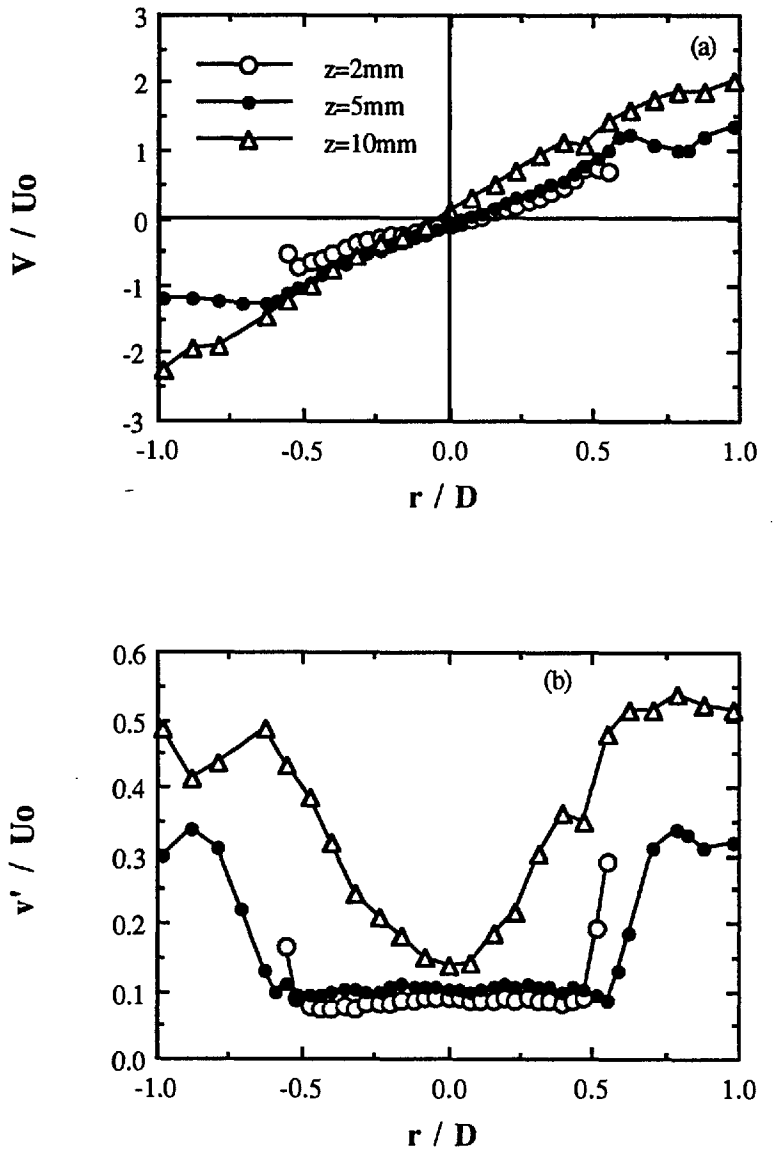


Figure 3.3.40 Radial variations at different axial positions of the radial velocity in single premixed flames with H=20mm, H_p=55mm, U_o=2.0m/s, and ϕ=0.95.

Figures for Chapter 3, Section 3.4

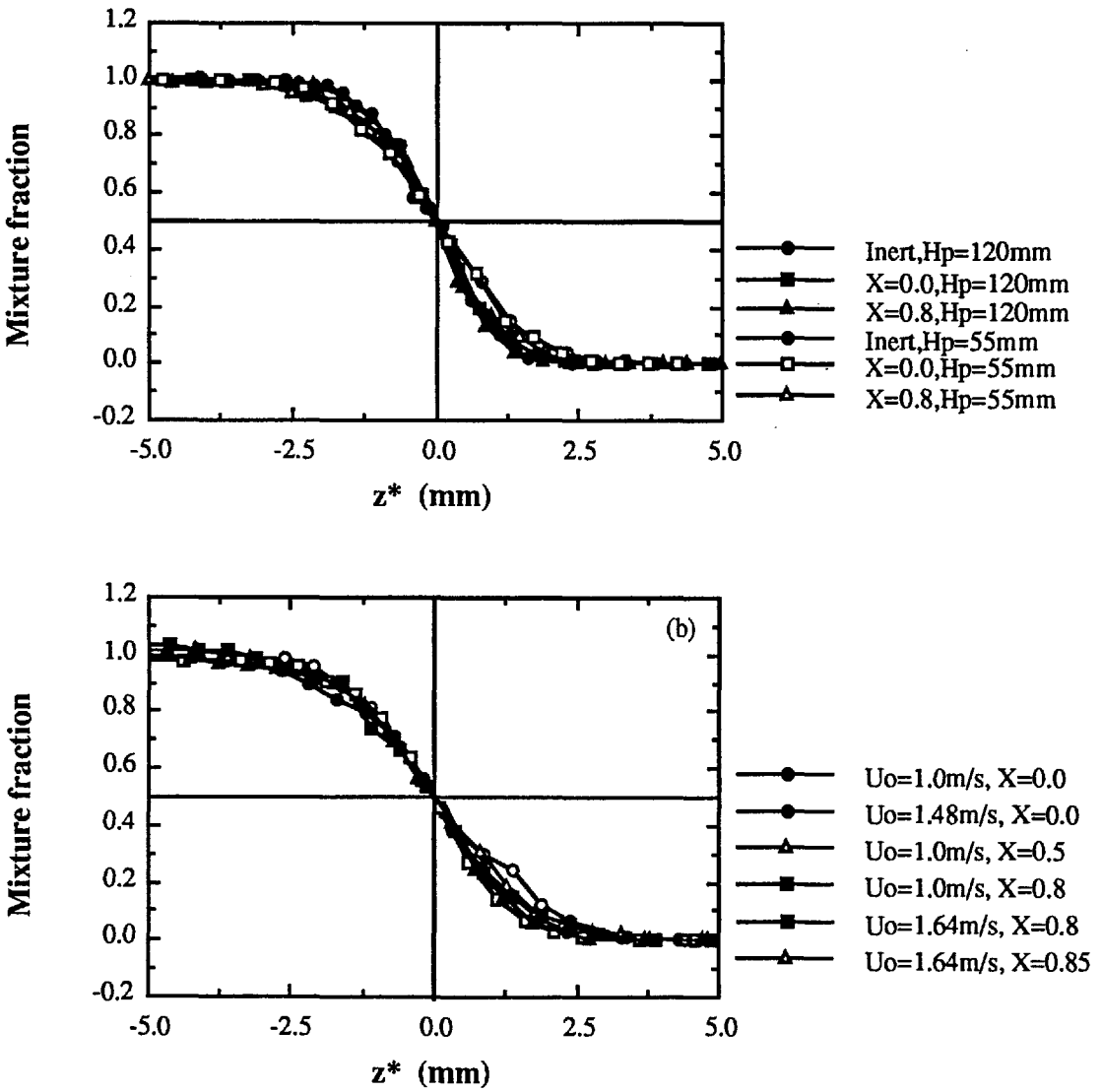


Figure 3.4.1 (a) The mean mixture fraction variation from the species measurements during combustion (Figs. 3.3.15, 3.3.16, 3.3.17 & 3.3.19) and the inert flow measurements (Fig. 3.2.17) for weak and strong turbulence for H=20mm. (b) The mean mixture fraction from combustion measurements for pure and partially premixed flames with H=20mm and different bulk velocities and premixedness.

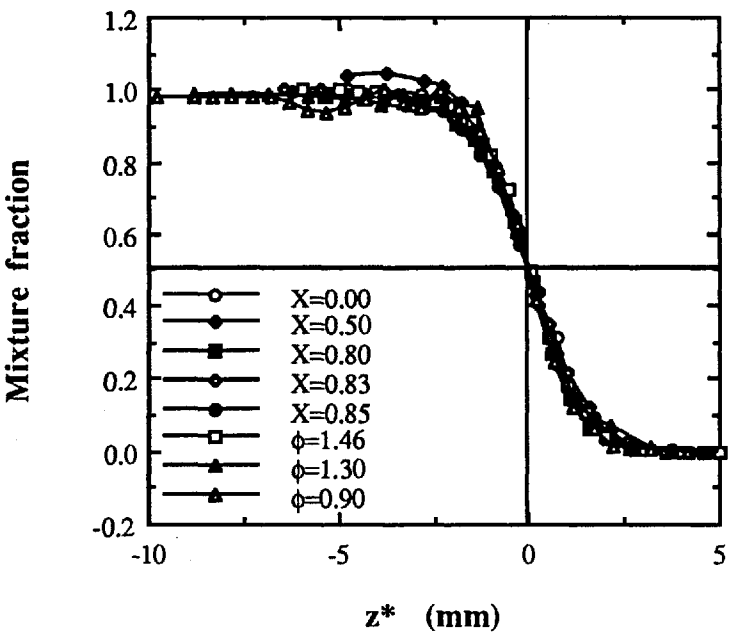


Figure 3.4.2 The mean mixture fraction from measurements of species mole fractions in diffusion and single premixed flames with H=20mm, H_p=55mm, and U_o=1.64m/s (1.48m/s for the flame with X=0.0).

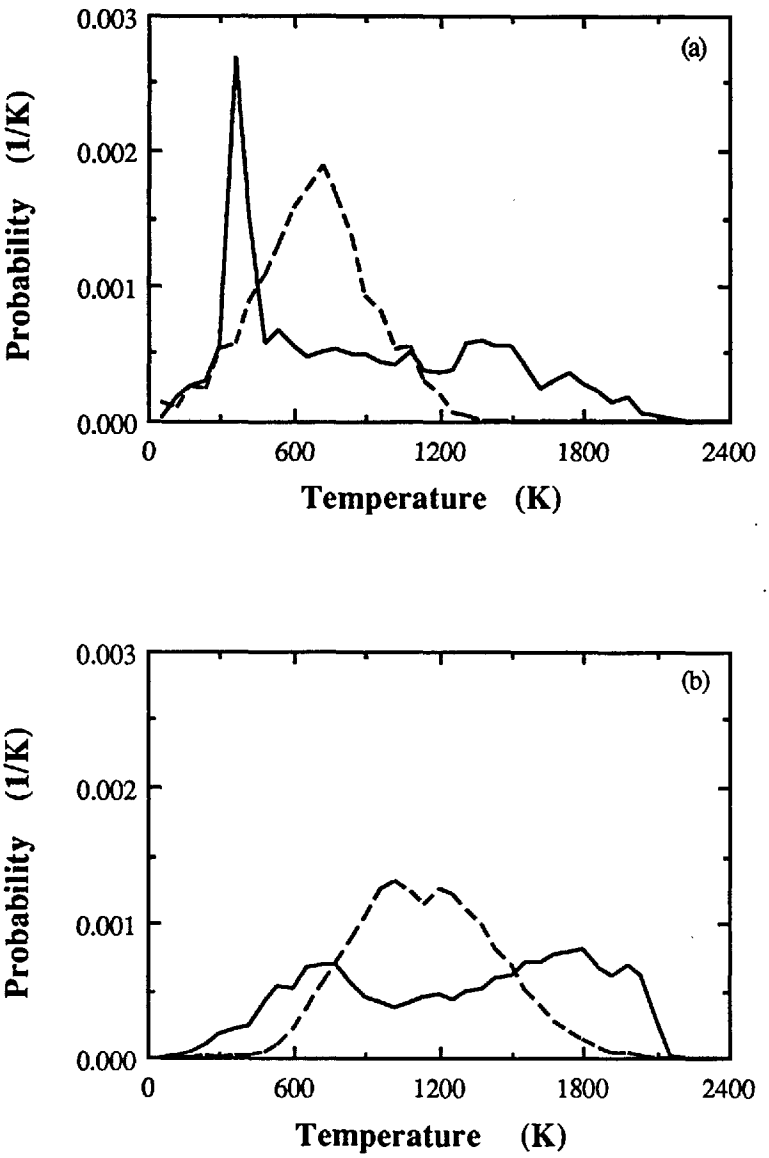


Figure 3.4.3 The pdf of temperature before (solid line) and after (dashed line) high–pass filtering at 20Hz for the diffusion flame of Fig. 3.3.10 at (a) z=8mm, and (b) z=10.5mm.

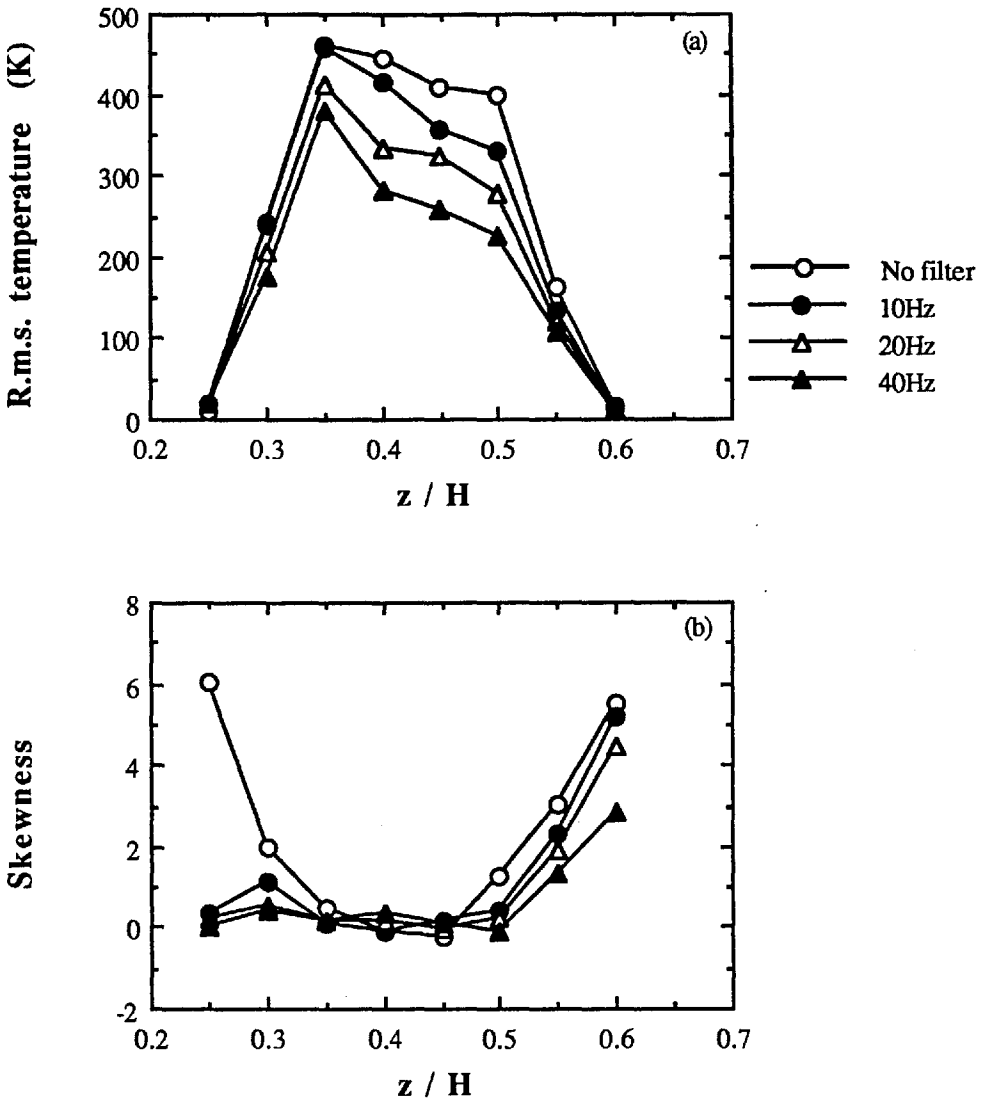


Figure 3.4.4 The effect of high–pass filtering on the axial variation of (a) the r.m.s. temperature and (b) the skewness of the pdf of the temperatures of Fig. 3.3.6b and for H_p=55mm.

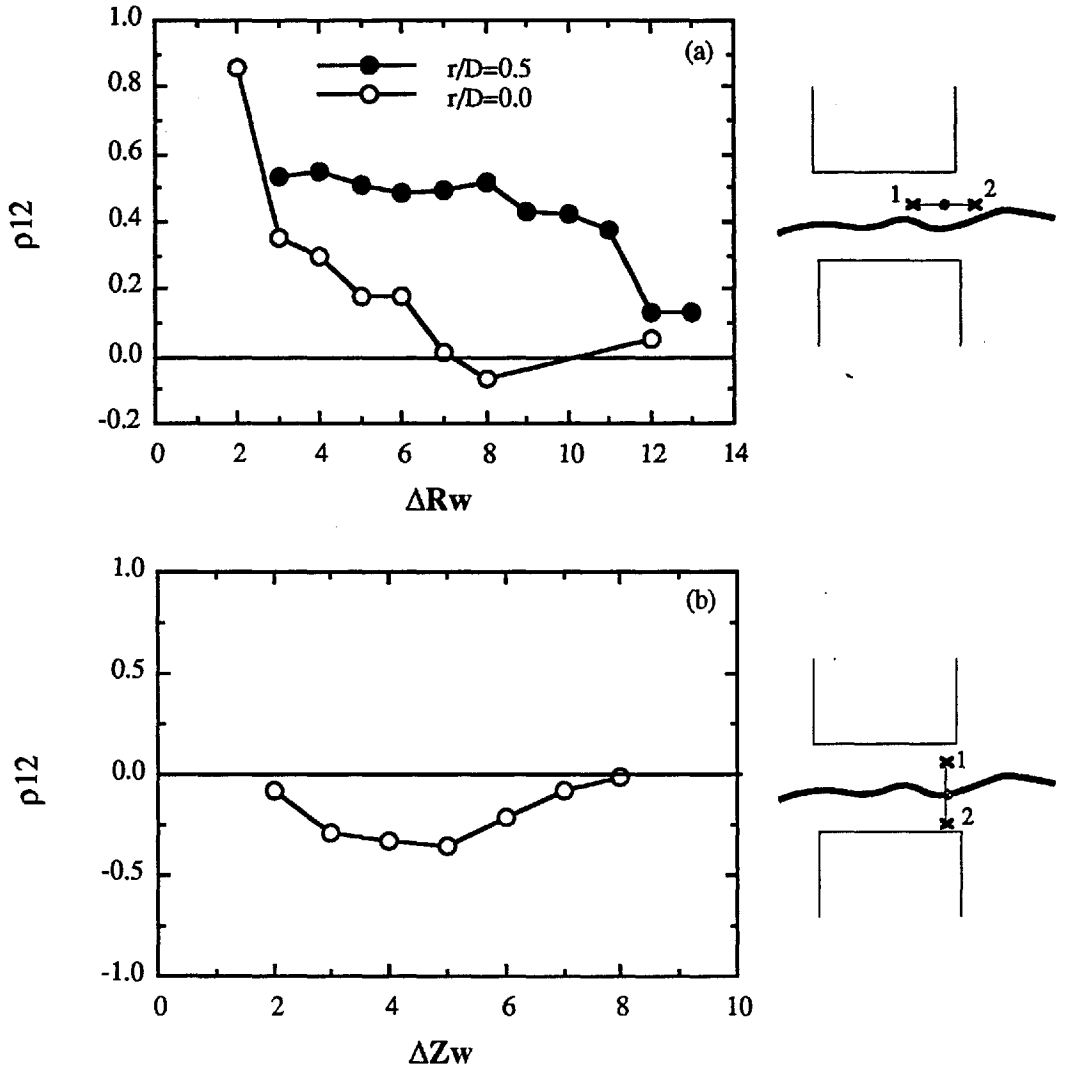


Figure 3.4.5 (a) The correlation coefficient of the temperature fluctuations in two points in the diffusion flame of Fig. 3.3.6b with H_p=55mm as a function of radial distance between the thermocouples. Both thermocouples were kept at approximately the same axial location and the mid–point between the thermocouples (indicated as the dot between 1 and 2 in the "cartoon" next to the graph) was at r=13mm (blocked symbols) and at the centreline (open symbols). (b) The correlation coefficient as a function of axial separation when the two thermocouples were at the same radial location (r=13mm) and their mid–point corresponded to the maximum temperature.

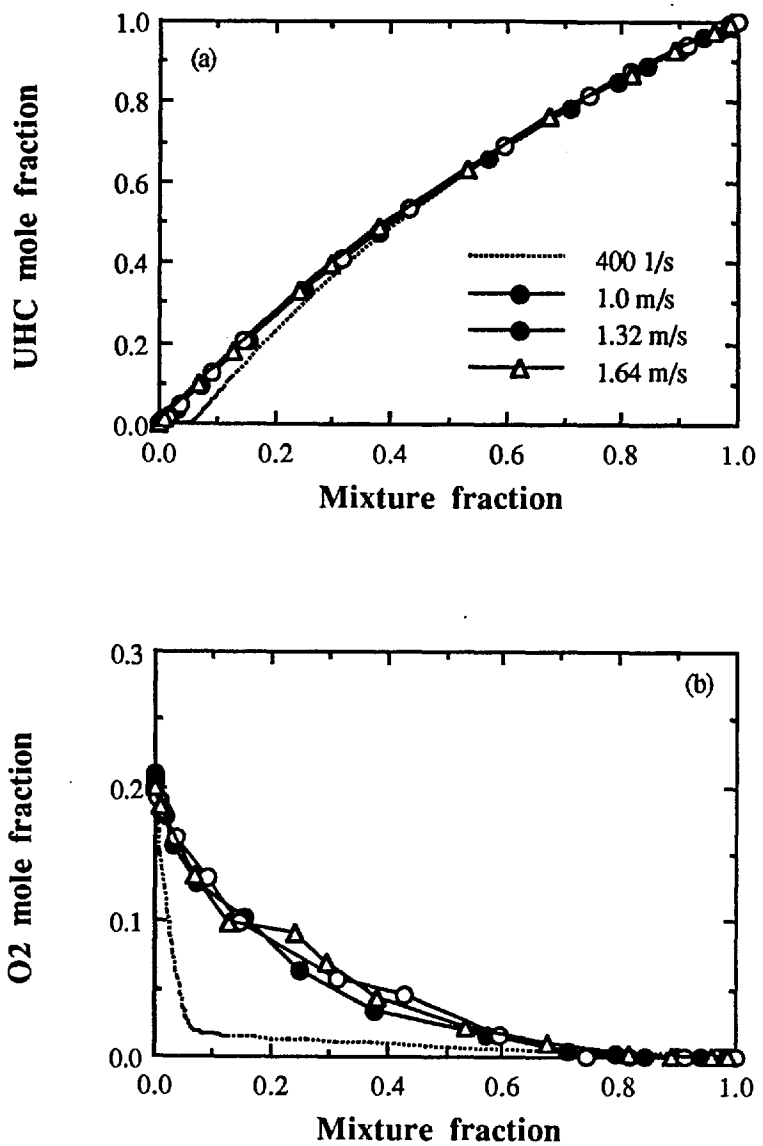


Figure 3.4.6 Measured concentrations of UHC (a), O_2 (b), CO_2 (c), CO (d), and H_2 (e) in diffusion flames with H=20mm, X=0.0, H_p=55mm, and the indicated bulk air velocity plotted as a function of mean mixture fraction. The stoichiometric mixture fraction for this flame was equal to f_{st}=0.055. Blocked circles : U_o=1.0m/s; open circles : U_o=1.32m/s; triangles : U_o=1.64m/s. Included are calculations (Lindstedt, 1992; personal communication) from laminar counterflow diffusion flames at 151 s^{-1} (solid line) and at 400 s^{-1} (dashed line), the latter flame close to extinction.

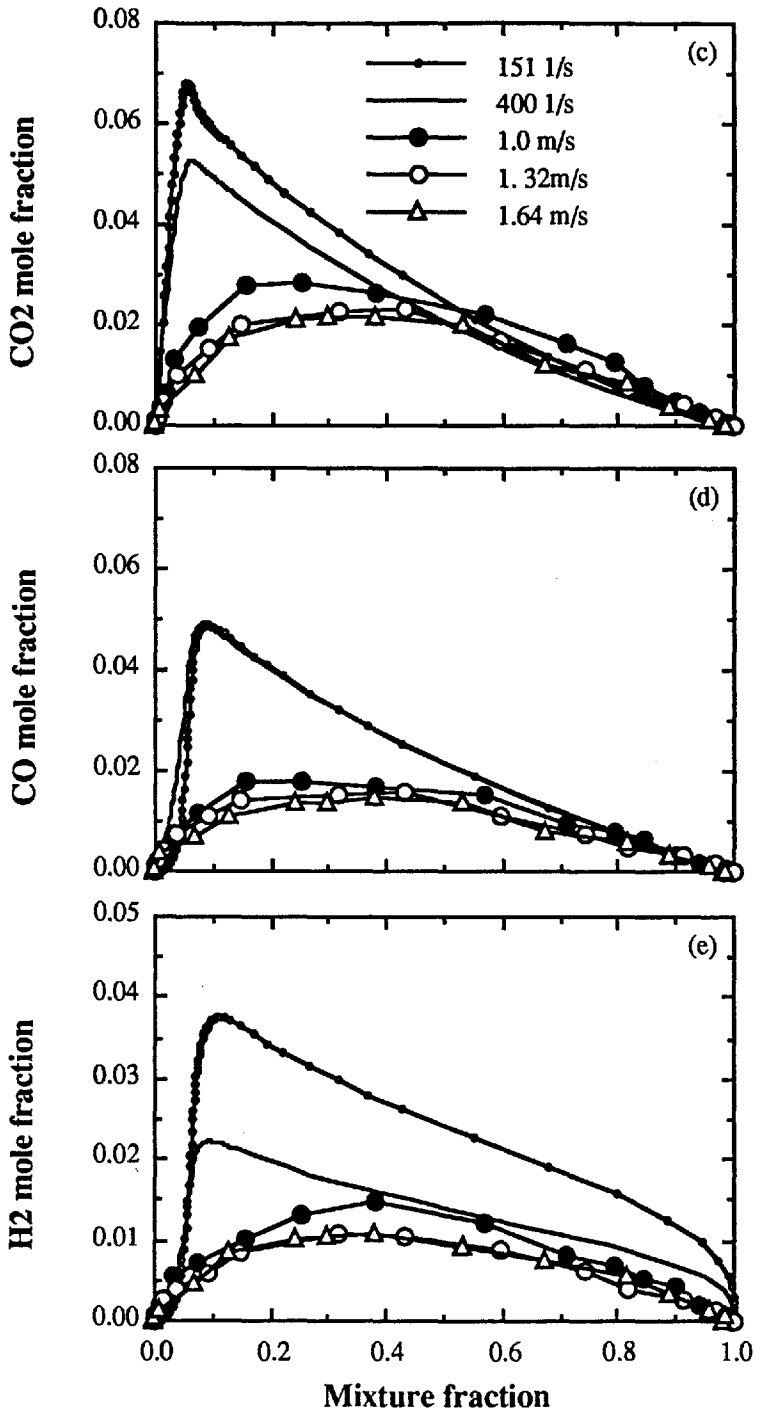


Figure 3.4.6 Continued and concluded.

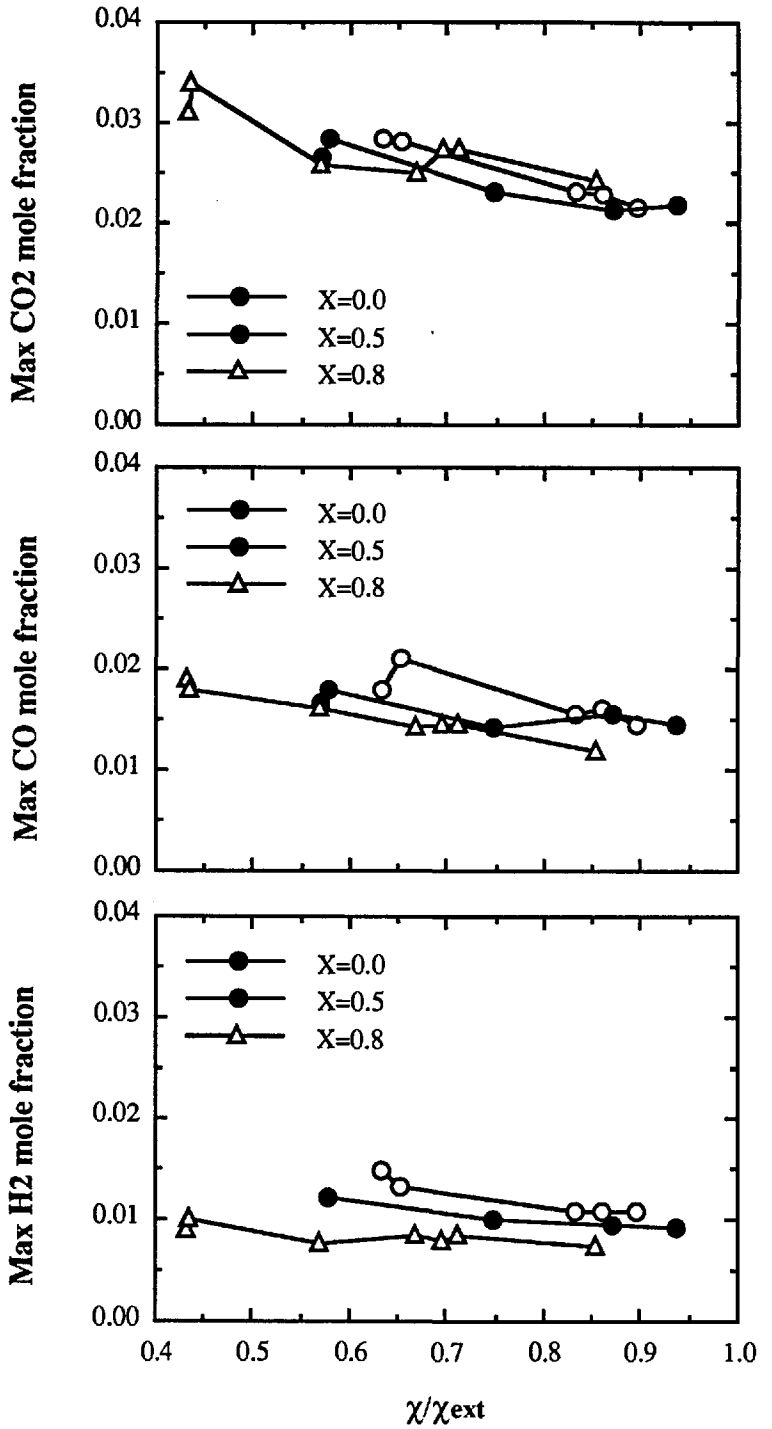


Figure 3.4.7 The maximum mole fractions of CO_2, CO, and H_2, from the profiles in Figs. 3.3.15 to 3.3.20, plotted as a function of the ratio of the estimated scalar dissipation rate from Eq. (3.2.8) for each velocity U_o, jet separation H, and perforated plate location H_p, to the value at extinction of each flame (see Fig. 4.16, and Section 4.3.4). The ratio χ/χ_{ext} is a way to quantify the approach to extinction for diffusion flames (see Section 4.3.4). For each point, χ was estimated by evaluating Eq. (3.2.8) using $q'=C_q U_o$, with C_q from Eq. (3.2.2), L_{turb}=4mm, and f' from numerical calculations as in Fig. 3.2.12b for the corresponding value of α calculated from Eq. (3.2.19).

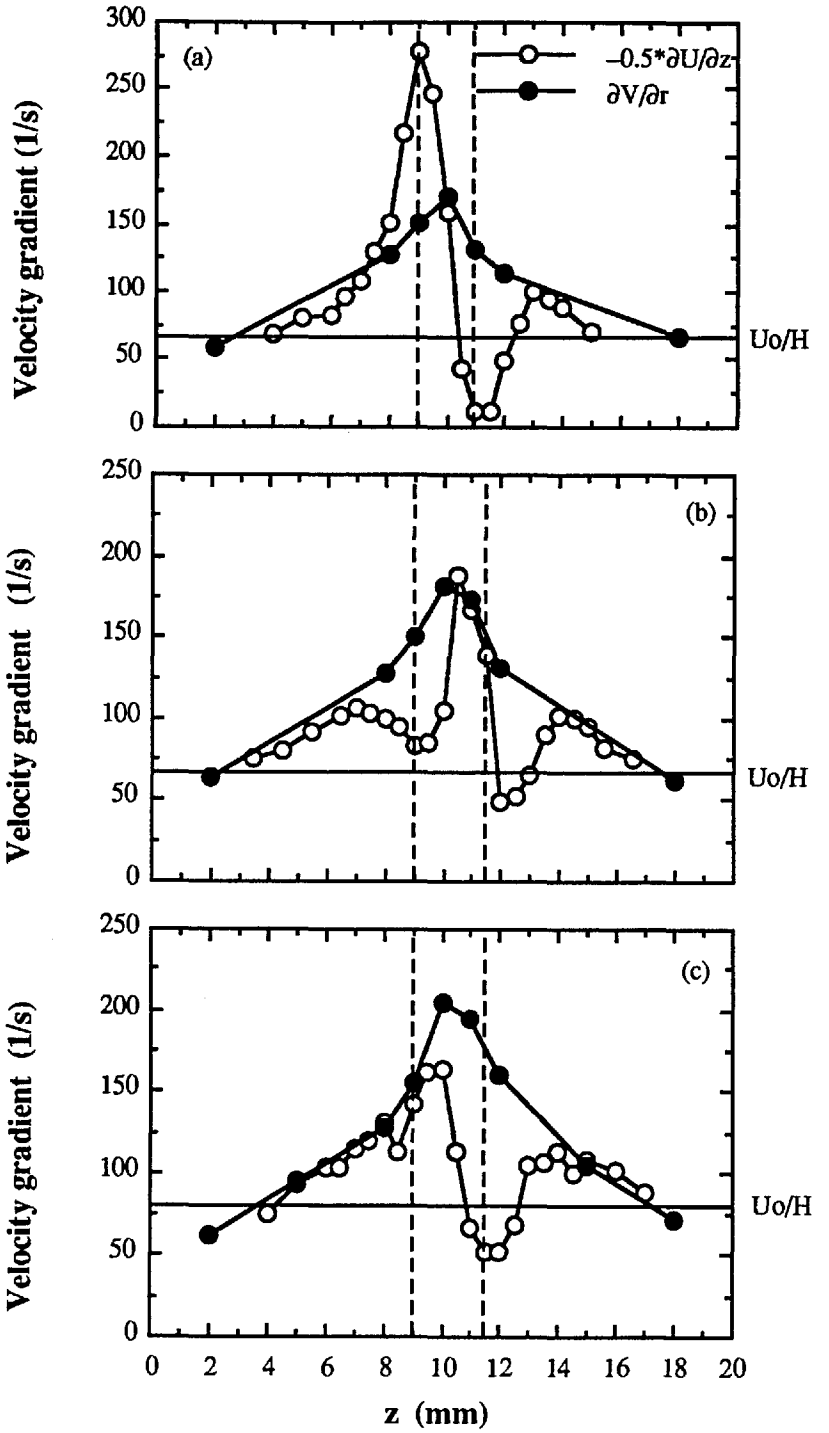


Figure 3.4.8 The axial variation of $-\partial U/\partial z$ and $\partial V/\partial r$ along the centreline of diffusion flames, the former measured from central differences from the data in Figs. 3.3.22 and subsequent smoothing (performed by a 3–point running average), and the latter from straight line fits to radial profiles such as those of Fig. 3.3.28 from measurements in $-6 \le r \le 6$mm. For all measurements, H=20mm, H_p=55mm, and for (a) X=0.0, U_o=1.32m/s; (b) X=0.5, U_o=1.32m/s; (c) X=0.8, U_o=1.64m/s. In all graphs, the luminous zone, as judged by eye, has been marked by the dashed lines.

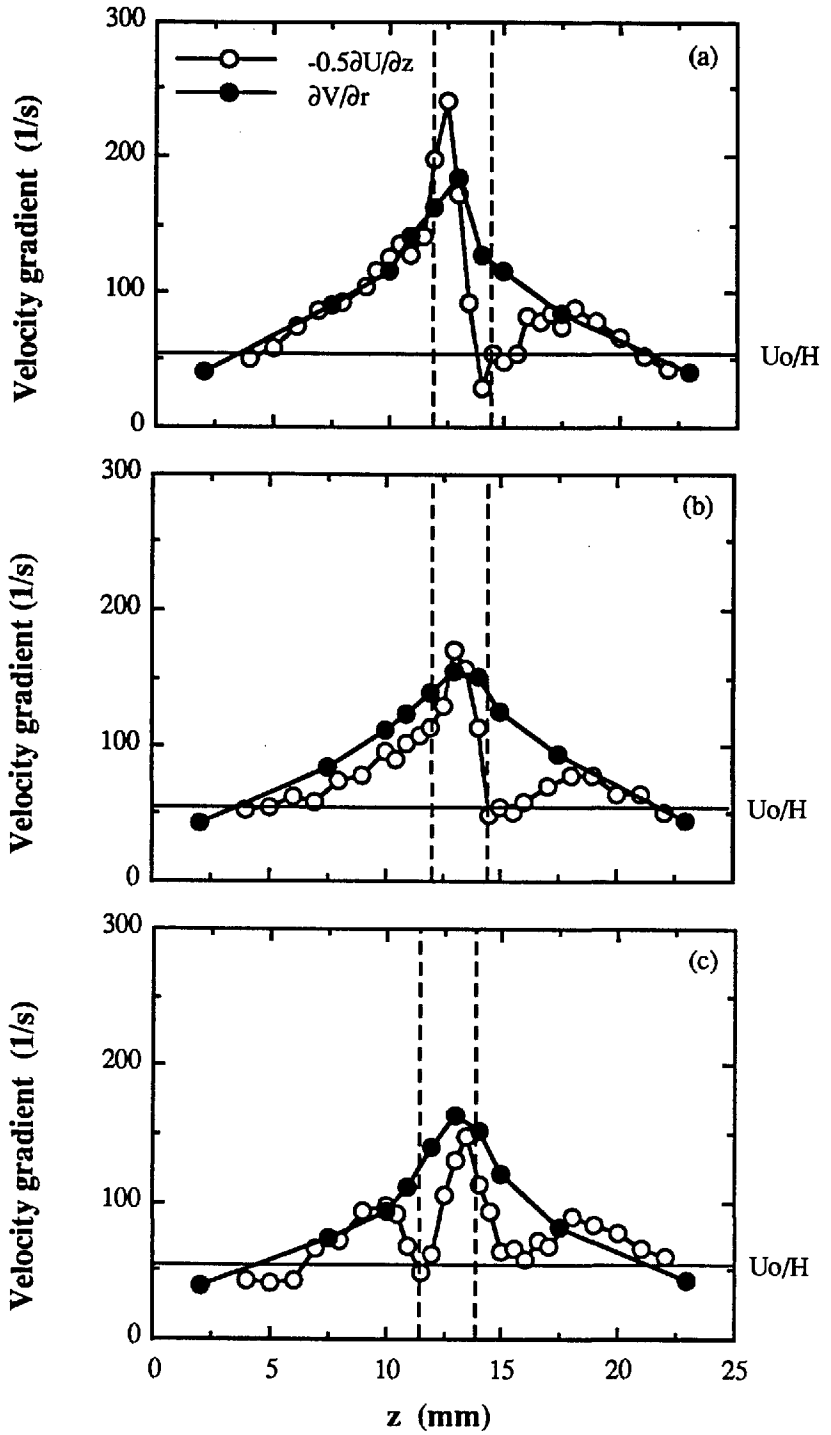


Figure 3.4.9 The centreline variation of $-\partial U/\partial z$ and $\partial V/\partial r$ for diffusion flames with H=25mm, H_p=55mm, and U_o=1.32m/s. (a) : X=0.0; (b) : X=0.5; (c) : X=0.8. See caption to Fig. 3.4.8 and Section 3.4.5 for calculation method. The dashed lines indicate the location of the luminous zone.

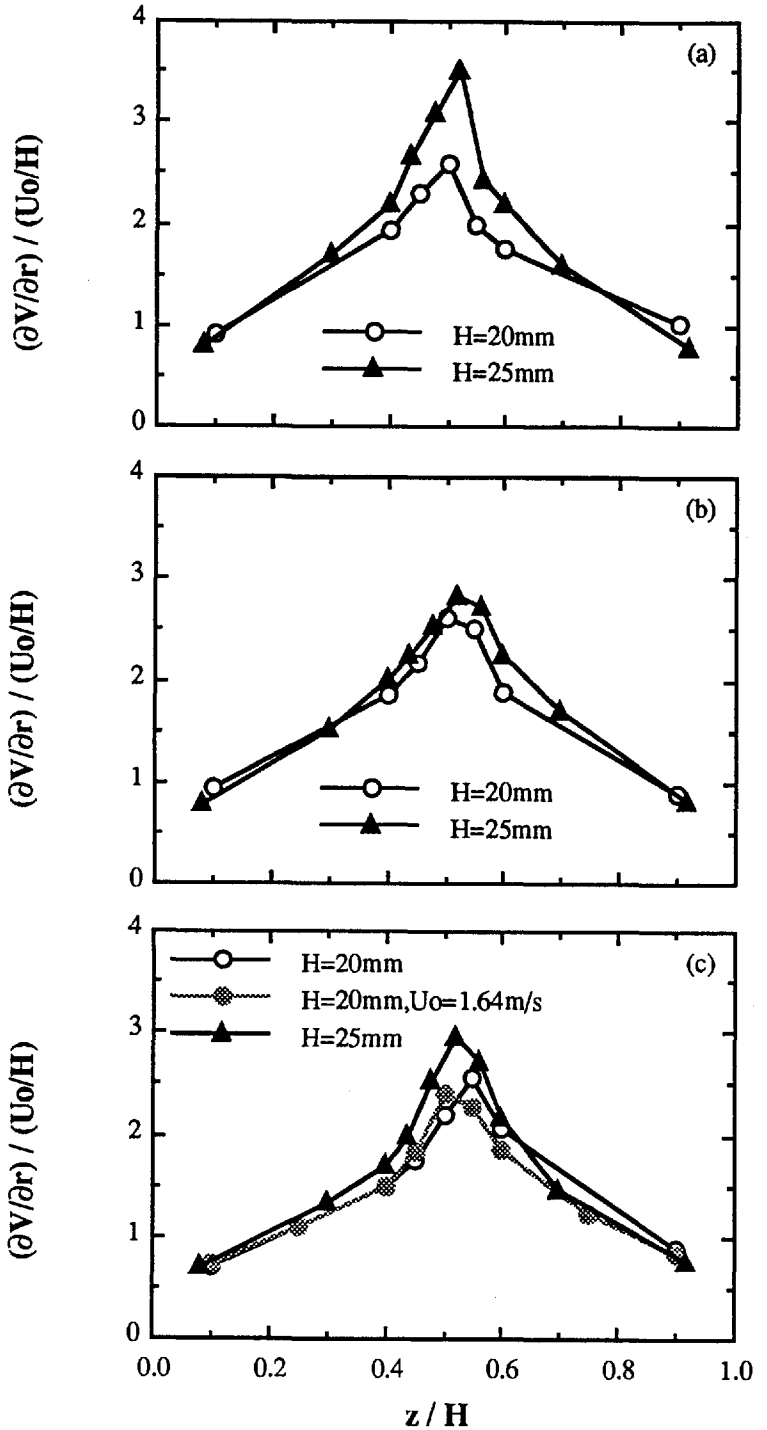


Figure 3.4.10 The centreline variations of the radial bulk stretch rate $\partial V/\partial r$ normalised by U_o/H for the data of Figs. 3.4.8 and 3.4.9.

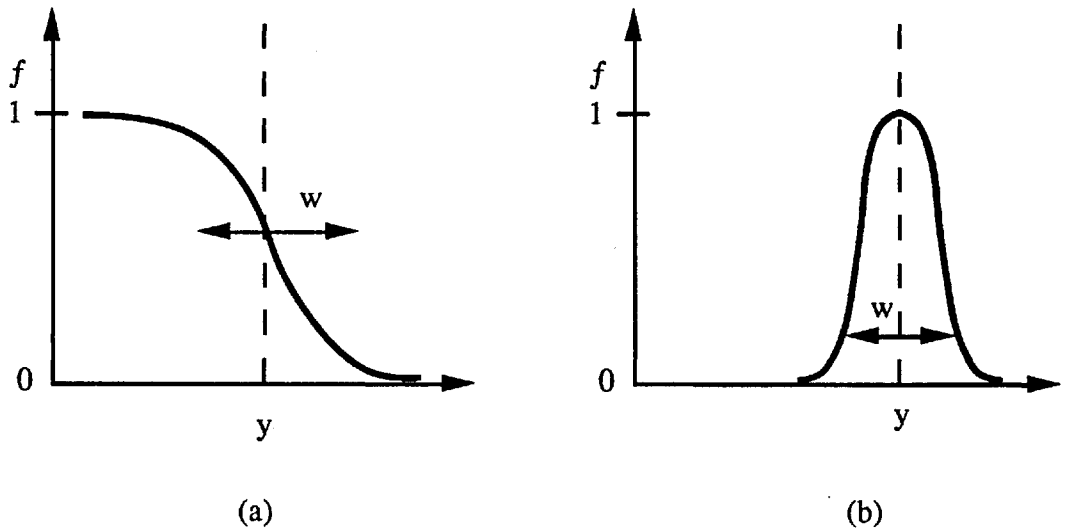


Figure 3.4.11 Schematic of the Flapping Model. The scalar profile depicted by the solid line is assumed to remain invariant and be located randomly at y relative to the measuring point, which is assumed to be located at the origin. The resulting ensemble averages at the measuring point can be found by averaging over all possible locations of this profile. In (a) an error–function profile is depicted with a characteristic width w and is used to predict the statistics of mixture fraction in inert opposed jet flows. In (b), a Gaussian profile is shown that is used for predictions of flame temperature fluctuations. These profiles have been described by the following functional forms for the predictions presented in Figs. 3.4.12 to 3.4.15: for (a), $f = 0.5\ [1-\mathrm{erf}(y/w)]$ and for (b), $f = \exp(-y^2/w^2)$.

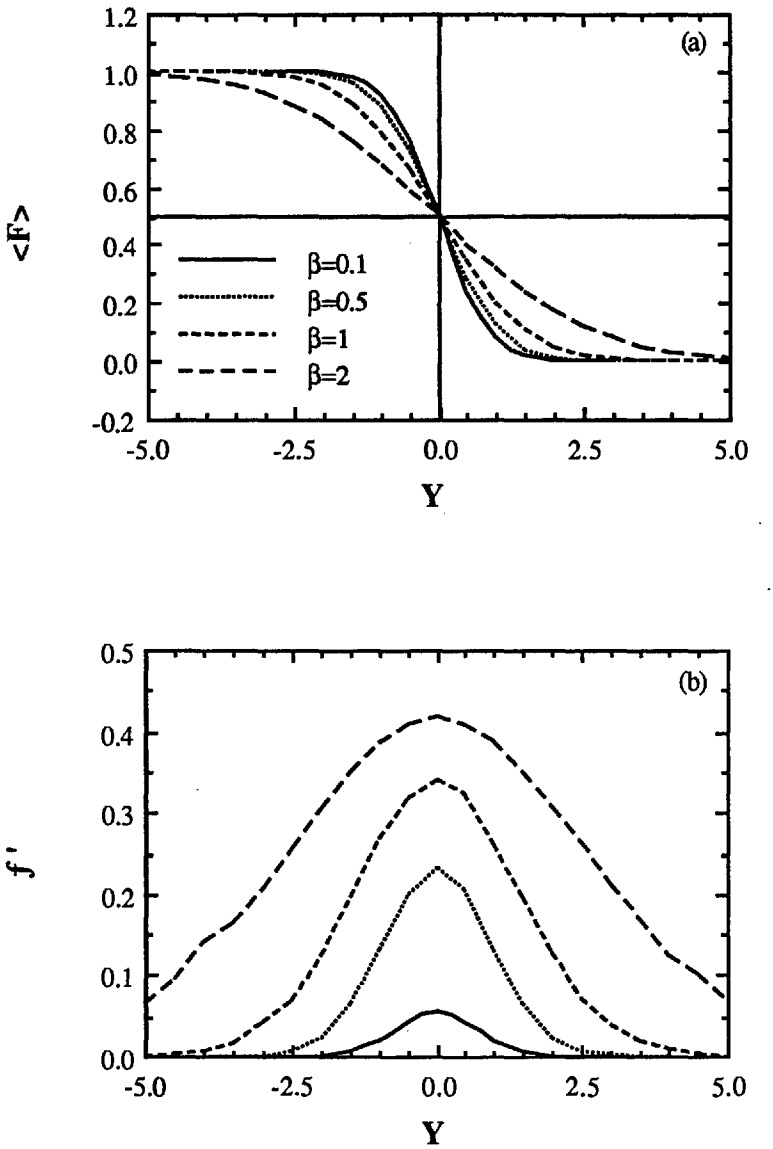


Figure 3.4.12 The mean and r.m.s. of a scalar predicted by the Flapping Model in which a small–scale scalar error–function profile of width w is located from the origin at a random distance obeying a Gaussian distribution with mean Y and r.m.s. y', as a function of distance for various values of β (=y'/w). See Fig. 3.4.11 and Section 3.4.6.

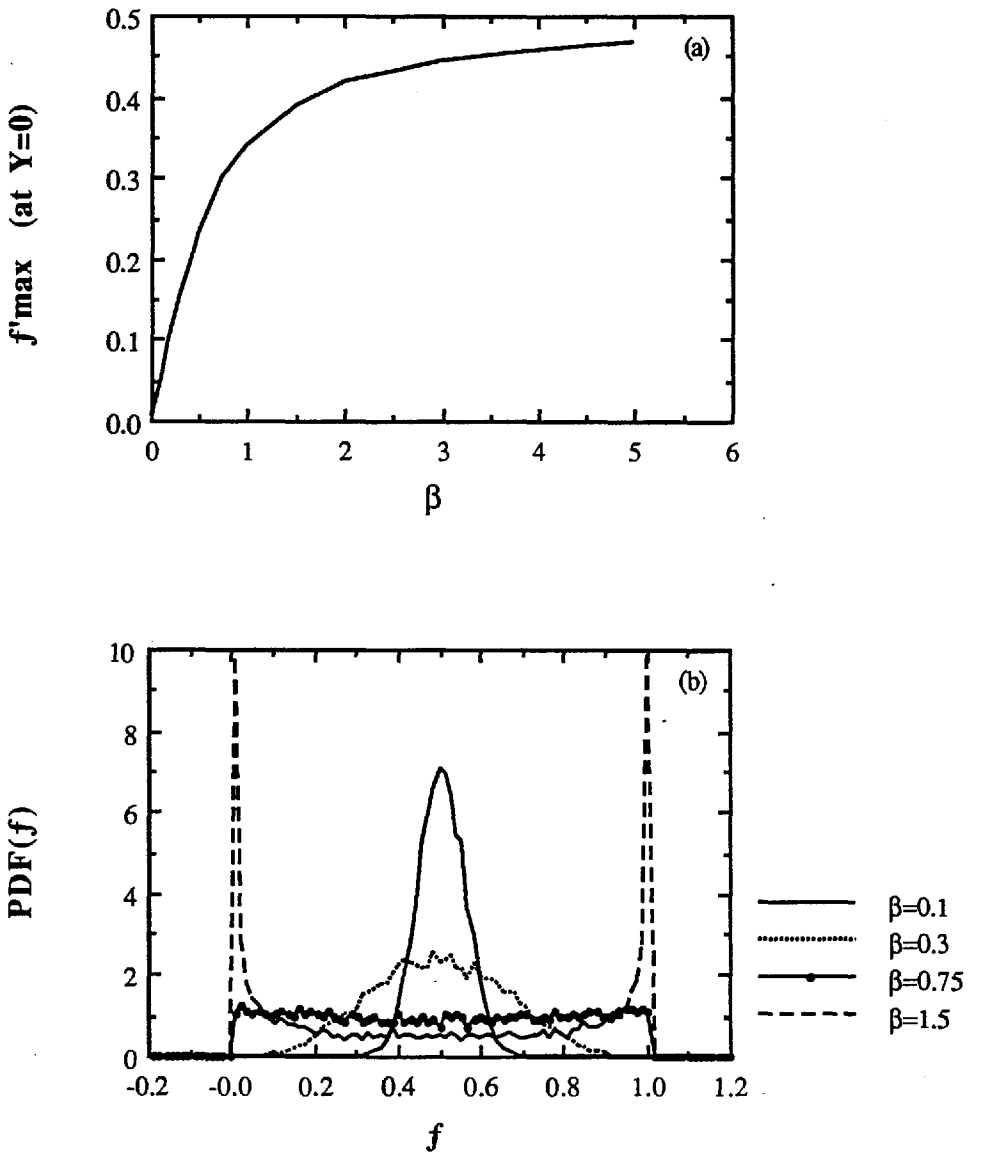


Figure 3.4.13 (a) The maximum scalar r.m.s. fluctuations at the location of ⟨F⟩=0.5 (Y=0) as a function of β. (b) The associated pdfs with β as parameter.

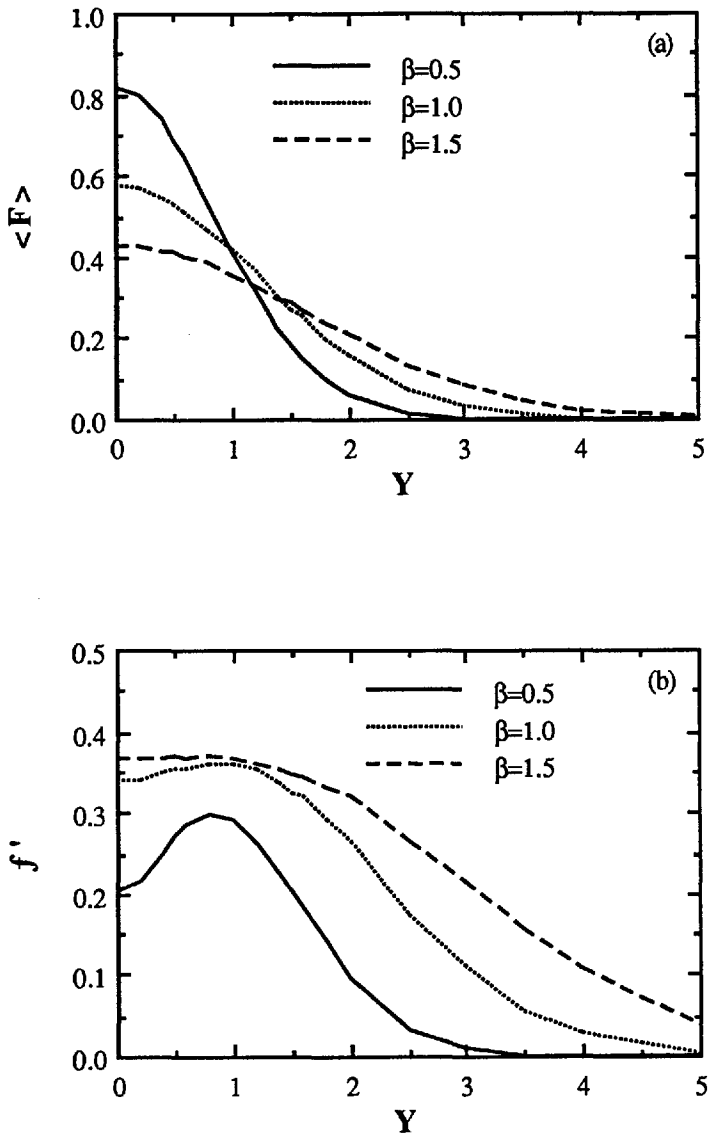


Figure 3.4.14 The mean (a) and r.m.s. (b) values of the scalar predicted by the Flapping Model for a Gaussian small-scale scalar profile with width w and peak of unity, located at a random distance y obeying a Gaussian distribution with mean Y and r.m.s. y'. Curves for different values of β (=y'/w) are shown.

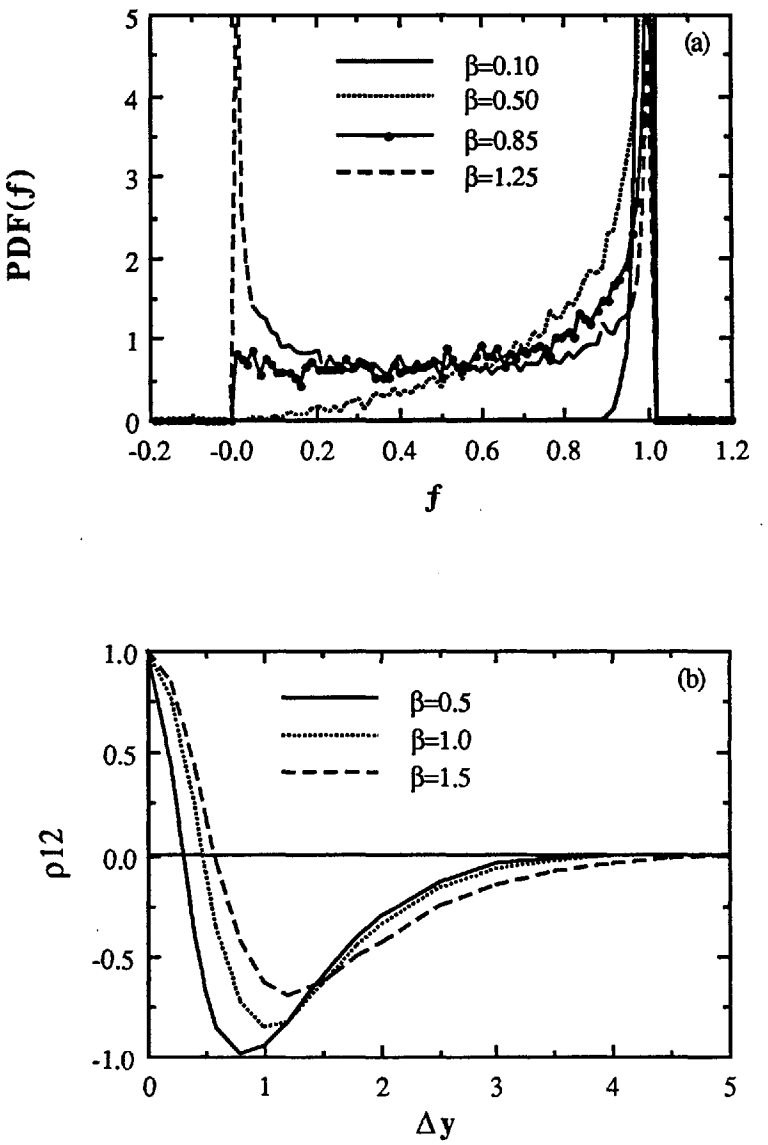


Figure 3.4.15 (a) The pdfs of the scalar f predicted by the Flapping Model for a Gaussian small–scale profile at the location of maximum mean scalar (Y=0) with β as parameter. (b) The correlation coefficient between fluctuations at points placed symmetrically about the origin as a function of separation distance Δy.

Chapter 4. Extinction of turbulent counterflow flames

4.1 INTRODUCTION

4.1.1 Structure of this Chapter

As was mentioned in the introduction to the thesis, the extinction of turbulent flames is an important subject because it affects the operation of combustion devices and is interesting from a fundamental viewpoint and here, measurements of the extinction limits of the turbulent counterflow premixed and diffusion flames examined in Chapter 3 are presented. The results provide insight into the parameters that affect the stability of turbulent flames and help distinguish between current theories of turbulent flame extinction.

The Chapter begins with a review of the stability of turbulent premixed and diffusion reacting flows by considering theories that treat the local structure of the flame and its extinction, while Section 4.2 presents the methods used to determine the extinction limits and the reader is referred to Chapter 2 for a detailed description of the geometric configuration. In Section 4.3, the results are presented and discussed separately for premixed and for diffusion flames and compared with the extinction of similar laminar flames. Finally, in Section 4.4 the major conclusions are summarised.

4.1.2 Background on extinction of laminar flames

It is widely believed that flames extinguish when the reaction rates are slower than the rate at which reactants are supplied to the reaction zone. Extinction can be achieved when the temperature drops excessively, thereby slowing the kinetics, and this can be caused by dilution with an inert gas, contact with a cold solid surface, or by diffusion or convection of heat from the reaction zone. The last possibility is often associated with velocity gradients which lead to flame stretch. A Damköhler number, Da, can be defined for both premixed and diffusion laminar flames as the ratio of an aerodynamic timescale, equal to the inverse of the stretch rate for counterflow flames, to a chemical timescale that, for example, increases with deviations from stoichiometry for premixed flames, and extinction occurs when Da falls below a critical value, as was mentioned in Chapter 1. The concept that extinction occurs when an aerodynamic timescale becomes short compared to a chemical timescale has motivated extinction theories of *turbulent* flames, and such applications are reviewed below. The reader should consult the original papers for details.

4.1.3 Extinction of turbulent premixed flames

Flamelet combustion

When the spatial thickness of the reaction zone is smaller than the Kolmogorov lengthscale, the Bray–Moss–Libby model applies and flamelet models of the turbulent flame can be formulated to calculate the time-average reaction rate in the turbulent flame (Peters, 1986). In such models, the mean reaction rate is the ensemble average over all laminar flamelets that experience strain rates smaller than the strain rate required for extinction, and only these flamelets contribute to the overall creation of products and heat release (e.g. Bradley *et al.*, 1992). The success of this method rests on the accurate representation of the statistics of the strain rates in the small–scale motions and on the accurate estimation of the quenching strain rate of the laminar flamelet. Flamelet descriptions are often used with a numerical calculation of the time–averaged conservation equations together with a turbulence model and have shown promising results for predicting the overall stability of turbulent flames (Al–Masseeh *et al.*, 1990; Bradley *et al.*, 1990; Bray *et al.*, 1991). Extinction of the turbulent flame in the flamelet regime occurs when the small–scale strain rate is sufficiently high to quench a sufficient portion of the laminar flamelets forming the turbulent flame.

Combustion in Kolmogorov–scale vortices

Many authors do not take the view that the turbulent flame is a wrinkled continuous or fragmented sheet which can be treated by laminar flamelets, but that reaction occurs in isolated, Kolmogorov–scale vortices (Chomiak, 1979). This picture of turbulent premixed combustion uses the concept that the smallest scales of the turbulent motions are confined to twisted elongated eddies (vortices) of one Kolmogorov scale η_K diameter, one large–eddy lengthscale L_{turb} long, and with the lengthscale characterising the twisting equal to one Taylor microscale λ. Reaction occurs *inside* the vortex and, by relating the small scales with the energy–containing motions of high–Reynolds number turbulent flows, this model has produced an expression for the time–mean reaction rate (Chomiak, 1979). Such ideas have also been used to predict the extinction of premixed flames and, for example, Radhakrishnan *et al.* (1981) proposed that the turbulent flame locally extinguishes when the time taken by a laminar flame front to travel between different segments of the small–scale vortex, λ/S_L, is smaller than that for the eddy to die out, as given by the large–eddy turnover time L_{turb}/q', where S_L is the laminar flame speed and q' the r.m.s. turbulent fluctuations. This model successfully predicted the extinction limits of bluff–body stabilised premixed flames by making assumptions about L_{turb} and q' suitable for a bluff–body recirculating flow.

Byggstøyl and Magnussen (1983) did not make particular reference to the exact spatial structure of the small–scale vortices, but assumed that reaction proceeds inside these vortices which were treated as well–stirred reactors. They calculated the volume

that these small–scale well–stirred reactors occupy inside turbulent flows and the mass and heat exchange between the reacting vortices with the non–reacting surroundings, and then postulated that extinction occurs when the reactant supply to the Kolmogorov–scale reactors is larger than the amount of reactants they can consume. The resulting expression for flame extinction requires calculation of the turbulent kinetic energy and its dissipation rate and can be incorporated into a turbulence model such as the k–ε model. In this way, Byggstøyl and Magnussen (1983) calculated the lift–off heights of jet diffusion flames by assuming that the jet diffusion flame, once lifted, propagates at its base as a premixed flame.

Lockwood and Megahed (1978) used a different picture of combustion in Kolmogorov–scale vortices: two vortices, one containing burnt and the other unburnt fluid, were assumed to touch; reaction in the unburnt vortex will occur only when a flame front can propagate into the unreacted vortex by ignition due to the burnt material. A special characteristic of this model is that the speed at which the flame propagates into the unburnt vortex depends on the vortex rotational speed, and the resulting expression for extinction compares the Kolmogorov lengthscale η_K with a lengthscale which depends on *both* the laminar flame speed and the turbulent kinetic energy dissipation rate and which reduces to the laminar flame thickness at the limit of zero turbulence. This flame extinction model has been incorporated in calculations using a k–ε turbulence model by Chakravarty *et al.* (1984) to predict the spatial locations in the flow where reaction is extinguished for jet diffusion, bluff–body premixed, and bluff–body diffusion flames, and the authors show good reproduction of the experimentally–observed extinction trends.

Both Byggstøyl and Magnussen (1983) and Lockwood and Megahed (1978) used a flame extinction model that was developed for *premixed* combustion to predict *diffusion* flame extinction with the justification that, because reaction occurs in the small–scale vortices where the reactants are uniformly mixed, the mode of reactant supply (i.e. whether premixed or initially separated) in the large scales becomes irrelevant. This is a gross simplification, however, because in diffusion flames the topology of reaction surfaces (which follow the diffusive layers between the fuel and air streams) is not necessarily the same as the topology of the Kolmogorov–scale vortices. It is necessary therefore to examine theories for flame extinction developed especially for initially separate reactants, both for flames that may be treated with flamelet concepts and for flames for which these are not applicable.

4.1.4 Extinction of turbulent diffusion flames

Flamelet flames

Peters (1983, 1984a) has developed a theory for turbulent diffusion flames in the flamelet regime and Peters and Williams (1983) applied it to predict the lift–off of jet

diffusion flames. There are three major elements in this theory. Firstly, the flame is assumed to be composed of laminar flamelets that are modelled as quasi-steady laminar combusting diffusion layers, and if these are of the boundary–layer type with concentration gradients being much larger in the direction normal to the layer than in the directions along it, the flamelet is characterised only by the local instantaneous value of the dissipation rate of the mixture fraction at the stoichiometric surface, χ_{st}, defined as

$$\chi_{st} = 2\, D_{mol} \left[\frac{\partial f}{\partial x_i}\right]^2_{st}, \qquad (4.1.1)$$

where f is the mixture fraction, D_{mol} is the molecular diffusion coefficient, and the subscript st denotes a quantity at $f=f_{st}$. These laminar diffusion flames will exist only for values of the scalar dissipation rate below a critical value corresponding to quenching conditions χ_q (also called χ_{lam} later in this Chapter) because, as Peters (1983) put it, "we may look at χ_{st} as the inverse of a characteristic diffusion time. If χ_{st} is large, heat will be conducted to both sides of the flamelets at a rate that is not balanced by the heat production due to chemical reaction. Thus the maximum temperature will decrease until the flamelet is quenched at a value of $\chi_{st}=\chi_q$."

The second ingredient of the turbulent diffusion flame extinction theory is to consider the statistical distribution of the scalar dissipation rate and to recognise that flamelets that experience a χ larger than χ_q will be quenched and therefore do not contribute to the overall heat release. The probability of a burning flamelet is then determined by the probability of the scalar dissipation rate conditioned on the stoichiometric value of the mixture fraction, and the percentage of burning flamelets decreases monotonically to zero because more flamelets experience $\chi > \chi_q$ as the mean turbulent scalar dissipation rate increases. Finally, the third element of the theory uses concepts from percolation theory to relate the probability of the burning flamelets to the overall, sudden extinction of the turbulent flame by postulating that the whole flame sheet will disappear if a critical portion of the laminar flamelets has been quenched. Peters and Williams (1983) made assumptions appropriate for mixing in a jet and found that the previous arguments can reduce to a comparison between the mean turbulent scalar dissipation rate at the mean stoichiometric mixture fraction $\tilde{\chi}_{st}$, and the quenching value χ_q. They applied this theory to predict successfully the lift–off heights of jet diffusion flames by assuming that lift–off is due to flame extinction at all locations from the nozzle to the flame initiation point.

In Section 4.3.4, this theory is used to correlate the measured extinction limits of the present turbulent counterflow diffusion flames, which fall in the flamelet regime as shown in Section 3.4.1, by using estimates of the mean turbulent scalar dissipation rate based on the mixing analysis of Section 3.2.5.

Non–flamelet flames

One of the assumptions behind Peters (1983) extinction argument, is that the turbulent flame can be described as an ensemble of laminar flamelets, but there are diffusion flames for which this assumption may not be appropriate. Bilger (1988, 1989) suggested that a turbulent diffusion flame can be described by a flamelet model if the width of the reaction in mixture fraction space, Δf_R, is smaller than a "scalar scale" Σ_f defined as $(\tilde{\chi}\,\tau_K)^{1/2}$ where $\tilde{\chi}$ is the mean turbulent scalar dissipation rate and τ_K the Kolmogorov timescale (Section 3.4.1). If this condition is satisfied, there is a large instantaneous difference of the mixture fraction across the reaction zone and then the reaction zone can be treated as a laminar–like flame characterised by the local value of the scalar dissipation rate. However, if this condition is violated, there are variations of the instantaneous χ across the reaction zone and then the flamelet cannot be characterised solely by χ_{st}. Flame extinction based on this flame structure, which Bilger (1988) called "distributed reaction zones", occurs when the value of χ averaged between the contours of f bracketing the reaction zone (i.e. where $f - \Delta f_R/2 < f_{st} < f + \Delta f_R/2$), exceeds a critical value. This regime of combustion is not expected in the present flames, as shown in Section 3.4.1, but note that, as in the flamelet theory of Peters (1983), the turbulent scalar dissipation rate has to be excessive for flame extinction.

4.1.5 Application of extinction theories: the lifted jet flame

The previous review showed that many different quantitative theories for the local extinction of turbulent premixed and diffusion flames have appeared in the literature and many of them have examined, as a test case, the situation of the lifted jet flame. In particular, predicting the height at which the flame is stabilised once lifted from the fuel nozzle has been one of the aims and, in this Section, the literature is reviewed to identify features of this flow that may preclude its use as a "benchmark" flame extinction phenomenon, contrary to current trends.

The major experimental phenomena were measured by Kalghatgi (1984) and have been reviewed by Pitts (1988) in conjunction with proposed theories to explain these: the lift–off height, H_{lift}, increases linearly with the jet velocity, is independent of the jet diameter, and is inversely proportional to the square of the maximum laminar flame speed of fuel–oxidiser mixtures. A physical mechanism for flame stabilisation away from the nozzle is that the flame at its base is premixed and propagates against the incoming reactants with a turbulent flame speed determined by local stoichiometry. Flame extinction does not occur at all in this view. Peters and Williams (1983), on the other hand, considered that the flame is lifted because localised extinctions arise from high values of the scalar dissipation rate, and that the stabilisation height is the point where $\tilde{\chi}_{st}$ has fallen below the value that causes extinction. Because one of the issues

of debate between the different "schools" of thought is whether the lifted flame is premixed or not, Peters (1984b) amended the original proposal and also considered quenching of *partially premixed* flamelets since some premixing is bound to occur before the flame initiation point. Lockwood and Megahed (1978) and Byggstøyl and Magnussen (1983) used their extinction models to predict the lift–off heights and both concluded that their model was adequate to capture the basic extinction trends, and that lift–off was explained by localised extinctions. More recently, Bradley *et al.* (1990) used a flamelet model that included flamelet quenching incorporated in a full numerical calculation and concluded that flame lift–off cannot be explained by any of the previous simplified descriptions, but is the outcome of a "complex interplay of convection, diffusion, and heat release rate". Finally, an alternative view was provided by Broadwell *et al.* (1984), Dahm and Dibble (1988), Miake–Lye and Hammer (1988), and Dahm and Mayman (1990) who predicted lift–off and blow–out of jet diffusion flames by assuming that combustion occurs inside the large–scale structures of the jet with extinction occurring when a large–eddy timescale is shorter than a chemical timescale; success is claimed, but it is difficult to see how this view can be generalised into a local extinction theory that may be used in other than jet flames.

It is evident that there are many complications arising from interpreting the lift–off of jet diffusion flames and that no clear physical explanation exists yet. A theory that predicts lift–off heights would not necessarily represent the extinction limits in other flames because lift–off might not be associated with extinction. It is also clear that partial premixing occurs, and that this is being recognised now as a feature of many flows in which oxygen penetrates the flame at upstream locations due to large strain rates or localised quenching, hence resulting in fuel and oxygen being mixed before combustion takes place at downstream locations.

4.1.6 Localised extinction: the piloted jet diffusion flame of Masri *et al.* (1990)

The simultaneous measurement of the concentration of stable species and of short–lived radicals like OH and of the temperature in jet diffusion flames stabilised by a strong pilot flame at the nozzle exit has been attempted by pulsed Raman and Rayleigh scattering and laser–induced fluorescence (e.g., Masri *et al.*, 1990; Barlow *et al.*, 1990). The flow was designed so as to have high scalar dissipation rates with resulting localised extinctions, yet to provide overall stability by using a pilot flame. The joint probability density functions of reactive scalars and temperature have shown that fluid particles were quenched, as diagnosed by high probability of reactive composition and low temperature, at about 20 jet diameters where the effect of the pilot became weak. The possibility of quenching increased with jet velocity and turbulence levels and decreased with distance from the jet and, at downstream locations where the dissipation rate was smaller, the flame re–ignited by hot "pockets" of reaction products. This work

has provided detailed measurements against which computational models of turbulent combustion can be tested (for example, Masri and Pope, 1990), and has provided insight as to the structure of diffusion flames approaching extinction for flames within and outside the flamelet regime. The presence of the pilot flame, however, means that global extinction of the flame is complicated and cannot be predicted unless the effect of the pilot flame itself is adequately modelled. In the present work, the counterflow geometry is provided as an alternative in which to study the extinction limits of turbulent flames in a more straightforward way.

4.1.7 The turbulent counterflow premixed flames of Kostiuk *et al.* (1989)

Turbulent counterflow flames, as used in this thesis, have been examined by Kostiuk *et al.* (1989), who considered the stagnating flow of two turbulent impinging jets of premixed reactants such that two identical turbulent premixed flames were stabilised around the stagnation plane. This experiment was the turbulent equivalent of laminar counterflow twin (also referred to as "back–to–back") flames and the results showed that both the bulk stretching, identified by the jet velocity divided by the jet separation, and the turbulent stretching, identified by the inverse of the Kolmogorov timescale, could lead to global, sudden extinction of the flame. In particular, Kostiuk *et al.* (1989) were able to correlate, approximately, the measured extinction limits of these flames by considering the magnitude of the *total* strain rate (bulk plus small–scale turbulent) and this provided a useful way to incorporate both effects in a single concept. The extinction of these flames has been predicted successfully by Bray *et al.* (1991) who used a turbulence closure and the Bray–Moss–Libby model of turbulent combustion and found that extinction occurred when a Damköhler number became low and, at the same time, the mean concentration of product between the two flames approached zero.

4.1.8 Present contribution

The advantages that the turbulent counterflow flames offer for flame studies have been highlighted in Chapter 1; for extinction in particular, they are useful because the stretch rate is uniform and so the direct effect of the stretch rate on the flame can be examined without any complicating effects due to earlier quenching and re–ignition or to the stabilising action of pilot flames.

In this Chapter, measurements of the extinction limits of the premixed and diffusion flames described in Chapter 3 are provided. In particular, the extinction studies of Kostiuk *et al.* (1989) are extended to the case of *single premixed* flames, i.e. flames stabilised with one reactant stream impinging on an inert stream, and for these the extinction limits are measured in terms of the bulk and turbulent stretching and as a function of opposed stream temperatures to quantify the effect of post–flame heat loss on stability. Flames stabilised against a stream of hot combustion products (flames also

referred to as "unburnt–to–burnt") are also examined because theoretical analyses of their extinction predict a widening in their flammability limits, but so far without experimental verification.

Emphasis is put on the extinction of *diffusion* flames, stabilised in the impingement region of a fuel and an oxidiser turbulent stream, and the – not well–studied for turbulent flames – case of fuel partially premixed with air, and thus the extinction of the whole spectrum of flames from pure diffusion, through partially premixed, to premixed is examined. Estimates of the scalar dissipation rate at the extinction of turbulent diffusion flames are made since it was shown in this Section that this quantity determines flame extinction, and it will be concluded that extinction occurs at a critical value of the scalar dissipation rate. Finally, the extinction limits for diffusion flames using air diluted by hot combustion products are measured motivated by the importance of hot exhaust gas recirculation in many combustion applications.

4.2 EXPERIMENTAL METHODS

4.2.1 Flow configuration

The turbulent flames described here were stabilised in the opposed jet burner described in Section 2.1.1 (see Fig. 2.1). This burner comprises two identical straight pipes of inner diameter D=25.4mm fitted with perforated plates with solidity 45% and hole diameter of 4mm, and both upper and lower pipes were surrounded by tubes of 51.8mm inside diameter that carried nitrogen to shield the inner flows from entraining ambient air and thus to limit reaction to the impinging region between the two jets. The turbulence intensity was determined by the distance H_p of the perforated plate from the tube exit plane; for large distances, the turbulence was less than for small distances because turbulence was given time to decay (Fig. 3.2.4). The reactant composition could be varied in both streams from pure fuel to pure air and the flow rates were metered by rotameters calibrated by the manufacturer.

Turbulent flames with vitiated air (i.e. air mixed with hot combustion products) were stabilised in the burner shown in Fig. 2.3a. The lower assembly was identical to that used for the unheated, undiluted flames, but, to provide a flow of hot products, a second perforated plate on which a laminar, "supply" flame was ignited was fitted inside the upper tube 40D upstream of the jet exit. In a slightly different configuration (Fig. 2.3b), the laminar flame was ignited on the perforated plate in the upper tube previously used to promote turbulence so that the distance from the supply flame to the stagnation plane was small (in the range 2 to 10D), and this configuration achieved larger temperatures of the hot product stream but less flexibility in the oxygen concentration.

Finally, laminar flames were stabilised in the opposed well–contoured nozzle burner (Fig. 2.2) to find extinction limits of pure and partially premixed laminar diffusion flames in order to compare with the measurements in the turbulent flames.

4.2.2 Determination of extinction points

Cold reactants, diffusion flames

The extinction limits were defined by the sudden loss of the whole flame, which always coincided with loss of flame at the centerline, and they were measured by keeping the two jets at a fixed distance, establishing equal velocities in each pipe, igniting the flame with a torch at a low velocity to obtain a stable flame, and increasing simultaneously the velocities of the two opposed flows in steps of 0.05 m/s. For partially premixed diffusion flames, the air flow in the fuel stream was kept constant and the fuel and upper air flow rates were increased, allowing hence the simultaneous decrease of the air volume fraction of the fuel stream, and the extinction velocity was then determined for each jet separation as a function of air premixedness. For most

experiments, the velocities of the two jets were kept equal, rather than the momentum, and the asymmetry in the resulting flowfield was largest for unpremixed flames because then the difference in density between the two jet fluids was the largest, but it was found that the extinction velocity, when the velocities were kept equal, was very close to the air velocity at extinction when the momenta were kept the same. The reported extinction velocity is an average of 5 measurements with an estimated uncertainty at about ±10% and at about ±7.5% for the air volume fraction.

Cold reactants, premixed flames

Single premixed flames were stabilised in the impingement region of a fuel–air premixed jet and an opposing jet of air, and the extinction limits of these flames were found by igniting the flame at stable conditions and then reducing the equivalence ratio in steps of about 0.03 until the flame was extinguished, resulting in a repeatability within the metering error. The extinction limits of twin premixed flames, which were stabilised when both opposed streams were premixed at the same equivalence ratio, were measured by decreasing simultaneously the equivalence ratio of both flames until extinction; because this involved metering errors from the *two* natural gas flowmeters metering, independently, the flows in the two jets, the repeatability was slightly worse than for single flames. However, it was found that this method gave more reliable results than the method used by Kostiuk *et al.* (1989) who reduced the jet separation while keeping the equivalence ratio and velocity constant, and was therefore preferred. The estimated uncertainty in the extinction velocity is about ±5% and in the equivalence ratio about ±0.03 corresponding to the flow metering uncertainties.

Electrically heated reactants

Diffusion flames with electrically heated reactants were stabilised in the straight–pipe burner after allowing about 30 minutes for the metal to reach thermal equilibrium and the extinction limits of these flames were measured by reducing the air mixture fraction, while keeping the velocity of each jet constant and the two jet momenta equal. This method was selected based on the experience of extinction of flames with cold reactants so that the parameter to which extinction was most sensitive was altered. The uncertainty in the reported velocity is about ±10% and ±7.5% for the air volume fraction.

Reactants diluted by hot products

When the laminar, "supply" flame was operating in the burner of Fig. 2.3a, a flow of hot products and separately metered oxygen and nitrogen comprised the upper stream. The parameters at the experimenter's disposal were the composition of the lower stream and the relative flow rates of the O_2 and N_2 added to the hot products in the upper stream with the laminar flame being stable in the range of equivalence ratios between 0.6

to 0.75 before it extinguished or exhibited combustion–driven oscillations. It was found that the extinction of counterflow diffusion flames was most sensitive to the oxygen content and then the extinction limit was measured by selecting a jet separation, fuel stream premixedness and velocity, upper "supply" flame equivalence ratio, and N_2 and O_2 flow rates such that the resulting mixture momentum at the upper tube exit was equal to the lower stream, and then decreasing the oxygen supply while simultaneously increasing the nitrogen's flow rate keeping the sum constant. When the "supply" flame was located close to the tube exit (Fig. 2.3b), the distance from the exit plane and the equivalence ratio determined the temperature and the oxygen concentration, and for these experiments, the equivalence ratio of the "supply" flame was decreased so as to reduce the temperature until extinction of the stagnation point flame was observed (see below for the associated errors). The oxygen content was calculated from the flow rates of the reactants to the "supply" flame and of any extra oxygen or nitrogen added and complete combustion was confirmed by the negligible measured concentrations of CO and unburnt hydrocarbons at the exit plane of the upper burner. Details of the oxygen mole fraction calculation are presented in Appendix 2.1.

The uncertainties involved in these measurements are larger than in the experiments with cold reactants because the velocity, oxygen concentration, and temperature of the upper stream change simultaneously with variations of the flow rates, and because it was not easy to keep the momentum flow rates between the two jets equal *both* for a stable flame *and* for conditions corresponding to an extinguished flame. These errors were minimised, and the repeatability was improved, by taking extra care to first locate the extinction limit, igniting the flame as close as possible to extinction, and then changing the parameter that gave the largest sensitivity. It is estimated that the reported value of oxygen mole fraction is accurate to within ±10%, the bulk velocity of the bottom stream to within ±5%, the bulk velocity of the upper stream ±10% (because it is estimated from the flow rates of the reactants when cold and the centreline measured temperature, which, in addition to the measurement uncertainty, was not uniform across the upper pipe), and the air volume fraction and equivalence ratio of the bottom stream as in the other experiments. The uncertainty in metering the equivalence ratio of the "supply" flame was about ±0.02.

Flames with fuels other than natural gas

A few measurements were made of the extinction of turbulent counterflow flames of natural gas mixed with hydrogen which were stabilised in the straight pipe burner (Fig. 2.1) and the extinction limits were determined by igniting a stable flame and then reducing the hydrogen content until extinction was observed. The estimated uncertainty in the reported value of the hydrogen mole fraction in the H_2 / natural gas mixture is ±5%.

4.3 RESULTS

Results on the extinction of premixed and diffusion turbulent counterflow flames are presented in this Section. As discussed in Section 2.2, flames are deemed "premixed" if the air volume fraction in the fuel stream was higher than the rich limit of laminar flame propagation (X_{air}>0.86), "diffusion" if X_{air}<0.86, and the term "pure diffusion" is reserved for flames without partial premixing. The symbol X_{air} is used in this Chapter, rather than X as in the rest of the thesis, to avoid possible confusion with the oxygen mole fraction in the air stream, X_{ox}. Unless otherwise stated, the flames were established in the straight pipe burner without any preheat or dilution by inerts, and the extinction velocities correspond to the bulk velocity of the flow leaving the pipes and were calculated from the metered flow rates.

Results for premixed flames are presented for single and twin flames, and for single premixed flames stabilised against hot products of varying temperature. For diffusion flames, results on the extinction velocity of pure and partially premixed flames are given as a function of premixedness with the jet separation as parameter and *vice versa*, with the turbulence intensity as parameter, and for the minimum oxygen requirement in the air stream, X_{ox}, as a function of the fuel stream premixedness and as a function of the air stream temperature. The results with cold and undiluted reactants are correlated by two different concepts of extinction and compared with laminar flames. Finally, the implications of these results for the stability of turbulent premixed and diffusion flames in other geometries are discussed in the respective Sections.

4.3.1 General observations

The extinction of the present flames was sudden, with the whole flame disappearing when any of the parameters that cause extinction, for example the bulk velocity, exceeded a critical value. Similar observations were made for the extinction of laminar flames, and for the extinction of twin turbulent premixed flames by Kostiuk *et al.* (1989). The extinction of counterflow flames was therefore easy to observe and avoided the complexities associated with, for example, flame lifting from a stabilisation point as in jet diffusion flames. The velocity of the nitrogen co–flow was greater than 0.5m/s because at smaller velocities, and only for diffusion flames with small premixing, it was found that the unburnt fuel would form a large, buoyant flame outside the burner and this sometimes resulted in large–scale buoyant motions that would extinguish the flame. No such effects were observed with a co–flow larger than 0.5m/s and this value was kept for all experiments.

It was observed during temperature measurements in diffusion flames that the presence of the thermocouple at the *centreline* would induce extinction at a velocity

smaller by a few percent than when the thermocouple was absent, possibly due to the introduction of extra strain rates associated with the wakes of the thermocouple posts. The region of this influence was limited to a radius of about 2–3mm; at larger radii, no effect on the extinction limit was observed. Similarly, when the sampling probe for the species measurements was at the centreline, extinction would occur at a smaller bulk velocity than with the probe absent but, as with the thermocouple, no influence on the extinction limits was observed when the probe was at radii larger than about 5mm. These observations suggest that the centreline region is most important for the stability of counterflow flames and that distortions of the flow there affect the stability of the whole flame. A similar conclusion was reached by Kostiuk (1990; personal communication) in twin premixed flames by observing in a high-speed video that the whole flame disappeared very quickly after the centreline region had been quenched, and these observations imply that the stability of the whole flame depends critically on the stability of the flame at the centreline. In view of the radial uniformity of the flame with the velocity gradients, turbulences, temperatures, and compositions varying only in the axial direction, the result that the whole flame extinguished when the centreline region was extinguished is welcome because it highlights that extinction in the counterflow flames is localised, but has a global manifestation, or, conversely, because inferences about the occurrence of localised extinctions at the centreline can be made by observing the existence of the whole flame.

4.3.2 Premixed flames

Single and twin flames

The extinction limits of single and twin turbulent premixed flames with reactants at room temperature are presented here. The fuel was natural gas, ambient air was used, and the flow rates of the two jets were kept equal.

The extinction velocity of a *single* turbulent counterflow flame peaks at about stoichiometric equivalence ratio and decreases as the flame becomes leaner or richer than stoichiometric (Fig. 4.1), as expected, and it increases with jet separation (Fig. 4.1a) and decreased with increasing turbulence intensity (Fig. 4.1b). These trends are consistent with the results of Kostiuk *et al.* (1989) for *twin* premixed flames and suggest that the present single flames extinguish due to the combined action of bulk and turbulent stretching, as the twin premixed flames. The results are qualitatively consistent with a view that the flame extinguishes at small values of a Damköhler number, which decreases in flows with intense turbulence or with departures from stoichiometric mixtures (Bray *et al.*, 1991).

Figure 4.1a also includes some measurements of twin flames stabilised in the same burner as the single flames and it is evident that the twin flames extinguish at larger velocities than the single flames at lean and stoichiometric conditions, but this is

eventually reversed at rich equivalence ratios with the single flames extinguishing at higher velocities than the twin flames. Lean single flames extinguish earlier than twin flames possibly because the cold counterflowing air in the single premixed flames extracts thermal energy and causes extinction, while each of the two twin flames provides heat for the stabilisation of the other. It seems possible that the temperature of the opposing jet for single premixed counterflow flames has an effect on their extinction limits and this is examined next.

Heated opposed stream

The extinction of single counterflow premixed flames stabilised in the "vitiated air burner" (Fig. 2.3) where the bottom stream that carried the reactants was identical to that of the straight pipe burner, is examined here. Results are presented in terms of the equivalence ratio of the lower mixture ϕ_1, the centerline temperature of the upper stream T_2, the equivalence ratio of the laminar "supply" flame inside the upper tube ϕ_2 whose products opposed the lower, reactants, stream at velocity U_1. For all experiments, the momenta of the two jets were equal such that $\rho_1 U_1^2 = \rho_2 U_2^2$ with $\rho_1 \approx \rho_{air}$ because the mixtures were lean and with ρ_2 calculated from the measured temperature.

Figure 4.2 shows that the leanest equivalence ratio necessary for a premixed flame to exist at a given bulk velocity decreases slightly as the opposed stream temperature T_2 increases from room temperature up to 1400K. Below this temperature, the flames were ignited by a torch and their extinction was sudden and brought about by gradually decreasing the equivalence ratio ϕ_1; the opposed stream was composed of reaction products with an oxygen content between $0.02<X_{ox}<0.10$, but the measurements can be compared without reference to the opposed stream oxygen content because the flames were lean premixed and the top stream fluid did not participate in combustion (Fig. 3.3.3)[1]. The bulk and turbulent stretching that these flames experienced are expected to be similar to those with unheated opposed streams because the flow rates were adjusted such that $\rho_1 U_1^2 = \rho_2 U_2^2$ and so the bulk stretch rate in the cold, reactant stream was approximately equal to $2U_1/H$, and because the turbulence on the reactant side of the flame was determined by the approach flow; therefore the stretching on the flames shown in Fig. 4.2 depended only on U_1 and was independent of T_2. Increasing T_2 probably reduces the temperature gradient from the flame to the opposing stream and thus the heat loss from the reaction zone and, therefore, the results in Fig. 4.2 show that the effect on flame stability is not large, but in the expected direction, i.e. increasing T_2 up to 1400K helps stability, albeit slightly.

For T_2 between 1450 and 1550 K and $\phi_1>0.45$, the effect on the flame is much larger, for the flame would intermittently *ignite without* an external source in "patches" of

[1] The oxygen content of the hot product stream was calculated in the manner described in Appendix 2.1.

luminous and non–luminous areas, possibly due to fluctuations of temperature and strain rate that made conditions locally and instantaneously favourable for ignition. In this temperature range, the ignition equivalence ratio, ϕ_{ign}, was determined by increasing ϕ_1 from zero to the value when "patchy" ignition first occurred, and it was found that ϕ_{ign} increased with bulk velocity and with decreasing temperature. For equivalence ratios leaner than about 0.45, no flame and no intermittent ignition was observed in this temperature range.

At opposed stream temperatures higher than about 1550K, it was observed that the flame ignited steadily without any external source as soon as the mixture was formed in the bottom stream. *No extinction* was observed for ϕ_1 as low as 0.2, which corresponded to the minimum measurable fuel flow rate. Lean flames were visible, with luminosity increasing with T_2 and ϕ_1 in the range $0.2 < \phi_1 < 0.7$ and for bulk velocities up to U_1=3.5m/s, and these ultra–lean flames were thinner and less luminous than the stable and vigorous premixed flames with $\phi_1 > 0.7$. The oxygen content of the top hot product stream was determined by the equivalence ratio of the laminar "supply" flame in the range $0.6 < \phi_2 < 0.75$ and it was found that X_{ox} did not affect the extinction of lean premixed flames, as expected, with the temperature T_2 being the major parameter that affected the transition from sudden extinction to no–extinction.

The observation that ultra–lean premixed flames could exist at high temperatures of the opposing top stream is interesting because it shows that chemical reaction can proceed at seemingly very lean conditions in the presence of a high temperature region and deserves more attention in view of the relevance of lean combustion to practice (Weinberg, 1986). Results on the structure of these flames follow next.

Structure of ultra–lean counterflow premixed flames

Here, some details on the temperature, mean species compositions, and velocity fields of the mixing layer formed in the opposed jet flow between air and hot products are presented and the difference that a small amount of methane in the air jet, thus sustaining an ultra–lean visible flame, makes to the mixing layer is examined. The reaction location is emphasised and a conjecture as to why ultra–lean flames can exist is given.

Figure 4.3 shows that the mean temperature in the inert opposed jet mixing flow between hot products at 1700K and cold air follows a profile like an error function and that there are finite fluctuations. In Fig. 4.3 the temperature is normalised so that it is zero in the cold stream and unity in the other and the mean temperature measurements in this opposed jet flow are similar to those in opposed jets with a smaller (T_2–T_1) at about 150K (Section 3.2.6), such that the temperature acted like a passive scalar. Figure 4.4 shows that the probability density functions of the temperature at different axial locations

across the mixing layer are bimodal, as in Chapter 3, but with finite probability of intermediate temperatures, probably due to the high molecular thermal conductivity caused by the high temperatures. Figure 4.5 shows that the temperature fluctuations have a frequency spectrum without any low frequency peak and with a roll–off at about 10Hz following a decay with a slope of approximately –5/3 which then becomes steeper after about 100Hz. Such spectra are typical of "well–behaved" turbulent flows and therefore any suspicions of strong buoyancy effects, instabilities of the mixing layer, or instabilities of the "supply" flame, are without foundation. Finally, the mean axial velocity along the centerline, Fig. 4.6a, shows the expected trend with the stagnation point lying half–way between the two nozzles and r.m.s. velocities (Fig. 4.6b) similar to those in isothermal jets (Section 3.2.4), with the exception of the turbulence at the hot product stream which, although of equal numerical value to that at the bottom stream, is a much smaller fraction of the bulk velocity there and therefore the hot product flow is of low turbulence; recall that these flows were realised in the burner shown in Fig. 2.3b without a turbulence–promoting perforated plate in the top tube.

Ultra–lean flames involve very small heat releases (see below) and it is hence expected that the presence of the flame would not change the velocity field. The amount of bulk stretching that counterflow flames experience is described by the velocity gradient and Fig. 4.6a shows that the axial velocity gradient is larger in the hot stream than in the cold stream, in agreement with the calculations of Kim and Williams (1990) for a similar laminar flow, and thus the stretch rate on a flame would depend on the flame location. Vigorous, propagating flames with a high equivalence ratio burn inside the reactant (lower) stream (Fig. 3.3.3), but evidence presented below shows that ultra–lean flames, which are not self–sustaining, are located inside the hot product stream, and therefore are expected to experience a *bulk* stretch rate higher than $2\ U_1/H$, which is a measure of the bulk strain rate in the cold stream. It is difficult to estimate the *turbulent* stretch rate on these lean flames because, even with the turbulent intensities of Fig. 4.6b, the absence of a turbulence–promoting perforated plate in the hot product stream does not allow a reasonable estimate of the turbulence lengthscale; however, in view of the experimental observation and theoretical expectation that the existence of these ultra–lean flames is a very strong function of the hot stream temperature with the strain rate playing a minor role, the turbulent stretch rate may not be treated in detail.

When the bottom tube carried an ultra–lean mixture of ϕ_1=0.3 that resulted in a luminous flame, Figs. 4.7 and 4.8 show respectively that the mean temperature and concentrations of O_2 and CO_2 in the reacting flow were almost indistinguishable from those with inert flow of air against hot products. Although the flame was clearly visible at this equivalence ratio, it did not result in enough heat release to increase the temperature and did not generate enough CO_2 to be distinguished from the inert opposed jet flow to within experimental error. However, these lean premixed flames produced

measurable quantities of CO, Fig. 4.9, and visual observations confirmed that the peak concentration of CO across the mixing layer was located at the position of the luminous zone. Figures 4.9a and 4.9b show respectively that the CO mole fraction increases with the equivalence ratio of the reactant stream and with the temperature of the hot product opposed stream, and Fig. 4.10 shows that the maximum CO mole fraction across the flame (found from the peak in profiles as in Fig. 4.9) approaches zero as T_2 approaches 1400K; these trends are consistent with the observation that the luminosity of the flame increased with equivalence ratio and increasing temperature.

Figure 4.11 shows that the maximum CO corresponds to a local temperature above 1500K, as found by plotting the CO concentration against the measured mean temperature (i.e. cross–plotting the data of Figs. 4.7 and 4.9), and therefore the mean luminous zone was located in the high–temperature region *inside* the hot product stream. This is an important observation and it implies that the reaction of the flammable mixture from the lower jet occurs *only* when mixed with the hot products from the upper jet and that the local equivalence ratio where the reaction occurs is even smaller than that of the supplied mixture. The present result agrees with the discussion by Law (1988) that counterflow laminar premixed flames when burning against hot products can "migrate across the stagnation surface and thereby assume a negative flame speed. Combustion in this situation is supported by diffusion of the reactants against the unfavourable convection", and here Law's statement is extended to turbulent flames. The ultra–lean flames did not exist with opposing streams with temperatures *less* than 1500K and are to be contrasted with premixed flames at richer equivalence ratios. Self–sustaining flames are stabilised at the axial location where the mean flow velocity is equal to their propagation speed; ultra–lean flames, however, cannot propagate into cold reactants because the mixture is so lean that it cannot generate enough heat release (Weinberg, 1986) and hence ultra–lean flames *require* the high temperature of the opposing stream for their existence. Thus partial conversion of fuel will locally occur even under ultra–lean conditions provided that the mixture achieves temperatures above about 1500K, qualitatively emphasised also by Weinberg (1986) in his discussion of burner designs for lean combustion. It is not surprising that such flames do not show abrupt extinction (Fig. 4.2) because the presence of the hot products, if at sufficiently high temperature, ensures that chemical reaction will take place resulting in a luminous zone.

Discussion and comparison with laminar flames

The single counterflow flames stabilised against cold air streams extinguish with a combination of bulk and turbulent stretch rates, as the twin premixed flames of Kostiuk *et al.* (1989), and this observation confirms that the extinction of these flames depends on a Damköhler number (Bray *et al.*, 1991). However, the single flames extinguish

earlier than the twin flames, which suggests that each flame "helps" the other and that, in the single–flame configuration, the post–flame heat loss is important for reducing stability. When the opposed stream comprises adiabatic hot reaction products, it was observed that flames with ultra–lean equivalence ratios, or equivalently, small Damköhler numbers, were visible when the hot products had temperatures in excess of about 1550K.

The latter observation is consistent with that of Smooke *et al.* (1990) and the predictions of Libby and Williams (1983) that *laminar* counterflow premixed flames of methane formed against a fully–burnt hot product stream would never extinguish due to strain when the temperature of the opposing hot stream was high, and confirm the prediction of Bray *et al.* (1991) that the same is true for *turbulent* counterflow premixed flames. It is evident that there is a drastic change in the behaviour of the flame extinction for T_2>1550K, and laminar flame studies have identified this temperature with the transition of a non–monotonic to a monotonic gradual decrease of the heat release rate with decreasing Damköhler number (i.e. the classic S–shaped curve is replaced at high opposed stream temperatures by a monotonic curve that does not show the "catastrophic" reduction with decreasing Da; Libby and Williams, 1983; Darabiha *et al.*, 1988)[2].

There is, therefore, a large widening of flammability limits when the opposed stream temperature is high. Quantitatively, this happened when the hot product temperature was above 1550K in this work and above 1500K in Smooke *et al.* (1990), and a related observation is that the luminous zone of ultra–lean flames was located at the spatial location with a mean temperature higher than about 1500K. Gover *et al.* (1992) found that methane–air lean combustion cannot occur in heat–recirculating burners when the final flame temperature fell below 1550K for a range of equivalence ratios and heat–recirculation rates, while Yamaoka and Tsuji (1988) found that nitrogen–diluted lean premixed flames all extinguish at a limiting flame temperature of about 1400K. These observations are consistent with the view of Dixon–Lewis (1990) that extinction of the flame will occur when the system fails to become chain–branching, i.e. the net rate of radical production fails to become positive, a phenomenon which occurs at a well–defined "ignition" temperature. The present results and those mentioned above suggest that this temperature is about 1500 ±100K for methane–air premixed combustion. It is also interesting to compare this limit–flame value with that obtained for the extinction of *diffusion* methane–air flames: Tsuji (1982) quotes a value of 1480K and Puri and Seshadri (1986) found 1595K, both values similar to the limit–flame temperature for premixed flames. Also, Mauß *et al.* (1990) reported detailed time–dependant calculations *through* the extinction process and found that as a laminar diffusion flamelet extinguished

[2] In the present experiments, the strain rate could not be increased very much because of limitations in the supply; therefore Da was made very small by making the mixture ultra–lean.

after applying a high strain rate, it might re–ignite if the temperature had not fallen (by diffusion) below *ca.* 1600K.

This "universality" of a limit reaction zone temperature of about 1500K suggests that the concept of an "ignition" temperature is valid for both diffusion and premixed flames. As mentioned in the previous paragraph, Dixon–Lewis (1990) suggested that failure to achieve chain–branching in the air–hydrocarbon chemical mechanism is responsible for extinction, and that this occurs at a specific temperature, and the same conclusion was drawn from examination of reduced reaction mechanisms without resort to complete kinetic descriptions (Bilger, 1993; Peters, 1993b). An example of a reduced mechanism for methane is

$$CH_4 + 2H + H_2O \Leftrightarrow CO + 4H_2 \qquad \text{(I)},$$
$$CO + H_2O \Leftrightarrow CO_2 + H_2 \qquad \text{(II)},$$
$$H + H + M \Leftrightarrow H_2 + M \qquad \text{(III), and}$$
$$O_2 + 3H_2 \Leftrightarrow 2H_2O + 2H \qquad \text{(IV)}$$

(Yang and Seshadri, 1992), and the competition between the chain–terminating reaction (I) and the chain–branching reaction (IV) determines the overall rate of the reaction in the flame (Bilger, 1993). Reaction (IV) dominates only above a certain temperature, and so extinction will occur when the temperature falls below some "ignition" temperature.

The ultra–lean flames discussed here and in the heat–recirculating burners of Gover *et al.* (1992) attain the "ignition" temperature with the help of heat sources *outside* the reaction zone (the hot product stream and the rise in the initial reactant temperature respectively), while in a "normal" self-sustaining flame, the "ignition" temperature is achieved by back–diffusion of heat produced by the reaction zone itself. This puts a more stringent requirement on the amount of heat released from the reaction and so the equivalence ratio of a self–sustaining flame needs to be higher than the equivalence ratio of flames "helped" by outside agents. This perhaps provides a physical justification for the theoretical prediction that reaction at small Damköhler numbers can occur if the post–flame gases are adiabatic, or close to adiabatic, products of combustion (Libby and Williams, 1983).

These ideas are now applied to the stability of a more practically–important flame in a qualitative manner. A model for the stabilisation mechanism of turbulent premixed flames stabilised by recirculation zones is that the hot products inside the recirculation zone ignite the incoming reactants (e.g. Zukoski and Marble, 1956) and, in view of the previous discussion, all that is necessary for the reaction to proceed is to bring the reactants to a minimum "ignition" temperature. Therefore reaction is ensured if the recirculation zone temperature is high; because the hot products in the recirculation zone are created by the flame itself, they will not be hot enough if the equivalence ratio of the

mixture is low, and thus the ultra–lean flames of the type observed in the present work, that have a very small heat release, could not have been stabilised in a recirculation zone.

In the light of the previous discussion that hot products in the post–flame region help a single premixed flame exist at ultra–lean conditions, questions arise as to why *twin* flames extinguish at all, because no sudden extinction should be observed since in this configuration the post–flame region always comprises hot products. This apparent conflict is resolved by considering the theoretical prediction of Bray *et al.* (1991) and the results in Chapter 3 (Figs. 3.3.4, 3.3.33, and 3.3.38), which showed that the twin flames come close to each other at large strain rates thereby reducing the size of the region containing hot products and consistent with the suggestion by Law (1988), and the recent experimental verification by Sung and Law (1993), that *laminar* twin methane–air lean premixed flames in this configuration *touch* at large strain rates. Thus, approaching extinction, the reaction becomes incomplete which decreases the temperature of the hot product region (Sato, 1982; Yamaoka and Tsuji, 1988), and if the latter falls below the critical value of around 1500K necessary to ensure combustion, the flames extinguish. This explanation is also appropriate for *rich* methane–air flames, which have Lewis number smaller than unity and so can extinguish by straining alone without the requirement that the flames touch, because the temperature of the flame products falls with strain rate even as the flames are away from the stagnation plane (Law, 1988; Sato, 1982).

The premixed flames discussed in this Section were stabilised when a premixed stream impinges on a cold stream of air, hot products, or an identical reactant stream, and it was found that the reaction ceased depending on the bulk and turbulent stretch rate and on the temperature of the gases in the post–flame region. It was also found that reaction will always occur if the local temperature is high, regardless of the reactant concentration. The extinction of diffusion flames in the counterflow geometry is examined next and the important physical difference between counterflow premixed and diffusion flames is that fluid from the upper stream is required for combustion in the diffusion flames, unlike the case of premixed flames. The fact that mixing between fuel and oxidiser is necessary before combustion has resulted in different theoretical treatments of flame extinction, as discussed in Section 4.1.

4.3.3 Diffusion flames

In this Section, measurements of the extinction limits of pure and partially premixed turbulent diffusion counterflow flames are presented with discussion to follow in Section 4.3.4 after these measurements are analysed.

Figure 4.12 shows that the velocity at extinction increases with tube separation for air volume fractions in the fuel stream (X_{air}) of 0.0, 0.5, and 0.8 and also that initial

premixing of the fuel stream with air makes the flame more strain-resistant. The former trend suggests that the bulk flow stretch rate, which is proportional to the bulk flow velocity and inversely proportional to the nozzle separation, affects the extinction of the flame since at small nozzle separations a smaller velocity is required for extinction. The trend that partial premixing stabilises the flame is demonstrated in more detail in Fig. 4.13 which shows that the velocity at extinction for flames with separation of 20 and 25mm increases by a factor of about 1.8 with initial air premixedness from X_{air} of zero to 0.8, and this result is typical for all separations. Figure 4.13 also includes data (open circles) for premixing corresponding to equivalence ratios higher that the rich limit for premixed flame propagation (ϕ_1=1.6 or X_{air}=0.86), and it is evident that there is a smooth continuation of the extinction limit from diffusion to premixed flames, with the pure diffusion flame exhibiting the least resistance to stretch and the stoichiometric premixed the strongest.

The effect of the turbulence intensity on the extinction of the counterflow non–premixed flame is apparent from Fig. 4.14, which shows that a decrease in the normalised turbulence intensity q' / U by a factor of about two, brought about by increasing the distance of the perforated plate from the tube exit (Fig. 3.2.4), results in an increase in the bulk extinction velocity for the same tube separation. This result is consistent with the expectation that the higher strain rates due to higher turbulence lead to flame extinction and shows that it is not the bulk flow stretch rate *alone* that causes extinction since, if that were the case, the extinction velocity would be a function only of the tube separation.

It was mentioned in Section 4.1.6 that Kostiuk *et al.* (1989) showed that the extinction limits of turbulent counterflow *premixed* flames could be correlated in terms of a phenomenological criterion based on the total stretch rate (bulk plus small–scale turbulent). This provided a way to combine the observations that both the bulk and the turbulent stretching led to extinction, and in the next Section this concept is extended to *diffusion* flames based on the present data.

4.3.4 Discussion and correlations of the extinction of diffusion flames

Correlation in terms of total strain rate

The dependence of the extinction velocity on tube separation for the same normalised turbulence intensity (Fig. 4.12) and on turbulence intensity for the same tube separation (Fig. 4.14) suggest that the bulk and the turbulent strain rate affects extinction. Hence, following Kostiuk *et al.* (1989), the nominal total strain rate acting on the flame is estimated as the sum of the bulk flow stretch rate

$$S_{bulk} = \frac{2\,U}{H} \qquad (4.3.1)$$

and the small–scale turbulence stretch rate, equal to the inverse of the Kolmogorov timescale,

$$S_{turb} = Re_t^{1/2} \frac{q'}{L_{turb}} , \qquad (4.3.2)$$

which, together with $Re_t = \frac{q' L_{turb}}{\nu}$ and $q'=C_q U$, give

$$S_{total} = \frac{2\,U}{H} + \frac{C_q^{3/2}}{\nu^{1/2} L_{turb}^{1/2}} U^{3/2} \qquad (4.3.3)$$

with $C_q \approx 0.085$ for H_p = 55mm and $C_q \approx 0.045$ for H_p = 120mm (Section 3.2.3; Eq. 3.2.2), and L_{turb}=4mm, and the total strain rate given by Eq. (4.3.3) is evaluated at each measurement of bulk velocity at extinction[3]. The extinction data for $15 \le H \le 35$mm and for two values of H_p plotted in terms of the total strain rate from Eq. (4.3.3) against air volume fraction follow a single curve, Fig. 4.15, with a spread of ±20 %, which implies that the total strain rate at extinction depends *only* on the air volume fraction in the fuel. The extinction data for H = 10mm follow distinctly different curves, possibly due to the larger uncertainty in the approximation of the bulk strain rate term in Eq. (4.3.3) at small H due to the unrealistic limiting behaviour of Eq. (4.3.1) as H goes to zero. The fact that S_{total} is constant for a given value of air premixedness suggests that the nominal total strain rate acting on the flame is a convenient way to describe the stability of the counterflow diffusion flame with or without partial premixing and implies that the mean and the turbulent stretch rates act in combination to cause extinction, as in the premixed flames of Kostiuk *et al.* (1989).

In Section 4.1.4, it was shown that current theories of turbulent diffusion flame extinction relate extinction to the turbulent scalar dissipation rate; the total stretch rate that the flame experiences does not appear anywhere in those descriptions. Thus, the correlation of extinction in Fig. 4.15 based on the total stretch rate on the flame is of phenomenological nature because it lacks fundamental basis and it is interesting to see how extinction of the present diffusion flames is related to the turbulent scalar dissipation rate.

---

[3] It is assumed that q'/U is solely determined by the location of the turbulence generator in the tube and that the turbulent stretching at the flame is given by the state of the turbulence at the exit plane of the jet. This assumption results in estimates of the stretch rate that do not need the detailed measurements of Chapter 3 and its validity will be discussed later.

Correlation in terms of the scalar dissipation rate

In the introduction to this Chapter, the extinction of turbulent diffusion flames was related to the value of the mean turbulent dissipation rate of a conserved scalar like the mixture fraction. In particular, for flamelet flames, Peters (1983) proposed that extinction of the turbulent flame occurs when the mean turbulent scalar dissipation rate evaluated at the stoichiometric mixture fraction $\tilde{\chi}_{st}$ exceeds a critical value, and here, $\tilde{\chi}_{st}$ is estimated at the extinction conditions of turbulent counterflow flames.

An eddy–viscosity model for the mean mixture fraction and its r.m.s. fluctuations f' and numerical solutions for the latter was presented in Section 3.2.5 and the modelled equation for f' included a term for $\tilde{\chi}$ where it was assumed that

$$\tilde{\chi} = 2\, q'/L_{turb}\, f'^2. \qquad (4.3.4)$$

Equation (4.3.4) shows that the mean scalar dissipation rate increases with the *turbulent* strain rate q'/L_{turb}, and with the *bulk* strain rate U/H, because, as shown in Section 3.2.5, small values of H result in large f'^2 and large values of U result in the same f' but in large q'. Therefore, based on the experimental data in Figs. 4.12 and 4.14, the scalar dissipation rate estimated by the eddy–viscosity model of Section 3.2.5 increases with approach to extinction and quantitative estimates are presented below.

Evaluation of Eq. (4.3.4) and the measured values of q'/U at the exit plane of the jet, with $10 \le H \le 35$mm, $0.045 \le q'/U \le 0.085$, $L_{turb} = 4$mm, and Eq. (3.2.19) that defines the parameter α which determines f', lead to values of $0.225 \le \alpha \le 1.49$ for the conditions of the extinction measurements shown in Fig. 4.15. For each extinction point, the scalar dissipation rate is estimated from Eq. (4.3.4) with the experimental value of q' and the calculated value of f' based on the corresponding value of α. The r.m.s. fluctuations of the mixture fraction are calculated from solutions such as those in Fig. 3.2.12b at $\eta = \eta_{st}$ which corresponds to the location of the stoichiometric mixture fraction and which is found from Fig. 3.2.12a, while the stoichiometric mixture fraction for diffusion flames with partial premixing is found from

$$f_{st} = \frac{(1-X_{air})R_{MW} + X_{air}}{(1-X_{air})R_{MW} + (1-X_{air})/R_{molar}}\ , \qquad (4.3.5)$$

where $R_{MW} = MW_{fuel} / MW_{air}$, R_{molar} is the fuel to air molar ratio at stoichiometry and equal to 0.105 for methane–air flames, and X_{air} is the air volume fraction in the fuel stream (also Eq. 2.2.1). Having described how the experimental conditions are related to the non–dimensional parameters of the model of Section 3.2.5, quantitative estimates of the mean scalar dissipation rate at the extinction of counterflow non–premixed flames follow.

The scalar dissipation rate at extinction was determined in the manner described in the previous paragraph for each measured extinction point. Figure 4.16a shows that the estimated mean turbulent scalar dissipation rate at extinction χ_{ext} is constant to within about 7% for air volume fractions of 0, 0.5, and 0.8 and equal to 2.3, 6.8, and 17.4 s^{-1} respectively, while Fig. 4.16b shows that the estimated χ_{ext} increases with partial premixing and the data from different tube separations and turbulence intensities collapse on the same curve[4]. There are two reasons why χ_{ext} increases with partial premixing. The first is that partial premixing, by increasing the stoichiometric mixture fraction, changes the location at which the mixture fraction fluctuations are evaluated, from a location with small f' at large η for small f_{st}, to a location with large f' at small η when f_{st} increases, and so partially premixed flames have higher f' at the same α. The second reason is that the experimental value of the bulk velocity and therefore the value of the turbulent intensity q' at extinction is larger at high f_{st}, as Fig. 4.17 shows explicitly for a few extinction measurements. Figures 4.16a and 4.16b show that χ_{ext} depends *only* on the air volume fraction in the fuel stream and the constant value of χ_{ext} gives strong support to the theory of Peters and Williams (1983) that extinction of turbulent diffusion flames occurs at a critical value of the mean scalar dissipation rate.

Comparison with laminar flames – strain rate

The present extinction data for turbulent flames are consistent with measurements, performed in the opposed jet burner without turbulence generators with well-contoured nozzles (Fig. 2.2), of the strain rate at extinction of *laminar* counterflow diffusion flames, which have been included in Fig. 4.15. The laminar diffusion flame without partial premixing extinguished at about 430 s^{-1}, a value similar to that measured by Chelliah *et al.* (1990), and partial premixing resulted in increased resistance to strain, as for the turbulent flames, to about 630 s^{-1} for an air volume fraction of 0.75 in the fuel stream. A similar increase in the extinction strain rate of a partially premixed counterflow laminar flame was reported by Stårner *et al.* (1990) who found, with a numerical calculation of counterflow diffusion flames in the forward stagnation point of a porous cylinder, a value of about 820 s^{-1} for X_{air}=0.75. These values are close to the estimated total strain rate at extinction of the *turbulent* counterflow non–premixed flame (Fig. 4.15) and, based on this observation, the phenomenological correlation proposed in Section 3.4.1 is expanded and it is suggested that turbulent counterflow diffusion flames extinguish at a total strain rate equal to the strain rate at the extinction of similar *laminar* flames.

---

[4] The symbol χ_{ext}, is used for the *estimated* $\tilde{\chi}_{st}$ at extinction to contrast with $\tilde{\chi}_{st}$ which generally denotes the mean turbulent scalar dissipation rate at the stoichiometric mixture fraction.

Comparison with laminar flames – dissipation rate

In the context of Peters and Williams (1983) theory of turbulent flame extinction, the critical value of the turbulent mean scalar dissipation rate is numerically equal to the scalar dissipation rate

$$\chi_{lam} = 2\, D_{mol}\, (\partial f/\partial x_i)^2$$

for extinction of a *laminar* counterflow flame and the magnitude can be determined from a measurement of the extinction strain rate together with a solution for the mixture fraction f, from which the gradient $\partial f/\partial x_i$ at $f=f_{st}$ can be estimated. The measurements of the strain rate for extinction of laminar partially premixed counterflow flames (see previous paragraph and Fig. 4.15) lead to an estimate of the laminar scalar dissipation rate by using Eq. (3.2.22) to evaluate $(\partial f/\partial z)$ resulting in

$$\chi_{lam} = 2S/\pi \exp(-2\, S\, z_{st}^2 / D_{mol}) \qquad (4.3.6)$$

where $2S$ is the strain rate and z_{st} is the axial coordinate where the mixture fraction is equal to stoichiometric with non–dimensionalisation appropriate for laminar flow (Section 3.2.5; see also Peters, 1983, or Liñan, 1974). Assumptions underlying Eq. (4.3.6) are that the density is constant and that the velocity field conforms to potential flow. For pure diffusion flames, the experimental value of $2S = 430\ s^{-1}$ and evaluation of Eq. (4.3.6) results in $\chi_{lam} = 10.7\ s^{-1}$ and for partially premixed flames the magnitude of χ_{lam} increases with f_{st} because z_{st} becomes smaller and because of the higher measured extinction strain rate (Fig. 4.15). Figure 4.18 shows that the mean scalar dissipation rate at extinction of the *turbulent* partially premixed flame, normalised by its value for a flame without premixing, does not increase as fast as the similarly normalised scalar dissipation rate at the extinction of the *laminar* partially premixed flame, but the trend that partial premixing makes the flame more resistant to stretching is clear for both laminar and turbulent flames.

Comparison with laminar flames – partial premixing

The present observation that partial premixing of the fuel stream with air increases the resistance of diffusion flames to straining is consistent with the observation that partially premixed piloted turbulent jet diffusion flames blow–off at a higher jet velocity than without such premixing (Stårner *et al.*, 1990), with measurements of the extinction strain rate of laminar counterflow partially premixed diffusion flames (included in Fig. 4.15), and with the predictions of Spalding (1961) who used approximate expressions for the finite rate of chemical kinetics and showed that the critical strain rate

for extinction increased by a factor of two from X_{air}=0.0 to X_{air}=0.8. In Spalding's analysis, this was because partial premixing of the fuel stream with oxidant results in an increase in the stoichiometric mixture fraction f_{st} and the critical strain rate for extinction was predicted to increase with f_{st}.

The stabilising effect of partial premixing on diffusion flames can be understood by examining the chemical structure of a laminar strained diffusion flame at extinction. Jones and Lindstedt (1988) suggested that the fuel breakdown reaction in the rich side of the flame is the slowest of all the other reactions which constitute their four–step reduced mechanism and flame extinction occurs when the rate of this reaction becomes too low. Fuel breakdown is probably assisted by the presence of oxygen in the rich side of the flame, and therefore partial premixing will help to keep the rate of the breakdown reaction high. Laminar partially–premixed flames have also been examined by Yamaoka and Tsuji (1974, 1976) in the context of their chemical structure, not extinction, and they found that the flame had two luminous zones (as in Fig. 3.3.2) and that the inner flame produced most of the H_2 and CO that the outer flame consumed on the oxidiser side; since the concentration of H_2 is crucial for the progress of the reaction, as also discussed in Section 4.3.2, oxygen in the fuel stream helps in the creation of hydrogen and therefore helps flame stability.

A different type of partially premixed flames has been examined by Peters (1984b), Seshadri *et al.* (1985), and Smooke *et al.* (1988), who considered the simultaneous premixing of fuel with air, and of the air stream with fuel, so as to keep the stoichiometric mixture fraction constant. These papers reported that the extinction strain rate can be smaller with dilution, but their results cannot be compared directly with the present measurements because of the different premixing which results in different definition of the mixture fraction and thus the scalar dissipation rate.

Discussion on the proposed correlations

In this Section, two extinction criteria were presented for turbulent counterflow diffusion flames with and without partial premixing: one says that the flame will extinguish when the total stretch rate acting on the flame exceeds the strain rate necessary to extinguish a similar laminar flame, i.e. $S_{total} > S_{lam}$. The other concludes that extinction will occur when the mean turbulent scalar dissipation rate at the location of the stoichiometric mixture fraction exceeds an experimentally–determined critical value, i.e. $\tilde{\chi}_{st} > \chi_{ext}$.

The first correlation is useful for describing the operational limits of turbulent counterflow flames and is based on estimates, using Eq. (4.3.3), of the *nominal* total stretch rate on the flame based on the global mean flow parameters U and H, and estimates from the initial state of the turbulence produced by the perforated plate for q'/U and L_{turb}. Questions arise as to whether these estimates represent the *actual* stretch rate

that the flame experiences, and these questions have also been discussed in Section 3.4.5, but there are various reasons for the reluctance to attempting to estimate here the true stretch rate on the flame. First, the purpose of this correlation was to show in a easily–calculated way the operational limits of counterflow burners, without need to resort to detailed measurements. Secondly, although the velocity measurements of Chapter 3 allow estimates of the actual mean velocity gradient on the flame and the r.m.s. values are known, estimates of the small–scale strain rate would still require approximations for the turbulent lengthscales. Finally, even if the actual total stretch rate on the flame could be estimated, the resulting correlation would still lack fundamental basis because it is not a quantity appearing in existing diffusion flame extinction theories.

In the context of the second correlation, which is physically more legitimate for describing the approach of a flame to extinction, the effect of the bulk strain rate on the extinction of the flame is to provide a flow pattern which makes the mixture fraction fluctuations increase and thereby increase the scalar dissipation rate, and the effect of the turbulence stretch rate is to increase $\tilde{\chi}_{st}$ directly, as seen from Eq. (4.3.4). There is no conflict between the two descriptions of flame extinction for the present counterflow flames; the second one, however, is a concept that can be extended to turbulent diffusion flames in other geometries.

Peters (1983) predicted that extinction occurs when $\tilde{\chi}_{st} > \chi_{lam}$, but in Fig. 4.18 the estimated χ_{ext} at extinction of the turbulent flame does not agree quantitatively with the estimated χ_{lam} at the extinction of the laminar flame with, for example, $\chi_{ext} = 2.3s^{-1}$ and $\chi_{lam} = 10.7s^{-1}$ at $X_{air} = 0$. There are four reasons for this discrepancy. The first is that the determination of χ_{lam} based on a measured extinction velocity and an assumed potential flow isothermal solution to the mixture fraction in laminar counterflow flames involves approximations that are, at present, difficult to quantify. The second reason is that in the theory the numerical value of the ratio $\tilde{\chi}_{st}/\chi_{lam}$ depends on the assumptions made about the statistical nature of the scalar dissipation rate in a turbulent flame and these were based by Peters and Williams (1983) on a limited number of measurements in free jet flows. Indeed, as these authors point out, the numerical value of this ratio is not to be trusted too much, and more research is necessary to determine the statistics of the small–scale motions in turbulent flames (Bradley *et al.*, 1992).

The third reason is that it is increasingly being recognised that laminar flamelets do not respond instantaneously to straining and extinguish only if the strain rate stays high for an adequately long time (Mauß *et al.*, 1990; Poinsot *et al.*, 1991; Stahl and Warnatz, 1991), and so it may not be true that flamelets with scalar dissipation rate higher than χ_{lam} do not exist in the turbulent flow, as assumed by Peters (1983). The physical explanation offered by Mauß *et al.* (1990) for laminar diffusion flames is that, even if instantaneously the chemical reaction ceases because of too large a value of the scalar dissipation rate, the temperature will decrease according to a diffusional timescale;

if the temperature has not decreased below some critical value and the dissipation rate is relaxed, the flamelet will re–ignite. Similarly, for laminar premixed flames interacting with vortices, Poinsot *et al.* (1991) found that large strain rates have to interact for a finite time with the flame to cause extinction, and Stahl and Warnatz (1991) found that the same applies to twin laminar counterflow premixed flames. Thus, flames take a finite time to respond to increases in straining and this implies that it is not sufficient to consider only the magnitude of the steady–state scalar dissipation rate at extinction of a laminar counterflow flame, χ_{lam}, in the description of the extinction of the turbulent flame.

The fourth reason is that approximations have been made in the eddy–viscosity model in Section 3.2.5, which led to the previous estimates of χ_{ext}: assumptions were made of a Hiemenz flow field, a constant eddy–viscosity, and a model for the mean turbulent scalar dissipation rate given by Eq. (4.3.4). The first two have been relaxed by Champion and Libby (1993) in a second–order closure model, but were warranted here because they enabled quick predictions of χ which revealed why both bulk and turbulent stretching can lead to extinction. The validity of the model for χ, also discussed in Section 3.4.6, relies on a constant value of the timescale ratio between the decay of the velocity and the scalar fluctuations (the factor 2 in Eq. 4.3.4). This timescale ratio, however, has been shown to vary by Warhaft and Lumley (1978) who found that the scalar dissipation rate depended on the way the scalar was introduced into the turbulent flow and, in particular, by the relative magnitudes of the lengthscales of the scalar and the velocity fluctuations. Using direct numerical simulations, Eswaran and Pope (1988) found that the timescale ratio depended additionally on the time of the scalar injection (the relative "age" of the scalar and the velocity turbulence) and that the scalar dissipation rate was larger than the estimate of Eq. (4.3.4) by as much as a factor of three at short times (i.e. for "young" scalar fluctuations).

It was shown in Section 3.4.6 that the turbulent counterflows examined in this thesis fall in the regime of timescales examined by Eswaran and Pope (1988) and so the scalar dissipation rate on the present diffusion flames is probably larger than the estimates in Fig. 4.16, and indeed, closer to χ_{lam}. However, the *correlation* of extinction limits is not expected to change even if such effects are introduced in the modelling of χ because *all* the flames examined here concern relatively similar scalar turbulence "ages" which means that although the estimate might be wrong, it s likely to be so by a *constant* factor, and thus extinction measurements from different jet separations and turbulence intensities would still collapse on the same curve, albeit at different numerical values of χ_{ext}.

Finally, as mentioned in Section 3.4.6, a qualitative model for the instantaneous structure of the mixture fraction based on the random movement of the laminar strained diffusion layers, along which the flamelet lie and on which the scalar dissipation rate has

non–zero values, reproduces the prediction from the eddy–viscosity model that high bulk stretching leads to high values of χ. Therefore, notwithstanding the numerous approximations made to reach the correlation presented in Fig. 4.16, the qualitative dependence of χ on the global flow parameters has been correctly represented and the present experimental evidence supports explicitly the view that turbulent diffusion flame extinction is associated with high values of the scalar dissipation rate.

4.3.5 Diffusion flames with vitiated air

Background and structure of this Section

Mixing of reactants with hot combustion products prior to combustion is currently used in various applications to reduce the amount of pollutants, as for example, exhaust gas recirculation in utility boilers which lowers NO_x emissions (van de Kamp *et al.*, 1992), and the stabilisation of flames by recirculation zones has long been attributed to the mixing of the unburnt reactants with hot combustion products (Beér and Chigier, 1972). The presence of hot products in the reactants is termed "vitiation" (Mullins, 1954) and results in an increase in the temperature and, at the same time, in the lowering of the reactant concentrations and, although the former is expected to have a beneficial effect on flame stability, it is not clear when this will be larger than the expected detrimental effect of the latter. Thus the net effect on flame stability is not known and the aim of this Section is to quantify the effects of the preheat and dilution due to vitiation on the stability of turbulent counterflow diffusion flames.

Based on experiments and examination of the literature, it was concluded in Section 4.3.2 that extinction is associated with small values of the flame temperature, and so the effects of reactant vitiation on flame temperature have to be considered. The maximum temperature of a diffusion flame is the same as the adiabatic flame temperature of a stoichiometric premixed flame and simple thermodynamic arguments (for example, Williams, 1985) show that reactant preheat (without dilution) results in a linear increase and reactant dilution by inert species (without preheat) results in a linear decrease in the flame temperature. With dilution with hot reaction products at the adiabatic flame temperature of a stoichiometric flame of undiluted reactants, the temperature rise of the reactants and their dilution are related so that the flame temperature is *identically* that of the undiluted, unheated mixture in the absence of heat losses, because the reduction in energy release due to the dilution is exactly counterbalanced by the gain in initial temperature. This special situation can be described as "self–vitiation" (Mullins, 1954) and the extinction of flames under this condition will be examined closely later in this Section.

Reducing the reactant concentrations leads to flame extinction and Tsuji (1982) reported that no laminar diffusion flame can exist at an oxygen mole fraction, X_{ox}, smaller than 0.143, while Puri and Seshadri (1986) and Chen and Sohrab (1991) found

a value of 0.150 for the same quantity. These measurements were taken with an oxidiser initial temperature of 300K, but, in view of the previous discussion on the relationship between extinction and flame temperature, it is expected that these limiting values of X_{ox} will be smaller for higher temperatures of the oxidiser. Mullins (1954) measured the stability limits of flames in gas–turbine combustors and found that "a reduction of 100°C in the inlet air temperature reduced the stability limit by the same amount as a diminution of 0.016" in X_{ox}, thus confirming, in a realistic burner, the trend expected from laminar flame studies.

In the experiments presented below, the temperature dependence of the limiting oxygen content for turbulent counterflow diffusion flames is measured and the results are then discussed through comparisons with the extinction trends of *laminar* counterflow flames. Finally, the Section closes with a discussion of the application of the results to the extinction of flames stabilised by recirculation zones.

Air stream preheat without dilution

The effect of a rise in the initial temperature of the air stream with X_{ox}=0.21 in a turbulent counterflow diffusion flame of gas, either pure or partially premixed with cold air, is to increase the velocity at which the flame extinguishes, as Fig. 4.19 shows for two jet separations. This trend is expected since increasing the initial air temperature increases the resulting flame temperature and thus the speed of the chemical reaction. When a *lean premixed* flame is formed by ejecting a flammable mixture of equivalence ratio $\phi_1<1$ from the bottom tube, the top air does not participate in combustion, and Fig. 4.19 shows that the curves for heated and unheated air merge at around stoichiometric conditions, so that a low T_2 has no effect on the stability of lean premixed flames, as discussed in Section 4.3.2.

Fuel stream preheat without dilution

Figure 4.19a also includes some data for partially–premixed diffusion flames in which the fuel–air mixture is heated and the ambient oxidiser air is not (open triangles), and comparison with the flames with heated *air* and unheated fuel streams (blocked triangles) shows that the flame extinguishes at a smaller velocity for the former. However, fuel–stream preheating is better than no preheating at all (open triangles and blocked circles). These trends are consistent with the expectation that preheat of the air stream will result in a larger increase in the flame temperature than preheat of the fuel stream as the stoichiometric mixture fraction of partially premixed flames is always smaller than 0.5 (Eq. 4.3.5). The effect of reactant dilution, which also affects the flame temperature, is discussed next.

Air dilution with and without preheat

Flames of pure, and partially–premixed, fuel were established against electrically–heated oxygen–nitrogen mixtures in the burner of Fig. 2.3a and extinction limits were measured by decreasing the oxygen flow rate and increasing correspondingly the nitrogen flow rate to keep the bulk velocity (hence the strain rate) and the temperature constant. Figure 4.20 shows that the minimum required oxygen mole fraction of the oxidiser (upper) stream decreases with increasing partial premixing of the fuel (lower) stream because oxygen for combustion is available in the fuel and, therefore, the requirement for oxygen from the oxidiser stream reduces. As the degree of partial premixing approaches the rich flammability limit, the minimum oxygen content requirement of the top stream decreases quickly and reaches zero when the bottom tube mixture corresponds to a *lean* premixed flame. The results show that a rise in the oxidiser stream temperature is beneficial for flame stability over the whole spectrum of partial premixing up to situations corresponding to premixed flames and that the required minimum oxygen mole fraction decreases as the temperature of the oxidiser increases.

Flames with hot combustion products as oxidiser

Measurements at oxidiser temperatures higher than 1000K were made in the burner of Fig. 2.3b with the "supply" flame closer to the tube exit plane and are presented below, but with the drawback that the turbulence in the oxidiser stream is not as large as before (Figs. 4.19 & 4.20) because the turbulence–promoting perforated plate was now used to stabilise the "supply" flame. The degree of stretching will therefore be described only qualitatively through the bulk velocity of either stream because a direct comparison of the stretch rates that these flames experience with the stretch rate of the previous flames (Figs. 4.15, 4.19 & 4.20) cannot be made because Eq. (4.3.3) cannot be evaluated.

Figure 4.21 shows that the minimum oxygen mole fraction required in the "air" stream increases with decreasing temperature by about 0.023/100K for turbulent unpremixed diffusion flames at the same velocity, in qualitative accord with expectations, and that this "elasticity" is, approximately, insensitive to strain rate. The bulk velocity for extinction is higher than that necessary to extinguish a diffusion flame without any reactant preheat or dilution (1.5m/s for the conditions of Fig. 4.21, from Fig. 4.12) and therefore the beneficial effect of the high oxidant temperature more than compensates for the detrimental effect of the reduced oxygen content[5].

---

[5] The velocities in the flows here are expected to be qualitatively similar to the measurements in Fig. 4.6. An under–estimate of the stretch rate acting on these diffusion flames can be obtained by considering the extreme case that the turbulence in the hot product stream is zero. Then the stretch rate on the flame is due *only* to the mean velocity gradient in the oxidiser stream (in view of the small stoichiometric mixture fraction which locates the flame inside the air stream) and which is estimated as $2U_2/H$, i.e. about 500 to 680s^{-1} for the flames of Fig. 4.21. Compare this with the 400s^{-1} of *total*

At the temperature range of Fig. 4.21, the flame needed an external ignition source and the extinction was sudden as the oxygen mole fraction or the temperature decreased below a critical value. It was found, however, that the flame ignited *without* external sources for high oxidant temperatures, as for turbulent *premixed* flames against hot products (Section 4.3.2; Fig. 4.2). Detailed measurements of the conditions under which this happened were not taken, but one condition was T_2=1700K, X_{ox}=0.02, and fuel diluted by nitrogen so that the methane volume fraction was as low as 0.03, and a reaction zone was visible as soon as the fuel was introduced in the lower stream. This observation is the equivalent for diffusion flames of the observation that premixed flames do not exhibit sudden extinction at high opposing stream temperatures (Fig. 4.2) and shows that sudden extinction occurs only when the initial reactant temperature is not too high (*ca.* 1500K for premixed flames, lower than 1700K for diffusion flames).

The quantification of the temperature dependence of the minimum oxygen content, the observation that dilution with hot products is always beneficial for stability, and the demonstration of the transition from sudden extinction to no–extinction at high vitiated air temperatures, are basic conclusions from this Section and will be supported by comparisons with *laminar* flame extinction below. The formula of Liñan (1974) is used to find the minimum Damköhler number for a stable laminar counterflow diffusion flame, as no experimental data for laminar flames with vitiated air are available, and results are given for a wider range of strain rates and oxidiser temperatures and oxygen mole fractions than could be achieved in the present experiments. The analysis is presented in the next sub–section, followed by the presentation and discussion of the results.

Comparison with laminar flames – analysis

The results of the theory of Liñan (1974) are, in principle, able to capture the extinction trends of flames with vitiated air because reactant vitiation changes the equilibrium flame temperature, the fuel and oxidant mass fractions, and the stoichiometric mixture fraction, quantities that appear as parameters in the analysis. In the following, most of the nomenclature of Liñan's paper is preserved and the reader should consult that paper for details.

Liñan showed that counterflow diffusion flames extinguish when a Damköhler number becomes smaller than a critical value which depends on the equilibrium flame temperature and the reaction rate. In particular, extinction occurs when

$$\delta = e\{(1-\gamma)-(1-\gamma)^2+0.26(1-\gamma)^3+0.055(1-\gamma)^4\} \qquad (4.3.7)$$

---

strain rate (bulk plus small–scale turbulent) necessary to extinguish a pure diffusion flame with unheated and undiluted air (Fig. 4.15).

where γ is defined later and δ is the reduced Damköhler number defined as

$$\delta = 8\pi \exp(z_e^2) \left(\frac{T_e^2}{T_a}\right)^3 (\alpha+1)^{-2} \mathrm{Da} \exp(-T_a/T_e) , \qquad (4.3.8)$$

with Da being the Damköhler number

$$\mathrm{Da} = Z \nu Y_{F,-\infty} / S . \qquad (4.3.9)$$

Z represents an inverse kinetic timescale, ν is the stoichiometric mass ratio of oxidiser to fuel (equal to 4 for oxygen–methane flames), $Y_{F,-\infty}$ the fuel mass fraction in the fuel stream, and S the strain rate, assumed constant. The other quantities that appear in Eqs. (4.3.7) and (4.3.8) are defined as follows: z is the axial coordinate measured from the stagnation plane and made non–dimensional by the characteristic length $\sqrt{D_{mol}/S}$ with D_{mol} being the molecular diffusion coefficient and with the fuel approaching from $z=-\infty$ and the oxidant from $z=\infty$ where the oxidant mass fraction is $Y_{O,\infty}$; z_e, defined later by Eq. (4.3.14), is the flame location. The temperature T has been normalised by the quantity $Q/(c_p Y_{F,-\infty})$ with Q being the heat release per unit mass of fuel and c_p the specific heat; T_a is the non–dimensional activation temperature and

$$T_e = T_\infty + (1-\beta)\alpha/(1+\alpha) \qquad (4.3.10)$$

is the non–dimensional adiabatic flame temperature[6]. Also,

$$\alpha = Y_{O,\infty} / (\nu Y_{F,-\infty}) \qquad (4.3.11)$$

represents the oxygen mass fraction in the oxidiser stream,

$$\beta = T_\infty - T_{-\infty} \qquad (4.3.12)$$

represents a non–dimensional temperature difference between the two streams, and

$$\gamma = 2(\alpha+\beta)/(1+\alpha) - 1 . \qquad (4.3.13)$$

[6] In this Section, T represents non–dimensional temperatures, apart from T_1 and T_2 which are the dimensional temperatures of the lower fuel stream and the upper air stream respectively.

Finally, z_e is the location of the flame in the Burke–Schumann limit of an infinitely thin flame located at the stoichiometric mixture fraction and is related to the mixture fraction f by

$$f = \frac{1}{2}[1 - \mathrm{erf}(z/\sqrt{2})] \qquad (4.3.14)$$

defined such that f=0 in the oxidiser and f=1 in the fuel stream and the stoichiometric mixture fraction is given by

$$f_e = \alpha / (\alpha+1)\,, \qquad (4.3.15)$$

which is the equivalent expression in Liñan's nomenclature of Eq. (4.3.5).

A flame far from extinction and close to equilibrium is thin, located at z_e, and has a temperature T_e, and the subscript e is used to emphasise the fact that a quantity at equilibrium is considered. Finite–rate kinetics set in when the strain rate is sufficiently high and then the temperature decreases and the flame acquires an internal structure; this structure was explored by Liñan using asymptotic methods and who found that above a certain Damköhler number, given by Eq. (4.3.7), stable solutions of the governing momentum, species, and energy equations do not exist, and this situation was deemed to correspond to flame extinction.

Vitiation of the air stream results in a reduction of the oxygen mass fraction $Y_{O\infty}$, an increase in the temperature T_∞, and a reduction in the stoichiometric mixture fraction, and these changes are manifested in the parameters α, β, and z_e, given by Eqs. (4.3.11), (4.3.12), (4.3.14) and (4.3.15). The counterflow flame with $Y_{F-\infty}$=1, $Y_{O\infty}$=0.23 and T_∞=$T_{-\infty}$=300/(Q/c_p) K (i.e. pure fuel burning with ambient air) is used as a "reference flame" and then the strain rate for extinction of a flame with vitiated air, S_{vit}, is related to the extinction strain rate of the "reference flame", S_{ref}, by

$$\frac{S_{vit}}{S_{ref}} = \frac{\delta_{ref}}{\delta_{vit}} \frac{\exp[(z_e^2)_{vit}]}{\exp[(z_e^2)_{ref}]} [T_{e,vit} / T_{e,ref}]^6 \frac{(\alpha+1)^2_{ref}}{(\alpha+1)^2_{vit}} \exp[T_a/T_{e,ref} - T_a/T_{e,vit}]\,. \qquad (4.3.16)$$

Numerical values of Q/c_p = 34545K and T_a = 0.4735 are obtained with the assumption that the adiabatic flame temperature of methane–ambient air flames is 2200K and the non–dimensional activation temperature corresponds to an overall activation energy of 32.5 Kcal/mol (Chen and Sohrab, 1991). Only diffusion flames with undiluted and unheated fuel streams are considered, i.e. $Y_{F-\infty}$=1 and $T_{-\infty}$ corresponding

to 300K, and results of S_{vit}/S_{ref} are presented in the next sub–section as a function of the dimensional air stream temperature T_2 and the oxygen mole fraction X_{ox}. The oxygen mass fraction $Y_{O\infty}$ is related to X_{ox} by considering the air mixture as composed of oxygen and nitrogen; this is a valid assumption for "air" mixtures of oxygen vitiated with hot reaction products because the molecular weights of nitrogen and stoichiometric combustion products differ by less than 1%. From the chosen values of T_2 and X_{ox}, the parameters α, β, f_e, z_e, T_e, γ, and δ are calculated and then Eq. (4.3.16) is evaluated.

During self–vitiation of the air stream with hot reaction products, the rise in temperature is associated with the reduction in the oxygen mole fraction in a well–defined way. Assuming that the "air" stream is ambient air adiabatically mixed with combustion products of a stoichiometric flame, the oxygen concentration X_{ox} is related to the final oxidant mixture temperature T_2 (the dimensional form of T_∞) by

$$T_2 = (1-Y_{air})T_{prod} + Y_{air}\,T_{air}$$

$$= T_{prod} - \frac{X_{ox}}{0.21R+(1-R)X_{ox}}\,(T_{prod} - T_{air})\,, \qquad (4.3.17)$$

where Y_{air} is the mass fraction of ambient air in the air–products mixture and $R=\frac{MW_{prod}}{MW_{air}}$ ≈ 1. T_{air} is taken as 300K and T_{prod} is taken to be equal to the adiabatic flame temperature of methane–air stoichiometric flames at 2200K.

Results of numerical evaluations of Eq. (4.3.16) for various combinations of X_{ox} and T_2 and for the special case when these two quantities are related by Eq. (4.3.17), are presented below and compared with the measurements in the turbulent flames presented previously.

Comparison with laminar flames – results

Figure 4.22 shows that the strain rate of laminar flames at extinction increases by two orders of magnitude when the ambient air is heated to a temperature of about 1500K, but that when the oxygen mole fraction is reduced to 0.09, such a large increase is achieved at about 2100K. For X_{ox}=0.21 and T_2=420K, the strain rate increases by a factor of 1.8, which is close to the measured ratio shown by the data of Fig. 4.19 for X_{air}=0. When the oxygen content decreases, the flame is extinguished more easily, as Fig. 4.22b shows in more detail. These predictions are consistent with the measurements and will be used in assembling contours of S_{vit}/S_{ref}, to be discussed shortly.

Figure 4.23 shows that the extinction of *self-vitiated* counterflow diffusion flames occurs at a higher strain rate than the reference case of unheated, undiluted air. It is also evident that the extinction strain rate increases almost exponentially at oxygen

mole fractions smaller than about 0.03, corresponding to $T_2 \geq 1800K$; the mathematical reason is that the second term increases very quickly compared to the other terms in Eq. (4.3.16) because as X_{ox} decreases, the stoichiometric mixture fraction decreases (Eqs. 4.3.12 & 4.3.16), the flame shifts deeper into the oxidiser stream, and z_e increases (Eqs. 4.3.15 & 4.3.16).

It is possible that the S–shaped curve of flame temperature *vs.* Damköhler number, the turning point of which corresponds to extinction and which forms the basis of Liñan's extinction prediction, becomes monotonic with Da as the initial reactant temperature gets closer to T_e; recall that during self-vitiation the final flame temperature is not altered because the initial reactant temperature is higher due to preheat, but the temperature rise is less due to dilution, and so the upper and lower curve of the S–shaped curve may merge. Recent numerical evidence by Darabiha and Candel (1992) shows that the S–shaped curve becomes monotonic for laminar diffusion flames with reactants at high initial temperatures, as for premixed laminar flames (Section 4.3.2; Libby and Williams, 1983), and this is consistent with the experimental observation mentioned previously that the turbulent flame would ignite without external sources and would not extinguish even for very low reactant concentrations for $T_2=1700K$.

Figure 4.24 presents contours of S_{vit}/S_{ref} calculated from Eq. (4.3.16) and includes data of Fig. 4.21 and selected data from Fig. 4.20 that were taken for *turbulent* flames[7]. The predictions are in reasonable agreement with the experiments when the extinction measurements are plotted in the $T_2 - X_{ox}$ plane. Note that, apart from the blocked squares in Fig. 4.24 (the data of Fig. 4.20) which correspond to extinction at the same velocity as that of unheated, undiluted air and thus $S_{vit}/S_{ref} \approx 1$, the strain rate ratio of the other data cannot be estimated accurately, but since those flames extinguished at a bulk velocity higher than that of the "reference" flame, it may be concluded that the predictions agree to within better than an order of magnitude with the data. A curve representing Eq. (4.3.16) has also been plotted in Fig. 4.24 and always lies above the $S_{vit}/S_{ref}=1$ contour and this, together with Fig. 4.23, shows that for diffusion flames with air *adiabatically* diluted by hot reaction products, the effect of the rise in temperature *always* dominates the effect of the loss of oxygen. A justification for the rise in temperature winning over the reduction in the oxygen concentration is that because the extinction strain rate scales with an inverse chemical timescale to a good approximation and because the chemical reaction rate is represented by an Arrhenius–like term, the chemical timescale changes more steeply with temperature than with reactant concentration.

[7] Comparing predictions for *laminar* flames with experiments from *turbulent* flames is reasonable because it was found in Section 4.3.4 that the total strain rate at extinction of a turbulent flame is close in magnitude to the extinction stretch rate of the corresponding laminar flame.

Application to recirculating flames

The temperature dependence of the minimum oxygen mole fraction in turbulent counterflow diffusion flames was quantified as 0.023/100K (Fig. 4.21), and only very weakly dependant on strain rate, and this value is close to the slope of the contours of the calculated laminar counterflow flame extinction strain rate in Fig. 4.24. The only other similar data the author knows are those of Mullins (1954) which show a slope of 0.016/100K, a value comparable to that found here. Such close agreement was unexpected because the data of Mullins were taken from measuring the maximum bulk flow rate of combustion air for a stable flame in a full–scale gas turbine burning liquid fuel, a situation very different from the (comparatively) simple counterflow flames described here. However, flame extinction occurs at a critical Damköhler number, and Plee and Mellor (1979) suggested that lean blowoff, as when the air velocity is increased to the point of extinction, is due to a competition between a fluid mechanical and a chemical time evaluated at the shear layer between the hot recirculation zone and the incoming reactants. The stability of a flame in a shear layer is not, in principle, different from the stability of flames in counterflows and thus the present results are applicable to different geometries as well.

Other evidence in recirculating diffusion flames (Namazian *et al.*, 1988) suggests that the flame starts at the stagnation region between the fuel jet and the opposed recirculating flow which is composed mostly of hot combustion products, and this implies that in realistic burners the flame initiation point resembles closely the counterflow flames examined here. It is interesting to compare the conditions of the present flames with the oxygen concentration and temperatures measured inside the swirl–induced recirculation zones of Milosavljevic (1993) where the temperature was in the range 1300 to 1600K and the oxygen mole fraction varied from 0.06 to 0.03, values similar to these discussed here. The bulk stretching rates in those recirculating flames were of the order of 5000 s^{-1}, a value very high compared to the extinction stretch rate of 400 s^{-1} in turbulent counterflow diffusion flames with unheated and undiluted reactants, and this high value raises the question of how the flame could exist. Figure 4.24 shows that an increase in the extinction strain rate of a laminar diffusion flame on the order of 10 is indeed possible at the temperatures and oxygen concentrations encountered by Milosavljevic (1993). Therefore, based on the present result that a high temperature is beneficial for flame stability, despite the loss of oxygen associated with the rise in temperature, it is evident that recirculating flames exist at high stretch rates because the recirculation zone is at a sufficiently high temperature. More discussion on the application of these results for the extinction of diffusion flames stabilised by recirculation zones is presented in Chapter 5.

4.3.6 Extensions to other fuels

H_2/CH_4 flames

Measurements of the extinction of turbulent counterflow diffusion flames of mixtures of natural gas and hydrogen are presented here. These experiments aim, first, to confirm the applicability of the correlation of extinction based on the scalar dissipation rate by examining a different fuel, and, secondly, to quantify in the counterflow geometry the expected trend that hydrogen improves the stability of the flame. An additional motivation is provided by the observation in Chapter 3 that the turbulent Reynolds number of the present flames is relatively low and it is expected that the stability of the flames to larger Reynolds numbers is extended with hydrogen addition.

Figure 4.25a shows the extinction velocity of hydrogen–natural gas flames as a function of the hydrogen mole fraction in the fuel mixture with the jet separation as parameter. It is evident that the velocity is higher for large jet separations, in agreement with the, by now expected, trend that bulk stretching leads to extinction, and that it increases with hydrogen content by a factor of 2 for 10% H_2 by volume. Figure 4.25b shows that the scalar dissipation rate at extinction, calculated as in Section 4.3.4, again collapses the measurements from different jet separations and this provides additional support for the proposed correlation of extinction in terms of χ. For these estimates, the stoichiometric mixture fraction was calculated by considering the air necessary to oxidise fully both the hydrogen and the natural gas.

The increase in the scalar dissipation rate shown in Fig. 4.25b corresponds to an increase in the scalar dissipation rate at the extinction of a similar laminar counterflow flame, but there are no data from such flames with which to compare the turbulent flame measurements. Yu *et al.* (1986) measured the laminar flame speeds of hydrogen–hydrocarbon–air mixtures and reported an increase of about 20% for hydrogen additions corresponding to 10% in CH_4. Considering that a chemical timescale as inferred from the laminar flame speed S_L is proportional to the inverse square of S_L, the chemical timescale of a $10\%H_2 - 90\%CH_4$ mixture burning in air in stoichiometric proportions would decrease by a factor of about 0.7, a value on the order of the inferred acceleration of the reaction with hydrogen addition from Fig. 4.25b. Hydrogen addition in relatively small quantities can therefore be used to extend significantly the stability limits of turbulent counterflow flames and thus result in higher turbulence Reynolds numbers in future studies of counterflow flame structure.

$CO/H_2/N_2$ flames

Turbulent diffusion flames with mixtures of H_2, CO, and N_2 as fuel, which has been used in the past by various authors to simulate city gas and the gas sometimes resulting from coal gasification processes, have been stabilised in the present burner. The major differences between this fuel and hydrocarbon fuels is the larger resistance to

stretching, the increase depending on the percentage of hydrogen, and that the stoichiometric mixture fraction and the width of the reaction zone in mixture fraction space are both larger than in hydrocarbon flames, which may imply that turbulent combustion of such fuels might not occur in the flamelet regime (Masri *et al.*, 1990). Extinction of laminar diffusion flames of a mixture with 45% CO, 15% H_2, and 40% N_2 occurs at a strain rate of about 1950 s^{-1} (or, equivalently, at $\chi_{lam} = 65\ s^{-1}$; Masri *et al.*, 1990), and such high values require velocities of the order of 10m/s which are beyond the capabilities of the gas delivery system of the present experiment and so the extinction of such flames was not measured. The large extinction strain rates, however, allow large Reynolds numbers be achieved, and so such flames are good candidates for future work. In particular, an effort to correlate the extinction of such flames, which are not expected to fall in the flamelet regime (Bilger, 1988), with the methods of Section 4.3.4 would result in interesting insights. For example, such experiments and estimates of the scalar dissipation at extinction could result in a direct testing of Bilger's conjecture that extinction of "distributed reaction zones" occurs at a mean scalar dissipation rate not calculated at f_{st}, but volume–averaged across the space corresponding to the width of the reaction zone in mixture fraction terms. Such an attempt would be the equivalent for non–flamelet flames of the effort here for flames in the flamelet regime.

4.4 SUMMARY OF CHAPTER 4

Measurements of the extinction limits of counterflow premixed flames as a function of bulk and turbulent stretch rates and opposing stream temperature, and of counterflow diffusion flames as a function of bulk and turbulent stretch rates, partial premixing, air or fuel stream preheat, air stream dilution, and air stream dilution by hot combustion products, have been presented in this Chapter. The extinction of these flames was sudden and with the whole flame disappearing, with the exception of flames burning against hot combustion products that did not extinguish when the hot product stream was at a sufficiently high temperature, as concluded below.

Increasing the jet separation and decreasing the turbulence intensity resulted in larger, and decreasing the equivalence ratio resulted in smaller, velocity for extinction of counterflow *single premixed* flames stabilised in the stagnation flow of a reactant stream against cold air, in agreement with the expectation that extinction occurs at low values of a Damköhler number. These flames extinguished at smaller strain rates than the "twin" flames which were established by impinging identical reactant streams because in the latter configuration each flame provides heat for the stabilisation of the other.

Motivated by the possible dependence of the extinction limit on the post–flame heat loss, single counterflow flames stabilised against heated air and hot combustion product streams of temperatures up to 1750K were examined. It was found that the leanest equivalence ratio for extinction of premixed flames at constant velocity decreased slightly as the opposing stream temperature increased from room temperature to 1400K. However, above 1550K, there was a major change in the flame behaviour: no sudden extinction was observed for ultra–lean equivalence ratios down to 0.2 and the flames were ignited by the action of the opposing hot products, results in agreement with expectations from previous laminar counterflow flame experiments and analyses that showed that premixed flames stabilised against hot products never extinguish with strain rate. These ultra–lean premixed flames were further examined in terms of their composition and temperatures and it was found that the reaction zone was located, in the mean, in the region corresponding to a local temperature above 1500K, and this value is close to the product–stream temperature that marks the difference in extinction behaviour of lean premixed flames and to the final flame temperature below which chemical reaction in not self-sustaining, as found from various observations in a spectrum of flame configurations reported in the published literature. This suggests that methane–air mixtures of any composition will always burn if kept at temperatures higher than about 1500K, and the "universality" of this temperature was traced to the sensitivity of hydrocarbon combustion to chain–branching reactions.

Both the bulk and the turbulent stretching led to extinction of turbulent counterflow *diffusion* flames stabilised in the impinging flow of cold fuel and air jets, as inferred from the observation that the extinction velocity increased with jet separation and decreased with turbulence intensity. Partial premixing of the fuel with air was beneficial for stability and there was a smooth variation of extinction from diffusion to premixed flames, as also discussed in Chapter 3, with the extinction velocity increasing from pure fuel to a peak at stoichiometric mixtures. Results from different jet separations and turbulence intensities were correlated in terms of the estimated total strain rate acting on the flame, taken as the sum of the bulk stretch rate 2U/H, and the small–scale turbulent stretch rate, taken as the inverse of the Kolmogorov timescale and equal to $Re_t^{1/2}\, q'/L_{turb}$ with q' and L_{turb} calculated at the exit plane of the jet. The results of Chapter 3 show that the strain rate on the flame is different from this estimate, but the resulting correlation provides a way to describe the operational limits of counterflow burners.

Theory, however, suggests that the appropriate quantity to describe diffusion flame extinction is the scalar dissipation rate, rather than the strain rate, and estimates of the mean turbulent scalar dissipation rate $\tilde{\chi}_{st}$ were made using the results of the mixing analysis of Chapter 3. It was found that extinction occurred at a critical value of $\tilde{\chi}_{st}$ that increased with partial premixing and this result provides support for the flamelet theory of diffusion flame extinction due to Peters (1983). Quantitative differences between the mean turbulent scalar dissipation rate and the corresponding laminar dissipation rate at extinction χ_{lam} imply that the statistical nature of χ has to be considered as well as its correct modelling, but the present results suggest that a suitable Damköhler number determining the extinction of turbulent diffusion flames is $(\tilde{\chi}_{st}/\chi_{lam})^{-1}$.

The extinction of turbulent counterflow diffusion flames stabilised between impinging jets of cold fuel and of hot products from a lean premixed flame (so that oxygen was present in the vitiated air) were also measured for different temperatures and oxygen contents of the vitiated air, motivated by the current trend in combustion applications to employ exhaust gas recirculation and the need to quantify the relative effects of dilution and preheat on flame stability. The extinction velocity increased with the air temperature and the oxygen mole fraction, and for every 0.023 of oxygen mole fraction lost by dilution, the temperature had to increase by 100K to achieve the same stability and these numbers did not vary by much with temperature, oxygen mole fraction, and strain rate. The trends measured in turbulent flames agreed with trends for the extinction of laminar counterflow diffusion flames with air vitiation predicted here by using Liñan's (1974) analysis and show that large increases in flame extinction stretch rate are obtained with adiabatic hot product dilution. The transition from sudden extinction to no–extinction at high reactant temperatures, as for premixed flames, was

also demonstrated for diffusion flames with vitiated air at 1700K by the fact that such flames ignited without an external source.

Flame stability is an important consideration in realistic combustion configurations, and the present results show that the extinction of turbulent diffusion flames is associated with high values of the scalar dissipation rate and that mixing with hot products is beneficial for stability, and these findings are used to predict the extinction trends of the technologically–important flames stabilised by recirculation zones in the following Chapter.

Figures for Chapter 4

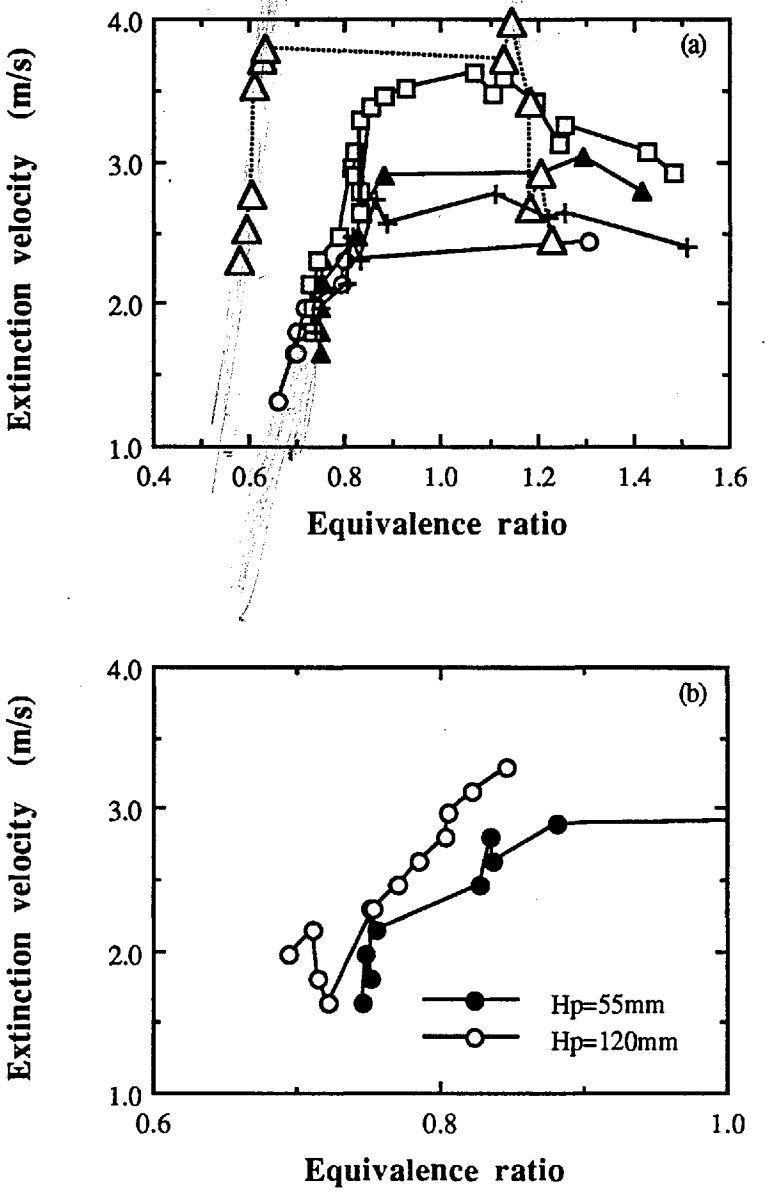


Figure 4.1 (a) The extinction velocity of single premixed flames as a function of equivalence ratio with jet separation as parameter. For all measurements, H_p=55mm. Open circles: H=10mm; crosses: H=15mm; blocked triangles: H=20mm; squares: H=25mm. For H=20mm, extinction points from twin premixed flames are included (open triangles) to compare with the single flames. (b) The extinction velocity of lean single premixed flames at H=20mm as function of equivalence ratio for two locations of the perforated plate. Large H_p results in smaller turbulence intensities at the flame due to the decay associated with the longer time from the turbulence generation (Fig. 3.2.4).

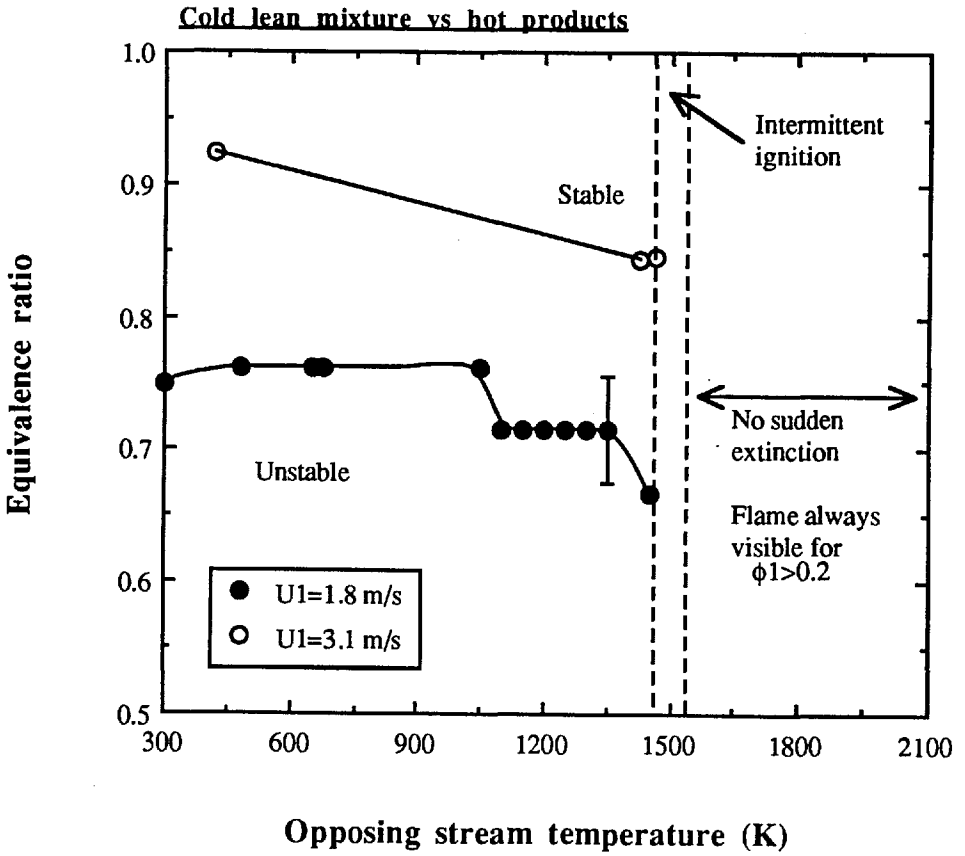


Figure 4.2 The leanest equivalence ratio for stable counterflow turbulent premixed flames as a function of the opposing stream temperature. Above 1550K, no external ignition source was needed and the flame was always visible for the lowest measurable ϕ_1 of 0.2; intermittent ignition of the flame was observed in the range $1450<T_2<1550$K. For all data, H=20mm and H_p=55mm. The oxygen content of the upper hot product stream did not affect these observations.

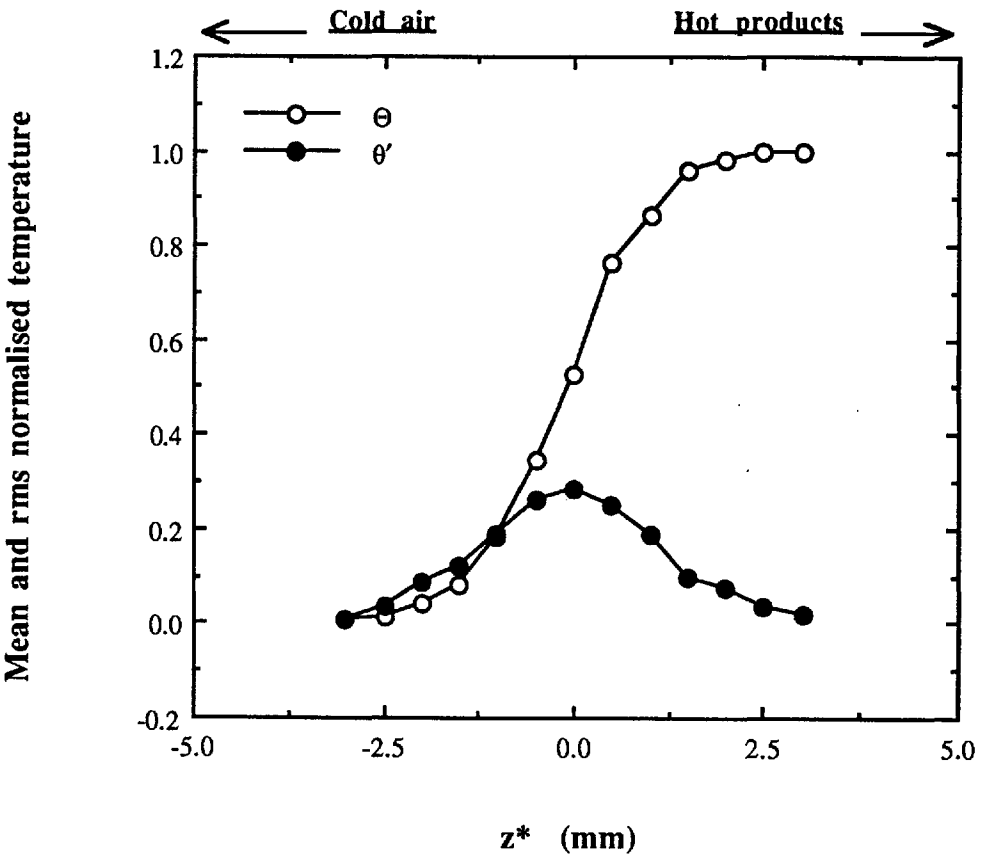


Figure 4.3 The mean (open symbols) and r.m.s. normalised temperature (blocked symbols) at a radial distance of 10mm across the mixing layer formed between a hot product stream at ϕ_2=0.63, T_2=1750K, and estimated U_2=6.1m/s, and air at T_1=300K and U_1=2.5m/s at H=20mm, H_p=55mm. H_{flame}=60mm. The flow rates were such that the momentum flow rates were equal and z* in the figure is the axial distance from the location where the mean temperature $\Theta = 0.5$. The temperature has been normalised as $\theta = (T-T_1)/(T_2-T_1)$ and $\Theta=\langle\theta\rangle$.

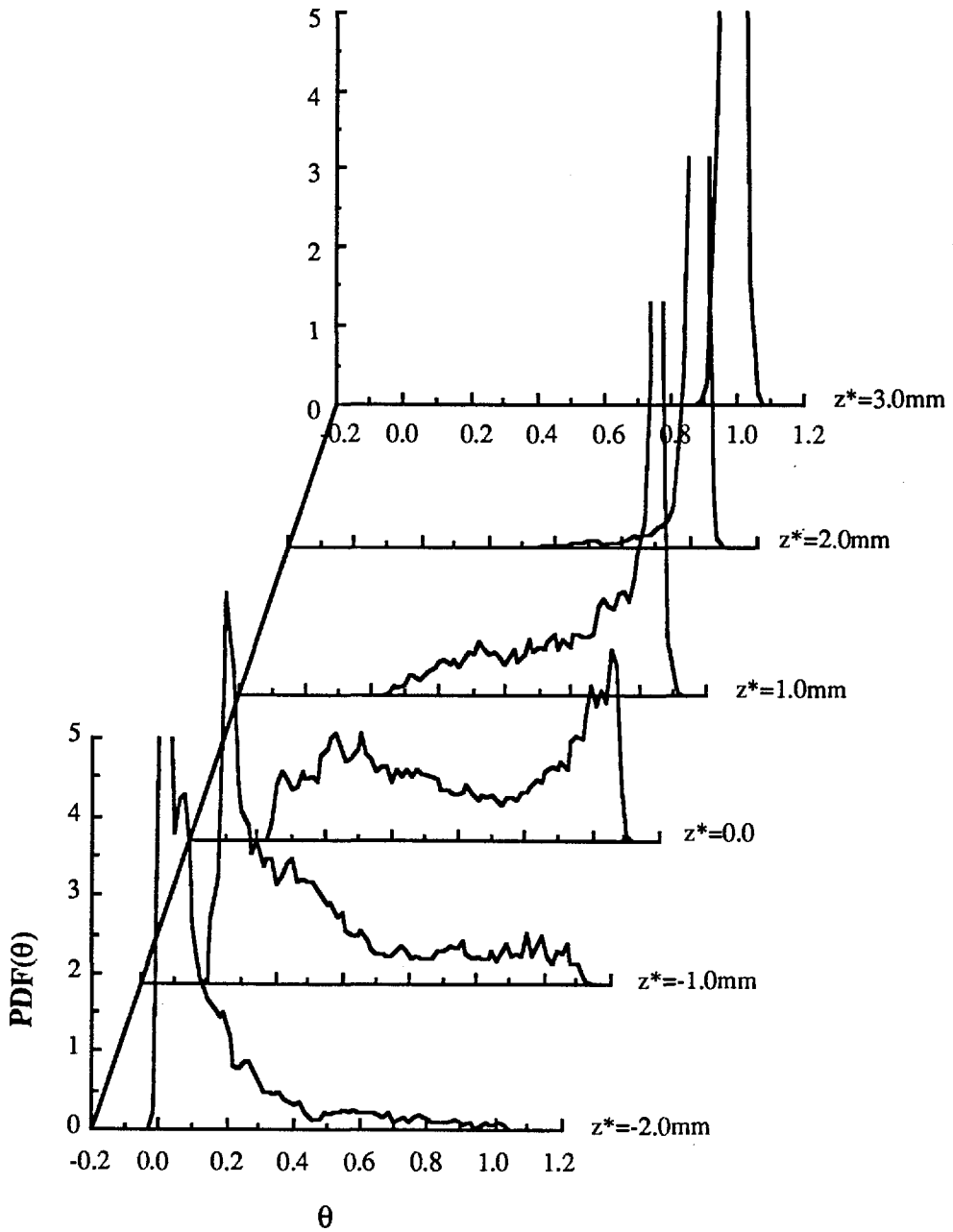


Figure 4.4 Normalised temperature probability density functions across the mixing layer under the conditions of Fig. 4.3. z* is the axial coordinate measured from the location where $\Theta = 0.5$.

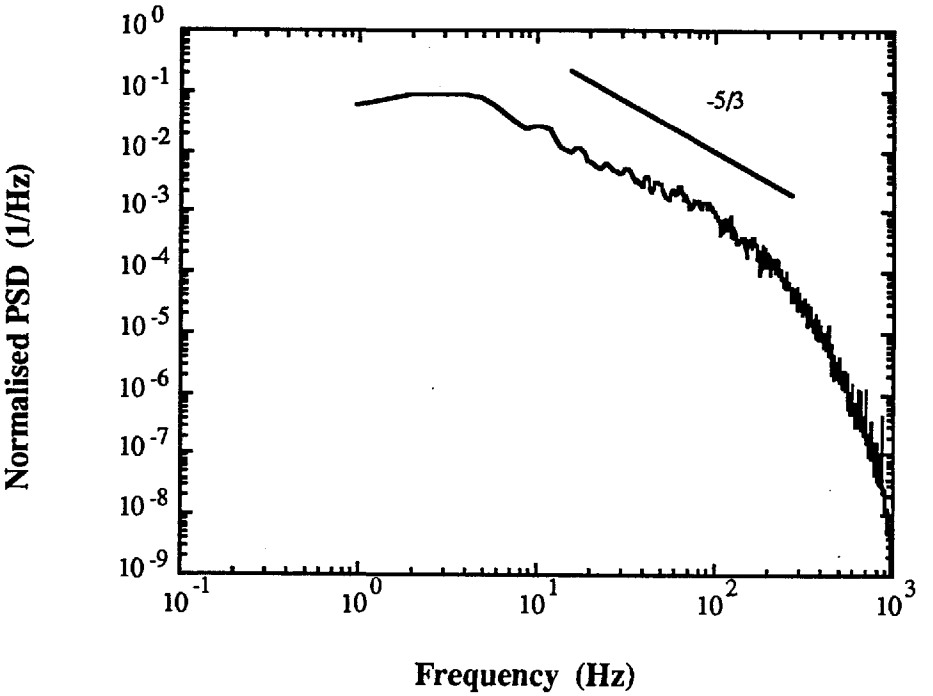


Figure 4.5 The power spectral density of the temperature fluctuations corresponding to the location of $\Theta = 0.5$ for the conditions of Fig. 4.3.

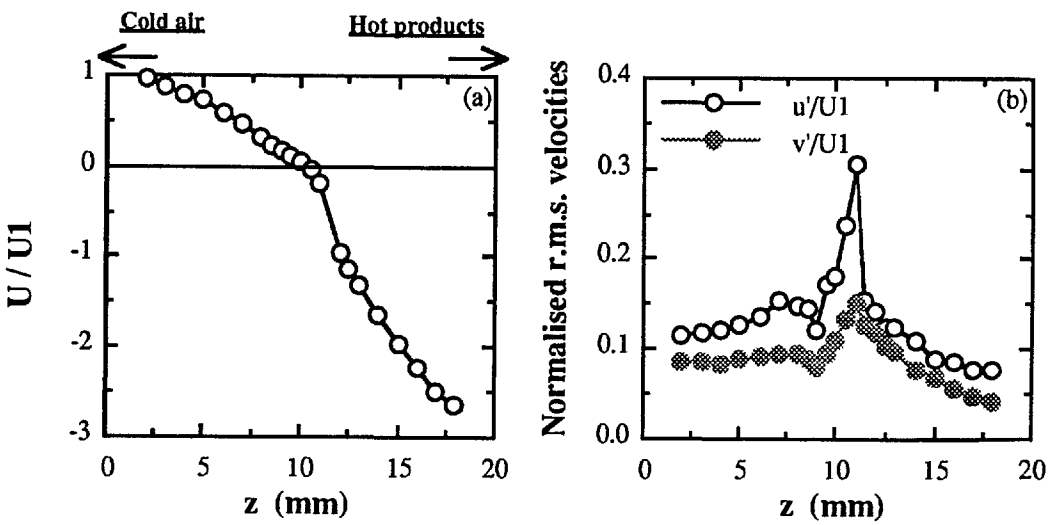


Figure 4.6 The mean (a) and r.m.s. (b) velocities along the centerline of the flow of Fig. 4.3. The velocities have been normalised by the bulk velocity U_1 in the bottom tube. z is the axial coordinate measured from the bottom nozzle.

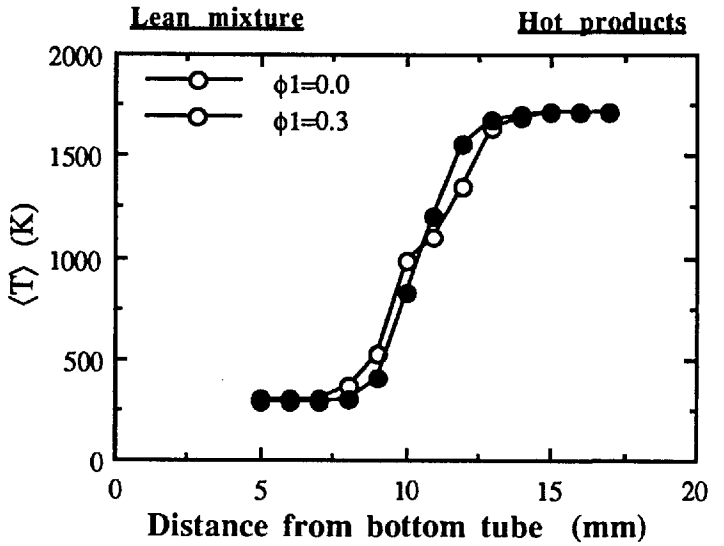


Figure 4.7 The mean temperature variation at the centreline of a mixing layer with the conditions of Fig. 4.3. Blocked circles: the bottom stream is a mixture of equivalence ratio ϕ_1=0.3; open circles: ϕ_1=0.0, same data as those of Fig. 4.3 but in dimensional form.

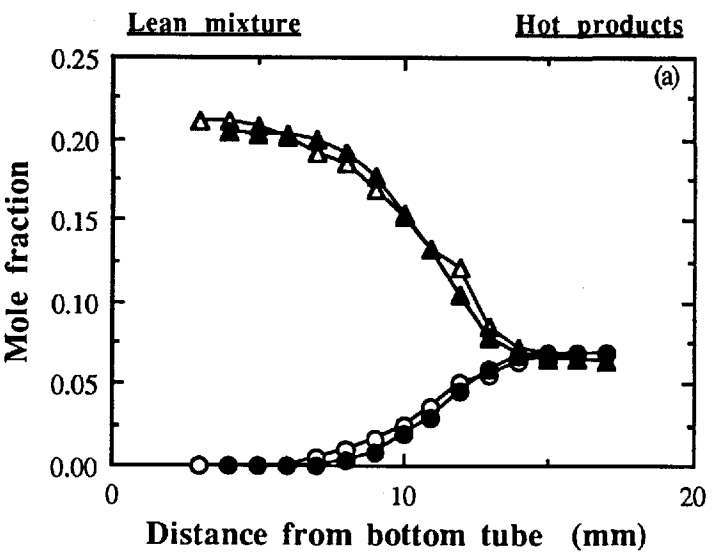


Figure 4.8 The mean concentrations across the mixing layer of O_2 (triangles) and CO_2 (circles) for the conditions of Fig. 4.7 at r=10mm. Open symbols: ϕ_1=0.0; blocked symbols: ϕ_1=0.3.

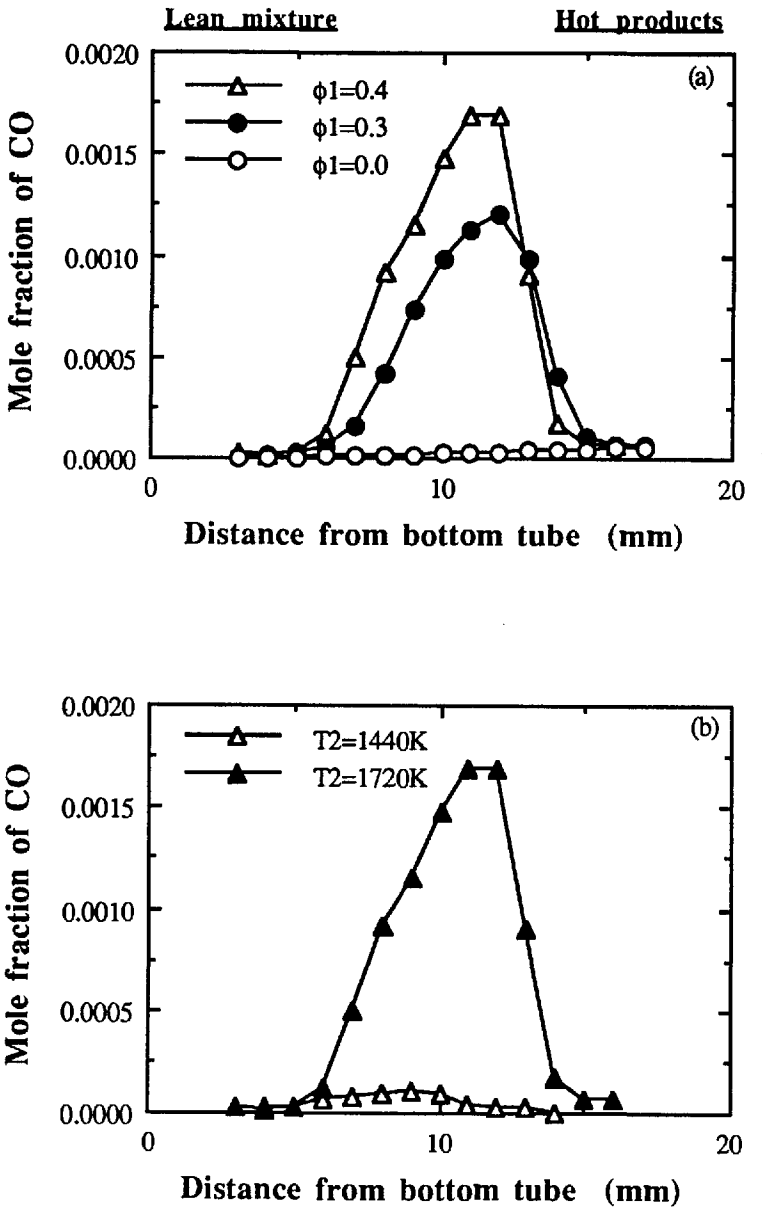


Figure 4.9 The mean concentration of CO across the mixing layer with the flow rates and geometric conditions of Fig. 4.3 for (a) different lower stream mixture equivalence ratios and (b) different temperatures of the upper opposing hot product stream. For the open triangles in (b), the distance of the "supply" flame from the nozzle exit was H_{flame}=200mm and the resulting velocity was estimated as U_2=5.1m/s.

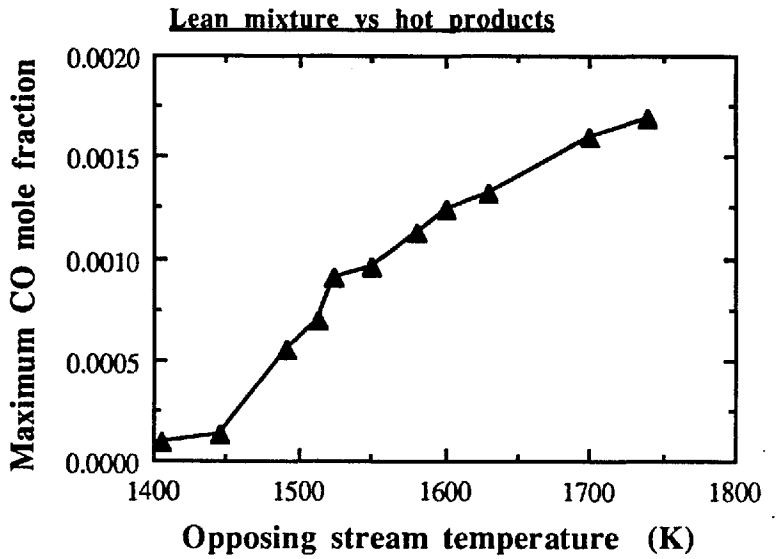


Figure 4.10 The maximum CO mole fraction in profiles such as those in Fig. 4.9 for ϕ_1=0.4 as a function of opposing stream temperature. T_2 was varied by changing ϕ_2 and H_{flame}. During these experiments, U_1 was kept constant at a value to balance the hot product flow corresponding to the highest temperature (T_2=1700K) and therefore the flow was slightly asymmetric at lower T_2.

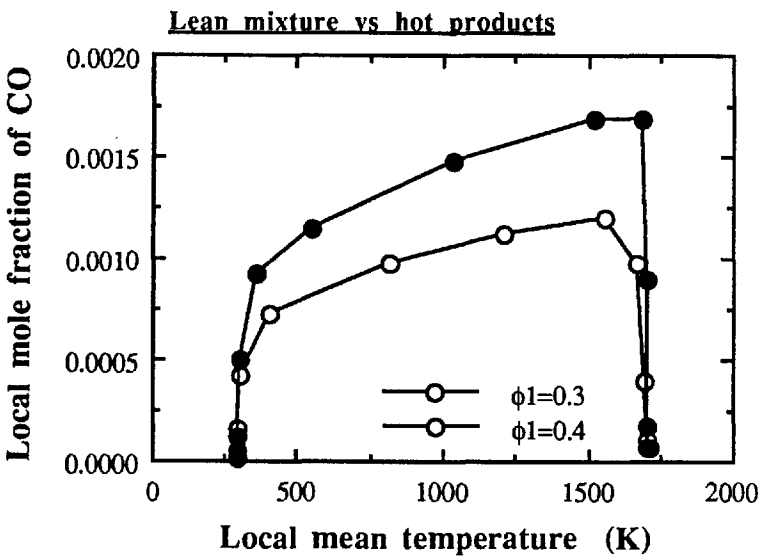


Figure 4.11 The CO mole fraction plotted as a function of the local mean temperature for the concentration data of Fig. 4.7 and temperature data of Fig. 4.9.

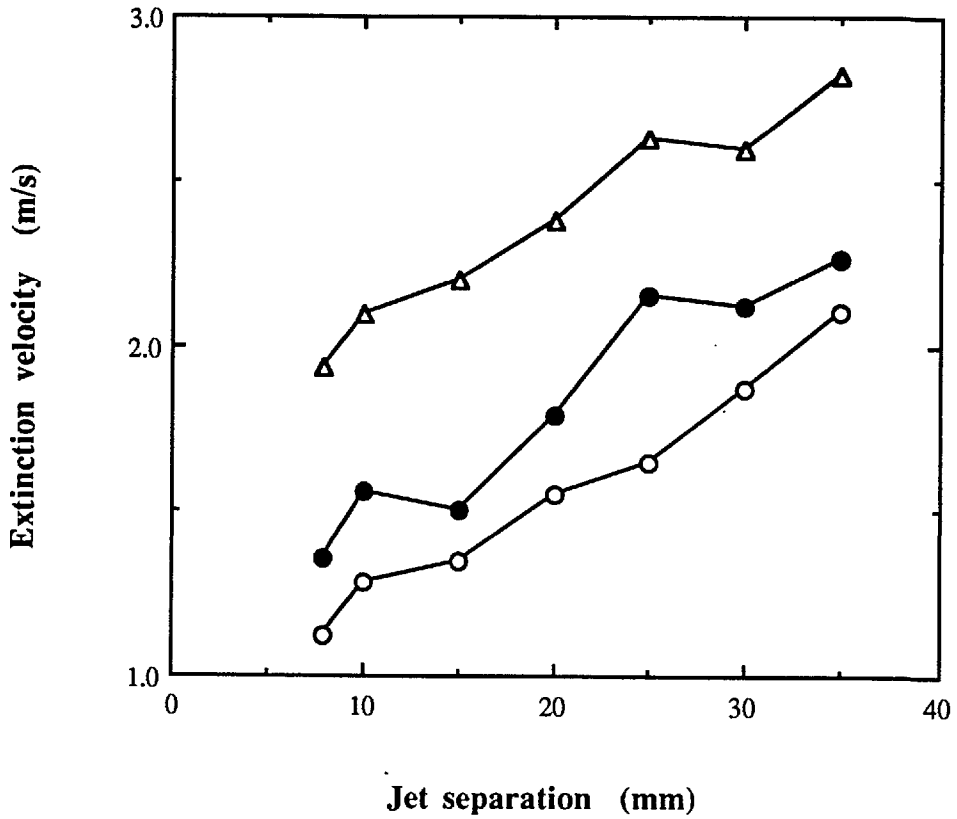


Figure 4.12 Bulk velocity at extinction of diffusion flames as a function of tube separation H for different air volume fractions in the fuel stream. Open circles : X_{air} = 0; blocked circles: X_{air} = 0.5; triangles: X_{air} = 0.8. For all measurements, H_p = 55mm.

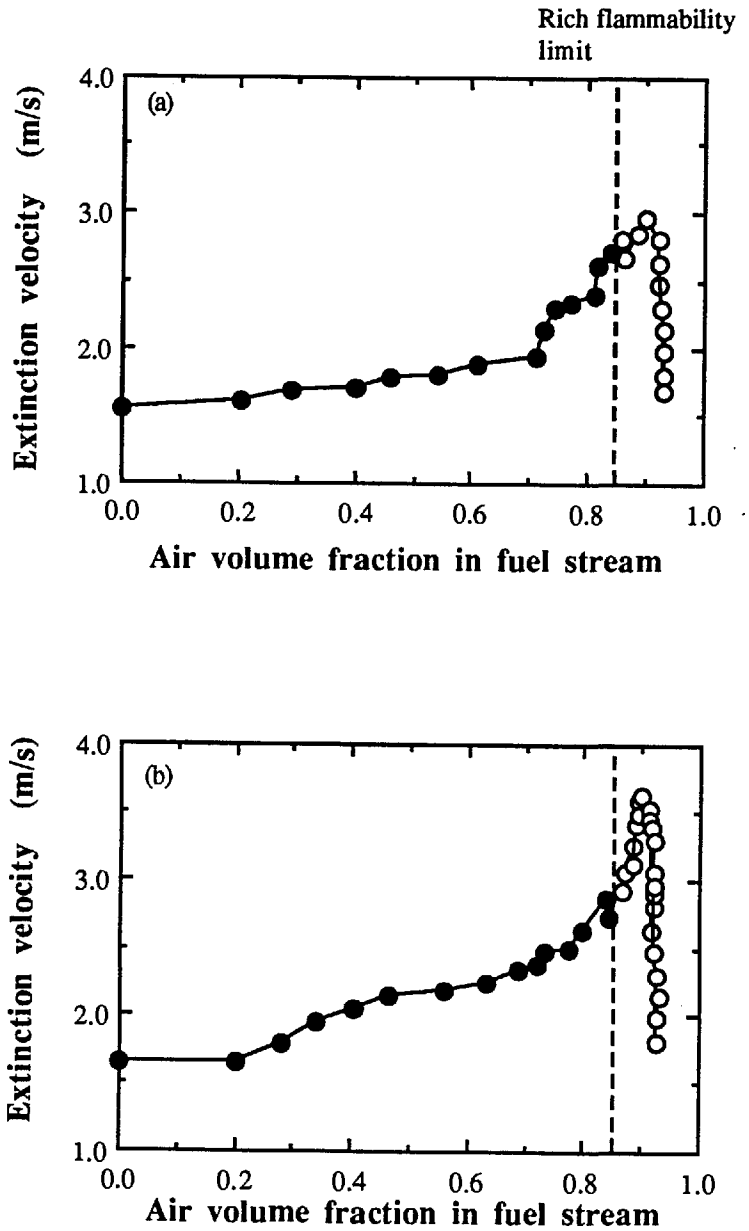


Figure 4.13 Bulk velocity for extinction as a function of air volume fraction for (a) H=20mm and (b) H=25mm. For both graphs, H_p = 55mm. Blocked symbols correspond to diffusion flames with $X_{air} \leq 0.86$, while the open symbols correspond to premixed flames with $X_{air} > 0.86$. The dashed line indicates the rich limit for premixed flame propagation.

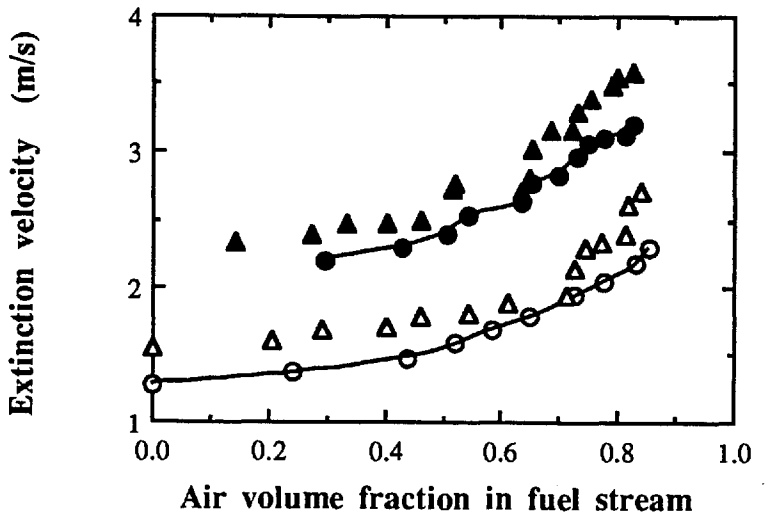


Figure 4.14 Bulk velocity for extinction as a function of air volume fraction for H_p = 55mm (open symbols) and 120mm (blocked symbols) for H=10mm (circles) and H=20mm (triangles). Large H_p results in smaller turbulence intensities at the flame due to the decay associated with the longer time from the turbulence generation (Fig. 3.2.4).

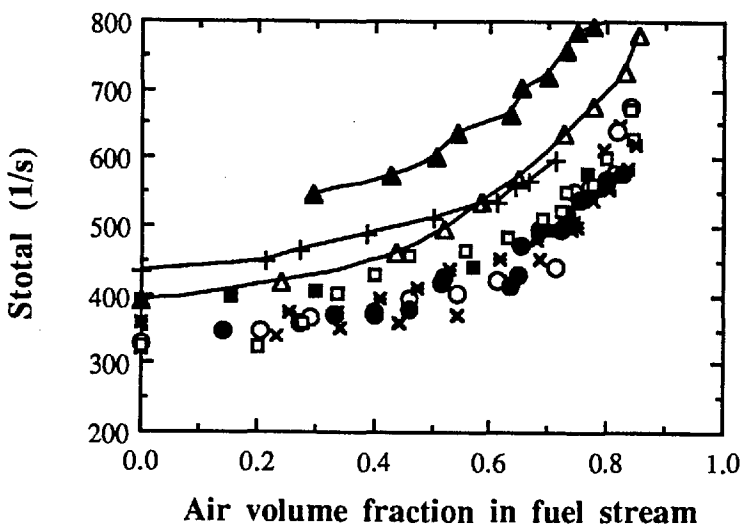


Figure 4.15 Total strain rate (Eq. 4.3.3) at extinction as a function of air volume fraction for different H and H_p. —△— : H=10mm, H_p= 55mm; —▲— : H=10mm, H_p=120mm; × : H=15mm; ○ : H=20mm, H_p=55mm; ● : H=20mm, H_p=120mm; □ : H=25mm; ✱ : H=30mm; ■ : H=35mm. Where not specified, H_p=55mm. Lines have been drawn through the data for H=10mm and H_p=120mm, H=10mm and H_p=55mm. The crosses correspond to laminar flame extinction with S_{total} being equal to 2U/H and H=15mm.

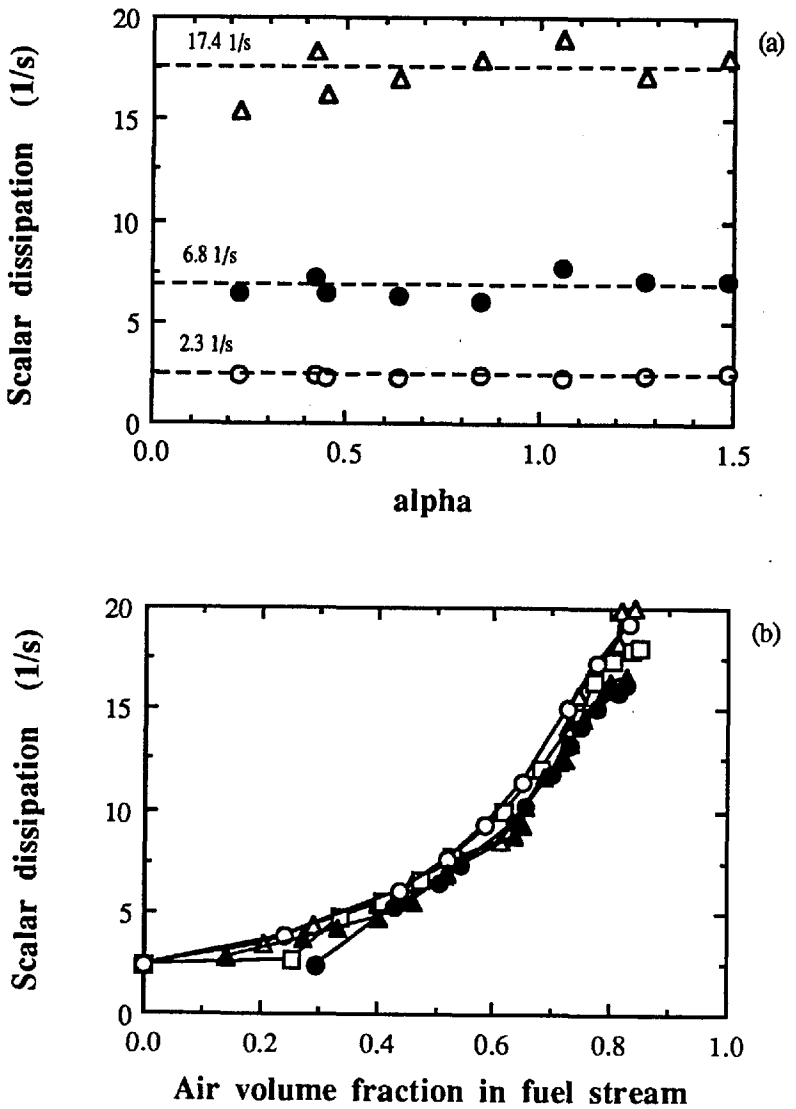


Figure 4.16 (a) Estimated scalar dissipation rate from Eq. (4.3.4) at extinction for different values of α ($=2q'H/UL_{turb}$; Section 3.2.5) for air volume fraction X_{air} equal to 0 (open circles), $X_{air} = 0.5$ (blocked circles), and $X_{air} = 0.8$ (triangles). See Section 4.3.4 for the determination of α in terms of the geometrical parameters in the counterflow flame. (b) Estimated scalar dissipation rate at extinction against air volume fraction from many experimental conditions. Symbols are as follows: H=10mm, H_p=55mm (open circles), H=10mm, H_p=120mm (blocked circles), H=20mm, H_p=55mm (open triangles), H=20mm, H_p=120mm (blocked triangles), and H=30mm, H_p=55mm (squares).

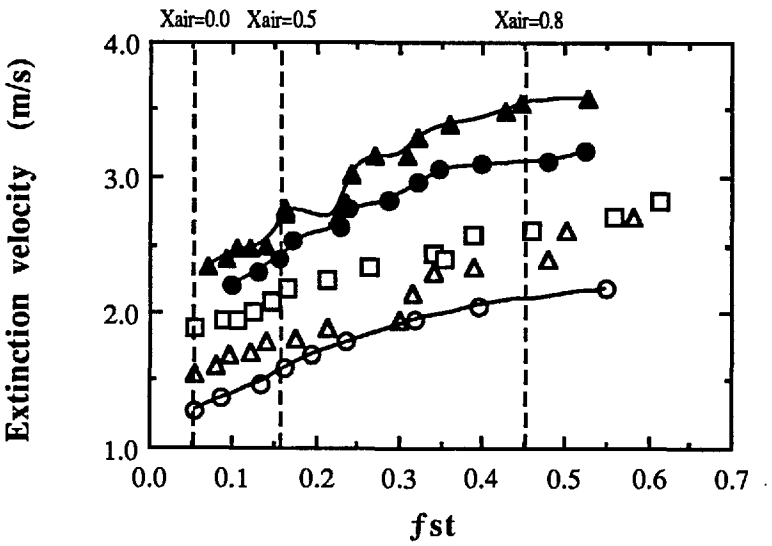


Figure 4.17 Data of the bulk velocity at extinction from Fig. 4.15 plotted as a function of stoichiometric mixture fraction f_{st} using the relationship between X and f_{st} in Eq. (4.3.5). Symbols as in Fig. 4.16b.

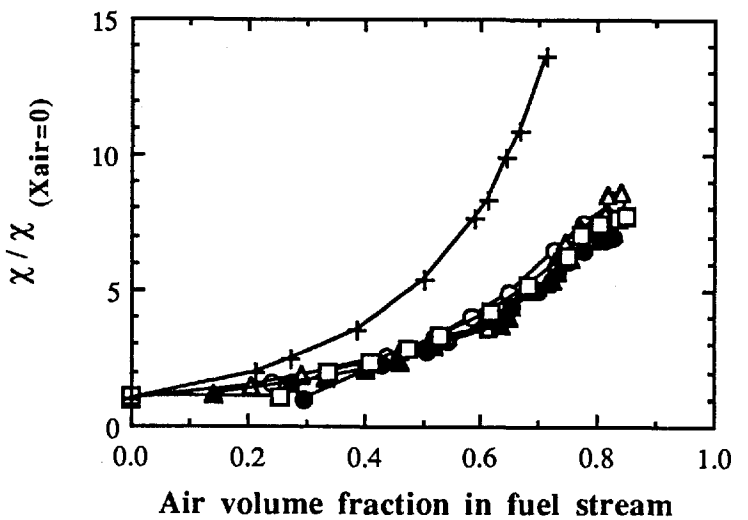


Figure 4.18 Ratio of the turbulent mean scalar dissipation rate data of Fig. 4.16b normalised by the average value for the flames without premixing (2.3 s^{-1}) against air volume fraction. Symbols as in Fig. 4.16b. Included are similarly normalised estimates of the laminar scalar dissipation rate calculated with Eq. (4.3.6) and experimental data for laminar partially premixed flames from Fig. 4.15 (crosses). The laminar scalar dissipation rate for the flame without premixing is 10.7 s^{-1}.

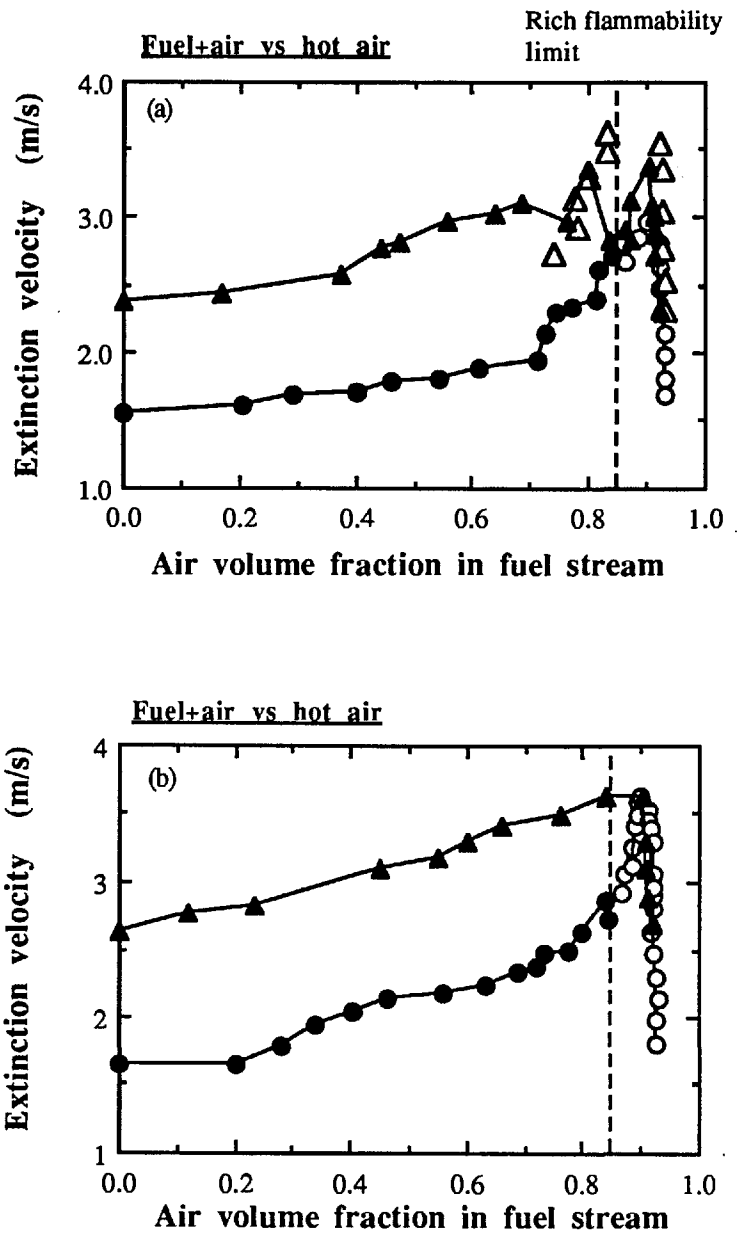


Figure 4.19 The extinction velocity of pure, partially premixed diffusion, and fully premixed flames as a function of the air volume fraction in the fuel stream for different conditions of opposed air stream preheat. Open circles: premixed flames with $\phi_1<1.6$; blocked circles: diffusion flames. Both correspond to unheated reactants. Blocked triangles: Air stream heated to 420K; open triangles: stream containing the fuel heated to 420K. H=20mm for (a) and H=25mm for (b). The data of unheated flames are from Fig. 4.13. For all data, H_p=55mm, X_{ox}=0.21, i.e. ambient air, the preheat was achieved by electric heating, and the flames were stabilised in the burner without the "supply" flame operating.

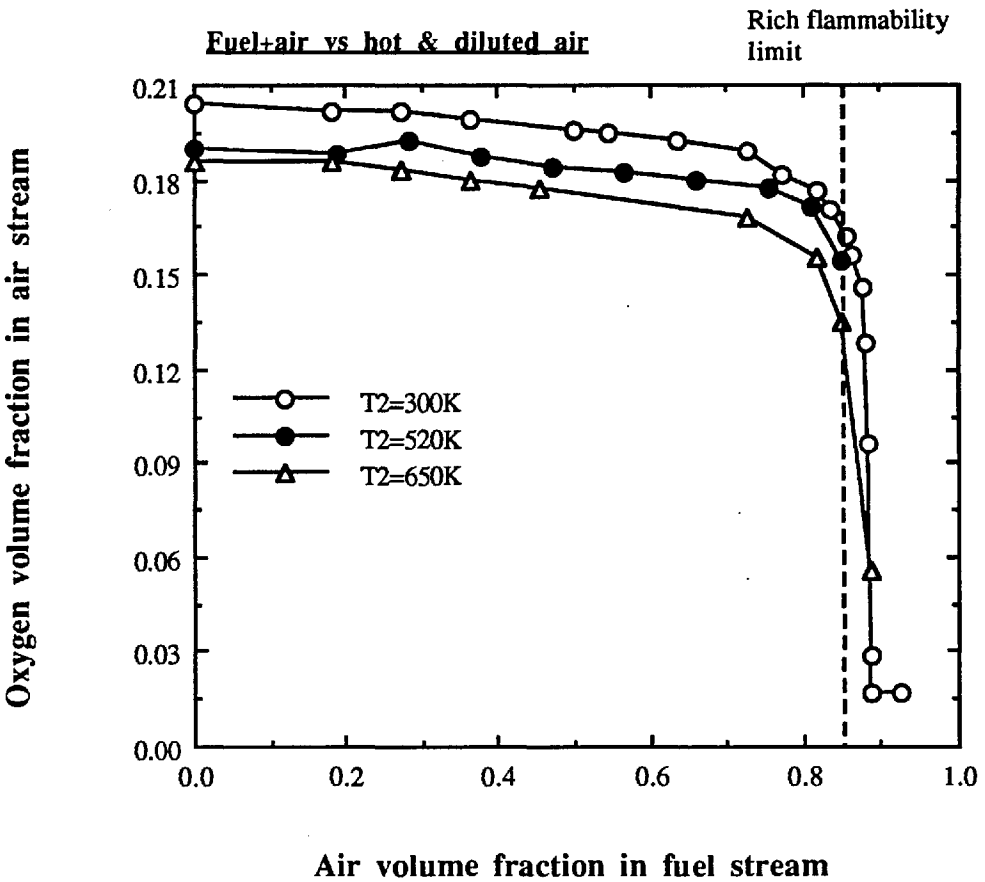


Figure 4.20 The minimum oxygen mole fraction required in the oxidiser stream for flames ranging from pure diffusion to fully premixed as a function of the air volume fraction in the fuel stream with opposed air stream temperature as parameter. The air premixed with the fuel was at ambient temperature and undiluted, while that in the oxidiser stream was diluted by nitrogen and electrically preheated, apart from the open triangles for which the preheat was achieved by mixing O_2–N_2 mixtures with hot products. Data for X_{air} higher than the dashed line correspond to premixed flames and all measurements were taken at the same fuel stream bulk velocity of 1.5m/s, H=20mm and H_p=55mm, so that the stretch rate was approximately the same as that at the extinction of unheated, unpremixed fuel burning in unheated, undiluted air (Fig. 4.12). This condition is referred to as $S_{vil}/S_{ref}=1$ in the text and in Fig. 4.24 and these flames were established in the burner shown in Fig. 2.3a.

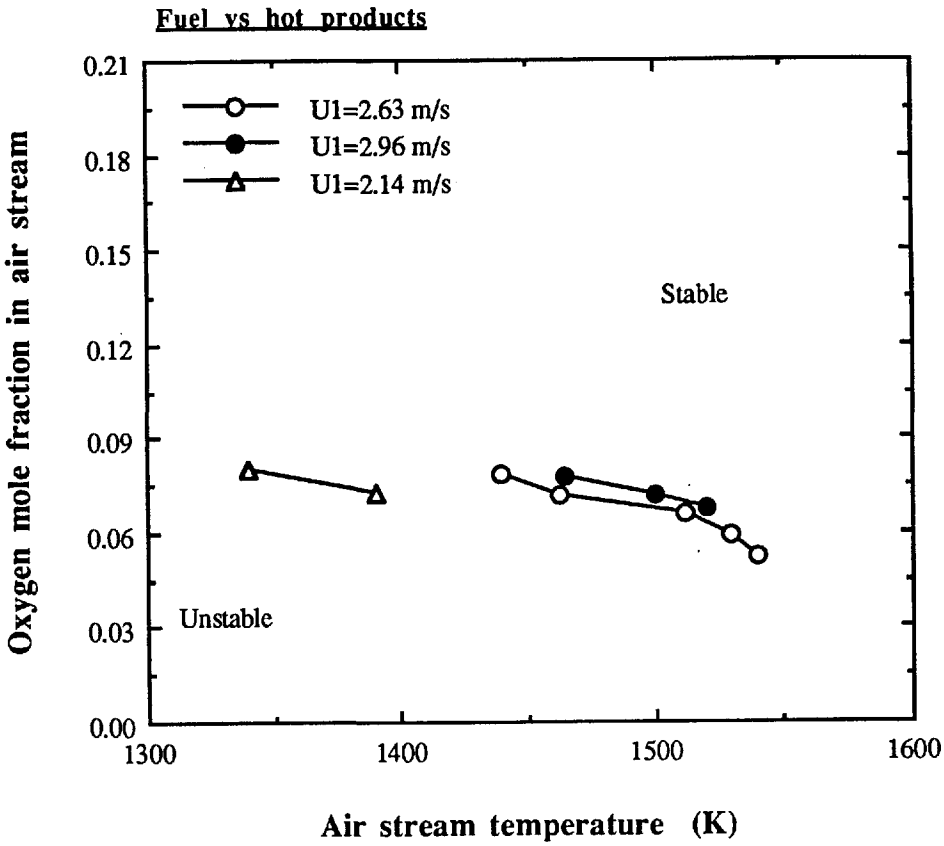


Figure 4.21 The minimum oxygen mole fraction in the hot product stream as a function of the temperature for counterflow turbulent diffusion flames of unheated, unpremixed fuel against the hot products of the lean "supply" flame for different bulk velocities. These flames were established in the burner shown in Fig. 2.3b and the data do not extend to higher T_2 because of the inability of the flow supply system to achieve higher fuel flow rates needed for extinction at high temperatures. One experiment showed that for T_2>1700K the flames would not extinguish suddenly, but the temperature corresponding to the transition between sudden and no extinction was not measured in detail (see Fig. 4.2 for equivalent measurements for premixed flames). The oxygen concentration was varied by changing the equivalence ratio and the temperature was also affected by the positioning of the supply flame relative to the top burner exit plane.

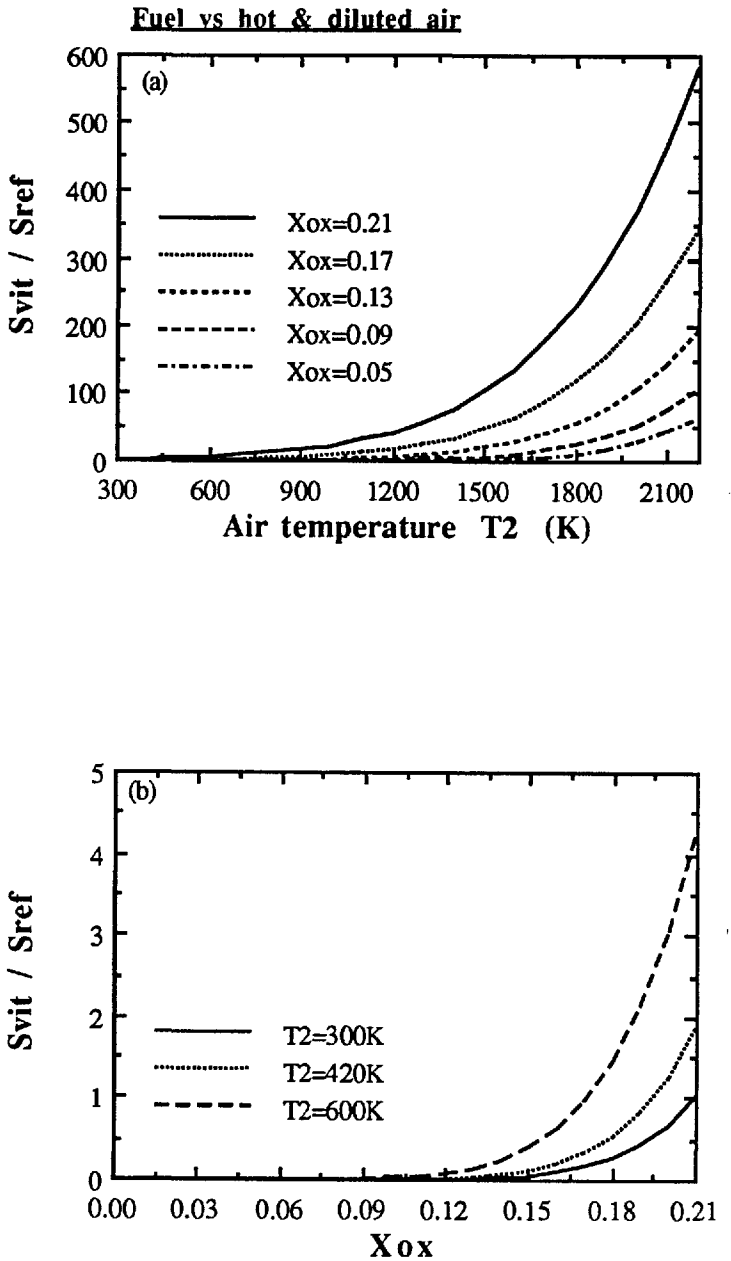


Figure 4.22 The predicted from Eq. (4.3.16) S_{vit}/S_{ref} for laminar counterflow pure diffusion flames as a function of air temperature for different oxygen mole fractions (a), and as a function of oxygen mole fractions in the oxidiser for different temperatures (b).

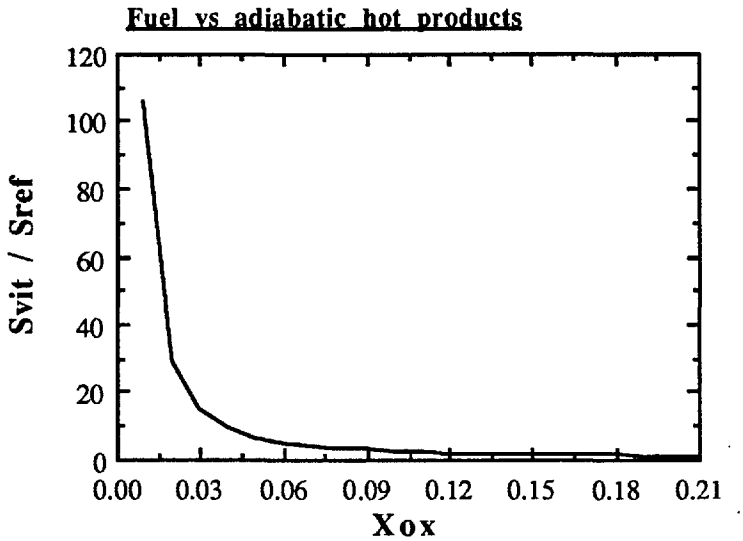


Figure 4.23 Predictions of Eq. (4.3.16) for laminar counterflow pure diffusion flames for the special case of adiabatic hot product dilution during which the oxidiser oxygen concentration and temperature are related by Eq. (4.3.17). Note that S_{vit}/S_{ref} is always larger than unity.

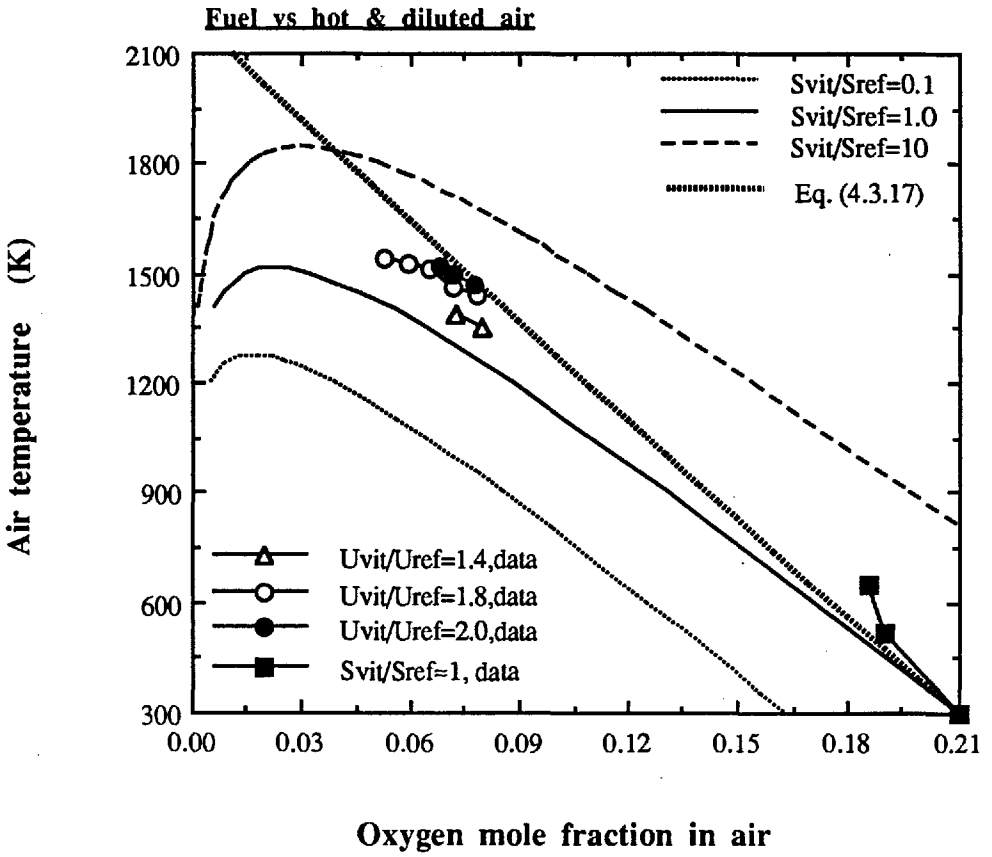


Figure 4.24 Contours of S_{vit}/S_{ref} from Eq. (4.3.16) in the $X_{ox} - T_2$ plane. Measurements are superimposed: the data of Fig. 4.21 for U_1=2.14m/s (open triangles); U_1=2.63m/s (open circles); U_1=2.96m/s (blocked circles); and data from Fig. 4.20 for X_{air}=0.0 (blocked squares). U_{ref} = 1.5m/s, i.e. the fuel velocity at extinction of the turbulent counterflow diffusion reference flame with unpremixed, unheated fuel burning with the unheated, undiluted ambient air with H=20mm and H_p=55mm, and this value is taken from Fig. 4.12. The heavy dotted line traces the adiabatic hot product dilution with the accompanying temperature rise (Eq. 4.3.17). Note that the slope of the data is similar to slope of the predicted contours and that the heavy dotted line is steeper than both which means that there is "room" for heat losses during self–vitiation before the stability becomes worse than the unvitiated case.

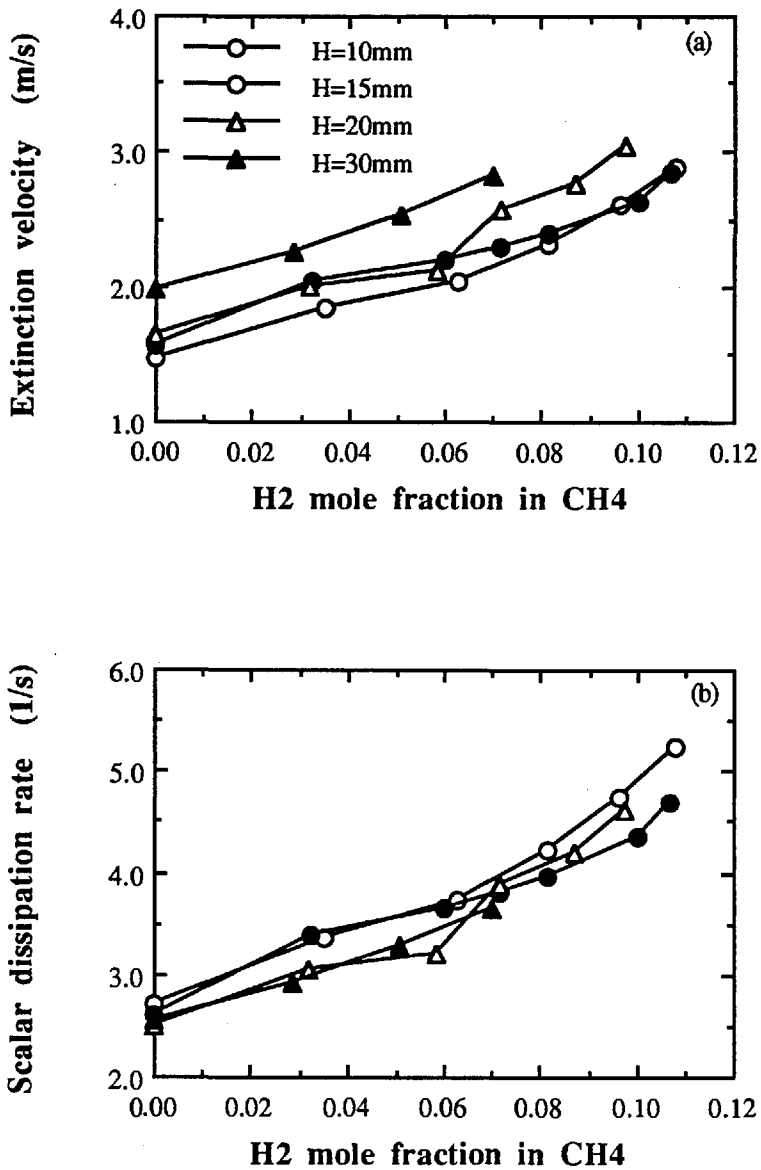


Figure 4.25 (a) Extinction velocity of turbulent counterflow pure diffusion flames with H_2–natural gas mixtures as fuel as a function of hydrogen mole fraction with the jet separation as parameter. For all measurements ambient air was used and H_p=55mm. (b) The scalar dissipation rate estimated as in Section 4.3.4 for the data of (a).

Chapter 5. Conjectures on the extinction of non–premixed flames stabilised by recirculation zones

5.1 INTRODUCTION

5.1.1 Purpose of this Chapter

Turbulent flames stabilised by recirculation zones have received attention because such configurations are used in most combustion applications, as in gas turbines and industrial burners of gas, liquid, or solid fuels. The stability of such flames is important, especially in view of current practice of lean operation to avoid excessive formation of pollutants, and hence research is needed to provide information on the operating conditions under which extinction occurs. A lot of work has been performed on laboratory–scale flames and efforts have been made to use these experiments to create correlations used to predict the extinction limits of flames in larger–scale combustors, and the success and generality of such correlations depends on how realistic are the physical foundations on which they are based. As will be shown by the literature review in this Section, existing correlations for the lean stability limits of recirculating non–premixed flames do not take into account the turbulent scalar dissipation rate, which is the aerodynamic quantity that determines extinction as concluded in Chapter 4, and so provide physically incomplete descriptions.

The aim of this Chapter is to present estimates of the scalar dissipation rate in recirculating non–premixed flames that result in a new scaling law for the approach to extinction which may be used to extrapolate from results in small–scale experiments to realistic–scale configurations. The description proposed here also qualitatively explains measured extinction trends that were not up to now well–understood and is hence expected to represent correctly the extinction of non–premixed recirculating flames.

Because the stability of such flames has been previously described by approaches originating from the extinction of *premixed* flames, a literature review of both types is given below.

5.1.2 Stability of recirculating premixed flames

As early as the late 40's, the stabilisation of flames in high-velocity premixed streams received attention because of the relevance to after–burners and rocket combustors. In most cases of flame stabilisation, a bluff–body is placed in the flow in order to create a recirculation zone and numerous theories have been proposed to explain and predict the stability limits of bluff–body premixed flames. There are two types of stability limits for such flames: the first is when the velocity is low and the flame flashes

back upstream of the bluff body into the mixture. The second, more important in practice and the one that will be examined here, is when the mixture velocity is high enough for the flame to blow–off the bluff body.

Longwell *et al.* (1953) assumed that chemical reaction is initiated and completed inside the recirculation zone that is uniform in composition and temperature and thus is similar to a well–stirred reactor. Because the convective heat transfer from the reactor eventually exceeds the heat release due to the chemical reaction, the temperature of the reactor falls and the reaction abruptly ceases, and so there is a maximum amount of reactants that can be consumed in the reactor. Extinction was predicted to occur when a chemical time becomes long compared to the residence time in the reactor, and Spalding and Tall (1954) showed that the result of Longwell *et al.* was equivalent to

$$\frac{U_b D}{\alpha_{th}} > C\left(\frac{S_L D}{\alpha_{th}}\right)^2 , \qquad (5.1.1)$$

where each grouping was interpreted as a Peclet number, U_b is the blow–off velocity, D a characteristic size of the flameholder, S_L the laminar flame speed of the mixture, α_{th} the thermal diffusivity, and C a constant. Spalding and Tall (1954) showed that dimensional analysis also leads to Eq. (5.1.1) and so a Peclet number correlation was proposed to be of general applicability for premixed flames stabilised by bluff bodies. The result of Longwell *et al.* (1953) is physically sound for a well–stirred reactor, but objections arise as to whether chemical reaction occurs *inside* the recirculation zone of bluff–body premixed flames because it is evident from measurements that the RZ is a volume of almost inert hot reaction products.

Zukoski and Marble (1956) correlated experimental measurements of blow–off limits by assuming that extinction occurs when the ignition time of the mixture, given by a timescale τ_{chem}, is longer than the residence time, given by L_{RZ}/U_b with L_{RZ} the length of the recirculation zone, i.e.

$$\frac{U_b}{L_{RZ}} > \frac{C}{\tau_{chem}} . \qquad (5.1.2)$$

The physical basis for this correlation is that the hot products of the recirculation zone mix with the reactants flowing outside it and that a flame will be established only when ignition of the reactants is successful. Marble and Adamson (1954) considered an idealisation of this mechanism by examining a laminar mixing layer between cold reactants and hot combustion products and found that the "time–of–flight" to the ignition point increases with the hot stream temperature and the mixture strength, as expected. In this view of bluff–body flame stabilisation, which is widely accepted (Beér and Chigier,

1972), it is the ignition of the reactants by mixing with the hot combustion products that provides the physical mechanism for flame stabilisation, and the importance of the mixing process between the recirculation zone and the incoming mixture in the shear layer is emphasised. Equation (5.1.1) is equivalent to Eq. (5.1.2) because the chemical timescale τ_{chem} can be written as the inverse of S_L^2/α_{th} and L_{RZ} is proportional to D, and a similar correlation has also been proposed by Plee and Mellor (1979).

Radhakrishnan *et al.* (1981) used a model of combustion in Kolmogorov–scale vortices and found that they could predict successfully the blow–off limits of bluff–body stabilised flames by using a model for the occurrence of extinctions in the small scales and reasonable expressions to relate the small–scale turbulence properties of the shear layer to U_b and L_{RZ}. Their result reduced to Zukoski and Marble's (1956) empirical expression and this equivalence emphasises the general applicability of Eq. (5.1.2) for bluff–body stabilised flames and is consistent with the expectation that in premixed flames the speed of the reaction is everywhere given by the same chemical timescale and that an aerodynamic timescale can be formed by L_{RZ} (or D) and U_b.

It is clear that the criteria proposed in the literature for the extinction of bluff–body stabilised premixed flames are equivalent to each other and there is general agreement that extinction occurs when U_b/D exceeds a critical value which is a function of the chemical timescale and the flameholder shape. Below, similar correlations are reviewed for *non–premixed* flames and it will be shown that no such consensus exists.

5.1.3 Stability of recirculating non–premixed flames

In non–premixed recirculating flames, the recirculation zone is usually established by a bluff body or by swirl and the fuel is injected at the centreline either axially or at an angle to the annular air flow. There are two types of stability limits for these flames: the rich limit usually involves flame lift–off and is due to large quantities of fuel with the fuel jet penetrating the recirculation zone and the resulting flame is analogous to a lifted jet diffusion flame and can be treated with the same concepts (Feikema *et al.*, 1990). The lean stability limit, which will be examined here, corresponds to the minimum amount of fuel that can burn stably with a given amount of air and is hence proportional to an overall equivalence ratio ϕ. It will be shown below that no satisfactory physical arguments exist in the literature for explaining the lean extinction limits.

The few measurements of lean extinction limits of swirl–stabilised diffusion flames that exist (Rawe and Kremer, 1980; Milosavljevic *et al.*, 1990a; Feikema *et al.*, 1991; Prade and Kremer, 1992) show that the minimum equivalence ratio, ϕ_{min}, increases with the air flow and the swirl number and that ϕ_{min} decreases with increasing burner size. Other trends will be examined in more detail in Section 5.3. It is important to realise that the equivalence ratio here refers to the *overall* equivalence ratio, not the local one, and that the flame is found at locations with approximately stoichiometric

fuel:air ratio. The location of the stoichiometric contour depends on the mixing pattern between the fuel and the jet, and motivated by the fact that these patterns can be different under different conditions of fuel flow rates and air swirl number, different physical explanations for the above mentioned trends have been put forward by various authors.

Rawe and Kremer (1980) suggested that close to the lean limit the flame is found at locations with high velocities, and therefore is de–stabilised in, presumably, the same way that a premixed flame is de–stabilised at high velocities. This physical explanation is similar to one of the mechanisms proposed for the lift–off of jet diffusion flames (Pitts, 1988) and it is not clear why it may be applied to the lean limit of *attached* flames. Rawe and Kremer (1980) proposed, with a correlation with dimensionless Peclet numbers motivated by the extinction of bluff–body premixed flames, that extinction occurs when

$$\frac{Sw U_b L_{RZ} R}{\alpha_{th}} > C \left(\frac{S_L L_{RZ} R}{\alpha_{th}} \right)^{1.6}, \qquad (5.1.3)$$

where Sw is the swirl number, the grouping SwU_b denotes the tangential velocity at the flame, R is a geometric parameter and equal to the ratio of the diameter of the fuel injector (D_{inj}) to the diameter of the annular air flow (D), and S_L is the laminar flame speed of a stoichiometric mixture. If the exponent in the r.h.s. was 2, and not 1.6, Eq. (5.1.3) would reduce to Eq. (5.1.2), and so it is concluded that this correlation reduces, approximately, to a Damköhler number (or residence time) criterion.

Feikema *et al.* (1991) found that the flame is located close to the fuel nozzle at lean extinction and so proposed that the large velocity gradients in the opposed flow between the fuel and the recirculating gases extinguished the flame. Although it is reasonable to state that high bulk stretching leads to extinction, this explanation for the specific flows may be false: these authors claimed that the flame is stable at high fuel jet velocities because the flame is located at regions of low velocity gradients, but it is more probable that when the fuel velocity increases, the velocity gradient at the fuel–air mixing region increases, and this should have a de–stabilising effect on the flame – contrary to experiment. Feikema *et al.* (1991) presented an approximate correlation of their experimental data from different burners in terms of ϕ_{min} plotted as a function of U_b/D and it was shown that ϕ_{min} increases with U_b/D along a unique curve but with large scatter, and so did not provide conclusive evidence that U_b/D is the appropriate parameter to describe extinction of recirculating non–premixed flames.

Although the experimental trends that increasing the bulk air velocity or the swirl number leads to extinction may be reasonably explained because the strain rate acting on the flame becomes high, there are other experimental trends that are not well–understood. Milosavljevic *et al.* (1990a) measured extinction data similar to those of Rawe and

Kremer (1980) and Feikema *et al.* (1991), but also found that long recirculation zones, created by long diffusers, deteriorate stability, so that the lean limit ϕ_{min} is higher than for short recirculation zones. Note that the criterion based on the aerodynamic timescale L_{RZ}/U_b in Eq. (5.1.3) predicts the *opposite* trend to that found in the experiment because it suggests that long recirculation zones are beneficial to stability. Finally, note that a physical explanation for the dependence on extinction on recirculation zone length has not been proposed yet.

This review showed that, unlike the state of knowledge for premixed flames, there has not been yet a successful lean stability prediction for diffusion flames stabilised by recirculation zones, and, more importantly, that the proposed physical mechanisms for flame extinction under lean conditions are not clear and they lack fundamental foundation. The difficulty for diffusion flames stems partly because of the need to examine the mixing between the fuel and the air flow and partly because the exact mechanism of local turbulent diffusion flame extinction is still the subject of research. There have been, it seems, no attempts yet to predict, with a complete numerical model, the *lean* stability limits, the way it has been done to predict *rich* stability limits (Bradley *et al.*, 1990; Chakravarty *et al.*, 1984), and so the way recirculating overall–lean diffusion flames are extinguished by too large an air flow still calls for explanation. It is hence challenging to attempt to apply the knowledge of extinction from Chapter 4 to, more interesting in practice, recirculating flames.

5.1.4 Structure of this Chapter

In the next Section, the stabilisation mechanism of non–premixed recirculating flames is discussed and in Section 5.3, estimates of the scalar dissipation rate and of an average temperature in the recirculation zone are made and used to explain qualitatively all the measured dependencies of the lean limits. The way extinction results from small–scale experiments may be scaled to larger–scale burners is discussed in the context of the proposed extinction criterion. The Chapter closes with a summary of the main findings in Section 5.4.

5.2 STABILISATION OF NON-PREMIXED RECIRCULATING FLAMES

Consider a swirl–driven recirculation zone (RZ) into which fuel is introduced at the centreline axially against the backflow. Usually, a diffuser (quarl) is placed at the inlet plane of the reactants (the throat) to promote a stronger recirculation and the central jet consists of unpremixed gaseous fuel and the annular swirling jet is ambient. This is the configuration used by Feikema *et al.* (1991), while Namazian *et al.* (1988) used a bluff–body to induce the recirculation zone. Milosavljevic *et al.* (1990a) also examined flames with fuel injected at a small angle and normal to the air flow by an annular and a radial injector respectively, but close to the lean extinction limit the momentum of the fuel jet was small compared to the momentum of the air flow, and therefore all the above configurations are qualitatively similar in the way the fuel and air mix.

Figure 5.1 shows a conceptual model of a recirculation zone induced by swirl with axial injection of fuel from a nozzle of diameter D_{inj} at velocity U_f centrally placed to an annular flow of air at a bulk velocity U_b at a diameter D. The heavy line in the Figure represents one possible realisation of the instantaneous contour of stoichiometric mixture fraction, while the light dashed lines represent contours leaner and richer than the stoichiometric to indicate the spatial width of the mixing layer between the fuel and the air flow. Subject to favourable conditions, most of the combustion will occur close to the stoichiometric contour and then it is possible, but not necessary, to have chemical reaction everywhere along the f_{st} contour; the flame is initiated somewhere along the f_{st} contour and some of the products so created flow back inside the central region of the RZ.

It is widely accepted that the hot products in the recirculation zone ignite the reactants, as in a premixed flame, but a factor often overlooked in this statement is that the heat transfer from the products to reactants occurs simultaneously with dilution, and so it is not clear whether reaction along the *inside* f_{st} contour is possible due to low oxidant concentrations there. However, results from Section 4.3.5 indicate that combustion *is* indeed possible because the high temperature wins over the reduced oxygen concentrations for usual operating conditions (temperatures in the range 1300 – 1600K, oxygen mole fractions in the range 0.03 to 0.06; Milosavljevic, 1993). Furthermore, because diffusion flames using hot products as oxidant withstand higher strain rates than flames with ambient air by increasing the reaction rates (Section 4.3.5), combustion is perhaps more favourable along the inside than in the outside part of the f_{st} contour of Fig. 5.1. Therefore it is expected that the temperature of the gases in the recirculation zone, T_{RZ}, affects the extinction limits of the recirculating flame, and evidence for the connection between low temperatures and lean extinction is provided by

the data of Rawe and Kremer (1980) who measured decreasing T_{RZ} with approaching extinction.

There are four regions along the contour, marked A to D in Fig. 5.1, differing mostly in the composition of the gases far from the mixing layer in a direction normal to it. Point A involves mixing between the central fuel jet and the recirculating gases and is reminiscent of the counterflow flames described in this thesis, while point B involves mixing along the shear layer between the fuel and the air flow and is reminiscent of mixing in a jet. Points C and D denote, respectively, flames at the shear layers between the fuel and the annular air, and the recirculating gases and the fuel, and here most of the fuel is burnt. The little magnified "cartoons" of laminar counterflows across the mixing layer are made to emphasise that a flamelet model of this turbulent flame would consider such elements, and therefore that the appropriate boundary conditions of the laminar flamelets comprising the "library" would depend on the flow location. In different parts of the flame, combustion occurs between fuel and oxidant at various degrees of dilution and initial temperatures, and as both affect the speed of the reaction, there is no *single* chemical timescale describing the reaction rate in a recirculating non–premixed flame. However, it is reasonable to assume that the reaction rate increases monotonically with T_{RZ} for all locations along the flame.

It is clear from this discussion and the results of Chapter 4 that the temperature of the recirculation zone is an important parameter for stabilisation because the speed of the chemistry is an increasing function of T_{RZ}, and then the extinction of the flame will depend on the scalar dissipation rate acting on the flame and on T_{RZ}. Estimates of both these quantities are performed in the next Section.

5.3 EXTINCTION OF NON–PREMIXED RECIRCULATING FLAMES

Approximations for the mixing and the turbulent scalar dissipation rate at the flame are made in this Section together with assumptions pertinent to the way the local flow variables like turbulent intensities and mixture fraction gradients scale with global operational parameters. The mixing model also results in an expression for the flame length, which is used to predict the temperature of the recirculation zone, and then the extinction of the flame is discussed through estimates of the scalar dissipation rate and T_{RZ}. The expressions developed here explain qualitatively the measured trends of non–premixed recirculating flame extinction.

5.3.1 Operational parameters of a recirculation–stabilised diffusion flame

A recirculation–zone stabilised diffusion flame is described by the fuel jet velocity U_f, the bulk air velocity U_b, the swirl number Sw, and by the throat diameter D, the fuel injector size D_{inj}, and the length of the diffuser L_{diff}. The following assumptions are made: (i) U_f/U_b is small enough for the central fuel jet not to penetrate the recirculation zone (Feikema et al., 1991; Rawe and Kremer, 1980; Prade and Lenze, 1992); (ii) the turbulence q' scales with the air bulk velocity U_b (Prade and Lenze, 1992) and increases with swirl number Sw (Milosavljevic, 1993); (iii) the turbulence integral lengthscale L_{turb} is proportional to D and does not depend on any other parameter; (iv) the length of the recirculation zone L_{RZ} is proportional to D, increases with L_{diff}, and is independent of Sw (Milosavljevic *et al.*, 1990a); (v) the recirculation zone has uniform temperature and composition (Milosavljevic, 1993); and (vi) close to lean extinction limit, the mode of fuel injection does not change the mixing field.

Below, the effects of changes in the parameters U_f, U_b, Sw, D, and L_{RZ} on the scalar dissipation rate are examined. Estimates of the recirculation zone temperature are also necessary and, to achieve both, a discussion about the mixing between the fuel and the air is a prerequisite and presented next.

5.3.2 Mixing of the fuel jet

Consider the turbulent mixing layer between the fuel and the air growing from the fuel injector to the tip of the flame. Mixing is effected by the action of a turbulent eddy diffusivity, proportional to $q' L_{turb}$, for a length x, where x is a coordinate along the mixing layer. It is assumed that the turbulent diffusivity is constant and does not depend on the velocity of the fuel with the turbulence q' proportional to the dominant air velocity U_b. This assumption is valid because the momentum of the fuel jet is small relative to that of the air flow at lean conditions, and because the turbulence lengthscale depends only on the burner size D. The fuel jet mixing is modelled as similar to the

dispersion from a line source of a contaminant in homogeneous, isotropic turbulence of constant mean velocity U_b and intensity q', for which the standard result is that

$$L_{mix}(x) \propto (q' L_{turb}\, x/U_b)^{1/2}\,, \tag{5.3.1}$$

and

$$F(x) \propto (U_f D_{inj})\,(q'\, L_{turb}\, U_b\, x)^{-1/2} \tag{5.3.2}$$

where L_{mix} is the thickness of the mixing layer at the axial location x, F is the mean mixture fraction at x, and the term $(U_f D_{inj})$ represents the "source strength" (Hinze, 1975, Eq. 5-161). Therefore the mean mixture fraction decays as $x^{-1/2}$, the mixing layer grows as $x^{1/2}$, and the decay is faster with increasing turbulence intensity and lower ratio of fuel to air velocity.

5.3.3 Scalar dissipation rate in the mixing layer

The mean turbulent scalar dissipation rate will have non–zero values at locations where the mixture fraction fluctuations are finite which, in turn, happens where the mean mixture fraction gradients are non–zero. A balance between the production and dissipation terms in the modelled governing equation for the r.m.s. fluctuations of mixture fraction (Section 3.2.5) gives

$$q' L_{turb}\left[\frac{\partial F}{\partial x_i}\right]^2 \propto \frac{q'}{L_{turb}}\, f'^2\,. \tag{5.3.3}$$

The mean mixture fraction gradients are dominant in the direction normal to the mixing layers between fuel and air and between fuel and the recirculating gases (Fig. 5.3.2) and then Eq. (5.3.3) can be approximated by

$$\chi \propto q' L_{turb}\left[\frac{\Delta F}{L_{mix}}\right]^2\,. \tag{5.3.4}$$

In the context of the previous mixing model (Eqs. 5.3.1 & 5.3.2), the scalar dissipation rate depends on the axial location and varies as

$$\chi(x) \propto (U_f D_{inj}/U_b D)^2\,(U_b/q')\;(U_b/L_{turb})\;(x/D)^{-2}\,, \tag{5.3.5}$$

where use has been made of Eqs. (5.3.1) and (5.3.2) and of $\Delta F \approx F(x)$. Equation (5.3.5) is used to estimate the mean scalar dissipation rate at the flame location and recall from Section 4.3.4 that extinction occurs when χ / χ_{lam} is greater than a critical value, where χ_{lam} is the scalar dissipation rate at extinction of a laminar counterflow flame at the

conditions of reactant premixing, vitiation, and initial temperature of the reactants reaching the turbulent flame zone. An expression for the temperature in the recirculation zone is also needed, because this affects χ_{lam}, and this is estimated next.

5.3.4 The temperature of the recirculation zone

The recirculation zone is composed of gases that were entrained along the RZ boundaries by turbulent diffusion; in the conceptual picture of Fig. 5.1, the recirculation zone is enclosed by the flame and therefore only combustion products can be entrained and this is in agreement with our expectations and with the measurements of Milosavljevic (1993). Assume that the recirculation zone entrains combustion products from the surrounding flame only along the flame's length: if $L_{flame}>L_{RZ}$, only combustion products can be entrained. However, if $L_{flame}<L_{RZ}$, there is a region along the RZ boundary which is composed of combustion products mixed with annular air and, possibly, fluid entrained from the outer stagnant atmosphere. Therefore the recirculation zone can entrain *cool* gases and then its temperature is expected to be lower and the oxygen content higher. Therefore an important parameter determining the RZ temperature is the flame length which is estimated below[1].

The flame length is given approximately by the axial location x that corresponds to $F(x)=F_{st}$, i.e. the tip of the stoichiometric mixture fraction contour. Solving Eq. (5.3.2) for x gives

$$L_{flame}/D \propto (U_f D_{inj}/U_b D)^2 (U_b/q') (D/L_{turb}) F_{st}^{-2}, \qquad (5.3.6)$$

which shows that the flame length increases with fuel jet velocity and decreases with swirl number because the turbulence q'/U_b increases with swirl, both trends consistent with the data of Milosavljevic (1993) and Rawe and Kremer (1980).

A volume–averaged value of the temperature of the RZ is therefore given approximately by

$$T_{RZ} \approx (L_{flame}/L_{RZ}) T_{flame} + (1 - L_{flame}/L_{RZ}) T_{amb}, \qquad (5.3.7a)$$

if $L_{flame} < L_{RZ}$, and by

$$T_{RZ} \approx T_{flame}, \qquad (5.3.7b)$$

---

[1] Of course, if there is significant temperature drop and reactant penetration through the flame zone due to high strain rates, the temperature of the fluid that the RZ entrains falls from the adiabatic value even if $L_{flame}>L_{RZ}$.

if $L_{flame} \geq L_{RZ}$, where T_{RZ} is a measure of the recirculation zone temperature, T_{flame} the adiabatic flame temperature, and T_{amb} the temperature of the fluid entrained along the RZ boundary *downstream* of the flame. Equations (5.3.6) and (5.3.7) show that as the fuel velocity decreases, the flame length decreases, an increasing portion of the RZ boundary is exposed, and entrainment of cold air and cold outer ambient fluid becomes possible thus reducing the temperature, and this is the basic mechanism whereby lean flames extinguish.

5.3.5 Final expressions

Substitution of Eq. (5.3.6) in Eq. (5.3.5) with $x=L_{flame}$ shows that the scalar dissipation rate at the flame tip is given by

$$\chi_{flame} \propto (U_f D_{inj}/U_b D)^{-2} (q'/U_b) (L_{turb}/D) (U_b/D) . \qquad (5.3.8)$$

Equation (5.3.8) shows that a representative value of the scalar dissipation rate increases with air bulk velocity, swirl number through an increase in q'/U_b, while it decreases with burner size and with fuel injection velocity. Writing the equivalence ratio as the ratio of fuel to air flow rates gives

$$\phi \propto \frac{U_f D_{inj}^2}{U_b(D^2-D_{inj}^2)}$$

and with $R=D_{inj}/D$,

$$\chi_{flame} \propto \phi^{-2} (1/R-R)^{-2} (q'/U_b) (L_{turb}/D) (U_b/D) \qquad (5.3.9)$$

and

$$L_{flame}/D \propto \phi^2 (1/R-R)^2 (U_b/q') (D/L_{turb}) F_{st}^{-2} , \qquad (5.3.10)$$

which relate the scalar dissipation rate and the flame length to the equivalence ratio and the fuel nozzle to the burner size. Equations (5.3.7), (5.3.9) and (5.3.10) are used to predict the dependence of flow parameters on the stability of the flame in the next Section.

5.3.6 Qualitative prediction of extinction

Effect of air bulk velocity

Equation (5.3.9) shows that the scalar dissipation rate increases with U_b for a given burner and equivalence ratio and so increasing the air bulk velocity will eventually cause extinction. On the chemical side, as U_f/U_b decreases, the flame length is reduced (Eq. 5.3.10), the temperature in the recirculation zone may decrease, and therefore combustion may become less favourable.

Effect of fuel bulk velocity

For given conditions of air velocity and diffuser geometry, increasing the fuel velocity U_f is beneficial for stability because it decreases the scalar dissipation rate at the flame by making the fuel jet "thicker" and hence the gradient smaller, and because it increases the temperature inside the recirculation zone which increases the advantageous effect of vitiation. Note that this explanation why overall rich flames are more stable than lean flames in diffusion flame configurations has not been presented before and is based on Eq. (5.3.9) and on the concept which emerged from the results of Chapter 4 that the high temperature, notwithstanding the small oxidiser content, is beneficial for the flame. It is different *in principle* from that given by Rawe and Kremer (1980) and by Feikema *et al.* (1991) that high fuel jet velocities "push" the flame towards regions of low velocities, a fact that those authors claimed has an advantage for stability but stated without any theoretical justification.

Effect of swirl number

Increasing the swirl number increases q'/U_b and so increases the mean turbulent scalar dissipation rate (Eq. 5.3.9), while it simultaneously reduces the flame length and possibly the temperature inside the recirculation zone, if the equivalence ratio is low such that the flame is not long enough to cover the RZ (Eqs. 5.3.6 & 5.3.7). In this case, the swirl number has an additional detrimental effect that it entrains *more* ambient fluid because the speed of entrainment increases with Sw (Wall *et al.*, 1986), thus cooling even further the RZ gases.

Effect of throat diameter D

Increasing the size of the burner increases the turbulence lengthscale L_{turb} proportionately; L_{flame}/D is unaffected (Eq. 5.3.10) if the fuel to air velocity ratio is the same and the fuel injector scales linearly with D. Then Eq. (5.3.9) shows that χ_{flame} decreases with increasing burner size, and so large burners can sustain flames at higher velocities.

Effect of diffuser length L_{diff}

A longer diffuser results in a longer recirculation zone, but the lengthscales of the turbulence and of the mixing layer between the fuel and the air jets are not affected because they depend only on D and the turbulence intensity is also expected to be unaffected. Equation (5.3.9) then shows that χ_{flame} is the same for long and short diffusers, but the temperature inside the RZ is smaller because of more entrainment, and then the chemical timescale increases. Therefore flames stabilised in long quarls are expected to have a richer lean limit than flames in short quarls.

Effect of fuel injection angle

The species concentrations measurements of Milosavljevic (1993) and of Rawe and Kremer (1980) and the visualisation of Feikema *et al.* (1991) show that when the reverse flow momentum dominates the fuel jet momentum, as at the lean extinction limit with axial injection, the mixing pattern resembles the one depicted in Fig. 5.1, the expressions for χ_{flame} and L_{flame} are expected to be valid, and therefore no qualitative changes in the extinction limits with different fuel injection angles are expected, consistent with the data of Milosavljevic *et al.* (1990a).

Effect of ambient temperature

Increasing the temperature T_{amb} of the surroundings to the recirculating flame improves flame stability because T_{RZ} increases (Eq. 5.3.7), consistent with the observation of Milosavljevic *et al.* (1990b) that enclosed gas–supported swirl–stabilised coal–fired flames are more stable than flames without enclosure. The enclosure traps hot products and thus the reduction of T_{RZ} caused by the entrainment of ambient fluid is less pronounced.

5.3.6 Discussion

Comparison with experiment

The previous predictions agree with the lean stability measurements of Milosavljevic (1993), Milosavljevic *et al.* (1990a), Feikema *et al.* (1991), and Rawe and Kremer (1980) in most respects, namely that increasing the bulk air velocity and the swirl number cause extinction, that flames with high swirl numbers and in small burners need a higher equivalence ratio for stability, and that flames with long quarls are less stable. Note that the first two trends could be explained by a simple argument relating the swirl number and the bulk velocity with the strain rate on the flame[2], as by Feikema

[2] Recall that the strain rate is not appropriate for a description of the extinction of diffusion flames, the scalar dissipation rate is, but the two are approximately proportional if the mixing field is the same. In recirculating flames, however, the mixing field changes with the operational parameters and so examination of the strain rate alone is not sufficient to explain extinction.

et al. (1991), but the trend that the leanest equivalence ratio increases with recirculation zone length could not be explained without introducing the dependence of the RZ temperature on flow parameters, which also provided the correct demonstration why rich flames are stable.

A feature of the measurements of Rawe and Kremer (1980) and, to a lesser extent, of Milosavljevic *et al.* (1990a), that the present predictions apparently do not reproduce is the non–monotonic dependence of the equivalence ratio on swirl number in a small range of Sw. The explanation given by Milosavljevic *et al.* (1990a) for the presence of "bulges" in some of the plots of ϕ_{min} against Sw was that at these swirl numbers, the turbulence *decreased* with Sw instead of increasing, with subsequent changes in the mixing patterns. If that is the case in the measured extinction data, it would suggest that the ratio q'/U_b in Eq. (5.3.9) does not vary monotonically with swirl number, and the validity of the present model is not affected.

The only feature of the measurements of Rawe and Kremer (1980) that the present model does not reproduce is the marginal dependence of the leanest equivalence ratio on fuel nozzle diameter: the experiment showed that increasing the ratio $R=D_{inj}/D$ resulted in a slightly leaner equivalence ratio at extinction at the same bulk velocity. Contrary to the experiment, Eq. (5.3.9) shows that if R increases, ϕ has to increase in order to achieve the same level of χ_{flame} and Eq. (5.3.10) shows that the flame length decreases with increasing R, which are both detrimental for flame stability. Recall that the injector size appears only in the expression of the "source strength" in Eqs. (5.3.1) and (5.3.2) and that the conical mixing layer between the fuel and the air flow was represented as planar two–dimensional, and this might cause the discrepancy.

Scaling laws

In the present model for the extinction of recirculating non–premixed flames, the scaling parameters are the ratio of fuel to air flow rates, the linear dimension of the fuel injector to the burner size, the swirl number because it determines the proportionality constant between the bulk velocity and the turbulence, the ratio U_b/D, and the temperature in the recirculation zone. Extinction is determined by the ratio χ_{flame}/χ_{lam}, and it was shown previously that *both* can change with the operating conditions: for example, increasing U_b increases χ_{flame} by increasing the turbulence, and decreasing U_f increases χ_{flame} by increasing the mixture fraction gradient and also decreases χ_{lam} by reducing the temperature. Therefore a laboratory–scale experiment will simulate truly the approach to extinction of a larger–scale burner with the same fuel if the temperature of the recirculation zone T_{RZ} (and thus χ_{lam}) and χ_{flame} given by Eq. (5.3.9) are kept the same at the small and the large scales. Equivalently, a Damköhler number defined as $(\chi_{flame}/\chi_{lam})^{-1}$ should be the same, and the present contribution shows how this can be accomplished. For example, doubling the size of the burner means that both the bulk

velocities of the air and fuel should also be doubled to achieve the same χ_{flame}, and the presence of radiation heat transfer into the recirculation zone from, say, refractory materials in an industrial furnace, may be simulated by reactant preheat so as to achieve the same T_{RZ}. Other trends that the present scaling imply are that the flame length close to the lean limit increases with the square of the overall equivalence ratio, is independent of the bulk air velocity, and decreases with increasing swirl because the latter increases the turbulence and hence the eddy diffusivity.

Extinction correlations

The success of the ratio χ_{flame}/χ_{lam} in correlating quantitatively the extinction of jet diffusion flames (Peters and Williams, 1983) and of turbulent counterflow diffusion flames (Chapter 4), and in predicting qualitatively the experimental trends of extinction of diffusion flames stabilised by recirculation zones, emphasises that this ratio correctly identifies the approach of turbulent diffusion flames to extinction. In contrast to previous expressions that use only the parameter U_b/D to determine extinction by Feikema *et al.* (1991) and the equivalent expressions by Rawe and Kremer (1980) and Prade and Lenze (1992), the present model predicts that the appropriate aerodynamic timescale, χ_{flame}, does *not* scale uniquely with U_b/D (Eq. 5.3.9) because of the presence of the term representing the "source strength" in Eq. (5.3.2) and which introduces the dependence of the aerodynamic timescale on the equivalence ratio. The wide success of correlations based only on U_b/D for predicting extinction of *premixed* recirculating flames stems mostly from the fact that this problem is simpler because no considerations of the mixing are needed and so application of those correlations to *diffusion* flame configurations is not justified.

Justification of assumptions

The assumptions behind the analysis leading to Eqs. (5.3.7), (5.3.9), and (5.3.10) are warranted for the qualitative purposes of this Chapter. First, the momentum of the fuel relative to the air flow is small at conditions corresponding to lean extinction and therefore the dominant feature of the fuel mixing is the *air* flow velocity and turbulence, with the fuel acting passively. This is a different situation from that of a round jet diffusion flame of fuel into stagnant surroundings because there the *fuel* velocity dominates, and induces, the diffusion process, and therefore the lean extinction of recirculating flames cannot be treated with the same mixing model as the rich extinction. Secondly, the turbulence does not vary much across the mixing layer (Milosavljevic, 1993) and it is reasonable to assume that the lengthscale behaves in the same way, and so the eddy viscosity is approximately constant. Thirdly, it has been assumed that the bulk velocity is constant although the mean velocity gradients in the mixing region are not negligible, but this will result in a small error such that the

qualitative *dependencies* of χ_{flame} and L_{flame} on flow conditions in Eqs. (5.3.9) and (5.3.10) are correct. Finally, the assumption that production equals dissipation that led to Eq. (5.3.6) is a standard assumption in turbulent shear flows and, again, it is expected that the basic dependencies on flow conditions have been captured.

The effect of the r.m.s. mixture fraction fluctuations, f', has not been discussed yet. The major influence f' may have on the arguments presented here is not as to the accuracy of the estimate of the scalar dissipation rate, because by evaluating the production term in the governing equation for f', the problem of calculating f' was circumvented. The fluctuations are more important for determining whether the flame is in the flamelet regime or not and thus for deciding on the appropriateness of the extinction criterion based on the scalar dissipation rate that was developed for flamelet flames (Section 4.1.4). However, the extinction of non–flamelet flames is also caused by large values of χ, as shown by Bilger (1988), and therefore the results for the extinction trends of this Chapter are qualitatively correct without being restricted to a flamelet flame.

Quantitative predictions

The chemical timescale, χ_{lam}^{-1}, changes with flow conditions through changes in the temperature and the dependence of χ_{lam} on T_{RZ} is difficult to quantify, especially because the exact composition and initial temperature of the laminar flamelets burning in the recirculating flame (Fig. 5.1) are not known. Therefore, although estimates of χ_{flame} can be made with Eq. (5.3.9), the ratio χ_{flame}/χ_{lam} cannot be calculated numerically, as would be desirable in order to obtain a simple correlation, and so the present predictions are mostly of qualitative value and highlight scaling laws. It is believed, however, that all the physical phenomena of importance to the stability of such flames have been captured by considering the scalar dissipation rate at the flame and the temperature in the recirculation zone.

It is hence suggested that quantitative attempts for the stability of recirculating diffusion flames may be performed with models that are able to (i) predict successfully the mean mixing field and (ii) the scalar dissipation rate; (iii) include the probability of partial premixing and reactant vitiation in the flamelet "library" or other combustion model and their effects on extinction; and (iv) allow for ambient fluid entrainment. Such an effort has not been accomplished to date, but Al–Masseeh *et al.* (1990) calculated successfully the extinction of swirling recirculating *premixed* flames with a Reynolds–stress turbulence model and a laminar flamelet description of the combustion that included the possibility of flamelet quenching, and it is in this spirit and to at least this level of complication that calculations of *diffusion* flames stabilised by recirculation zones should be tried.

5.4 SUMMARY OF CHAPTER 5

It was found in Chapter 4 that the extinction of turbulent non–premixed flames is determined by the ratio of the mean turbulent scalar dissipation rate χ_{flame} to the scalar dissipation rate at the extinction of a laminar flame χ_{lam}, and the dependence of both these quantities on the operational parameters of non–premixed flames stabilised by recirculation zones was discussed in this Chapter. The motivation behind the present effort was provided by a review of appropriate literature that revealed that some of the explanations offered for the extinction of such flames are not consistent with physically correct results of flame extinction and hence that proposed correlations of lean stability limits are not of general applicability.

It is widely accepted that the recirculation zone is composed of reaction products which ignite the incoming reactants, and a justification for this general statement can be based on the results from Chapter 4 that demonstrated that combustion with hot reaction products as oxidant, albeit the low oxidant concentration, is more resistant to extinction than with ambient air due to the high initial reactant temperature. It follows that mixing with the recirculating hot products is beneficial for flame stability and, because χ_{lam} is an increasing function of temperature, it is sufficient for the stability of diffusion flames in recirculating zones to consider χ_{flame} and T_{RZ}, as parameters describing, respectively, the aerodynamic and the chemical timescales.

The fuel was assumed to spread from the fuel nozzle similarly to the way matter is diffused from a line source in a homogeneous turbulent flow, and together with a model for the scalar dissipation rate, it was found that :

$$L_{flame} / D \propto \phi^2 (1/R-R)^2 (U_b/q') (D/L_{turb}) F_{st}^{-2}$$

and

$$\chi_{flame} \propto \phi^{-2} (1/R-R)^{-2} (q'/U_b) (L_{turb}/D) (U_b/D) ,$$

and the temperature of the recirculation zone was modelled by

$$T_{RZ} \approx (L_{flame}/L_{RZ}) T_{flame} + (1 - L_{flame}/L_{RZ}) T_{amb} ,$$

motivated by the expectation that entrainment of cool ambient fluid becomes possible if the flame is shorter than the recirculation zone thus lowering the temperature. These expressions show the effects of the flame operating conditions on the flame length and on the scalar dissipation rate, and the major extinction trends, in agreement with experiments found in the literature, were predicted as follows: (i) as the air bulk flow velocity increases at constant equivalence ratio, the scalar dissipation rate increases thus

leading to extinction; (ii) as the equivalence ratio increases, the flame is longer and the temperature in the RZ may increase, thus increasing χ_{lam}, and also the fuel jet is thicker and so χ_{flame} decreases, both trends beneficial for flame stability; (iii) large burners have lower values of χ_{flame} than small burners at the same velocity and so can support leaner flames; (iv) high swirl numbers lead to extinction because the turbulence is increased, the flame is shortened allowing more ambient fluid entrainment hence reducing χ_{lam}, and also because χ_{flame} increases; and (v) increasing the recirculation zone length increases the leanest equivalence ratio for stable flames because T_{RZ} decreases.

These explanations for the lean extinction trends of recirculating diffusion flames have not been suggested before and have a sound theoretical basis contrary to others found in the literature. The proposed description implies that scale similarity of the approach to extinction of recirculating flames requires invariance of the Damköhler number $(\chi_{flame}/\chi_{lam})^{-1}$, and so T_{RZ} and χ_{flame} should be the same in laboratory–scale experiments and burners of larger size with the same fuel.

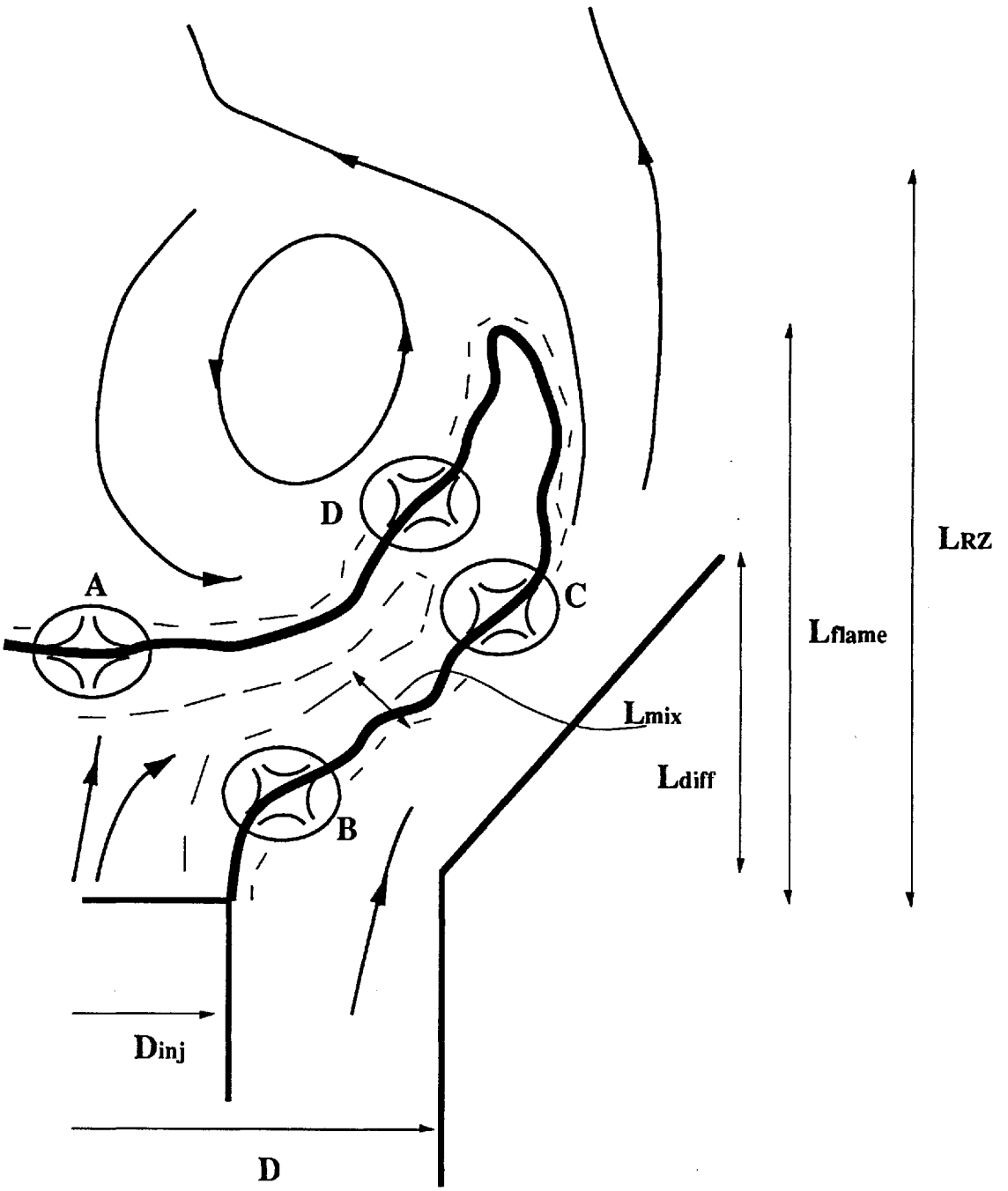


Figure 5.1 A conceptual model for a diffusion flame stabilised by a recirculation zone. The heavy line depicts a plausible shape of the instantaneous stoichiometric contour, the light dashed lines at either side of the stoichiometric depict rich and lean contours, and streamline portions are also indicated. The "cartoons" of counterflows along the stoichiometric contour denote that a laminar flamelet description of this flame would consider such flamelets, and the flamelets A to D are qualitatively different in the composition and initial temperature of the fuel and oxidant sides of the flame.

Chapter 6. Closure

This thesis described research with turbulent combustion in opposed jet flows in which flat and axisymmetric stretched non–premixed, partially premixed, and fully premixed flames were established. The work presented in the previous Chapters contributed to two areas: the first concerns the effects of stretch on the aerodynamic and chemical structure of turbulent flames, summarised at the end of Chapter 3, and the second concerns turbulent flame extinction, which was summarised at the ends of Chapters 4 and 5. In the next Section, the main findings are repeated and the thesis closes with suggestions for further research.

6.1 CONCLUSIONS FROM THIS WORK

The stretching rate on turbulent counterflow flames was partly due to the bulk flow strain rate and partly due to the superimposed turbulent fluctuations, and both the bulk flow and the turbulent stretch rates were discussed based on results from the present velocity measurements. It was found that the straining involved in the stagnation of opposed jet flows enhanced the turbulence, but that the turbulent intensity did not affect the mean velocity field, so that the turbulence can be treated by tracking its evolution in the straining flow, as, for example, by Rapid Distortion Theory. This de–coupling was suggested by the fact that mean residence times in the flow were smaller than typical turbulent timescales, and this had profound implications for mixing between the two jets, as discussed next.

Appreciable mixing did not have time to occur, and so the measurements of the instantaneous mixture fraction, denoting the concentration of fluid originating from one of the jets and determining approximately the location of diffusion flames, showed sharp transitions between low and high extreme values, with small probabilities of well–mixed fluid. It was suggested that the scalar fluctuations were due to the random movement of small–scale diffusion layers separating the two jets and techniques from the Flapping Model of scalar turbulence predicted qualitatively the trends in the mixture fraction measurements. The disparity of the velocity and the scalar fluctuation timescales suggests that widely–used models for the turbulent scalar dissipation rate, which is a quantity that determines the mean reaction rate and the extinction of turbulent diffusion flames, as shown in Chapter 4, might fail in the present flows. Finally, the large anisotropy measured in the velocities and the turbulent lengthscales suggest that standard modelling approaches should be used with care in opposed jet flows.

Non–premixed, partially premixed diffusion, and fully premixed flames showed smaller concentrations of combustion products as the stretch rate increased, and the transition from diffusion, through partially premixed, to premixed flames was smooth in terms of appearance, velocity field, scalar concentrations, and extinction limits. Non–premixed and partially premixed flames required mixing between the two streams prior to combustion, but fully premixed flames did not, and this implied a different location of the flames relative to the stagnation point, which, in turn, altered the mean velocity gradients and turbulence intensities in the flame neighbourhood. Non–premixed and partially premixed diffusion flames flames in turbulent opposed jet flows had not been observed before, and the present data are useful for guiding theoretical descriptions of stretch on non–premixed turbulent combustion.

Diffusion flames extinguished at high bulk velocities, small jet separations, and high turbulence intensities, and it was found that the mean turbulent scalar dissipation rate, χ, acquired a critical value at extinction conditions, supporting hence the extinction theory of Peters (1983) and suggesting that the appropriate Damköhler number describing diffusion flame stability should be based on the scalar dissipation rate. Partial premixing improved the stability of diffusion flames, reactant dilution by inerts was detrimental, preheat was beneficial, and for the special case where the oxidiser stream comprised hot products of combustion, as in certain practical combustion applications employing exhaust gas recirculation, the flame was more resistant to straining, and these results are consistent with expectations from the extinction of laminar counterflow flames, as found in the literature and as calculated in Chapter 4 based on the analysis due to Liñan (1974).

For premixed flames opposed by a hot stream and for diffusion flames with hot products as oxidant, extinction would *not* occur when the hot product stream had a temperature above about 1550K. Instead, the flames would ignite without an external source and luminous zones were observed even for very small reactant concentrations; this result agrees with recent views of hydrocarbon combustion that suggest that fuel conversion will proceed if the chain–branching steps in the reaction mechanism dominate the chain–termination steps, which occurs when the local temperature is above a critical value, and examination of flame extinction literature showed that this "universal" value is close to 1500K, supported by the present experiments.

The ideas of flame extinction developed in Chapter 4 were used for predicting the stability of non–premixed flames stabilised by recirculation zones in the following way. Motivated by the fact that recirculation zones contain mostly hot combustion products, by the finding that mixing with hot products is beneficial for stability, and by the appearance of the scalar dissipation rate in the appropriate Damköhler number representing

extinction, the stability of recirculating flames was attributed to small values of the recirculation zone temperature, hence increasing the chemical timescale, and to large values of the scalar dissipation rate, hence decreasing the aerodynamic timescale. Estimates of both quantities were performed based on a mixing model and predicted qualitatively all the extinction trends observed in laboratory–scale flames. This description of the extinction trends of recirculating flames is new and is not empirical in nature, in contrast to others found in the literature and, although qualitative, is expected to represent successfully the stability of realistic–scale burners because it encompasses most of the physical phenomena important to flame extinction.

6.2 SUGGESTIONS FOR FURTHER RESEARCH

A particular feature of the opposed jet flows examined here is that mean residence times are short compared to eddy turnover times, which means that the turbulence is distorted as it evolves in the flow and there is no time available for substantial mixing, and this disparity of timescales implies special effort for the correct modelling of mixing. One approach was suggested in Chapter 3 based on the conceptual picture that strained diffusion layers separate the two jets and that the amplitude and the thickness of these interfaces determine the scalar fluctuations. Diffusion flames lie along these interfaces and the instantaneous scalar dissipation rate is deteremined by the thickness of these layers. It is hence recommended that single and two–point measurements with better temporal and spatial resolution than can be provided by numerically–compensated thermocouples are performed to identify the thickness of these interfaces. Measurements in a range of bulk and turbulent strain rates may reveal the evolution from "early" times to the, better–understood, mixing at "long" times and thus provide insight in a relatively unexplored regime of turbulent mixing flows. Such an effort has already been started in the Thermofluids Section (Appendix 6.1).

A companion study in reacting flows may concentrate on two–dimensional imaging in diffusion and partially–premixed flames, as for example, by oil droplets which evaporate at the flame and thus give the instantaneous 2–D flame shape if illuminated by a laser sheet. Diffusion flames are located, approximately, along iso–concentration surfaces and premixed flames along iso–velocity surfaces in turbulent flows, and since the counterflow flames presented here span both regimes, useful insight in the transition between diffusion to premixed flames may be obtained and the results could be analysed with the help of techniques developed in the "G–equation model" of Peters (1993a).

Simultaneous measurements of velocity and temperature will provide data on the heat flux and are recommended because of the possible presence of counter–gradient

diffusion in these stagnating flames that involve large adverse pressure gradients. Temperature measurements in a wider range of premixed flames are also necessary in order to find the effects of stretch on flame temperature.

An effort was made in this thesis to extrapolate the knowledge of flame extinction obtained in the counterflow geometry to recirculating flames, but many approximations were made. It is recommended that a detailed experimental and theoretical examination of the scalar dissipation rate in recirculation zones is performed to show its dependence on various flow parameters, and hence quantify the qualitative scaling law proposed here. Such a contribution would be, I believe, welcome by combustion engineers.

Appendix 2.1. Calculation of oxygen mole fraction in the vitiated air burner

In this Appendix, the calculation method of the oxygen mole fraction in the vitiated air burner of Fig. 2.3 is described. The lower stream was composed of air and fuel at room temperature flowing at $V_{1,air}$ and $V_{1,fuel}$ l/min. The air and fuel flowing to the "supply" flame were metered as $V_{f,air}$ and $V_{f,fuel}$ l/min respectively, and to the products of this flame were added $V_{2,Ox}$ and $V_{2,Nit}$ l/min of bottled oxygen and nitrogen respectively. Complete combustion of the fuel in the "supply" flame is assumed so that the combustion products consist only of N_2, CO_2, H_2O, and O_2 (confirmed by measurements which showed that the mole fraction of CO was less than 0.007% and the unburnt hydrocarbons were about 5ppm at the tube exit plane). The chemical reaction is

$$CH_4 + \frac{1}{0.105}\,(0.21\,O_2 + 0.79\,N_2) \Rightarrow CO_2 + 2H_2O + \frac{0.79}{0.105}\,N_2$$

which shows that twice the number of moles of oxygen are required to burn completely the fuel and that no moles are produced during combustion. The oxygen mole fraction in the resulting mixture is then given by

$$X_{ox} = [\,0.21V_{f,air} + V_{2,Ox} - 2\,V_{f,fuel}\,] / [V_{f,air} + V_{f,fuel} + V_{2,Ox} + V_{2,Nit}]\,.$$

Note that the above formula applies both to the case of a few experiments in which ambient air was added to the hot products, which meant that $V_{2,Ox} = \frac{0.79}{0.21}\,V_{2,Nit}$, and to the case for no oxygen or nitrogen addition at all. Allowing for the fact that natural gas contains 94% methane and 1% propane, alters the oxygen concentration calculated from the formula above by 2% at most. For the experiments shown in Fig. 4.20, an electric heater was used for nitrogen–oxygen mixtures for which the oxygen mole fraction was calculated by $X_{ox} = V_{2,Ox} / (V_{2,Ox} + V_{2,Nit})$.

The mixtures flowing in the upper tube have a molecular weight close to air's, and so a measurement of the temperature is enough to determine the density. Based on this estimate, the velocity of the oxygen–nitrogen–combustion products in the upper tube can be determined and then the flow rates of either the upper or the lower stream can be adjusted to give $\rho_1 U_1^2 = \rho_2 U_2^2$, where $\rho_1 = X_{air}\,\rho_{air} + (1-X_{air})\,\rho_{fuel}$, X_{air} is the air volume fraction in the lower stream given by $X_{air}=V_{1,air}/(V_{1,air}+V_{1,fuel})$, $\rho_2=300/T_2\,\rho_{air}$, $\rho_{air}=1.19$ kg/m^3, $\rho_{fuel}=0.664$ kg/m^3, and T_2 is the measured temperature of the mixture at the upper tube exit in K.

Appendix 6.1. Published work

Portions of the work described in this thesis have appeared in archival literature and in conference proceedings and below, the references for these papers are given.

1. Mastorakos, E. & Taylor, A. M. K. P. (1992) Visualisation of counterflow flames. Flow Visualisation VI, Tanida, Y. & Miyashiro, H. (Eds.), Springer–Verlag, 580–584.

2. Mastorakos, E., Taylor, A. M. K. P. & Whitelaw, J. H. (1992) Extinction and temperature characteristics of turbulent counterflow diffusion flames with partial premixing. *Comb. Flame* **91**, 40–54.

3. Mastorakos, E., Taylor, A. M. K. P. & Whitelaw, J. H. (1992) Scalar dissipation rate at the extinction of turbulent counterflow non–premixed flames. *Comb. Flame* **91**, 55–64.

4. Mastorakos, E., Taylor, A. M. K. P. & Whitelaw, J. H. (1993) Turbulent counterflow flames with reactants diluted by hot products. Proceedings the Joint Meeting of the British and German Sections of the Combustion Institute, Cambridge, March 1993.

5. Mastorakos, E., Taylor, A. M. K. P. & Whitelaw, J. H. (1993) Mixing in turbulent opposed jet flows. To be presented at the 9th Symposium on Turbulent Shear Flows, Kyoto, August 1993.

Paper (5) describes measurements as in Section 3.2.6, but made with 5μm cold wire systems, not thermocouples, and so are more reliable because the time response was better and there were not uncertainties associated with the compensation procedure. However, the same conclusions as in Section 3.2.6, 3.2.7, and 3.4.6 were reached.

References

Abbas, N. S. T., Lockwood, F. C., Hussein, A. M. M. & Hassan, M. A. (1992) A study of extinction and NO_x in stretched premixed flames. *J. Institute of Energy* **65**, 77.

Abd Al–Masseeh, Bradley, D., Gaskell, P. H. & Lau, A. K. C. (1990) Turbulent premixed, swirling combustion: direct–stress, strained flamelet modelling and experimental investigation. 23rd Symposium (Int.) on Combustion, 825.

Anagnostou, E. & Potter, A. E. (1962) Flame strength of propane–oxygen flames at low pressures in turbulent flow. 9th Symposium (Int.) on Combustion, 1.

Attya, A. E. M. A. (1983) Kerosene spray flames. PhD Thesis, University of London.

Ballantyne, A. & Moss, J. B. (1977) Fine wire thermocouple measurements of fluctuating temperature. *Combust. Sci. and Tech.* **17**, 63.

Barlow, R. S., Dibble, R. W., Stårner, S. H. & Bilger, R. W. (1990) Piloted diffusion flames of nitrogen–diluted methane near extinction: OH measurements. 23rd Symposium (Int.) on Combustion, 583.

Becker, H. A. (1993) Physical Probes. In Intrumentation for flows with combustion, Taylor, A. M. K. P. (Ed.), Academic Press, London.

Beér, J. M. & Chigier, N. A. (1972) Combustion Aerodynamics. Applied Science Publishers, London.

Bendat, J. S. & Piersol, A. G. (1971) Random data: analysis and measurement procedures. Wiley–Interscience, New York.

Bilger, R. W. (1977) Probe measurements in turbulent combustion. AIAA Progress in Astronautics and Aeronautics, vol. 53, Zinn, B. T. (Ed.), 49.

Bilger, R. W. (1980) Turbulent flames with non–premixed reactants. In Turbulent Reacting Flows, Libby, P. A. & Williams, F. A. (Eds.), Springer.

Bilger, R. W. (1988) The structure of turbulent non–premixed flames. 22nd Symposium (Int.) on Combustion, 475.

Bilger, R. W. (1989) Turbulent diffusion flames. *Ann. Rev. Fluid Mech.* **21**, 101.

Bilger, R. W. (1993) Basic considerations. In Instrumentation for flows with combustion, Taylor, A. M. K. P. (Ed.), Academic Press, London.

Bird, R. B., Stewart, W. E. & Lightfoot, E. N. (1960) Transport Phenomena. Wiley, New York.

Bloor, M. I. G., David, T., Dixon–Lewis, G. & Gaskell, P. H. (1986) The influence of combustion on the fluid structure in a counter–flow diffusion flame. 21st Symposium (Int.) on Combustion, 1501.

Bradley, D. & Mathews, K. J. (1968) Measurements of high gas temperatures with fine wire thermocouples. *J. Mech. Eng. Sci.* **10**, 229.

Bradley, D., Lau, A. K. C. & Missaghi, M. (1989) Response of compensated thermocouples to fluctuating temperatures: computer simulations, experimental results and mathematical modeling. *Combust. Sci. and Tech.* **64**, 119.

Bradley, D., Gaskell, P. H. & Lau, A. K. C. (1990) A mixedness–reactedness flamelet model for turbulent diffusion flames. 23rd Symposium (Int.) on Combustion, 685.

Bradley, D., Lau, A. K. C. Lau, & Lawes, M. (1992) Flame stretch as a determinant of turbulent burning velocity. *Phil. Trans. R. Soc. Lond. A* **338**, 359.

Bray, K. N. C. (1993) University of Cambridge. Personal communication.

Bray, K. N. C. & Cant, R. S. (1991) Some applications of Kolmogorov's turbulence research in the field of combustion. *Proc. R. Soc. Lond. A* **434**, 217.

Bray, K. N. C., Champion, M. & Libby, P. A. (1991) Premixed flames in stagnating turbulence: Part I. The general formulation for counterflowing streams and gradient models for turbulent transport. *Comb. Flame* **84**, 391.

Bray, K. N. C., Champion, M. & Libby, P. A. (1992) Premixed flames in stagnating turbulence. Part III– The k–ε theory for reactants impinging on a wall. *Comb. Flame* **91**, 165.

Bray, K. N. C. & Libby, P. A. (1990) Premixed turbulent combustion. In Fluid Dynamical Aspects of Combustion Theory, Onofri, M. & Tesei, A. (Eds.), Longman, London.

Britter, R. E., Hunt, J. C. R. & Mumford, J. C. (1979) The distortion of turbulence by a circular cylinder. *J. Fluid Mech.* **92**, 269.

Broadwell, J. E., Dahm, W. J. A. & Mungal, M. G. (1984) Blowout of turbulent diffusion flames. 20th Symposium (Int.) on Combustion, 303.

Buckmaster, J. D. & Mikolaitis, D. (1982) The premixed flame in a counterflow. *Comb. Flame* **47**, 191.

Buckmaster, J. D. & Ludford, G. S. S. (1982) Theory of laminar flames. Cambridge University Press, Cambridge.

Byggstøyl, S. & Magnussen, B. F. (1983) A model for flame extinction in turbulent flow. Proc. 4th Symposium on Turbulent Shear Flows, p. 10.32.

Chakravarty, A., Lockwood, F. C. & Sinicropi, G. (1984) The prediction of burner stability limits. *Combust. Sci. and Tech.* **42**, 67.

Champion, M. & Libby, P. A. (1993) Reynolds stress description of opposed and impinging turbulent jets. Part I: Closely spaced opposed jets. *Phys. Fluids A* **5**, 203.

Chandran, S. B. S., Komerath, N. M., Grissom, W. M., Jagoda, J. I. & Strahle, W. C. (1985) Time resolved thermometry by simultaneous thermocouple and Rayleigh scattering measurements in a turbulent flame. *Combust. Sci. and Tech.* **44**, 47.

Chelliah, H. K., Law, C. K., Ueda, T., Smooke, M. D. & Williams, F. A. (1990) An experimental and theoretical investigation of the dilution, pressure and flow–field

effects on the extinction condition of methane–air–nitrogen diffusion flames. 23rd Symposium (Int.) on Combustion, 503.

Chen, C. L. & Sohrab, S. H. (1991) Simultaneous effects of fuel/oxidizer concentrations on the extinction of counterflow diffusion flames. *Comb. Flame* **86**, 383.

Cho, P., Law, C. K., Hertzberg, J. R. & Cheng, R. K. (1986) Structure and propagation of turbulent premixed flames stabilised in a stagnation flow. 21st Symposium (Int.) on Combustion, 1493.

Cho, P., Law, C. K., Cheng, R. K. & Shepherd, I. G. (1988) Velocity and scalar fields of turbulent premixed flames in stagnation flow. 22nd Symposium (Int.) on Combustion, 739.

Chomiak, J. (1979) Basic considerations in the turbulent flame propagation in premixed gases. *Prog. Energy Combust. Sci.* **5**, 207.

Collis, D. C. & Williams, M. J. (1959) Two dimensional convection from heated wires at low Reynolds number. *J. Fluid Mech.* **6**, 357.

Colket, M. B. III, Chiappetta, L., Guile, R. N., Zabielski, M. F. & Seery, D. J. (1982) Internal aerodynamics of gas sampling probes. *Comb. Flame* **44**, 3.

Dahm, W. J. A. & Dibble, R. W. (1988) Coflowing turbulent jet diffusion flame blowout. 22nd Symposium (Int.) on Combustion, 801.

Dahm, W. J. A. & Mayman, A. G. (1990) Blowout limits of turbulent jet diffusion flames for arbitrary source conditions. *AIAA Journal* **28**, 1157.

Darabiha, N., Giovangigli, V., Candel, S. & Smooke, M. D. (1988) Extinction of strained premixed propane–air flames with complex chemistry. *Combust. Sci. and Tech.* **60**, 267.

Darabiha, N. & Candel, S. (1992) The influence of the temperature on extinction and ignition limits of strained hydrogen–air diffusion flames. *Combust. Sci. and Tech.* **86**, 67.

Dimotakis, P. E. (1989) Turbulent shear layer mixing with fast chemical reactions. In Turbulent reactive flows, Borghi, R. & Murthy, S. N. B. (Eds.), Springer.

Dixon–Lewis, G. (1990) The structure of laminar flames. 23rd Symposium (Int.) on Combustion, 305.

Durst, F., Melling, A. & Whitelaw, J. H. (1976) Principles and practice of laser–Doppler anemometry. Academic Press, London.

Durst, F., Dornberger, E., Jakob, G., Veynante, D. & Martin, J. P. (1992) Laser Velocity and density measurement of a flat counterflow diffusion flame. In Aerothermodynamics in Combustors, Lee, R. S. L., Whitelaw, J. H. & Wung, T. S. (Eds.), Springer–Verlag, Berlin.

Eswaran, V. & Pope, S. B. (1988) Direct numerical simulations of the turbulent mixing of a passive scalar. *Phys. Fluids* **31**, 506.

Feikema, D., Chen, R.–H. & Driscoll, J. F. (1990) Enhancement of flame blowout limits by the use of swirl. *Comb. Flame* **80**, 183.

Feikema, D., Chen, R.–H. & Driscoll, J. F. (1991) Blowout of nonpremixed flames: maximum coaxial air velocities achievable, with and without swirl. *Comb. Flame* **86**, 347.

Fujibayashi, A. (1992) Thermofluids Section, Imperial College. Personal communication.

Gaydon, A. G. & Wolfhard, H. G. (1960) Flames: Their Structure, Radiation and Temperature. 2nd Edition, Chapman & Hall, London.

Gibson , C. H. (1968) Fine structure of scalar fields mixed by turbulence. I. Zero–gradient points and minimal gradient surfaces. *Phys. Fluids* **11**, 2305.

Godoy, S. (1982) Turbulent diffusion flames. PhD Thesis, University of London.

Goix, P. J. & Talbot, L. (1991) Turbulent counterflow diffusion flame structure and dilution effects. *Combust. Sci. and Tech.* **79**, 175.

Gover, M., Kermani, N. & Weinberg, F. J. (1992) Near–limit combustion in spouted and in crater beds. *Combust. Sci. and Tech.* **81**, 1.

Heitor, M. V. (1985) Experiments in turbulent reacting flow. PhD Thesis, University of London.

Heitor, M. V., Taylor, A. M. K. P. & Whitelaw, J. H. (1985) Simultaneous velocity and temperature measurements in a premixed flame. *Exp. in Fluids* **3**, 323.

Heitor, M. V., Laker, J. R., Taylor, A. M. K. P. & Vafidis, C. (1984) Instruction manual for the FS "Model 2" Doppler–frequency counter. Report No. FS/84/10, Mechanical Engineering Department, Imperial College.

Hinze, J. O. (1975) Turbulence. McGraw–Hill, New York.

Ishizuka, S, & Law, C. K. (1982) An experimental study on extinction and stability of stretched premixed flames. 19th Symposium (Int.) on Combustion, 327.

Jones, W. P. & Lindstedt, R. P. (1988) The calculation of the structure of laminar counterflow diffusion flames using a global reaction mechanism. *Combust. Sci. and Tech.* **61**, 31.

Jones, W. P., McDonnell, V., McGuirk, J. J., Milosavljevic, V. D. & Taylor, A. M. K. P. (1992) The calculation of mean mixture fractions in turbulent non–premixed methane flames from aspiration–probe measurements. Report No. FS/88/24, Mechanical Engineering Dept., Imperial College. Revised in 1992.

Jones, W. P. & Whitelaw, J. H. (1982) Calculation methods for reacting turbulent flows: a review. *Comb. Flame* **48**, 1.

Kalghatgi, G. T. (1984) Lift–off heights and visible lengths of vertical turbulent jet diffusion flames in still air. *Combust. Sci. and Tech.* **41**, 17.

Katsuki, M., Mizutani, Y. & Matsumoto, Y. (1987) An improved thermocouple technique for measurement of fluctuating temperatures in flames. *Comb. Flame* **67**, 27.

Kaye, G. W. C. & Laby, T. M. (1986) Tables of physical and chemical constants. 15th Edition, Longman, London.

Kee, R. J., Miller, J. A., Evans, G. H. & Dixon–Lewis, G. (1988) A computational model of the structure and extinction of strained, opposed flow premixed methane–air flames. 22nd Symposium (Int.) on Combustion, 1479.

Kennedy, I. M. & Kent, J. H. (1981) Scalar measurements in a coflowing turbulent diffusion flame. *Combust. Sci. and Tech.* **25**, 109.

Kerstein, A. R. (1991) Flapping model of scalar mixing in turbulence. *Phys. Fluids A* **3**, 2838.

Kim, J. S. & Williams, F. A. (1990) Theory of counterflow mixing of fuel with hot reaction products. *Combust. Sci. and Tech.* **73**, 575.

Kim, J. S., Libby, P. A. & Williams, A. (1992) On the displacement effects of laminar flames. *Combust. Sci. and Tech.* **87**, 1.

Kostiuk, L. W. (1991) Premixed turbulent combustion in counterflowing streams. PhD Thesis, University of Cambridge.

Kostiuk, L. W., Bray, K. N. C. & Chew, T. C. (1989) Premixed turbulent combustion in counterflowing streams. *Combust. Sci. and Tech.* **64**, 233.

Kostiuk, L. W., Bray, K. N. C. & Cheng, R. K. (1993)a Experimental study of premixed turbulent combustion in opposed streams. Part I– Nonreacting flow field. *Comb. Flame* **92**, 377.

Kostiuk, L. W., Bray, K. N. C. & Cheng, R. K. (1993)b Experimental study of premixed turbulent combustion in opposed streams. Part II– Reacting flow field and extinction. *Comb. Flame* **92**, 396.

Kuo, K. K. (1986) Principles of Combustion. Wiley, New York.

Labfacility Ltd. (1982) Temperature sensing with thermocouples and resistance thermometers. A practical handbook. London.

Laker, J. R. (1992) Thermofluids Section, Imperial College. Personal communication.

Law, C. K. (1988) Dynamics of stretched flames. 22nd Symposium (Int.) on Combustion, 1381.

Law, C. K., Ishizuka, S. & Mizomoto, M. (1980) Lean–limit extinction of propane/air mixtures in the stagnation–point flow. 18th Symposium (Int.) on Combustion, 1791.

Law, C. K., Zhu, D. L., & Yu, G. (1986) Propagation and extinction of stretched premixed flames. 21st Symposium (Int.) on Combustion, 1419.

Lawton, J. & Weinberg, F. (1969) Electrical aspects of combustion. Clarendon Press, Oxford.

Lee, M. J. (1989) Distortion of homogeneous turbulence by axisymmetric strain and dilatation. *Phys. Fluids A* **1**, 1541.

Libby, P. A. (1993) University of California San Diego. Personal communication.

Libby, P. A. & Williams, F. A. (1981) Structure of laminar flamelets in premixed turbulent flames. *Comb. Flame* **44**, 287.

Libby, P. A. & Williams, F. A. (1983) Strained premixed flames under nonadiabatic conditions. *Combust Sci. and Tech.* **31**, 1.

Liñan, A. (1974) The asymptotic structure of counterflow diffusion flames for large activation energies. *Acta Astronautica* **1**, 1007.

Lindstedt, R. P. (1992) Thermofluids Section, Imperial College. Personal communication.

Liu, Y. & Lenze, B. (1988) The influence of turbulence on the burning velocity of premixed CH_4–H_2 flames with different laminar burning velocities. 22nd Symposium (Int.) on Combustion, 747.

Liu, Y., Lenze, B. & Leuckel, W. (1990) Investigation on the combustion–turbulence interaction in premixed stagnation flames of H_2–CH_4 mixtures. In Turbulent Shear Flows 7, Springer–Verlag, Berlin.

Liu, Y., Ziegler, M. & Lenze, B. (1993) Burning velocity of premixed flames as a function of turbulence and physico–chemical fuel properties. Proceedings of the Meeting of the British and German Sections, Combustion Institute, Cambridge, March 1993, p. 64.

Lockwood, F. C. & Megahed, I. E. A. (1978) Extinction in turbulent reacting flows. *Combust. Sci. and Tech.* **19**, 77.

Longwell, J. P., Frost, E. E. & Weiss, M. A. (1953) Flame stability in bluff body recirculation zones. *Ind. and Eng. Chem.* **45**, 1629.

Marble, F. E. & Adamson, A. (1954) Ignition in a laminar mixing layer. In Selected combustion problems: fundamentals and aeronautical applications, Butterworths, London.

Masri, A. R. & Bilger, R. W. (1986) Turbulent non–premixed flames of hydrocarbon fuels near extinction: mean structure from probe measurements. 21st Symposium (Int.) on Combustion, 1511.

Masri, A. R., Bilger, R. W. & Dibble, R. W. (1990) The local structure of turbulent nonpremixed flames near extinction. *Comb. Flame* **81**, 260.

Masri, A. R. & Pope, S. B. (1990) PDF calculations of piloted turbulent nonpremixed flames of methane. *Comb. Flame* **81**, 13.

Mastorakos, E. (1992)a Description of a system for measuring the mean composition of flame gases with on–line analysers. Report No. TF/92/39, Mechanical Engineering Dept., Imperial College.

Mastorakos, E. (1992)b Thermocouple signal acquisition and processing system: an instruction manual. Report No. TF/92/08, Mechanical Engineering Dept., Imperial College.

Mauß, F., Keller, D. & Peters, N. (1990) A Lagrangian simulation of flamelet extinction and re–ignition in turbulent jet diffusion flames. 23rd Symposium (Int.) on Combustion, 693.

Miake–Lye, R. C. & Hammer, J. A. (1988) Lifted turbulent jet flames: a stability criterion based on the jet large–scale structure. 22nd Symposium (Int.) on Combustion, 817.

Milosavljevic, V. (1993) PhD thesis, Imperial College (in preparation).

Milosavljevic, V. D., Taylor, A. M. K. P. & Whitelaw, J. H. (1990)a The influence of burner geometry and flow rates on the stability and symmetry of swirl-stabilized nonpremixed flames. *Comb. Flame* **80**, 196.

Milosavljevic, V. D., Taylor, A. M. K. P. & Whitelaw, J. H. (1990)b Stability of pulverised coal flames. 23rd Symposium (Int.) on Combustion, 957.

Morel, T. (1975) Comprehensive design of axisymmetric wind tunnel contractions. *J. Fluids Engng.* **21**, 225.

Mounaïm–Rousselle, Ch. & Gökalp, I. (1993) Turbulent premixed combustion in counterflow geometry. The influence of a coflow. Presented at the Spring Meeting of the Western States Section of the Combustion Institute, Utah, March 1993.

Mullins, B. P. (1954) Combustion in vitiated air. In Selected combustion problems: fundamentals and aeronautical applications, Butterworths, London.

Namazian, M., Kelly, J. & Schefer, R. W. (1988) Near–field instantaneous flame and fuel concenration structures. 22nd Symposium (Int.) on Combustion, 627.

Pandya, T. P. & Weinberg, F. J. (1962) The study of the structure of laminar diffusion flames by optical methods. 9th Symposium (Int.) on Combustion, 587.

Perez–Ortiz, R. (1992) Thermofluids Section, Imperial College. Personal communication.

Peters, N. (1983) Local turbulent quenching due to flame stretch and non–premixed turbulent combustion. *Combust. Sci. and Tech.* **30**, 1.

Peters, N. (1984)a Laminar diffusion flamelet models in non–premixed turbulent combustion. *Prog. Energy Combust. Sci.* **10**, 319.

Peters, N. (1984)b Partially premixed diffusion flamelets in non–premixed turbulent combustion. 20th Symposium (Int.) on Combustion, 353.

Peters, N. (1986) Laminar flamelet concepts in turbulent combustion. 21st Symposium (Int.) on Combustion, 1231.

Peters, N. (1993)a Premixed, non–premixed and partially premixed turbulent combustion with fast chemistry. Proceedings of the Meeting of the British and German Sections of the Combustion Institute, Cambridge, March 1993, p. 26.

Peters, N. (1993)b University of Aachen. Personal communication. See also J. Göttgens, Mauß, F. & Peters, N. (1993) Analytic approximations of burning velocities and flame thicknesses of lean hydrogen, methane, ethylene, ethane, acetylene, and propane flames. 24th Symposium (Int.) on Combustion, 129.

Peters, N. & Williams, F. A. (1983) Liftoff characteristics of turbulent jet diffusion flames. *AIAA Journal* **21**, 423.

Pitts, W. M. (1988) Assessment of theories for the behavior and blowout of lifted turbulent jet diffusion flames. 22nd Symposium (Int.) on Combustion, 809.

Plee, S. L. & Mellor, A. M. (1979) Characteristic time correlation for lean blowoff of bluff–body–stabilised flames. *Comb. Flame* **35**, 61.

Poinsot, T., Veynante, D. & Candel, S. (1991) Quenching processes and premixed turbulent combustion diagrams. *J. Fluid Mech.* **228**, 561.

Potter, A. E. & Butler, J. N. (1959) A novel combustion measurement based on the extinguishment of diffusion flames. *ARS Journal* **29**, 54.

Potter, A. E., Heimel, S. & Butler, J. N. (1960) Apparent flame strength. A measure of maximum reaction rate in diffusion flames. 8th Symposium (Int.) on Combustion, 1027.

Prade, B. & Lenze, B. (1992) Experimental investigation in extinction of turbulent non–premixed disk stabilised flames. 24th Symposium (Int.) on Combustion, 369.

Press, W. H., Flannery, B. D., Teukolsky, S. A. & Vetterling, W. T. (1986) Numerical recipes. University Press, Cambridge.

Puri, I. K. & Seshadri, K. (1986) Extinction of diffusion flames burning methane and diluted propane in diluted air. *Comb. Flame* **65**, 137.

Radhakrishnan, K., Heywood, J. B. & Tabaczynski, R. J. (1981) Premixed turbulent flame blowoff velocity correlation based on coherent structures in turbulent flows. *Comb. Flame* **42**, 19.

Rawe, R. & Kremer, H. (1980) Stability limits of natural gas diffusion flames with swirl. 18th Symposium (Int.) on Combustion, 667.

Rolon, J. C., Veynante, D., Martin, J. P. & Durst, F. (1991) Counter jet stagnation flows. *Exp. Fluids* **11**, 313.

Sato, J. (1982) Effects of Lewis number on extinction behavior of premixed flames in a stagnation flow. 19th Symposium (Int.) on Combustion, 1541.

Schlichting, H. (1979) Boundary–Layer Theory. 7th Edition, McGraw–Hill, New York.

Schoenung, S. M. & Hanson, R. K. (1981) CO and temperature measurements in a flat flame by laser absorption spectroscopy and probe techniques. *Combust. Sci. and Tech.* **24**, 227.

Seshadri, K. & Williams, F. A. (1978) Laminar flow between parallel plates with injection of a reactant at high Reynolds number. *Int. J. Heat Mass Transfer* **21**, 251.

Seshadri, K., Puri, I. & Peters, N. (1985) Experimental and theoretical investigation of partially premixed diffusion flames at extinction. *Comb. Flame* **61**, 237.

Shepherd, I. G., Cheng, R. K. & Goix, P. J. (1990) The spatial structure of premixed turbulent stagnation point flames. 23rd Symposium (Int.) on Combustion, 781.

Simmons, R. F. & Wolfhard, H. G. (1957) Some limiting oxygen concentrations for diffusion flames in air diluted with nitrogen. *Comb. Flame* **1**, 155.

Smith, D. (1992) British Gas Plc. Personal communication.

Smooke, M. D., Puri, I. K. & Seshadri, K. (1986) A comparison between numerical calculations and experimental measurements of the structure of a counterflow diffusion flame burning dilute methane in diluted air. 21st Symposium (Int.) on Combustion, 1783.

Smooke, M. D., Seshadri, K. & Puri, I. K. (1988) The structure and extinction of partially premixed flames burning methane in air. 22nd Symposium (Int.) on Combustion, 1555.

Smooke, M. D., Crump, J., Seshadri, K. & Giovangigli, V. (1990) Comparison between experimental measurements and numerical calculations of the structure of counterflow, diluted, methane–air, premixed flames. 23rd Symposium (Int.) on Combustion, 463.

Spalding, D. B. (1961) Theory of mixing and chemical reaction in the opposed–jet diffusion flame. *ARS Journal* **31**, 763.

Spalding, M. A. & Tall, B. S. (1954) Flame stabilisation in high velocity gas streams and the effect of heat losses at low pressures. *Aeronautical Quarterly* **5**, 195.

Stahl, G. & Warnatz, J. (1991) Numerical investigation of time-dependent properties and extinction of strained methane– and propane–air flamelets. *Comb. Flame* **85**, 285.

Stapountzis, H., Sawford, B. L., Hunt, J. C. R. & Britter, R. E. (1986) Structure of the temperature field downwind of a line source in grid turbulence. *J. Fluid Mech.* **165**, 401.

Stårner, S. H., Bilger, R. W., Dibble, R. W. & Barlow, R. S. (1990) Piloted diffusion flames of diluted methane near extinction: mean structure from Raman/Rayleigh/Fluorescence measurements. *Combust. Sci. and Tech.* **70**, 111.

Stårner, S. H., Bilger, R. W., Dibble, R. W. & Barlow, R. S. (1992) Measurements of conserved scalars in turbulent diffusion flames. *Combust. Sci. and Tech.* **86**, 223.

Sung, C. J. & Law, C. K. (1993) On the structure and response of aerodynamically–strained planar premixed flames. AIAA paper 93–0246. Presented at the 31st Aerospace Sciences Meeting, Reno, January 1993. Also submitted to *Comb. Flame.*

Tennekes, H. & Lumley, J. L. (1972) A first course in turbulence. MIT Press, Cambridge, Mass..

Tien, J. H. & Matalon, M. (1991) On the burning velocity of stretched flames. *Comb. Flame* **84**, 238.

Tsuji, H. (1982) Counterflow diffusion flames. *Prog. Energy Combust. Sci.* **8**, 93.

Tsuji, H. & Yamaoka, I. (1966) The counterflow diffusion flame in the forward stagnation region of a porous cylinder. 11th Symposium (Int.) on Combustion, 979.

van de Kamp, W. L., Ikeda, I. & Smart, J. P. (1992) The combustion of pulverised coal using simulated turbine exhaust gas as oxidant. Report No. 37/y/29, International Flame Research Foundation, Ijmuiden, The Netherlands.

Vargaftik, N. B. (1975) Tables of the thermophysical properties of liquids and gases. 2nd Edition, Wiley, New York.

Veeravalli, S. & Warhaft, Z. (1990) Thermal dispersion from a line source in the shearless turbulence mixing layer. *J. Fluid Mech.* **216**, 35.

Wall, T. F., Phelan, W. J. & Bortz, S. (1986) The prediction and scaling of burn–out in swirled pulverised coal flames. Report No. F 388/a/3, International Flame Research Foundation, Ijmuiden, The Netherlands.

Warhaft, Z. & Lumley, J. L. (1978) An experimental study of the decay of temperature fluctuations in grid–generated turbulence. *J. Fluid Mech.* **88**, 659.

Wei, C. Y. & Miau, J. J. (1992) Stretching of freestream turbulence in the stagnation region. *AIAA Journal* **30**, 2196.

Weinberg, F. J. (1986) Advanced Combustion Methods. Academic Press, London.

Whitelaw, J. H. (1986) Lecture notes of the post–experience course "Experimental methods for turbulent flows", October 1986, Mechanical Engineering Dept., Imperial College.

Williams, F. A. (1985) Combustion Theory. Benjamin–Cummins, New York.

Wolfhard, H. G. (1956) Problems of combustion under altitude condition (treated from fundamental viewpoint). In Selected Combustion Problems – II, Butterworths, London.

Yahagi, Y., Ueda, T., Mizomoto, M. (1992) Extinction mechanism of lean methane / air turbulent premixed flame in a stagnation point flow. 24th Symposium (Int.) on Combustion, 537.

Yamaoka, I. & Tsuji, H. (1974) The structure of rich fuel–air flames in the forward stagnation region of a porous cylinder. 15th Symposium (Int.) on Combustion, 637.

Yamaoka, I. & Tsuji, H. (1976) Structure analysis of rich fuel–air flames in the forward stagnation region of a porous cylinder. 16th Symposium (Int.) on Combustion, 1145.

Yamaoka, I. & Tsuji, H. (1988) Extinction of near–stoichiometric flames diluted with nitrogen in a stagnation flow. 22nd Symposium (Int.) on Combustion, 1565.

Yang, B. & Seshadri, K. (1992) Asymptotic analysis of the structure of nonpremixed methane air flames using reduced chemistry. *Combust. Sci. and Tech.* **88**, 115.

Yanta , W. J. & Smith, R. A. (1978) Measurements of turbulence–transport properties with a laser–Doppler velocimeter. *AIAA paper no.* 73–169, 11th Aerospace Sciences Meeting, Washington.

Yoshida, A., Kubozuka, S. & Nakamura, S. (1989) Compensation of thermocouple signals by digital FIR filters for temperature measurement in turbulent premixed flames. *Combust. Sci. and Tech.* **65**, 317.

Yu, G., Law, C. K. & Wu, C. K. (1986) Laminar flame speeds of hydrocarbon + air mixtures with hydrogen addition. *Comb. Flame* **63**, 339.

Zukoski, E. E. & Marble, F. E. (1956) Experiments concerning the mechanism of flame blowoff from bluff bodies. Proc. Gas Dynamics Symp. on Aerothermochemistry, Northwestern University, 205.